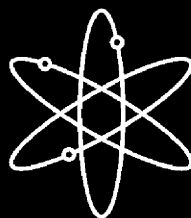
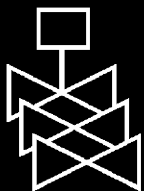




GSI-191 PWR Sump Screen Blockage Chemical Effects Tests: Thermodynamic Simulations



Center for Nuclear Waste Regulatory Analyses



**U.S. Nuclear Regulatory Commission
Office of Nuclear Regulatory Research
Washington, DC 20555-0001**



AVAILABILITY NOTICE

GSI-191 PWR Sump Screen Blockage Chemical Effects Tests: Thermodynamic Simulations

Manuscript Completed: November 2006

Date Published: December 2006

Prepared by

J. McMurry, V. Jain, X. He, D. Pickett

R. Pabalan, Y.-M. Pan

Center for Nuclear Waste Regulatory Analyses

Southwest Research Institute

6220 Culebra Road

San Antonio, TX 78238-5166

B.P. Jain, NRC Project Manager

Prepared for

Division of Fuel, Engineering and Radiological Research

Office of Nuclear Regulatory Research

U.S. Nuclear Regulatory Commission

Washington, DC 20555-0001

NRC Job Codes N6121 and N6278



ABSTRACT

This report summarizes chemical modeling studies and experiments performed to support the resolution of GSI-191. Along with entrained debris components, the formation of secondary precipitates and gels have the potential to impede the performance of Emergency Core Cooling System pumps, Containment Spray System pumps, or other components downstream of the sump strainer after a loss-of-coolant accident (LOCA). The purpose of this study was to examine the use of chemical modeling software as a tool in predicting whether secondary precipitates would be likely to form in specific post-LOCA chemical environments. Within the limits of the available thermodynamic data for the model, the software also identified which solids would be expected to form and their quantities, and it indicated how the containment water chemistry was affected by these reactions. Several existing, widely available chemical modeling programs—EQ3/6 (Lawrence Livermore National Laboratory, 1995), OLI Systems StreamAnalyzer (OLI Systems, Inc., 2005), The Geochemist's Workbench[®] REACT (RockWare, Inc., 2004), and PHREEQC (U.S. Geological Survey, 2003)—and their accompanying thermodynamic database files were evaluated to simulate the potential formation of precipitates under post-LOCA conditions. Detailed simulations were performed for five representative post-LOCA environments, in which alkaline or neutral borated containment waters interacted with metals, concrete, and insulation materials at 60 °C [140 °F] for times up to 720 hours. The modeled conditions corresponded to the Integrated Chemical Effects Test (ICET) experiments conducted at the University of New Mexico, and results of the experiments were used to benchmark and calibrate the simulations. The input water compositions for the simulations were estimated from specified initial containment water compositions, previously derived corrosion rates for the metals of interest, and dissolution rates from new experiments involving insulation materials and concrete. The modeling programs EQ3/6 and PHREEQC were used to perform blind predictions of the experiment results. Analytical data and qualitative observations of precipitation (or lack of it) from the ICET experiments were used to refine the conceptual model. Revised dissolution rates were obtained from additional experiments at the Center for Nuclear Waste Regulatory Analyses, after which informed simulations were performed using StreamAnalyzer and PHREEQC. A more detailed simulation considered the gradual changes in chemistry of the solution water over time, based on kinetic reaction rates with the reactive materials and ongoing equilibration (precipitation) with oversaturated secondary phases.

The study determined that the most important requirements for developing more accurate chemical effects simulations were (i) a realistic estimate of starting water compositions and dissolution rates, and (ii) the availability of an adequate set of thermodynamic data, particularly for amorphous or metastable solids that would be expected to form under the simulated conditions. The study concluded that the codes as tested were broadly useful in assessing whether precipitation of secondary solid phases was likely under the specified conditions and the quantity of material that was predicted to form. In applying chemical modeling software to other plant-specific sets of conditions, the effectiveness of the simulations and confidence in their predictions would be considerably improved by a more complete characterization of source-term materials and release rates for the conditions of interest, and by development of an appropriate thermodynamic database for modeling purposes that includes more realistic amorphous or metastable solids for the conditions of interest.

References:

OLI Systems, Inc. "StreamAnalyzer." Version 2.0. Morris Plains, New Jersey: OLI Systems, Inc. 2005.

Lawrence Livermore National Laboratory. "EQ3/6." Version 7.2b. Livermore, California: Lawrence Livermore National Laboratory. 1995.

RockWare, Inc. "The Geochemist's Workbench®." Version 5.0. Golden, Colorado: RockWare, Inc. 2004.

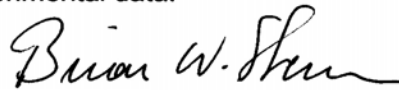
U.S. Geological Survey. "PHREEQC." Version 2.8. Reston, Virginia: U.S. Geological Survey. 2003.

FOREWORD

The U.S. Nuclear Regulatory Commission (NRC) is engaged in research activities related to resolving Generic Safety Issue (GSI) 191, "Assessment of Debris Accumulation on PWR Sump Performance." Following a loss-of-coolant accident (LOCA) in pressurized-water reactor (PWR) plants, corrosion products attributable to chemical interactions between the emergency core cooling system (ECCS) containment spray water and exposed materials (such as metal surfaces, paint chips, and fiberglass insulation debris) could impede the performance of ECCS recirculation. To assess whether gelatinous products could form following a LOCA event, the NRC initiated an integrated chemical effects tests (ICET) research program at the University of New Mexico. That ICET program consisted of a set of five tests conducted in an environment that represented expected containment pool conditions during recirculation. In addition, in order to gain insights into important test parameters and develop the predictive capability of ICET results, the NRC initiated a study at the Center for Nuclear Waste Regulatory Analyses (CNWRA) to evaluate the feasibility of utilizing commercially available thermodynamic simulation computer codes to predict the formation of chemical species in a typical post-LOCA PWR containment environment.

This report provides an evaluative summary of the predictive capability of four commercially available thermodynamic simulation computer codes (EQ3/6, PHREEQC, Geochemist's Workbench REACT, and OLI Systems StreamAnalyzer). The code comparison exercise considered representative post-LOCA conditions in alkaline, borated containment water at temperatures between 60 °C (140 °F) and 110 °C (230 °F). The reactor system components included galvanized steel, carbon steel, aluminum scaffolding, and copper fans and instrument lines, as well as glass fiber insulation material, calcium silicate insulation material, and concrete. The modeling software was used to identify the oversaturated secondary solids that would precipitate, and to calculate the final solution composition. The most important differences in results were traceable to different sets of solids in the thermodynamic database files accompanying each modeling code, rather than different capabilities of the codes themselves. Other simulations were benchmarked to the five ICET experiments.

Results of this study demonstrate that thermodynamic simulation modeling software is broadly useful in assessing the potential effects of post-LOCA interaction on sump screen blockage. However, its predictive capability is often hindered by insufficient thermodynamic data for relevant phases and aqueous species in the code database, as well as limitations in the kinetic data for dissolution of reactive materials in the presence of co-dissolving materials. Based on those findings, this study provides some insights for predicting what would happen in environments outside ICET tests, although the modeling alone is insufficient to make blind predictions with confidence. When thermodynamic simulations modeling is refined using ICET data and observations, the predictions broadly agreed with experimental results. Overall, prediction of chemical byproduct concentrations and species is most accurate when analytical models are properly benchmarked using experimental data.



Brian W. Sherron, Director
Office of Nuclear Regulatory Research
U.S. Nuclear Regulatory Commission

CONTENTS

Section	Page
ABSTRACT	iii
FOREWORD	v
FIGURES	ix
TABLES	xi
EXECUTIVE SUMMARY	xiii
ACKNOWLEDGMENTS	xix
1 INTRODUCTION	1-1
2 EVALUATION OF AQUEOUS CHEMICAL MODELING SOFTWARE	2-1
2.1 Selection of Codes for a Comparison Exercise	2-2
2.2 Code Comparison Exercise	2-5
2.3 Results of Temperature Variation Exercise	2-8
2.4 Results of Exposure Time Variations Exercise	2-13
2.5 Evaluation of Codes	2-16
3 DEVELOPMENT OF SOURCE TERMS FOR CHEMICAL EFFECTS SIMULATIONS	3-1
4 BLIND PREDICTIONS OF INTEGRATED CHEMICAL EFFECTS TEST RESULTS .	4-1
4.1 Blind Predictions for ICET #1	4-1
4.2 Blind Predictions for ICET #2	4-6
4.3 Blind Predictions for ICET #3	4-9
4.4 Blind Predictions for ICET #4	4-13
4.5 Blind Predictions for ICET #5	4-19
4.6 Assessment of Blind Prediction Results	4-19
5 INFORMED PREDICTIONS OF INTEGRATED CHEMICAL EFFECTS TEST RESULTS	5-1
5.1 Informed Predictions for ICET #1	5-2
5.2 Informed Predictions for ICET #2	5-7
5.3 Informed Predictions for ICET #3	5-10
5.4 Informed Predictions for ICET #4	5-18
5.5 Informed Predictions for ICET #5	5-23
5.6 Assessment of Informed Predictions Results	5-29
6 ADDITIONAL SIMULATIONS OF INTEGRATED CHEMICAL EFFECTS TEST CONDITIONS	6-1
6.1 PHREEQC Database Modifications	6-1
6.2 Source-Term Water Compositions	6-3

CONTENTS (continued)

Section	Page
6.3	Results of Blind and Informed Predictions 6-3
6.3.1	PHREEQC Simulations for ICET #1 6-9
6.3.2	PHREEQC Simulations for ICET #2 6-12
6.3.3	PHREEQC Simulations for ICET #3 6-15
6.3.4	PHREEQC Simulations for ICET #4 6-17
6.3.5	PHREEQC Simulations for ICET #5 6-20
6.3.6	Assessment of Blind and Informed PHREEQC Simulations 6-24
6.4	Example Simulation of Evolving Chemical Conditions in ICET #4 6-24
6.4.1	Source-Term Composition for the Evolved Prediction 6-25
6.4.2	Results 6-26
7	CONCLUSIONS 7-1
7.1	Post-LOCA Interactions Involving Metals 7-1
7.2	Post-LOCA Interactions Involving Insulation Materials 7-2
7.2.1	Nukon Low-Density Glass Fiber Insulation 7-2
7.2.2	Calcium-Silicate Insulation 7-2
7.3	Post-LOCA Interactions Involving Concrete 7-4
7.4	Limitations of the Modeling Predictions 7-4
7.4.1	Estimating Source-Term Concentrations for Modeling 7-4
7.4.2	Limitations of Thermodynamic Data 7-5
7.5	Assessment of Modeling Approach for Plant-Specific Conditions 7-6
8	REFERENCES 8-1
APPENDIXES	
A	DISSOLUTION RATE MEASUREMENTS FOR INSULATION MATERIALS A-1
B	SIMULATED OUTPUT FILE FOR INTEGRATED CHEMICAL EFFECTS TEST (ICET) #1 AT 60 °C [140 °F] AT 148 HOURS, USING EQ3/6 VERSION 7.2B B-1
C	SIMULATION CALCULATION SUMMARY FOR INTEGRATED CHEMICAL EFFECTS TEST (ICET) #1 AT 60 °C [140 °F] AT 148 HOURS, USING OLI STREAMANALYZER VERSION 2.0 C-1
D	SIMULATED OUTPUT FILE FOR ICET #1 USING PHREEQC D-1

FIGURES

Section		Page
2-1	Source-Term (Input) and Final (Modeled) Aqueous Concentrations as Predicted in Code Comparison for Simulated Containment Water for 30 Minutes of Exposure . . .	2-9
2-2	Initial (Source-Term) and Final (Modeled) Aqueous Concentrations as Predicted in Code Comparison for Simulated Containment Water at 60 °C [140 °F] at Exposure	2-14
3-1	ICET Test Chamber and Loop Components	3-1
4-1	Comparison of Blind Predictions With Results of Experiment ICET #1	4-5
4-2	Comparison of Blind Predictions With Results of Experiment ICET #2	4-10
4-3	Comparison of Blind Predictions With Results of Experiment ICET #3	4-14
4-4	Comparison of Blind Predictions With Results of Experiment ICET #4	4-18
4-5	Comparison of Blind Predictions With Results of Experiment ICET #5	4-22
4-6	Predicted Total Masses of Precipitated Solids in ICETs #1– #5	4-23
5-1	Aluminum Concentration From Informed Predictions (OLI) Compared With Data From ICET #1 ... Tests in the Presence of Aluminum	5-5
5-2	Calcium Concentration From Informed Predictions (OLI) Compared With Data From ICET #1 ... Tests in Alkaline Borated	5-5
5-3	Silicon Concentration From Informed Predictions (OLI) Compared With Data From ICET #1 ... Tests in Alkaline Borated	5-6
5-4	pH Values From Informed Predictions (OLI) Compared With the pH Measured in ICET #1	5-7
5-5	Silicon Concentration From Informed Predictions (OLI) Compared With Data From ICET #2 and CNWRA Glass Fiber Dissolution	5-11
5-6	Magnesium Concentration From Informed Predictions (OLI) Compared With Data From ICET #2 and CNWRA Glass Fiber Dissolution	5-11
5-7	Calcium Concentration From Informed Predictions (OLI) Compared With Data From ICET #2 and CNWRA Calcium Silicate Glass Fiber Dissolution	5-12
5-8	Silicon Concentration From Informed Predictions (OLI) Compared With Data From ICET #3 and CNWRA Dissolution Tests	5-15
5-9	Calcium Concentration From Informed Predictions (OLI) Compared With Data From ICET #3 and CNWRA Calcium Silicate Dissolution Tests	5-16
5-10	Phosphorous Concentration From Informed Predictions (OLI) Compared With Data From ICET #3 and CNWRA Calcium Silicate Dissolution Tests	5-16
5-11	Magnesium Concentration From Informed Predictions (OLI) Compared With Data From ICET #3 and CNWRA Calcium Silicate Dissolution Tests	5-17
5-12	pH Values From Informed Predictions (OLI) Compared With the Measured pH in ICET #3	5-18
5-13	Silicon Concentration From Informed Predictions (OLI) Compared With Data From ICET #4 and CNWRA Calcium Silicate Dissolution Tests in Alkaline	5-21
5-14	Calcium Concentration From Informed Predictions (OLI) Compared With Data From ICET #4 and CNWRA Calcium Silicate Dissolution Tests	5-22
5-15	Aluminum Concentration From Informed Predictions (OLI) Compared With Data From ICET #4 and CNWRA Calcium Silicate Dissolution Tests	5-22

FIGURES (continued)

5-16	Silicon Concentration From Informed Predictions (OLI) Compared With Data From ICET #5 in Sodium Borate Containment Water	5-26
5-17	Calcium Concentration From Informed Predictions (OLI) Compared With Data From ICET #5 in the Sodium Borate Containment Water	5-27
5-18	Aluminum Concentration From Informed Predictions (OLI) Compared With Data From ICET #5 in Sodium Borate Containment Water	5-27
5-19	pH Values From the Informed Predictions (OLI) Simulation Compared With Measured pH in ICET #5 in Sodium Borate Containment Water at 60 °C [140 °F]	5-28
6-1	Predicted Precipitates in ICET #1 Simulations	6-10
6-2	Predicted and Observed Variations in ICET #1 Water Chemistry	6-11
6-3	Predicted Precipitates in ICET #2 Simulations	6-13
6-4	Predicted and Observed Variations in ICET #2 Water Chemistry	6-14
6-5	Predicted Changes in Saturation in ICET #2	6-16
6-6	Predicted Precipitates in ICET #3 Simulations	6-17
6-7	Predicted and Observed Variations in ICET #3 Water Chemistry	6-18
6-8	Predicted Precipitates in ICET #4 Simulations	6-19
6-9	Predicted and Observed Variations in ICET #4 Water Chemistry	6-21
6-10	Predicted Precipitates in ICET #5 Simulations	6-22
6-11	Predicted and Observed Variations in ICET #5 Water Chemistry	6-23
6-12	Modeled Evolution of Solution Chemistry in ICET #4, Contrasted With Source-Term Calculations and Informed Predictions at Specified Times	6-27
6-13	Change in Evolution of Calcium and Silicon Concentrations if Precipitation of Monohydrocalcite Is Suppressed and Equilibration With Tobermorite	6-29

TABLES

Section	Page
2-1 Availability and Accessibility of Chemical Modeling Programs Used in This Study . .	2-3
2-2 Source-Term Water Compositions for Code Comparison Exercise	2-6
2-3 Comparison of Predicted Precipitation for Alkaline Containment Waters at Three Different Temperatures After 0.5 Hours of Exposure	2-10
2-4 Comparison of Predicted Aqueous Speciation for Modeled Variations Based on Temperature After 0.5 Hours	2-11
2-5 Comparison of Predicted Precipitation for Alkaline Containment Waters at Various Times of Exposure at 60 °C [140 °F]	2-15
3-1 Key Variations in the ICET Experiments	3-2
3-2 ICET Containment Water Initial Additives	3-3
3-3 Estimated Source-Term Contributions From Corrosion of Metals	3-4
3-4 Estimated Source-Term Contributions From Leaching of Concrete	3-5
3-5 Representative Chemical Analysis of Nukon® Glass Fiber	3-6
3-6 Derivation of Source-Term Contributions From Dissolution of Nukon® Glass Fiber . .	3-6
3-7 Representative Chemical Analysis of Calcium Silicate Insulation Compared With Stoichiometric Composition of Crystalline Tobermorite	3-7
3-8 Source-Term Contributions From Dissolution of Calcium Silicate Insulation	3-8
3-9 Modeling Test Matrix for ICET Simulations	3-9
4-1 Blind Predictions for ICET #1	4-3
4-2 Blind Predictions for ICET #2	4-7
4-3 Blind Predictions for ICET #3	4-11
4-4 Blind Predictions for ICET #4	4-16
4-5 Blind Predictions for ICET #5	4-20
5-1 Source-Term Water Compositions in Borated Alkaline Containment Water at 60 °C [140 °F] for StreamAnalyzer Simulations of ICET #1 Experiment Conditions .	5-3
5-2 Predicted Amount (mol) of Solid Phases Formed at 60 °C [140 °F], ICET #1 Environment	5-4
5-3 Main Aqueous Species Predicted in the Alkaline Borated Containment Water at 60 °C [140 °F], ICET #1 Environment	5-4
5-4 Source-Term Water Compositions in Borated Trisodium Phosphate Containment Water at 60 °C [140 °F] for StreamAnalyzer Simulations of ICET #2	5-8
5-5 Predicted Amount (mol) of Solid Phases Formed in Trisodium Phosphate Borated Containment Water at 60 °C [140 °F], ICET #2 Environment	5-9
5-6 Main Aqueous Species Predicted in the Trisodium Phosphate Borated Containment Water at 60 °C [140 °F], ICET #2 Environment	5-10
5-7 Source-Term Water Compositions in Borated Trisodium Phosphate Containment Water at 60 °C [140 °F] for StreamAnalyzer Simulations of ICET #3	5-13
5-8 Predicted Amount (mol) of Solid Phases Formed in Trisodium Phosphate Borated Containment Water at 60 °C [140 °F], ICET #3 Environment	5-14
5-9 Main Aqueous Species Predicted in the Trisodium Phosphate Borated Containment Water at 60 °C [140 °F], ICET #3 Environment	5-15

TABLES (continued)

5-10	Source-Term Water Compositions in Borated Alkaline Containment Water at 60 °C [140 °F] for StreamAnalyzer Simulations of ICET #4 Experiment Conditions	5-19
5-11	Predicted Amount (mol) of Solid Phases Formed at 60 °C [140 °F], ICET #4 Environment	5-20
5-12	Main Aqueous Species Predicted in the Trisodium Phosphate Borated Containment Water at 60 °C [140 °F], ICET #4 Environment	5-20
5-13	Source-Term Water Compositions in Borated Slightly Alkaline Containment Water at 60 °C [140 °F] for StreamAnalyzer Simulations of ICET #5 Experiment	5-24
5-14	Predicted Amount (mol) of Solid Phases Formed at 60 °C [140 °F], ICET #5 Environment	5-25
5-15	Main Aqueous Species Predicted in the Slightly Alkaline Borated Containment Water at 60 °C [140 °F], ICET #5 Environment	5-26
6-1	Modified PHREEQC Database of Solid Phases for Integrated Chemical Effects (ICET) Simulations	6-2
6-2	Source-Term Water Compositions for Integrated Chemical Effects Test (ICET) #1 Simulations	6-4
6-3	Source-Term Water Compositions for Integrated Chemical Effects Test (ICET) #2 Simulations	6-5
6-4	Source-Term Water Compositions for Integrated Chemical Effects Test (ICET) #3 Simulations	6-6
6-5	Source-Term Water Compositions for Integrated Chemical Effects Test (ICET) #4 Simulations	6-7
6-6	Source-Term Water Compositions for Integrated Chemical Effects Test (ICET) #5 Simulations	6-8
6-7	Initial Source-Term Water Composition for Integrated Chemical Effects Test (ICET) #4 Example Evolved Prediction	6-25
6-8	Source-Term Release Rates for Integrated Chemical Effects Test (ICET) #4 Example Evolved Prediction	6-26
7-1	Comparison of Aqueous Concentrations for ICET #1 Environment With and Without Aluminum in Borated Alkaline Containment Water at 60 °C [140 °F]	7-3

EXECUTIVE SUMMARY

The possible consequences of a loss-of-coolant accident (LOCA) include dissolution and corrosion reactions between the post-LOCA containment environment and containment materials such as metal scaffolding and piping, insulation materials, and concrete in the containment building. These reactions could lead to supersaturation of secondary phases in the containment system water. Along with entrained debris components, the precipitated solids might have the potential to clog and impede the performance of the Emergency Core Cooling System pumps, Containment Spray System pumps, or other components of the sump strainer. As part of a joint U.S. Nuclear Regulatory Commission and industry sponsored program to evaluate potential problems associated with the clogging of water recirculation systems by formation of secondary precipitates, this report summarizes an evaluation of chemical modeling software that could be used to assess whether precipitation of secondary solids would be expected in specific post-LOCA environments. The study evaluated existing, available modeling software and tested the application of suitable modeling codes by simulating five experiments representative of post-LOCA conditions that were conducted in the Integrated Chemical Effects Test (ICET) project. The range of applicability limits of the software with respect to plant-specific containment system environments was assessed in terms of the conclusions of the modeling study.

As an initial step in this study, four chemical modeling software programs—EQ3/6 (Lawrence Livermore National Laboratory, 1995), PHREEQC (U.S. Geological Survey, 2003), The Geochemist's Workbench[®] REACT (RockWare, Inc., 2004), and OLI Systems StreamAnalyzer (OLI Systems, Inc., 2005)—were evaluated in terms of their ability to perform aqueous speciation and mass transfer calculations relevant to post-LOCA conditions. The code comparison exercise considered seven example simulations, each of which was representative of post-LOCA conditions in an alkaline, borated containment water at temperatures between 60 °C [140 °F] and 110 °C [230 °F]. The containment materials modeled in the code comparison exercise included galvanized steel (a source of dissolved zinc), carbon steel (a source of dissolved iron), aluminum (e.g., from scaffolding or other components), copper (e.g., from fans and instrument lines), glass fiber insulation material and concrete. The modeling software was used to identify the oversaturated secondary solids that would precipitate and to calculate the final solution composition. Despite some convergence problems for simulations at high initial concentrations, all of the codes performed the main tasks of the comparison exercise. The most important differences in results were traceable to different sets of solid phases in the thermodynamic database files accompanying each modeling code, rather than to different capabilities of the codes themselves.

The code comparison exercise did not test additional features of some of the codes, such as the ability to maintain equilibrium with atmospheric gases or to block the precipitation of certain solids that would not be expected to form for kinetic reasons under representative post-LOCA conditions. The additional capabilities were examined in more detail in other simulations using three of the codes, EQ3/6, OLI StreamAnalyzer, and PHREEQC. The additional simulations were benchmarked to the ICET experiments, corresponding to five representative post-LOCA environments in which alkaline or neutral borated containment waters interacted with metals, concrete, and insulation materials (glass fiber and calcium silicate) at 60 °C [140 °F] for times up to 720 hours. The input values for water compositions at specified times of exposure were estimated from initial containment water additives, from pre-determined corrosion rates for the metals of interest, and from a set of dedicated Center for Nuclear Waste Regulatory Analyses

experiments that provided release rate data for the dissolution of insulation materials and concrete.

The benchmarked simulations began with a set of blind predictions using EQ3/6, and the predicted results were compared to data from the corresponding ICET experiment. In some cases, observed final concentrations in the sampled water were higher than the initial source-term estimates, indicating that the input value source-term contribution for that element had been underestimated. In other cases, the identity and quantity of precipitate did not conform to observations from the ICET experiment, indicating kinetic restrictions on precipitation under the conditions modeled. The main contributors to the formation of precipitates in the simulations were predicted to be calcium silicate insulation, glass fiber insulation, and aluminum metal. The addition of trisodium phosphate as a pH buffer in the presence of calcium silicate insulation was predicted to lead to the scavenging of all dissolved phosphorous from the water and the formation of a significant quantity of calcium phosphate precipitate, results that were also observed experimentally in ICET #3. Other metals in the system, such as galvanized steel, copper, and carbon steel, contributed to the modeled formation of precipitates but only in minor quantities. Revised dissolution rates for glass fiber insulation in the presence of aluminum metal and for calcium silicate insulation materials were obtained from additional in-house dissolution experiments to improve the estimated source-term contributions of these materials. The conceptual model for the simulations was refined to suppress the precipitation of certain oversaturated phases for kinetic reasons.

Another set of simulations, which were called informed predictions, used the OLI StreamAnalyzer simulation software and its accompanying thermodynamic database file. The general modeling approach was similar to the approach used for the EQ3/6 blind predictions. Each ICET experiment was represented by a set of source-term water compositions at different times of exposure, estimated from the initial composition of the containment water and the experimentally determined corrosion rates of sample materials. Simulations were performed for assumed times of exposure of up to 720 hours, which corresponded to the duration of the ICET experiments. Each modeling simulation assumed that the source-term water composition at the time of interest had not been modified by prior precipitation of secondary phases, regardless of the time of exposure. Solid phases that were excluded from precipitation included all aluminum oxides, hydroxides, and oxyhydroxides and all silicate minerals except amorphous silicon dioxide. No carbonate minerals were allowed to form because the source-term water composition in the StreamAnalyzer simulations did not include equilibration with atmospheric carbon dioxide.

The results of the informed predictions corresponded to the ICET experiment results more closely than the blind predictions did, largely due to the revised element release rates for aluminum and for insulation materials, for exposure times of up to 148 hours. Beyond this timeframe, final concentrations of calcium, silicon, and aluminum were typically overpredicted, indicating possible passivation of the metal surface or formation of an inhibitive surface coating on the insulation material during the experiment. These changes in release rate were not included in the source-term water concentrations for the informed predictions.

The differences in results for the blind predictions and the informed predictions also were attributed to the thermodynamic database files that accompanied the modeling software, which contained different lists of potential precipitates. To facilitate comparisons of results, a complete set of blind and informed predictions was performed using a single modeling program,

PHREEQC, which provided modeling advantages in terms of its flexibility in suppressing the precipitation of specified solids and the ease with which its thermodynamic database could be modified. The new simulations addressed additional conditions of interest, such as the potential precipitation of carbonate minerals and aluminum oxyhydroxide. Although the informed predictions were hindered by incomplete characterization of the precipitates that formed in the ICET experiments, the list of potential phases in the database file was edited to include only a small set of solids, such as carbonates, phosphates, and metal oxides, that would realistically be expected to form under the relatively low-temperature, short-term conditions associated with the ICET experiments. To assess the effect of changes in source-term water compositions, one set of blind predictions was performed with the same input values as used in the original EQ3/6 blind predictions, and a second set of blind predictions was performed using the modified source-term water compositions that had been used for the previous set of informed predictions. In these comparisons, the same precipitates were predicted to form, but the amounts differed according to differences in the source term. The only exception was for the ICET #4 simulation, which included the dissolution of calcium silicate under alkaline conditions. The original blind prediction conservatively overestimated the dissolution rate of the insulation material, which caused amorphous silicon dioxide to be oversaturated. In the modified source term, based on a more realistic dissolution behavior, no amorphous silicon dioxide was predicted to precipitate.

The PHREEQC informed predictions also used the modified source-term concentrations as input values. The precipitation of certain oversaturated phases was suppressed to produce results that conformed more closely to the ICET experiments.

For the informed PHREEQC simulations in which the solution chemistry was affected by precipitation, good agreement was obtained between predicted and observed results for calcium concentration under ICET #1 conditions (alkaline water buffered to pH values near 10 by sodium hydroxide) due to the precipitation of monohydrocalcite, for silicon concentration under ICET #2 and #3 conditions (solution buffered to near-neutral pH by trisodium phosphate) due to the precipitation of amorphous silicon dioxide, and for phosphorous concentration in ICET #3 due to the precipitation of calcium phosphate. The simulated equilibrium with amorphous silicon dioxide under ICET #2 conditions, in which the only insulation material present was glass fiber insulation, suggested that the glass may have reached its solubility limit during the experiment.

The development of source-term compositions for the chemical effects simulations was based on the simplifying assumption that the water chemistry represented interactions with the sample materials over a specified interval of time without any prior precipitation. For long exposure times, in some cases this assumption resulted in unrealistically large source terms and strongly oversaturated phases. To compensate for this simplification, a more detailed modeling approach was also evaluated for one of the informed predictions, using ICET #4 conditions as an example (alkaline water buffered to pH values near 10 by sodium hydroxide, in the presence of calcium silicate and glass fiber insulation materials), to provide a more realistic simulation that addressed precipitation as well as dissolution or corrosion reactions at each timestep to indicate how the composition of the water would evolve gradually over a 30-day period in response to interactions with the solids in the system. Although the conceptual models in the evolved prediction and the informed predictions were based on several different assumptions, the results in terms of total source-term contributions and the solids identified as potential precipitates were similar. More detail was provided by the evolved prediction in terms of the timing of precipitation. For example, the evolved prediction indicated that the silicon

concentration initially would increase steadily, due mainly to dissolution of calcium silicate, but after about 16 days the concentration would increase to the point that the solution was oversaturated with respect to amorphous silicon dioxide. Subsequent precipitation of this phase, in small amounts at each timestep, would limit the silicon concentration to a fixed value. Similarly, if the precipitation of calcium carbonate was suppressed for kinetic reasons, the evolved prediction indicated that the calcium and silicon concentration would increase steadily until the solution equilibrated with tobermorite, a calcium silicate mineral that was the main constituent of the calcium silicate insulation material. The modeled final concentrations of calcium and silicon in this case were higher than the concentrations observed in the experiment, but the trend of stabilized concentrations for both elements conformed to the predicted results.

On the basis of the various simulations and comparison with experimental results, the main finding of this study was that the usefulness of chemical modeling depended on two important factors—a realistic estimate of source-term contributions to the water composition, and an appropriate set of thermodynamic data for the relevant solids and aqueous species at the conditions of interest. In this respect, important practical advantages are provided by modeling programs such as PHREEQC that easily allow the user either to suppress the precipitation of solids unlikely to form for kinetic reasons or to edit the thermodynamic database to limit the solids to a set of reasonably expected precipitates. The informed predictions, which were calibrated on the basis of observations from the experiments being simulated, corresponded reasonably well to the experiment data over the first hours or days of exposure, an important period of interest in terms of post-LOCA chemical effects on sump screen blockage. Predictions at longer times of exposure tended to be more disparate because the estimated source-term contributions to water chemistry did not incorporate the observed changes in the corrosion or dissolution rates of some of the sample materials. In several of the ICET experiments, the dissolution rates of sample materials were affected by the co-dissolution of other materials in the system. To represent the source-term contributions accurately for different plant-specific containment systems, the effect of multiple materials on release rates needs to be characterized separately.

The study concludes that chemical modeling software is a broadly useful tool in assessing the potential effects of post-LOCA interaction on sump screen blockage, but the predictive capability of this approach was hindered by insufficient thermodynamic data in the code database for relevant phases and aqueous species and by limitations in the kinetic data for the dissolution of reactive materials in the presence of co-dissolving materials. These uncertainties are not insurmountable but do require more detailed characterization of the components being modeled.

References:

OLI Systems, Inc. "StreamAnalyzer." Version 2.0. Morris Plains, New Jersey: OLI Systems, Inc. 2005.

Lawrence Livermore National Laboratory. "EQ3/6." Version 7.2b. Livermore, California: Lawrence Livermore National Laboratory. 1995.

RockWare, Inc. "The Geochemist's Workbench®." Version 5.0. Golden, Colorado: RockWare, Inc. 2004.

U.S. Geological Survey. "PHREEQC." Version 2.8. Reston, Virginia: U.S. Geological Survey. 2003.

ACKNOWLEDGMENTS

This report was prepared to document work performed by the Center for Nuclear Waste Regulatory Analyses (CNWRA) for the U.S. Nuclear Regulatory Commission (NRC) under Purchase Order Nos. NRC-DR-04-05-067 and NRC-DR-04-06-046. The activities reported here were performed on behalf of the NRC Office of Nuclear Regulatory Research, Division of Fuel, Engineering and Radiological Research (DFERR). This report is an independent product of CNWRA and does not necessarily reflect the views or regulatory position of NRC.

The authors express their gratitude to J. Apps for his thoughtful review and discussions of this work. The authors thank J. Myers for technical review and D. Turner for programmatic review of this report. The authors also thank L. Selvey and N. Naukam for document preparation and E. Pearcy for editorial review.

QUALITY OF DATA, ANALYSES, AND CODE DEVELOPMENT

DATA: Sources of data are referenced in the report. The respective sources of non-CNWRA data should be consulted for determining levels of quality assurance. CNWRA-generated data that are presented in Appendix A of this report meet quality assurance requirements described in the Geosciences and Engineering Division Quality Assurance Manual. Experimental data and details of modeling simulations have been recorded in scientific notebooks numbered 723E, 679E, 722, and 738.

ANALYSES AND CODES: Four commercially or publicly available versions of chemical modeling computer codes were used by CNWRA to perform aqueous speciation and mass transfer calculations in this report. All four software packages are controlled under the Technical Operating Procedure (TOP)-18, Development and Control of Scientific and Engineering Software (Revision 10, Change 0). The modeling codes used are StreamAnalyzer Version 2.0 (OLI Systems, Inc., 2005), EQ3/6 Version 7.2b (Lawrence Livermore National Laboratory, 1995), Geochemist's Workbench Version 5.0 (RockWare, Inc., 2004), and PHREEQC Version 2.8 (U.S. Geological Survey, 2003).

References:

OLI Systems, Inc. "StreamAnalyzer." Version 2.0. Morris Plains, New Jersey: OLI Systems, Inc. 2005.

Lawrence Livermore National Laboratory. "EQ3/6." Version 7.2b. Livermore, California: Lawrence Livermore National Laboratory. 1995.

RockWare, Inc. "The Geochemist's Workbench®." Version 5.0. Golden, Colorado: RockWare, Inc. 2004.

U.S. Geological Survey. "PHREEQC." Version 2.8. Reston, Virginia: U.S. Geological Survey. 2003.

1 INTRODUCTION

A loss-of-coolant accident (LOCA) causes rapid changes in the temperature and pressure of the containment environment. The system is further modified by contact between the reactor coolant water and the submerged parts of the containment system, which could include metal components such as scaffolding and piping, in addition to debris materials (e.g., insulation), and concrete. The consequences of a LOCA potentially include the suspension of debris components from these materials or the formation of secondary precipitates. Both processes have the potential to clog and impede the performance of pumps and other downstream components that recirculate water in the emergency core cooling system and containment spray system.

Strainer clogging events reported at some U.S. boiling water reactor plants in the early to mid-1990s led the U.S. Nuclear Regulatory Commission (NRC) to require licensees of boiling water reactors to install suction strainers with larger surface areas (NRC, 1996). Subsequently, NRC published Generic Safety Issue (GSI)–191, Assessment of Debris Accumulation on PWR Sump Performance, to determine whether sump pump failure was a plausible generic concern for pressurized water reactors (PWRs). The GSI–191 technical assessments have considered the sources, generation, and transport of debris in a containment system and have characterized the relationship between debris clogging and sump screen head loss. In addition, GSI–191 studies have investigated post-LOCA chemical interactions between coolant water and exposed reactor system components. Chemical interactions may impede pump performance by producing additional debris through corrosion of existing materials or by precipitation of secondary solid phases. For example, small-scale chemical effects experiments have indicated that the formation of amorphous precipitates of aluminum, iron, and zinc could result in head loss across a sump screen that would be much higher than the loss from clogging by debris components such as fiberglass insulation alone (Johns, et al., 2003).

Aqueous chemical modeling software is potentially useful in determining whether, or to what extent, the changes in water chemistry associated with post-LOCA conditions would contribute to sump screen blockage due to precipitation of secondary solid phases. The computer programs allow the rapid and relatively inexpensive identification of the effects of changes in important variables such as temperature, pressure, and reactive solids. For example, thermodynamic simulations by Jain, et al. (2005) used measured corrosion rates, estimated exposed surface area, and exposure time to conclude that the formation of secondary solid phases under several representative sets of post-LOCA interactions would be controlled mainly by reactions between containment water and a subset of the solid materials in the containment system, namely aluminum, concrete, and insulation materials. These insights led to other supporting experiments, which are reported in the present study, to improve estimates of dissolution rates for Nukon® low-density glass fiber and for calcium silicate, both of which are commonly used insulation materials in containment buildings.

The main objective of the present study was to evaluate the feasibility of utilizing commercially available thermodynamic simulation computer codes to predict the formation of chemical species in a typical post-LOCA PWR containment environment. Several commercially available thermodynamic simulation software programs were tested and compared in a modeling exercise, after which selected modeling programs were used to perform more detailed simulations benchmarked with experimental data from Integrated Chemical Effects Tests Program, a related set of GSI–191 experiments conducted at the University of New Mexico.

2 EVALUATION OF AQUEOUS CHEMICAL MODELING SOFTWARE

In the decades since the seminal research that presented mathematical equations for the speciation of ions in natural waters (Garrels and Thompson, 1962) and for mass transfer reactions between water and minerals (Helgeson, et al., 1969, 1970), numerous versions of thermodynamic simulation software programs have been developed to represent chemical equilibria in aqueous systems. The computer programs that are used to study natural systems typically are called geochemical modeling codes. The equilibrium modeling approach also has been adopted for industrial and environmental applications.

Zhu and Anderson (2002) provide descriptions of specific geochemical modeling computer programs and an overview of the main features of such programs in general. Most programs consist of two main parts: a computer code and a related file of thermodynamic data, called a database file, that is accessed by the code to solve the equilibrium calculations. The computer code is simply a set of commands, written in a programming language, that includes algorithms for solving mathematical equations for chemical equilibria and mass balance, bookkeeping details, and management of input and output files. The mathematical frameworks for most modeling codes are similar to each other. Although the codes differ in terms of the computational and accounting techniques employed, all attempt to solve the same set of algebraic equations, typically by multiple iterations. A user may select different options in a computer modeling program, but the commands themselves cannot be amended without substantial effort. In contrast, the accompanying database file is typically designed to be easily edited by the user, or it can be substituted with a different file. The database file contains essential thermodynamic information such as standard-state equilibrium constants or free-energy values for aqueous speciation reactions involving the set of chemical elements that are listed in the database. Depending on the capabilities and requirements of the particular modeling program and input file, a database file will also have equilibrium constants for reactions involving solid phases, values for enthalpies of reaction or coefficients for calculations of speciation or mass transfer at non-standard states, or data for kinetic reactions or surface properties.

At least one appropriately formatted database file commonly is supplied with each modeling program. This enables the user to run the code and perform many types of calculations immediately. The developers of geochemical modeling programs make no assurance, however, about the completeness, quality, or accuracy of such a database. Users are encouraged to create their own database files, but the compilation and maintenance of thermodynamic data for computer modeling is a formidable task (Nordstrom and Munoz, 1986). As Zhu and Anderson (2002) noted, judging the quality, accuracy, and internal consistency of thermodynamic data is a job for specialists, and even they often do not agree among themselves. The amount of time and effort required to prepare such a database for complex chemical systems (those with many or unusual elements) is likely to be greater than the resources allotted for the modeling project itself. Consequently, certain preexisting large and accessible database files tend to be widely used in modeling studies, with little or no modification by the user. This approach is sufficient in many cases (Zhu and Anderson, 2002), given that widely distributed thermodynamic database files generally contain similar information for common minerals and aqueous species, even when they have been compiled from different sources (Nordstrom, et al., 1979). Modelers will generally obtain comparable results for studies involving these common phases and species, regardless of which database they use. Whether or not specific values are accurate, or whether the set of thermodynamic values is internally consistent, is a separate, broader issue that must

be weighed against the many other uncertainties associated with the representation of any complex system by an abstract model.

2.1 Selection of Codes for a Comparison Exercise

Many different versions of aqueous chemical modeling programs are publicly available. There is no single software that is best for all modeling tasks. Rather, the selection depends on the problem being studied and the capabilities of the particular program to represent the relevant conditions and processes for the system of interest. Another factor is the availability of an appropriate database file or one that can be readily adapted with thermodynamic data relevant to the problem being studied.

In terms of representing conditions in a post-loss-of-coolant accident (LOCA) containment water that could affect sump pump strainer performance, chemical modeling software needs to be able to

- Perform aqueous speciation and saturation calculations
- Perform mass transfer reactions (precipitation of solids)
- Perform calculations for standard and elevated temperatures
- Model aqueous processes at ionic strengths of up to 0.5
- Maintain fixed conditions (e.g., pH, redox, gas fugacities), if required

In addition, the database file needs to contain a sufficient set of thermodynamic data for the elements, aqueous species, and solids of interest, so that the problem modeled is representative of the system chemistry. In this particular study, one such requirement was an adequate set of thermodynamic data for boron. High concentrations of boron are added to containment water because the B-10 isotope provides a large capture cross section for thermal neutrons during a LOCA. Boron is not abundant in most natural waters, so it is not routinely included in some of the standard database files that accompany geochemical modeling programs. The database file also needs to contain appropriate thermodynamic values to allow the code to simulate reactions over a relevant temperature range of approximately 25 to 110 °C [77 to 230 °F] and for ionic strengths up to values of approximately 0.5.

On the basis of such requirements, versions of four chemical modeling programs validated by the Center for Nuclear Waste Regulatory Analyses were compared to assess their suitability for studies of post-LOCA chemical effects (Table 2-1). The accompanying database files contained thermodynamic information that was appropriate for the problems studied, including data for the most common aqueous borate species and the most common low-temperature boron-bearing mineral phases.

(1) EQ3/EQ6 Version 7.2b (Lawrence Livermore National Laboratory, 1995)

This computer program has two separately named parts. EQ3 is a stand-alone code that performs equilibrium speciation and mineral saturation calculations. It is run to prepare input data for EQ6, which is a larger and more complex reaction-path code. EQ6 allows the user to simulate open-system, closed-system, or titration conditions; mixing of fluids; heating or cooling of solutions; dissolution or precipitation of minerals; and evolution or adsorption of gases. It has several kinetic options, allows the use of ion

Table 2-1. Availability and Accessibility of Chemical Modeling Programs Used in This Study

	EQ3/6	PHREEQC	Geochemist's Workbench (REACT)	OLI (StreamAnalyzer)
Supplier	Lawrence Livermore National Laboratory	U.S. Geological Survey	Rockware, Inc.	OLI Systems, Inc.
Availability	Purchase (~\$1K)	Free	Purchase (~\$3K)	Lease (3-year term) (~\$17K)
Accessibility	<ul style="list-style-type: none"> • Large user manual but limited formal customer support • Input files, though user-friendly, are very sensitive to changes in formatting • Not interactive or graphical 	<ul style="list-style-type: none"> • Detailed (but not comprehensive) user manual with multiple examples • Online help, including list of frequently asked questions • Interactive input version available (PHREEQCI) 	<ul style="list-style-type: none"> • Includes set of three user manuals • Interactive input and graphing features • Online frequently asked questions • Online support group 	<ul style="list-style-type: none"> • Marketed for users who have limited chemistry experience • Marketed for industrial applications
Accompanying thermodynamic database files	data0.alt.R2 data0.chv.R2 data0.com.R2* data0.hmw.R2 data0.nea.R2 data0.pit.R2 data0.sup.R2	phreeqc.dat wateq4f.dat winteq.dat llnl.dat*	thermo.dat thermo.com.v8.r6+.dat* thermo_pitzer.data thermo_hmw.dat thermo_hdata.dat thermo_phrqpitz thermo_wateq4f.dat thermo_phreeqc.dat thermo_minteq.dat	Public.ddb*
Code version used	7.2b	2.8	5.0	2.0

*Used as a database in the code comparison exercise.

association or ion interaction models, and includes an H₂O mass balance constraint. EQ3/6 can be run at a range of temperatures.

Originally developed to model hydrothermal fluid/rock interactions (Wolery, 1978), EQ3/EQ6 is now administered by Lawrence Livermore National Laboratory (<http://www.llnl.gov>), from which it is available for a fee. It is the main geochemical modeling computer program used and supported by the U.S. Department of Energy to develop geochemical process-level model abstractions for the potential geologic repository for high-level waste at Yucca Mountain, Nevada. Various database files have been developed and distributed for EQ3/6 over the years, including a number that are for specialized applications (e.g., high ionic strength). The thermodynamic database file distributed with EQ3/6 that was used for the code comparison exercise is the data0.com.R2 file, the main thermodynamic file issued with the code for general use.

(2) REACT, Geochemist's Workbench7 Version 5.0 (RockWare, Inc., 2004)

Geochemist's Workbench7 is a set of interactive software tools for solving problems in aqueous geochemistry, including those encountered in environmental protection and remediation, the petroleum industry, and economic geology. It is commercially marketed and distributed by Rockware, Inc. (www.rockware.com). The full set of software tools, which includes the reaction-path modeling program REACT that was selected for this modeling code comparison exercise, enables the user to balance chemical reactions, calculate solution speciation and mineral saturation, model ion sorption and surface complexation processes, and perform mass transfer and reaction-path calculations over a range of temperatures. REACT also can account for kinetic rate laws, isotope fractionation, and microbial metabolism and growth. Geochemist's Workbench7 also has interactive graph-plotting tools that are not available in most other geochemical modeling computer programs.

The thermodynamic database file distributed with Geochemist's Workbench7 that was used for the code comparison exercise is the thermo.com.v8.r6+ database file. This file, one of several included with the Geochemist's Workbench7 package, is reformatted from the database file "thermo.com.V8.R6.full" that was developed at Lawrence Livermore National Laboratory as a combined dataset based on many sources of thermodynamic data (Wolery and Daveler, 1992). A commendable feature of this database, which includes aqueous species and solid phase data for many minor and trace elements is that the sources of thermodynamic data are individually documented and traceable.

(3) PHREEQC Version 2.8 (U.S. Geological Survey, 2003)

PHREEQC, a widely used geochemical modeling program, is fully supported and distributed free of charge by the U.S. Geological Survey. The acronym is derived from PH (pH), RE (redox), EQ (equilibrium), and C (written in C programming language). PHREEQC is capable of performing speciation and saturation calculations, mass transfer calculations (including sorption, ion exchange, and precipitation and dissolution reactions), inverse mass balance modeling, and some one-dimensional transport modeling. Although input files that provide reaction-path modeling can be constructed, PHREEQC differs from a number of other reaction-path codes in that the user must determine separately which phases are allowed to react in the simulation.

PHREEQC is currently distributed with four database files, one of which is a reformatted variant of the same Lawrence Livermore National Laboratory dataset that was used with REACT in the code comparison exercise. The PHREEQC version of this database file, llnl.dat, was also selected for use in the code comparison exercise.

(4) OLI StreamAnalyzer Version 2.0 (OLI Systems, Inc., 2005)

Unlike the other programs, OLI StreamAnalyzer Version 2.0 was developed for industrial engineering applications such as refinery processes rather than for geochemical modeling. With input data supplied from a process model, OLI StreamAnalyzer can be used to determine an aqueous phase equilibrium composition over a range of temperatures and elevated pressures. The thermodynamic framework used by the code predicts behavior of multi-component aqueous systems including aqueous liquid, vapor, organic liquid, and multiple solid phases for the general ranges of 0 to 30 molal, -50 to 300 °C [-58 to 572 °F], and 0 to 150 MPa [0 to 1,480 atm]. Calculations can be done at conditions of particular importance to corrosion such as aqueous phase dew point and bubble point. With regard to a post-LOCA chemical environment, changes in water phase chemistry can be evaluated for a wide range of conditions (e.g., Jain, et al., 2005).

The OLI StreamAnalyzer code uses a proprietary data file, the "OLI Public" database (Public.ddb), for its thermodynamic equilibrium modeling calculations. The database contains coefficients for thermodynamic, transport, and physical properties for 80 chemical elements and their associated aqueous inorganic species, in addition to data for more than 5,000 organic species.

2.2 Code Comparison Exercise

The code comparison exercise considered seven examples, each of which was representative of potential conditions in a post-LOCA chemical environment similar to ICET #1 (Table 2-2). The examples were divided into two sets of exercises, a temperature variation exercise and an exposure time variation exercise. The conceptual model for all of the examples assumed that during a post-LOCA sequence of events, a hot alkaline borated solution had contacted various metals, insulation materials, and concrete in the containment building. Dissolution or corrosion reactions between the water and these materials modified the initial (pre-LOCA) composition of the coolant water. In the modeling exercises, this modified (post-LOCA) water was used as the starting input (source term) composition. If the chemical modeling code determined that any secondary solid phases were oversaturated in the source-term water, they were allowed to precipitate until they were in equilibrium. The reported final composition of the water was calculated on the basis of the composition and amount of precipitated solids removed from solution.

The input values, or source-term water compositions, in the code comparison exercise were adapted from source-term compositions listed in Jain, et al. (2005). The temperature variation exercise consisted of three examples representing containment water that had reacted with debris components for the same amount of time (30 minutes), but at different temperatures {110, 90, or 60 °C [230, 194, or 140 °F]}. The remaining four examples, which comprised the exposure time variation exercise, represented containment water that had reacted with debris components at the same temperature {60 °C [140 °F]} for different times (4, 72, 148, and

Table 2-2. Source-Term Water Compositions for Code Comparison Exercise*

Example No.	T110-H30M	T90-H30M	T60-H30M	T60-H4	T60-H72	T60-H148	T60-H360
Temperature (°C)†	110	90	60	60	60	60	60
Exposure Time (hours)	0.5	0.5	0.5	4	72	148	360
Concentration (mol/L)							
Al	1.19×10^{-4}	7.10×10^{-5}	2.42×10^{-5}	1.66×10^{-4}	2.93×10^{-3}	6.01×10^{-3}	1.11×10^{-2}
B	2.59×10^{-1}	2.59×10^{-1}	2.59×10^{-1}	2.59×10^{-1}	2.62×10^{-1}	2.65×10^{-1}	2.66×10^{-1}
Ca	2.60×10^{-4}	1.55×10^{-4}	6.69×10^{-5}	2.32×10^{-4}	3.44×10^{-3}	7.03×10^{-3}	8.80×10^{-3}
Cu	3.82×10^{-6}	2.00×10^{-7}	1.84×10^{-7}	1.48×10^{-6}	2.66×10^{-5}	5.46×10^{-5}	1.33×10^{-4}
Fe as Fe ³⁺	1.25×10^{-7}	4.49×10^{-8}	2.06×10^{-8}	1.65×10^{-7}	2.96×10^{-6}	6.09×10^{-6}	1.48×10^{-5}
Mg	1.27×10^{-4}	6.48×10^{-5}	1.36×10^{-5}	1.09×10^{-4}	1.96×10^{-3}	4.02×10^{-3}	4.94×10^{-3}
Na	2.31×10^{-1}	2.30×10^{-1}	2.30×10^{-1}	2.31×10^{-1}	2.43×10^{-1}	2.56×10^{-1}	2.62×10^{-1}
SiO _{2(aq)}	1.78×10^{-3}	9.72×10^{-4}	2.99×10^{-4}	1.55×10^{-3}	2.58×10^{-2}	5.29×10^{-2}	6.51×10^{-2}
Zn	2.34×10^{-6}	4.06×10^{-7}	3.58×10^{-7}	2.86×10^{-6}	5.15×10^{-5}	1.06×10^{-4}	2.57×10^{-4}
pH	10.0	10.0	10.0	10.0	10.0	10.0	10.0
Eh (V)	-0.600	-0.600	-0.600	-0.600	-0.600	-0.600	-0.600

*From Jain, V., X. He, and Y.-M. Pan. NUREG/CR-6873, "Corrosion Rate Measurements and Chemical Speciation of Corrosion Products Using Thermodynamic Modeling of Debris Components to Support GSI-191." Washington, DC: NRC, 2005.

†Temperature conversion: 110 °C [230 °F], 90 °C [194 °F], 60 °C [140 °F]

360 hours). Containment components that influenced the source-term water composition included galvanized steel (source of dissolved zinc), carbon steel (source of dissolved iron), aluminum metal scaffolding (source of dissolved aluminum), fan coolers and instrument lines (source of dissolved copper), concrete (source of calcium, silica, and aluminum), and Nukon[®] glass fiber insulation (source of silica and trace amounts of other elements). The source-term concentrations were calculated from published or estimated corrosion rates for the various solids, as listed in Jain, et al. (2005). In addition, it was assumed that the borated containment water in each example contained 0.259 mol/L [0.068 mol/gal] of B(OH)₃ and that the initial pH of the water had been adjusted to 10.0 at the temperature of interest by the addition of sodium hydroxide.

The computer program OLI StreamAnalyzer Version 1.2 calculated that the starting solution in each case had a strong reducing capacity, expressed as $V_{\text{SHE}} = -0.600$ V. For consistency, the same redox condition was specified as an initial condition for the other three modeling programs. Other relevant assumptions and simplifications to standardize the modeling comparison exercise were as follows:

- Each example was modeled separately from the other examples on a stand-alone basis.
- The starting compositions were not modified by previous precipitation of any solids.
- Reactions occurred at atmospheric pressure (any elevated pressure effects were ignored).
- The system was in thermodynamic equilibrium (any kinetic effects were ignored).
- Any oversaturated solid was allowed to precipitate.
- The initial pH of the containment water was input as a specified value (10.0), but it was adjusted slightly by the computer program at the start of the calculations to provide charge balance.
- The pH was allowed to vary with reaction.
- The effects of dissolved gases such as O₂ and CO₂ were not included (equilibration with atmospheric oxygen and carbon dioxide was not considered).

Another important assumption in the code comparison exercise was that no kinetic restrictions were placed on the precipitation of oversaturated phases. If the modeling code predicted that a relevant solid phase listed in the database file would be oversaturated in the aqueous solution, the phase was allowed to equilibrate with the solution by precipitation. In reality, the precipitation of many crystalline solids is hindered kinetically, particularly at the temperatures and timeframes of interest in the code comparison exercise. Many of the solids that are listed in the thermodynamic databases are complex igneous or metamorphic minerals that are kinetically hindered from forming over short timeframes and under the relatively low-temperature conditions that are found at or near the Earth's surface, although many are subject to dissolution in such environments. They are included in aqueous chemical modeling programs mainly to represent interactions between water (e.g., groundwater) and rocks that contain these minerals.

Most modeling codes, including those considered here, provide an option by which the user can suppress the precipitation of oversaturated phases that are not expected to form under the conditions of interest. In the code comparison exercise, this option was not exercised so that a more direct comparison could be made of differences between the thermodynamic database files associated with the different codes.

2.3 Results of Temperature Variation Exercise

Results of the code comparison exercise for the three examples at different temperatures are summarized in Figure 2-1. The graphs indicate how each modeling code predicted changes in containment water composition by the removal of oversaturated solid phases. Final aqueous concentrations less than 10^{-10} mol/L [2.6×10^{-11} mol/gal] are indicated schematically as small bars below the axis on each graph.

All of the codes predicted large decreases in the dissolved concentration of magnesium, copper, and iron. Variations in the predicted concentrations for aluminum and zinc result from the prediction of different precipitated solids by the modeling codes, based on differences in the solids that are included in the various databases. For example, aluminum concentration for the EQ3/6, PHREEQC, and REACT simulations was limited by the formation of several aluminosilicate clay minerals (Table 2-3), but those phases are not present in the OLI database. In the OLI simulation, the concentration-limiting aluminum-bearing solid was the sodium feldspar mineral albite, $\text{NaAlSi}_3\text{O}_8$.

The most abundant solid phases predicted to precipitate in these examples were silicate minerals (Table 2-3). OLI StreamAnalyzer identified the most abundant precipitates to be albite, which is a sodium-rich aluminosilicate, and the amphibole tremolite, a calcium-magnesium silicate. Note that the abundant precipitation of albite predicted by OLI StreamAnalyzer produces a final solution composition that is much more depleted in dissolved aluminum than that predicted by the other three modeling codes (Figure 2-1). The other three codes predicted that the most abundant solid to form would be either the pyroxene diopside, which is a calcium-magnesium silicate, or the zeolite mesolite, a sodium-calcium aluminosilicate. However, for kinetic reasons none of these structurally complex silicate minerals are likely to form from an aqueous, low-temperature solution over the timeframe of interest.

Due to the strong reducing capacity that was assumed in each example, all of the modeling codes predicted that the precipitation of metallic copper in each case would effectively remove all copper ions from the final solution. All of the codes predicted that the garnet andradite, a calcium-iron silicate, would greatly limit the concentration of dissolved iron in the containment waters at 110 and 90 °C [230 and 194 °F] (Table 2-3). Similarly, three of the codes predicted that precipitation of a zinc silicate, Zn_2SiO_4 , would limit the concentration of dissolved zinc. EQ3/6 did not have Zn_2SiO_4 in its database and instead predicted that zinc concentration would be limited by the precipitation of zincite, a zinc oxide.

Table 2-4 compares the calculated aqueous speciation results for each of the modeling codes. The speciation results predicted by OLI StreamAnalyzer differ considerably from those predicted by the three geochemical modeling codes, particularly with respect to minor species. This is largely due to differences in the database files accessed by the codes. Many of the aqueous species indicated in Table 2-4 are in the OLI StreamAnalyzer database but not in the databases used by the other three codes.

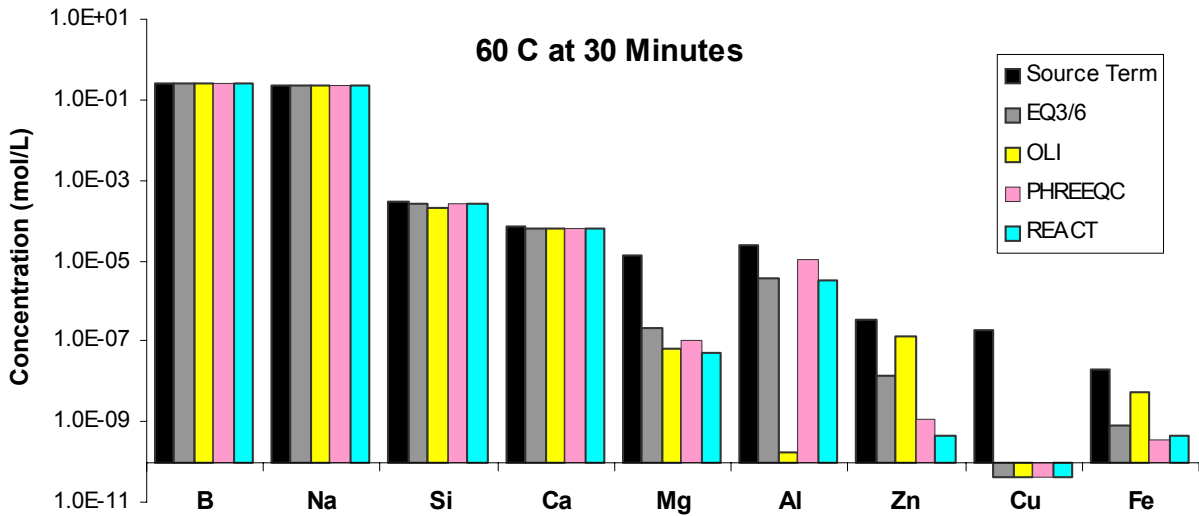
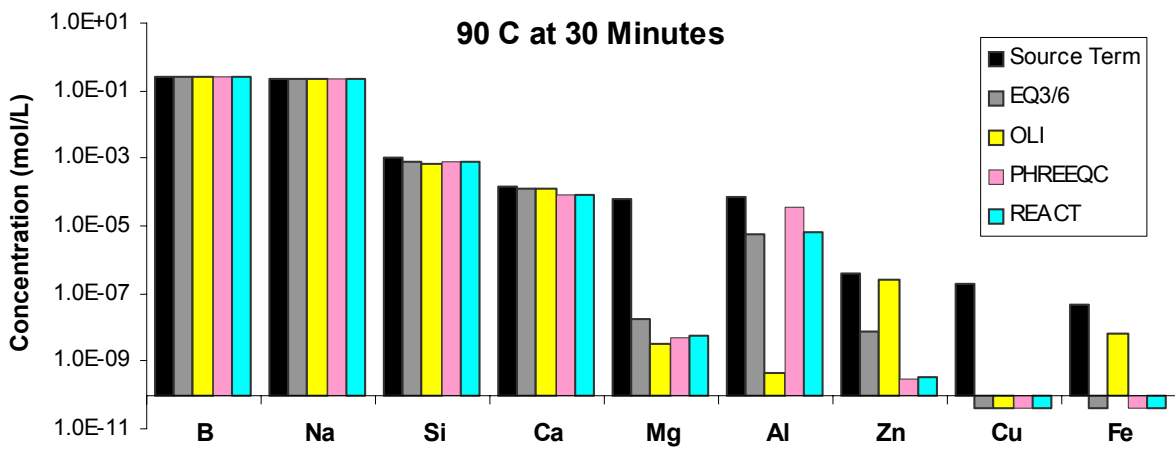
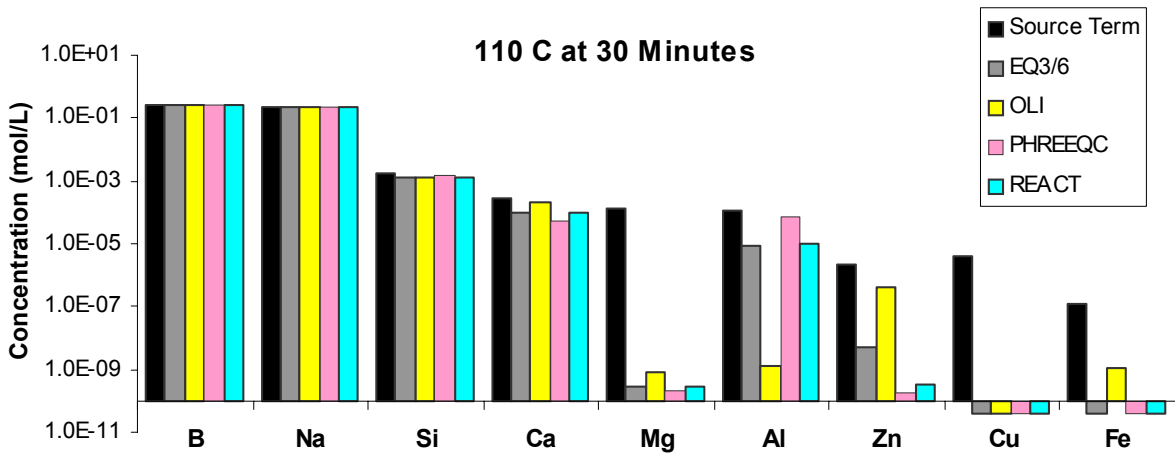


Figure 2-1. Source-Term (Input) and Final (Modeled) Aqueous Concentrations as Predicted in Code Comparison for Simulated Containment Water for 30 Minutes of Exposure at Temperatures of 110 °C [230 °F], 90 °C [194 °F], and 60 °C [140 °F]

Table 2-3. Comparison of Predicted Precipitation for Alkaline Containment Waters at Three Different Temperatures After 0.5 Hours of Exposure												
Precipitates (mol/L)*	Temperature = 110 °C†			Temperature = 90 °C†			Temperature = 60 °C†					
	EQ3/6	OLI	PHREEQC	REACT	EQ3/6	OLI	PHREEQC	REACT	EQ3/6	OLI	PHREEQC	REACT
Albite	—	1.2 × 10 ⁻⁴	—	—	—	7.1 × 10 ⁻⁵	—	—	—	2.4 × 10 ⁻⁵	—	—
Andradite	6.3 × 10 ⁻⁸	6.2 × 10 ⁻⁸	6.3 × 10 ⁻⁸	6.3 × 10 ⁻⁸	2.2 × 10 ⁻⁸	1.9 × 10 ⁻⁸	2.3 × 10 ⁻⁸	2.2 × 10 ⁻⁸	—	—	—	—
Copper (metal)	3.8 × 10 ⁻⁶	3.8 × 10 ⁻⁶	3.9 × 10 ⁻⁶	3.8 × 10 ⁻⁶	2.0 × 10 ⁻⁷	2.0 × 10 ⁻⁶	2.0 × 10 ⁻⁷	2.0 × 10 ⁻⁷	1.8 × 10 ⁻⁷	1.8 × 10 ⁻⁷	1.9 × 10 ⁻⁷	1.8 × 10 ⁻⁷
Daphnite-14A	—	—	—	—	—	—	—	—	4.0 × 10 ⁻⁹	—	4.1 × 10 ⁻⁹	—
Diopside	1.3 × 10 ⁻⁴	—	1.3 × 10 ⁻⁴	1.3 × 10 ⁻⁴	—	—	6.5 × 10 ⁻⁵	4.0 × 10 ⁻⁵	—	—	—	—
Greenalite	—	—	—	—	—	—	—	—	—	—	—	6.7 × 10 ⁻⁹
Grossular	—	—	2.6 × 10 ⁻⁵	—	—	—	—	—	—	—	—	—
Mesolite	5.5 × 10 ⁻⁵	—	—	5.5 × 10 ⁻⁵	2.9 × 10 ⁻⁵	—	1.8 × 10 ⁻⁵	3.2 × 10 ⁻⁵	9.5 × 10 ⁻⁶	—	6.5 × 10 ⁻⁶	9.8 × 10 ⁻⁶
Saponite-Na	—	—	—	—	2.2 × 10 ⁻⁵	—	—	—	4.5 × 10 ⁻⁶	—	4.5 × 10 ⁻⁶	4.5 × 10 ⁻⁶
Tremolite	—	2.5 × 10 ⁻⁵	—	—	—	1.3 × 10 ⁻⁵	—	5.0 × 10 ⁻⁶	—	2.7 × 10 ⁻⁶	—	—
Zincite	2.3 × 10 ⁻⁶	—	—	—	4.0 × 10 ⁻⁷	—	—	—	3.4 × 10 ⁻⁷	—	—	—
Zn ₂ SiO ₄	—	9.5 × 10 ⁻⁷	1.2 × 10 ⁻⁶	1.2 × 10 ⁻⁶	—	7.7 × 10 ⁻⁸	2.0 × 10 ⁻⁷	2.0 × 10 ⁻⁷	—	1.1 × 10 ⁻⁷	1.8 × 10 ⁻⁷	1.8 × 10 ⁻⁷
Final pH	9.5	9.6	10.0	9.5	9.5	9.7	10.0	9.6	9.7	10.0	10.0	9.7
Albite	Composition			Composition								
Albite	NaAlSi ₃ O ₈			Grossular	Ca ₃ Al ₂ Si ₃ O ₁₂							
Andradite	Ca ₃ Fe ₂ Si ₃ O ₁₂			Mesolite	Na _{0.676} Ca _{0.657} Al _{1.999} Si _{3.01} O ₁₀ ·2.647H ₂ O							
Copper (metal)	Cu			Saponite-Na	Na ₃₃ Mg ₃ Al ₃₃ Si _{3.67} O ₁₀ (OH) ₂							
Daphnite-14A	Fe ₉ Al ₂ Si ₃ O ₁₀ (OH) ₈			Tremolite	Ca ₂ Mg ₅ Si ₈ O ₂₂ (OH) ₂							
Diopside	CaMgSi ₂ O ₆			Zincite	ZnO							
Greenalite	Fe ₃ Si ₂ O ₅ (OH) ₄			Zn ₂ SiO ₄	Zn ₂ SiO ₄							

*mol/L = mol/0.26 gal

†Temperature conversion: 110 °C [230 °F], 90 °C [194 °F], 60 °C [140 °F]

Table 2-4. Comparison of Predicted Aqueous Speciation for Modeled Variations Based on Temperature After 0.5 Hours

Aqueous Species	Temperature = 110 °C*						Temperature = 90 °C*						Temperature = 60 °C*						
	OLI	REACT	EQ3/6	PHRQ	OLI	PHRQ	REACT	EQ3/6	PHRQ	OLI	PHRQ	REACT	EQ3/6	PHRQ	OLI	PHRQ	REACT	EQ3/6	PHRQ
	(mol/L)/t																		
AlO ₂ ⁻		8.9 × 10 ⁻⁶	8.6 × 10 ⁻⁶	6.4 × 10 ⁻⁵			6.1 × 10 ⁻⁶	5.4 × 10 ⁻⁶	3.4 × 10 ⁻⁵			3.1 × 10 ⁻⁶	3.7 × 10 ⁻⁶	9.8 × 10 ⁻⁶			3.1 × 10 ⁻⁶	3.7 × 10 ⁻⁶	9.8 × 10 ⁻⁶
B(OH) _{3(aq)}	2.0 × 10 ⁻²	3.3 × 10 ⁻²	3.3 × 10 ⁻²	9.6 × 10 ⁻³	1.8 × 10 ⁻²		3.1 × 10 ⁻²	3.1 × 10 ⁻²	1.1 × 10 ⁻²	1.4 × 10 ⁻²		3.0 × 10 ⁻²	3.0 × 10 ⁻²	1.6 × 10 ⁻²			3.0 × 10 ⁻²	3.0 × 10 ⁻²	1.6 × 10 ⁻²
B ₂ O(OH) ₅ ⁻	9.1 × 10 ⁻³				7.8 × 10 ⁻³					5.6 × 10 ⁻³									
B ₃ O ₃ (OH) ₄ ⁻	1.8 × 10 ⁻³				2.1 × 10 ⁻³					2.6 × 10 ⁻³									
B ₄ O ₅ (OH) ₄ ⁻²	6.9 × 10 ⁻⁴				1.0 × 10 ⁻³					2.6 × 10 ⁻³									
BO ₂ ⁻	2.0 × 10 ⁻¹	2.3 × 10 ⁻¹	2.3 × 10 ⁻¹	2.4 × 10 ⁻¹	2.0 × 10 ⁻¹		2.3 × 10 ⁻¹	2.1 × 10 ⁻¹	2.3 × 10 ⁻¹	2.0 × 10 ⁻¹		2.3 × 10 ⁻¹	2.1 × 10 ⁻¹	2.2 × 10 ⁻¹			2.3 × 10 ⁻¹	2.1 × 10 ⁻¹	2.2 × 10 ⁻¹
Ca ⁺²	3.6 × 10 ⁻⁵	9.8 × 10 ⁻⁵	9.7 × 10 ⁻⁵	2.4 × 10 ⁻⁵	2.5 × 10 ⁻⁵		8.3 × 10 ⁻⁵	5.2 × 10 ⁻⁵	3.0 × 10 ⁻⁵	1.3 × 10 ⁻⁵		6.0 × 10 ⁻⁵	1.8 × 10 ⁻⁵	1.8 × 10 ⁻⁵			6.0 × 10 ⁻⁵	1.8 × 10 ⁻⁵	1.8 × 10 ⁻⁵
CaB(OH) ₄ ⁺				3.3 × 10 ⁻⁵					8.3 × 10 ⁻⁵	4.9 × 10 ⁻⁵				4.2 × 10 ⁻⁵					4.5 × 10 ⁻⁵
CaH ₂ BO ₃ ⁺	1.7 × 10 ⁻⁴				1.0 × 10 ⁻⁴					4.8 × 10 ⁻⁵									
CaHSiO ₃ ⁺	6.7 × 10 ⁻⁸				2.2 × 10 ⁻⁸														
CaOH ⁺	4.2 × 10 ⁻⁶			1.3 × 10 ⁻⁸	1.2 × 10 ⁻⁶				1.7 × 10 ⁻⁸	1.6 × 10 ⁻⁷				1.1 × 10 ⁻⁸					
CaSiO ₂ (OH) ₂	6.4 × 10 ⁻⁸				3.5 × 10 ⁻⁸														
Fe ⁺²				1.3 × 10 ⁻⁸															
H ₂ SiO ₄ ⁻²	6.4 × 10 ⁻⁷			2.1 × 10 ⁻⁷	4.4 × 10 ⁻⁷				1.3 × 10 ⁻⁷	1.5 × 10 ⁻⁷				6.3 × 10 ⁻⁸					
H ₃ SiO ₄ ⁻	8.3 × 10 ⁻⁴				3.6 × 10 ⁻⁴					5.9 × 10 ⁻⁵									
HSiO ₃ ⁻		4.5 × 10 ⁻⁴	4.5 × 10 ⁻⁴	5.5 × 10 ⁻⁴			2.2 × 10 ⁻⁴	2.4 × 10 ⁻⁴	2.6 × 10 ⁻⁴			5.7 × 10 ⁻⁵	6.0 × 10 ⁻⁵	6.6 × 10 ⁻⁵			5.7 × 10 ⁻⁵	6.0 × 10 ⁻⁵	6.6 × 10 ⁻⁵
Mg ⁺²										5.9 × 10 ⁻⁸		5.0 × 10 ⁻⁸	4.9 × 10 ⁻⁸	2.2 × 10 ⁻⁸			5.0 × 10 ⁻⁸	4.9 × 10 ⁻⁸	2.2 × 10 ⁻⁸
MgB(OH) ₄ ⁺									1.2 × 10 ⁻⁸					7.7 × 10 ⁻⁸					
Na ⁺	2.2 × 10 ⁻¹	2.3 × 10 ⁻¹	2.3 × 10 ⁻¹	2.2 × 10 ⁻¹	2.2 × 10 ⁻¹		2.3 × 10 ⁻¹	2.1 × 10 ⁻¹	2.1 × 10 ⁻¹	2.2 × 10 ⁻¹		2.3 × 10 ⁻¹	2.1 × 10 ⁻¹	2.1 × 10 ⁻¹			2.3 × 10 ⁻¹	2.1 × 10 ⁻¹	2.1 × 10 ⁻¹
NaAlO _{2(aq)}		6.4 × 10 ⁻⁷	6.3 × 10 ⁻⁷	4.1 × 10 ⁻⁶			3.3 × 10 ⁻⁷	2.8 × 10 ⁻⁷	1.7 × 10 ⁻⁶			1.1 × 10 ⁻⁷	1.2 × 10 ⁻⁷	3.1 × 10 ⁻⁷			1.1 × 10 ⁻⁷	1.2 × 10 ⁻⁷	3.1 × 10 ⁻⁷
NaB(OH) _{4(aq)}	1.5 × 10 ⁻²			1.5 × 10 ⁻²	1.5 × 10 ⁻²				1.6 × 10 ⁻²	1.7 × 10 ⁻²				2.2 × 10 ⁻²					2.4 × 10 ⁻²
NaHSiO _{3(aq)}	3.5 × 10 ⁻⁴	8.0 × 10 ⁻⁴	8.0 × 10 ⁻⁴	8.8 × 10 ⁻⁴	2.8 × 10 ⁻⁴		4.7 × 10 ⁻⁴	4.9 × 10 ⁻⁴	5.1 × 10 ⁻⁴	1.4 × 10 ⁻⁴		1.7 × 10 ⁻⁴	1.7 × 10 ⁻⁴	1.8 × 10 ⁻⁴			1.7 × 10 ⁻⁴	1.7 × 10 ⁻⁴	1.8 × 10 ⁻⁴
NaOH _(aq)		9.3 × 10 ⁻⁵	9.1 × 10 ⁻⁵	2.9 × 10 ⁻⁴			4.5 × 10 ⁻⁵	4.0 × 10 ⁻⁵	1.2 × 10 ⁻⁴			1.4 × 10 ⁻⁵	1.1 × 10 ⁻⁵	2.4 × 10 ⁻⁵			1.4 × 10 ⁻⁵	1.1 × 10 ⁻⁵	2.4 × 10 ⁻⁵

Table 2-4. Comparison of Predicted Aqueous Speciation for Modeled Variations Based on Temperature After 0.5 Hours (continued)												
Aqueous Species	Temperature = 110 °C*			Temperature = 90 °C*			Temperature = 60 °C*					
	OLI	REACT	EQ3/6	PHRQ	OLI	REACT	EQ3/6	PHRQ	OLI	REACT	EQ3/6	PHRQ
$\text{SiO}_{2(\text{aq})}$	3.5×10^{-5}	1.1×10^{-4}	1.1×10^{-4}	3.9×10^{-5}	2.0×10^{-5}	6.5×10^{-5}	7.3×10^{-5}	2.7×10^{-5}	5.9×10^{-6}	2.3×10^{-5}	2.7×10^{-5}	1.4×10^{-5}
$\text{Zn}(\text{OH})_{2(\text{aq})}$	5.2×10^{-8}				5.0×10^{-8}				5.2×10^{-8}			
$\text{Zn}(\text{OH})_3^-$	3.5×10^{-7}				1.9×10^{-7}				7.1×10^{-8}			
$\text{Zn}(\text{OH})_4^{-2}$	1.8×10^{-8}				6.7×10^{-9}							
ZnOH^+	1.4×10^{-8}										1.3×10^{-8}	

(mol/L)†

*Temperature conversion: 110 °C [230 °F], 90 °C [194 °F], 60 °C [140 °F]
†Concentrations less than 10^{-8} mol/L not shown; mol/L = mol/0.26 gal

2.4 Results of Exposure Time Variations Exercise

The remaining four examples in the code comparison represented alkaline borated containment waters that reacted with reactor system components for different amounts of time at a constant temperature of 60 °C [140 °F]. Four starting concentrations (Table 2-2) were estimated for exposure times of 4, 72, 148, and 360 hours, based on reaction rates taken from the open literature for the various components as provided by Jain, et al. (2005). Due to the longer exposure times, the starting source-term concentrations were larger in these four examples than those of the previous three examples, which reacted at the same or higher temperatures but had exposure times of only 30 minutes.

For the higher initial starting concentrations in the examples and for the assumed strong reducing capacity, most of the modeling codes had computational difficulty in completing all four examples successfully. The main reason for the convergence problems appeared to be that at the high starting concentrations, a large number of the solid phases in the thermodynamic database files were oversaturated. The modeling programs were unable to equilibrate the water with an unrealistically large number of precipitated solids simultaneously. In order for OLI StreamAnalyzer to model the last three examples, the data for copper and iron had to be omitted from the input files, which reduced the number of solid phases that were considered as potential precipitates. REACT also experienced convergence problems for three of the four examples. For the containment water at an exposure time of 72 hours (T60-H72), the code ran successfully after copper and iron were omitted from the input file, but even with this approach REACT failed to converge for the other two examples [exposure times at 148 and 360 hours (T60-H148 and T60-H360)]. PHREEQC also experienced some convergence problems with these three examples, but trial-and-error modification of the input files produced a combination of solid phases that precipitated successfully and left no oversaturated phases in solution. EQ3/6 was the only modeling code to complete the entire exercise without convergence warnings or failure to converge.

As indicated by Figure 2-2, the composition of the containment water was most affected by the precipitation of solid phases that removed magnesium, aluminum, zinc, copper, and iron from solution. {Note that final aqueous concentrations less than 10^{-10} mol/L [2.6×10^{-11} mol/gal] in Figure 2-2 are indicated schematically as small bars below the axis.} Concentrations of silica and sodium also were affected by precipitation, but remained relatively high overall.

The solid phases that were predicted to precipitate in these examples (Table 2-5) are generally similar to the precipitated phases that were predicted in Table 2-3. All of the codes predicted that metallic copper would be strongly oversaturated. Zinc was removed from solution as the zinc silicate mineral Zn_2SiO_4 by all codes except EQ3/6, which removed zincite, a zinc oxide mineral. Dissolved iron and magnesium were strongly depleted by the precipitation of several iron-bearing or magnesium-bearing silicate minerals (except in simulations where iron had to be omitted from the file). High initial concentrations of silica and calcium resulted in the predicted precipitation of the minerals quartz (SiO_2) and wollastonite ($CaSiO_3$). For each case modeled, OLI StreamAnalyzer predicted that the precipitation of large amounts of the sodium-rich feldspar albite would remove dissolved aluminum almost entirely from the resulting solution, whereas the other three codes predicted that aluminum concentration would be lowered by the precipitation of the zeolite mineral mesolite. In practice, none of the predicted silica-bearing minerals would be expected to form at the temperature and timescales represented in the simulations.

The pH of each solution remained near the initial value of 10.0 in each case (Table 2-5). Values of pH predicted by PHREEQC ranged from 10.0 to 10.6, and variations predicted by EQ3/6 and

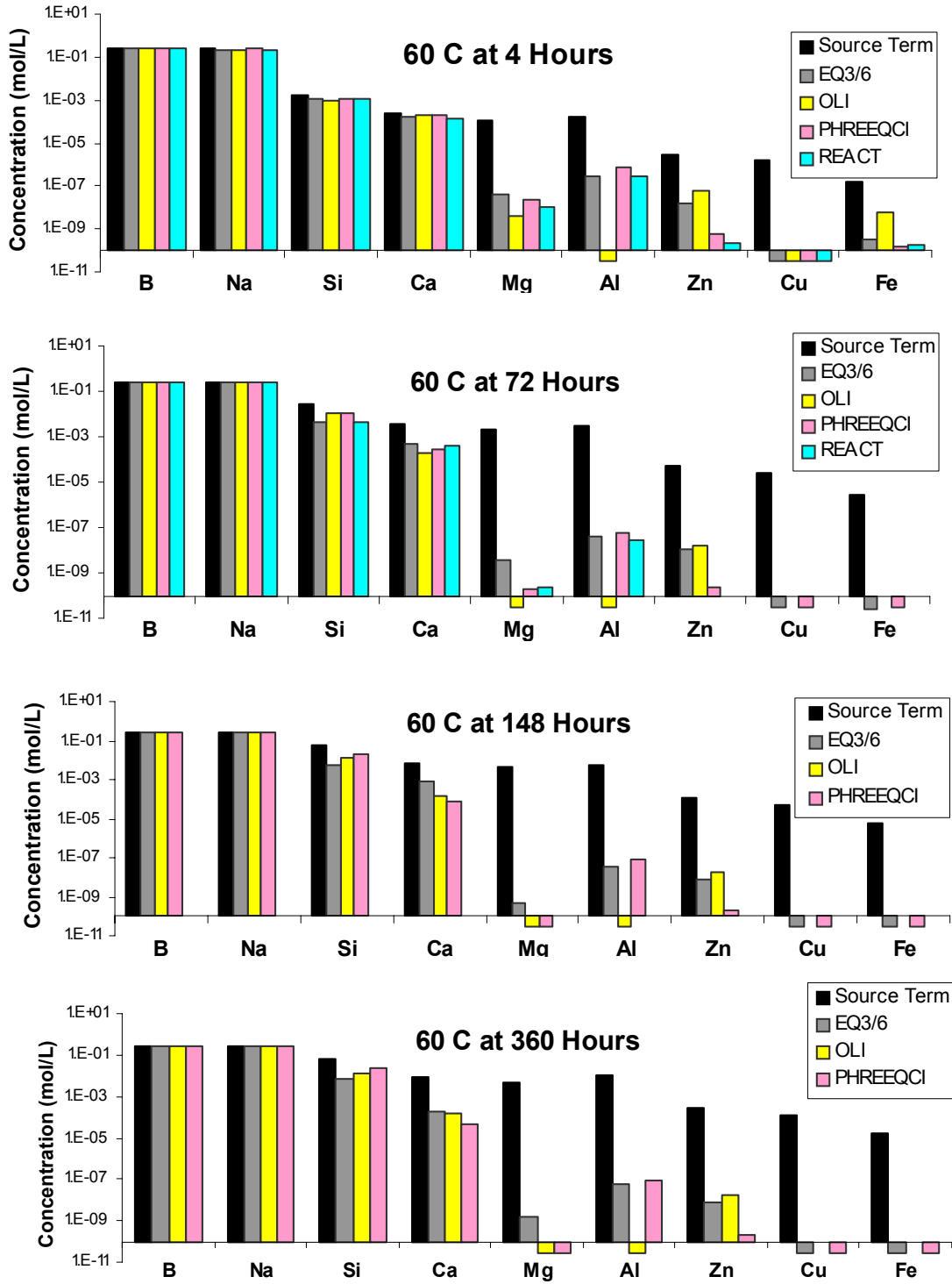


Figure 2-2. Initial (Source-Term) and Final (Modeled) Aqueous Concentrations as Predicted in Code Comparison for Simulated Containment Water at 60 °C [140 °F] at Exposure Intervals of 4, 72, 148, and 360 Hours

Table 2-5. Comparison of Predicted Precipitation for Alkaline Containment Waters at Various Times of Exposure at 60 °C [140 °F]

Precipitates (moles) per L of Water	Predictions at 4 Hours				Predictions at 72 Hours			
	EQ3/6	OLI	PHRQ	REACT†	EQ3/6	OLI	PHRQ	REACT
Albite		1.7×10^{-4}				2.9×10^{-3}		
Andradite					1.5×10^{-6}		1.5×10^{-6}	
Copper	1.5×10^{-6}	1.5×10^{-6}	1.5×10^{-6}	1.5×10^{-6}	2.7×10^{-5}		2.7×10^{-5}	
Diopside				2.0×10^{-3}	2.0×10^{-3}		2.0×10^{-3}	
Greenalite	5.5×10^{-8}	5.3×10^{-8}	5.5×10^{-8}	5.5×10^{-8}				
Hydrogen gas			3.0×10^{-3}				3.0×10^{-3}	
Mesolite	7.7×10^{-5}		7.8×10^{-5}	8.3×10^{-5}	1.5×10^{-3}		1.5×10^{-3}	1.5×10^{-3}
Quartz					1.3×10^{-2}	9.5×10^{-4}	7.3×10^{-3}	1.3×10^{-2}
Saponite-Na	3.6×10^{-5}		3.7×10^{-5}					
Tremolite		2.2×10^{-5}		2.2×10^{-5}		3.9×10^{-4}		
Wollastonite						2.5×10^{-3}	2.7×10^{-4}	8.6×10^{-5}
Zincite	2.8×10^{-6}				5.1×10^{-5}			
Zn ₂ SiO ₄		1.4×10^{-6}	1.4×10^{-6}	1.4×10^{-6}		2.6×10^{-5}	2.6×10^{-5}	2.6×10^{-5}
Final pH	9.68	9.96	10.00	9.72	9.79	9.93	10.21	9.82
Precipitates (moles) per L of Water	Predictions at 148 Hours				Predictions at 360 Hours			
	EQ3/6	OLI*	PHRQ	REACT†	EQ3/6	OLI*	PHRQ	REACT†
Albite		6.0×10^{-3}		—		1.1×10^{-2}		—
Andradite	3.0×10^{-6}		3.1×10^{-6}	—	7.4×10^{-6}		7.5×10^{-6}	—
Copper	5.5×10^{-5}		5.5×10^{-5}	—	1.3×10^{-4}		1.3×10^{-4}	—
Diopside	4.0×10^{-3}		4.1×10^{-3}	—	4.9×10^{-3}		5.0×10^{-3}	—
Hydrogen gas			3.0×10^{-3}	—			2.9×10^{-3}	—
Mesolite	3.0×10^{-3}		3.1×10^{-3}	—	5.6×10^{-3}		5.7×10^{-3}	—
Quartz	2.9×10^{-2}	1.0×10^{-2}	1.6×10^{-2}	—	3.2×10^{-2}	4.4×10^{-3}	1.4×10^{-2}	—
Saponite-Na				—				—
Tremolite		8.0×10^{-4}		—	2.4×10^{-6}	9.9×10^{-4}		—
Wollastonite	2.7×10^{-4}	5.3×10^{-3}	9.6×10^{-4}	—		6.7×10^{-3}	1.3×10^{-4}	—

Table 2-5. Comparison of Predicted Precipitation for Alkaline Containment Waters at Various Times of Exposure at 60 °C [140 °F] (continued)								
Precipitates (moles) per L of Water	Predictions at 148 Hours				Predictions at 360 Hours			
	EQ3/6	OLI*	PHRQ	REACT†	EQ3/6	OLI*	PHRQ	REACT†
Zincite	1.1×10^{-4}			—	2.6×10^{-4}			—
Zn ₂ SiO ₄		5.3×10^{-5}	5.4×10^{-5}	—		1.3×10^{-4}	1.3×10^{-4}	—
Final pH	9.97	10.00	10.48	—	10.00	10.00	10.60	—
	Composition				Composition			
Albite	NaAlSi ₃ O ₈			Mesolite	Na _{.676} Ca _{.667} Al _{1.99} Si _{3.01} O ₁₀ :2.647H ₂ O			
Andradite	Ca ₃ Fe ₂ (SiO ₄) ₃			Quartz	SiO ₂			
Copper	Cu			Saponite-Na	Na _{.33} Mg ₃ Al _{.33} Si _{3.67} O ₁₀ (OH) ₂			
Diopside	CaMgSi ₂ O ₆			Tremolite	Ca ₂ Mg ₅ Si ₈ O ₂₂ (OH) ₂			
Greenalite	Fe ₃ Si ₂ O ₅ (OH) ₄			Wollastonite	CaSiO ₃			
Grossular	Ca ₃ Al ₂ (SiO ₄) ₃			Zincite	ZnO			
Hydrogen gas	H _{2(g)}			Zn ₂ SiO ₄	Zn ₂ SiO ₄			
*Did not include Fe or Cu								
†Simulation did not converge								

REACT ranged from 9.7 to 10.0. Variation was due to two factors, the initial charge balance adjustment and the precipitation of solid phases that consumed hydrogen or hydroxide ions from solution.

The calculated aqueous speciation results (not shown here) are similar to the results for the previous three examples that were presented in Table 2-4. As in those examples, the main differences in speciation calculations resulted from different aqueous species listed in the database files for OLI StreamAnalyzer compared to the databases for the other three geochemical modeling codes.

2.5 Evaluation of Codes

The comparison exercise was designed to evaluate several modeling codes using seven examples that were representative of containment water chemistry in a post-LOCA environment. For the conditions modeled, only one of the codes, EQ3/6, completed all of the examples successfully without requiring adjustments to the input file to avoid convergence failure in the calculations. The main convergence difficulties were encountered in the examples where the concentrations of dissolved reactor debris components were relatively high and there was a large number of potentially oversaturated phases. In several cases, OLI StreamAnalyzer and REACT avoided convergence problems if dissolved copper and iron were omitted from the input file, but in two other examples this same approach did not work (Table 2-5).

The thermodynamic database accompanying OLI StreamAnalyzer has a slightly different set of aqueous boron species than the database of the other three modeling codes. The comparison exercise provided an opportunity to assess the importance of this difference, given the high concentration of boron in the containment water. However, most of the differences in the

databases were for minor boron species, and the overall result was that speciation differences were not significant.

In performing equilibrium mass transfer calculations, the modeling codes EQ3/6, OLI StreamAnalyzer, and REACT calculate the saturation index of all relevant solids that appear in the database file. The code then attempts to identify an equilibrium assemblage of minerals and allows the oversaturated phases to precipitate. In a single run, the code performs these trials iteratively until a successful combination of reacting phases is found, such that no oversaturated phases remain in the final aqueous solution. In contrast, the modeling code PHREEQC does not identify a reactive mineral assemblage automatically. However, the user can implement the process manually by executing the program and identifying the most oversaturated solid in a given simulation, running the program again to allow that phase to precipitate, saving the resulting solution composition, and determining which solid is the most oversaturated phase in the new solution. The user repeats these modeling steps, adding a new solid to the list of reacting phases each time until no oversaturated phases remain in the final solution.

PHREEQC successfully completed calculations for all examples without the need to omit elements from the initial solution compositions, but the reacting mineral assemblage had to be adjusted in several cases to ignore the precipitation of certain oversaturated solids while the sequence of precipitating solids was being developed. The PHREEQC results in the code comparison exercise were similar to those calculated by EQ3/6 and REACT, but the PHREEQC modeling approach required multiple user-generated iterations for each example and was more time-consuming and tedious to implement. Although this approach was a limitation in the code comparison exercise, in practice it could lead to more realistic modeling results. The approach provides the user with the opportunity to exercise a more careful consideration of geochemistry and mineralogy in order to select the concentration-limiting phases that are likely to form under the conditions modeled. This method avoids a black-box approach in which the identification of precipitates is largely controlled by the assumption that the system is in perfect thermodynamic equilibrium.

Most chemical modeling codes are similar enough in their mathematical approach that, given the same problem and the same set of thermodynamic data, they would produce similar results (Zhu and Anderson, 2002). In the examples where all four modeling codes completed the calculations successfully, the most conspicuous differences in results were traceable to the reacting solid phase assemblage that was predicted by OLI StreamAnalyzer, in contrast to the precipitating assemblages identified by the other three geochemical modeling codes. In every example, OLI StreamAnalyzer predicted that the containment waters would be oversaturated with respect to albite, $\text{NaAlSi}_3\text{O}_8$. Precipitation of this phase strongly depleted dissolved aluminum in the resulting waters compared to the predictions of the other codes. The thermodynamic database files for all four codes contained albite, but other aluminum-bearing silicate minerals, even more strongly oversaturated, were predicted to precipitate by EQ3/6, REACT, and PHREEQC. To a large extent, the code comparison exercise was an evaluation of the consequences of using different databases to perform a common simulation.

Despite some convergence problems for simulations at high initial concentrations and for strongly reducing conditions, all of the codes performed the main tasks of the comparison exercise. The most important differences in results were traceable to the listing of different sets of solid phases in the database files, not to the modeling codes themselves. These differences

would have been minimized if the list of potential precipitates had been restricted to phases that were common to all of the databases. The comparison exercise did not test some of the additional capabilities of the various codes, such as the ability to maintain fixed concentrations with atmospheric gases or to block the precipitation of solids that would not be expected to form for kinetic reasons under representative post-LOCA conditions. These capabilities have been examined in more detail by conducting additional simulations, as described in the following sections, using three of the codes—EQ3/6, OLI StreamAnalyzer, and PHREEQC—that were tested in the comparison exercise.

3 DEVELOPMENT OF SOURCE TERMS FOR CHEMICAL EFFECTS SIMULATIONS

The chemical effects simulations are based on the Integrated Chemical Effects Test (ICET) Project, a series of five experiments (ICET#1–#5) conducted at the University of New Mexico (Dallman, 2005a–e). The primary objectives of the ICET experiments were (i) to determine, characterize, and quantify chemical reaction products that may form in a containment sump in a representative post-loss-of-coolant accident (LOCA) environment and (ii) to determine and quantify any gelatinous material that could be produced during the post-LOCA phase of recirculating containment water. In each ICET experiment, 949 L [250 gal] of a simulated neutral or alkaline borated containment water was reacted in a large tank at 60 °C [140 °F] with a set of samples of various metallic and non-metallic reactor system materials (Figure 3-1). The materials included aluminum metal, copper, galvanized steel, carbon steel, concrete, and insulation materials. Sets of the materials, scaled proportionally to the submerged and unsubmerged exposed surface areas for debris components as defined in the U.S. Nuclear Regulatory Commission (NRC) test plan (NRC, 2005), were tested in all of the experiments. Two of the experiments, ICET #3 and ICET #4, tested calcium silicate insulation material in addition to Nukon glass fiber insulation (Table 3-1).

In the ICET experiments, samples of the solid components in the lower part of the tank were submerged in a simulated containment water for 30 days (720 hours). In addition, unsubmerged samples of components in the upper part of the tank were exposed to a uniform nozzle spray for the first four hours of each test to simulate early post-LOCA conditions. During the experiments, water samples were collected regularly and examined for turbidity, total suspended solids, and kinematic viscosity. Water compositions were determined by chemical analysis, and any debris accumulations or precipitates that formed were noted and characterized. Filtered as well as unfiltered water samples (using a glass micropore filter with a



Figure 3-1. ICET Test Chamber and Loop Components

Table 3-1. Key Variations in the ICET* Experiments				
ICET* Experiment No.	pH Buffering Agent	Initial pH	Relative Proportions of Insulation Materials	Containment Water Additives
1	NaOH (Sodium Hydroxide)	~10	100% (Nukon®) Glass Fiber	B(OH) ₃ LiOH HCl
2	Na ₃ PO ₄ (Trisodium Phosphate)	~7	100% (Nukon®) Glass Fiber	B(OH) ₃ LiOH HCl
3	Na ₃ PO ₄ (Trisodium Phosphate)	~7	80% Calcium Silicate 20% Glass Fiber	B(OH) ₃ LiOH HCl
4	NaOH (Sodium Hydroxide)	~10	80% Calcium Silicate 20% Glass Fiber	B(OH) ₃ LiOH HCl
5	Na ₂ B ₄ O ₇ •10H ₂ O (Sodium Tetraborate)	~8.2	100% Glass Fiber	B(OH) ₃ LiOH HCl

*ICET = Integrated Chemical Effects Test

nominal pore size of 0.7 micrometers [28 microinches]) were analyzed routinely. No significant differences in concentration between the two sets of samples were observed, though it should be noted that any colloidal solids smaller than the filter size would remain in solution. As would happen in a post-LOCA environment, in each experiment the starting composition of the water was modified by the dissolution (corrosion) of the sample materials. Many of the reactions were kinetically controlled, so the total dissolved concentration of elements tended to increase as exposure time increased. As concentrations increased, precipitation of oversaturated secondary solids further modified the solution chemistry in some cases. The chemical effects modeling studies focused on this latter effect. The objective of the simulations was to predict the type and amount of secondary solid phases that would be expected to precipitate from the modified containment water under the specified conditions. The predicted changes were compared to data and observations from the ICET experiments. The first set of simulations was blind predictions, which were performed without knowing the outcome of the experiments. The blind predictions were followed by “informed” simulations, in which the modeling approach was amended on the basis of data from the experiments, in an attempt to more closely adjust the simulations to the observed results.

In the blind prediction simulations, the time-dependent changes in water chemistry due to corrosion and dissolution reactions were represented schematically by a set of estimated source-term water compositions that corresponded to discrete exposure times of 0.5 hours,

32 hours [1.2 days], 148 hours [6.2 days], and 360 hours [15 days]. These estimates were based on the initial composition of the containment water (pre-LOCA) and its modification by exposure to the surfaces of the solid samples in the ICET experiments for a specified duration. The source term contribution of each solid, based on its corrosion or dissolution rate, surface area, and time of exposure, was calculated separately for each component and was added to the initial water composition. The source-term compositions were calculated only on the basis of the submerged samples. Contributions from the brief initial (4-hour) spray phase of the experiments were ignored.

In estimating the source-term concentrations of the containment water at various times of exposure, the initial (pre-experiment) composition for the containment water was based on the concentrations of additives listed for each experiment in the ICET test plan (NRC, 2005). The source-term concentrations of boron, chlorine, lithium, sodium, and phosphate that were contributed by the initial additives are indicated for each ICET experiment in Table 3-2.

Table 3-2. ICET* Containment Water Initial Additives				
Additive	Composition	Experiment No.	Concentration (mol/L)	Note
Boric Acid	B(OH) ₃	1, 2, 3, 4	0.259	
Boric Acid	B(OH) ₃	5	0.100	
Hydrochloric Acid	HCl	1, 2, 3, 4	0.00274	
Hydrochloric Acid	HCl	5	0.0011	
Lithium Hydroxide	LiOH	1, 2, 3, 4	0.000101	1
Lithium Hydroxide	LiOH	5	0.000101	2
Sodium Hydroxide	NaOH	1, 4	0.220	
Trisodium Phosphate	Na ₃ PO ₄	2, 3	0.012	
Sodium Tetraborate	Na ₂ B ₄ O ₇ •10H ₂ O	5	0.120	

*ICET = Integrated Chemical Effects Test

Note 1: The lithium hydroxide concentration of 1.01×10^{-4} mol/L corresponds to the ICET Test Plan (NRC. "Test Plan: Characterization of Chemical and Corrosion Effects Potentially Occurring During a Pressurized Water Reactor LOCA." Rev. 12b. ML050450478. Washington, DC: NRC. <www.nrc.gov/reading-rm/adams.html> 2005.) and was used as the source-term concentration in the blind predictions (Section 4) and informed predictions (Section 5). In the actual experiments, slightly less lithium hydroxide was added (2.93×10^{-5} mol/L).

Note 2: A lithium hydroxide concentration of 1.01×10^{-4} mol/L was used as the source-term concentration in the blind predictions (Section 4) and in the informed predictions (Section 5). In the actual ICET #5 experiment, the amount added was less (1.25×10^{-5} mol/L).

Because these conditioning agents were added only at the beginning of the experiment, their source-term concentrations did not increase with time.

Relevant corrosion rates for calculating the source-term contributions of copper, iron, aluminum, and zinc-bearing metals in the system were based on experimentally determined corrosion rates for the ICET sample materials as reported in NUREG-6873 (Jain, et al., 2005) and are listed in Table 3-3. The estimated exposed surface areas of the reacting materials were taken from the test plan (NRC, 2005). For the informed simulations, the aluminum metal corrosion rates were revised (Table 3-3) on the basis of observations from the ICET experiments and data from additional Center for Nuclear Waste Regulatory Analyses (CNWRA) corrosion rate tests, as described in Appendix A.

The source-term contribution from concrete was based on 14-day leaching tests at CNWRA under comparable conditions and for sample-to-solution proportions that corresponded to the ratio in the ICET experiments (Jain, et al., 2005). The CNWRA experiments indicated that the test solutions saturated with concrete leaching products within the first 24 hours. In addition to

Table 3-3. Estimated Source-Term Contributions From Corrosion of Metals					
Source Material	Elements Released to Solution	ICET* Experiment No.	Surface Area/ Volume [m²/m³]	Corrosion Rate [g/m²/h]	Used For
Scaffolding, Insulation	Al	1, 4, 5	0.57	0.99	Blind predictions
	Al	1, 5	0.57	1.31	Informed predictions
	Al	4	0.57	0.80	Informed predictions
	Al	2	0.57	0.0039	All simulations
	Al	3	0.57	0.0039	Blind predictions
	Al	3	0.57	0.028	Informed predictions
Galvanized Steel	Zn	1, 2, 3, 4, 5	1.31	0.036	All simulations
Carbon/Stainless Steel	Fe	1, 4, 5	0.17	0.014	All simulations
	Fe	2, 3	0.17	0.13	All simulations
Heat Exchanger; Fan Coolers	Cu	1, 2, 3, 4, 5	4.9	0.0048	All simulations

*ICET = Integrated Chemical Effects Test

the source-term contributions of calcium, silicon, and aluminum from leaching of concrete surfaces, a fixed amount of concrete dust was assumed to dissolve rapidly and completely in each simulation, as indicated in Table 3-4.

The glass fiber insulation material, Nukon, is composed mainly of silicon dioxide, but it also contains sodium, other minor elements, and some organic binders (Table 3-5). For the modeling study, it was assumed that the dissolution of the glass fibers would contribute silicon, aluminum, calcium, magnesium, and some additional boron, in proportion to their concentration in the glass itself (Table 3-6). Any contribution from organic binders was ignored. The overall source-term contribution from the glass fiber insulation material was estimated from leaching experiments in borated water at pH 7 and pH 10 (Appendix A). The need to measure the surface area of the fibrous material was circumvented by using a sample-to-solution ratio in the leaching tests that was equivalent to the proportions called for in the ICET test plan (NRC, 2005). Analogous to the effect of aluminum on quartz dissolution (Bickmore, et al., 2006), the leaching experiments determined that the Nukon dissolution rate at pH 10 decreased significantly in the presence of aluminum, so the lower glass dissolution rate was used for the source-term contribution of Nukon in alkaline containment waters (ICETs #1, #4, and #5). The glass dissolution rates for ICETs #3 and #4 are scaled by a factor of 0.20 (Table 3-6) to account for the smaller amount of Nukon used in those experiments. In addition, dissolution tests reported in Appendix A indicated that the amount of glass dissolution in alkaline borated containment water after 96 hours was inhibited in the presence of aluminum (Figure A-6). Accordingly, the input source term concentration for silicon for ICETs #1 and #5 was adjusted for time periods greater than 90 hours by fixing the contribution of silicon from dissolved glass fiber to the 90-hour release amount.

Table 3-4. Estimated Source-Term Contributions From Leaching of Concrete			
Concrete Walls			
Released to Solution	ICET* Experiment No.	Surface Area/Volume [m²/m³]	Corrosion Rate [g/m²/h]
Ca	1, 2, 3, 4, 5	0.05	1.00
Al	1, 2, 3, 4, 5	0.05	0.057
Si	1, 2, 3, 4, 5	0.05	0.081
Concrete Particulates (Dust)			
Released to Solution	ICET* Experiment No.	Amount Dissolved [mol] Per Liter of Water	
Ca	1, 2, 3, 4, 5	1.2 × 10 ⁻⁴	
Al	1, 2, 3, 4, 5	3.9 × 10 ⁻⁶	
Si	1, 2, 3, 4, 5	4.3 × 10 ⁻⁵	
*ICET = Integrated Chemical Effects Test			

Table 3-5. Representative Chemical Analysis of Nukon® Glass Fiber	
(Weight Percent)	
SiO ₂	63.67
Al ₂ O ₃	2.99
CaO	7.71
MgO	3.23
Na ₂ O	16.28
B ₂ O ₃	4.10
Total	97.98

Table 3-6. Derivation of Source-Term Contributions from Dissolution of Nukon® Glass Fiber				
Glass Dissolution Rate [mg/h] per Liter of Water			ICET* Experiment No.	
14.007 + 0.135 × h			1, 5	
0.76 × h			2	
(0.76 × h) × 0.20			3	
(14.007 + 0.135 × h) × 0.20			4	
Source-Term Releases from Dissolution of Glass				
Glass Composition† (Weight Percent Oxide)		Cation	Proportion of Cation in Oxide	Cation Released [mg] per Gram of Glass Dissolved
SiO ₂	63.67	Si	0.4674	297.1
Al ₂ O ₃	2.99	Al	0.5292	15.8
CaO	7.71	Ca	0.7147	55.1
MgO	3.23	Mg	0.6030	19.5
Na ₂ O	16.28	Na	0.7419	120.8
B ₂ O ₃	4.10	B	0.3106	12.7
*ICET = Integrated Chemical Effects Test				
†Based on representative analysis in Table 3-5				

X-ray diffraction analysis of the calcium silicate insulation material confirmed that it is composed mainly of the calcium silicate mineral tobermorite, $\text{Ca}_9\text{Si}_{12}\text{O}_{30}(\text{OH})_6 \cdot 4\text{H}_2\text{O}$. Calcium silicate insulation is manufactured from diatomaceous earth (a source of silica) and lime (a source of calcium), with lesser amounts of portland cement and sodium silicate. A small amount of the sodium silicate is unconsumed by manufacturing and acts as a corrosion inhibitor for stainless steel in the finished insulation by manufacturing. A representative chemical analysis of the calcium silicate insulation material used in the ICET experiments is listed in Table 3-7. Leaching rates and a chemical analysis of the sample material were not available when the first set of simulations (blind predictions) commenced. To estimate a source-term contribution from the insulation material for the blind predictions, it was assumed that the rapid dissolution of a fixed amount of material containing equal parts calcium oxide (CaO) and silicon dioxide (SiO_2) contributed equal molecular proportions of calcium and silicon ions to solution. For the later, informed predictions, the source-term contribution from the calcium silicate insulation material was estimated from leaching experiments in borated water at pH 7 and pH 10 (Table 3-8), as reported in Appendix A. For the experiment conditions of ICET #3, estimating the total calcium concentration in solution was complicated by the fact that the calcium released from the sample material quickly formed a calcium phosphate precipitate until all of the phosphorous was consumed, after which a steady increase in calcium concentration was observed. The source-term estimate therefore accounts for the amount of calcium that initially precipitated in the experiment in addition to the amount that remained in solution (Table 3-8). The source-term contribution of silicon for ICET #3 was based on the assumption that equal proportions of calcium and silicon ions were released by the dissolution of the insulation material.

Table 3-7. Representative Chemical Analysis of Calcium Silicate Insulation Compared with Stoichiometric Composition of Crystalline Tobermorite		
	Calcium Silicate Insulation (wt%)	Tobermorite (wt%)
SiO_2	18.5	53.3
TiO_2	2.6	
Al_2O_3	1.1	
Fe_2O_3	0.5	
MgO	0.5	
CaO	40.5	37.3
Na_2O	2.7	
K_2O	0.2	
Total	66.6	90.6
Loss on Ignition	35.2	

Table 3-8. Source-Term Contributions From Dissolution of Calcium Silicate Insulation		
	pH 7 with trisodium phosphate (ICET* #3 Conditions)	pH 10 no trisodium phosphate (ICET* #4 Conditions)
Blind Prediction Source Terms		
Ca [mol/L]	0.220	0.220
Si [mol/L]	0.220	0.220
Informed Prediction Source Terms		
Ca [mg/L]	$0.345 \times (5.61 \times [P]^\dagger + 3.02 \times h)^\ddagger$	$32.2 + 0.13 \times h$
Si [mg/L]	$0.242 \times (5.61 \times [P] + 3.02 \times h)$	$51.6 + 0.87 \times h$
*ICET = Integrated Chemical Effects Test †[P] = phosphorous concentration [mg/L] ‡h = time of exposure [hours]		

For all of the chemical effects simulations, the starting (input) composition of the water in each case was the sum of all contributions from all materials, including the original containment water additives, after the water had been exposed to the solids in the system for the specified amount of time at 60 °C [140 °F]. In each case, for simplicity it was assumed that the composition of the starting solution to that point in time had not been modified by prior precipitation of secondary phases.

The experimentally determined corrosion and dissolution rates were measured at CNWRA in test solutions at pH 7 and pH 10. This corresponded to the initial target pH in all ICET experiments except ICET #5, for which the initial target pH was an intermediate value of approximately 8.2. Because no relevant corrosion rates had been measured at this pH in the CNWRA tests, the source-term water composition for ICET #5 was developed by assuming the same corrosion rates applied as for ICET #1, the experiment with conditions that were the most similar to ICET #5. The source-term concentrations in ICET #5 were conservatively overestimated as a result of this assumption.

During each simulation, the modeling software used the input (source-term) water composition to calculate the aqueous speciation of the dissolved elements and calculated the saturation index (representing the proximity to equilibrium, or saturation) for all relevant solid phases in the accompanying thermodynamic database. Depending on restrictions imposed by the user (Table 3-9), the software then simulated the precipitation of oversaturated phases until they were in equilibrium with the resulting modified aqueous solution. In assessing the results of the simulation, the final calculated solution composition and final pH were compared with analytical data from the ICET experiment for water that was sampled after approximately the same amount of exposure time as was represented by the simulation. In addition, the amount and

Table 3-9. Modeling Test Matrix for ICET* Simulations		
	Input Water Compositions	
Database Manipulations	Original (Initial) Source-Term Estimates	Modified (Post-ICET) Source-Term Estimates
Used entire database (no user-suppressed solid phases)	EQ3/6 Blind predictions (Section 4)	—
Allowed User-suppressed solid phases	EQ3/6 Blind predictions (Section 4)	—
	PHREEQC Blind predictions (Section 6)	PHREEQC Modified blind predictions (Section 6)
Allowed solid phases as limited on basis of ICET results	—	OLI StreamAnalyzer Informed predictions (Section 5)
		PHREEQC Informed predictions (Section 6)

*ICET—Integrated Chemical Effects Test

composition of predicted secondary precipitates were compared qualitatively with descriptive and analytical observations of solids from the ICET experiment.

Several differences between the simulations and the experiments are noteworthy when comparing results. First, for modeling purposes it was assumed that the source-term contributions from various reactive components were time-dependent and followed a constant reaction rate. This does not account for passivation effects, which would eventually slow or stop the corrosion or dissolution reaction during the course of the experiment. As a result, the source-term concentration may be overestimated in some cases. Second, the rates generally are based on single material tests, but as was observed in separate and combined leaching tests for aluminum metal and Nukon glass fiber insulation, multiple material interactions can have a pronounced effect on corrosion/dissolution rates under certain conditions. This factor also would affect source-term water compositions, causing them to be underestimated or overestimated depending on the set of multiple material effects. Third, a simulation predicts the identity and amount of precipitated phases, but it does not provide any information about the physical appearance of a precipitate or its location within the system. The solid phase itself could be a colloidal suspension of very fine particles, a set of larger particles that settles visibly out of solution, or a grain or coating of a secondary corrosion product that remains firmly affixed to a solid substrate while it is forming.

4 BLIND PREDICTIONS OF INTEGRATED CHEMICAL EFFECTS TEST RESULTS

The blind predictions, which were initiated while the Integrated Chemical Effects Test (ICET) experiments were still in progress, were performed using the geochemical modeling code EQ3/6 and its accompanying thermodynamic database file data0.com0R2. To address the time-dependence of changes in the input source term concentrations, the blind predictions considered four cases for each experiment, based on estimated source-term compositions of post-loss-of-coolant accident (LOCA) containment water at four different exposure times. The source-term concentrations served as input values for the composition of the water, calculated from the rates and values presented in Section 3, after 0.5 hours, 32 hours [1.3 days], 148 hours [6.2 days], and 360 hours [15 days] of exposure to the sample materials at 60 °C [140 °F].

In each case for which an input file was developed, it was assumed that the composition of the source-term water at that point in time had not been modified by prior precipitation of secondary phases. The blind prediction simulations also assumed that the water supplied to the tank was in equilibrium initially with atmospheric oxygen and carbon dioxide, so each set of input parameters included an initial oxygen fugacity and an initial concentration of dissolved carbon dioxide. The subsequent speciation and precipitation calculations were performed for a closed system, based on the assumption that there would be limited exchange with the air after the tank was closed. Initial pH values were adjusted slightly from the test plan target values (Table 3-1) to conform to the reported pH values initially established in the experiments. The pH and redox conditions subsequently were allowed to vary in the speciation and precipitation calculations.

The EQ3/6 blind predictions were performed in two stages. First, using the same conceptual approach that was used in the code comparison exercise (Section 2), a baseline set of blind predictions was generated by assuming complete thermodynamic equilibrium for the system. For each starting composition of hypothetical post-LOCA containment water, the system was allowed to equilibrate with predicted oversaturated secondary phases without any restriction of solids that would not be expected to form for kinetic reasons. The second and more realistic set of blind predictions involved the suppression of precipitation for phases that were considered unlikely to form under the short-term, relatively low temperature conditions of the experiment. Results for both sets of EQ3/6 blind predictions are summarized in the following sections for simulations of each of the five ICET experiments.

4.1 Blind Predictions for ICET #1

ICET #1 was a 720-hour pilot-scale test at 60 °C [140 °F] in which coupons of aluminum, copper, galvanized steel, carbon steel and concrete, and bags of Nukon low-density fiber insulation were added to 949 L [250 gal] of alkaline borated containment water also containing small amounts of hydrochloric acid and lithium hydroxide (Table 3-2). In the test plan conditions (Table 3-1), the initial pH of the containment water was to be adjusted to a value of 10 by the addition of sodium hydroxide. The initial pH value obtained in the experiment was closer to 9.5, and an initial input value of 9.8 was used for the EQ3/6 simulations. A description of the ICET #1 test and its results are documented in the experiment final report (Dallman, et al., 2005a).

Table 4-1 summarizes the starting concentrations used for the EQ3/6 simulations of ICET #1 and the results of both sets of blind predictions. High initial dissolved aluminum values were estimated in the starting composition. For the baseline trial (complete thermodynamic equilibrium simulations), the code predicted that the chemistry of the solution would be modified mainly by the precipitation of a hydrated aluminum oxide phase, diaspore, which would remove almost all aluminum from the water. Dissolved copper, iron, and zinc were removed by the precipitation of metal oxides, a prediction that conformed to low observed concentrations of these elements in all of the ICET experiments. Precipitation of the carbonate mineral calcite was predicted to remove most of the calcium from the solution. Calcium and magnesium concentrations were also depleted by the precipitation of lesser amounts of dolomite and mesolite. The formation of the zeolite mineral mesolite also removed about 50 to 60 percent of the dissolved silica from the solution.

For the second set of ICET #1 blind predictions, the EQ6 input files were modified on a case-by-case basis to suppress precipitation of up to 40 solid phases that had been predicted by EQ3 to be oversaturated in the starting solutions, but that were considered unlikely to precipitate under the experiment conditions. The detailed results from an example EQ3/6 calculation with suppressed phases are presented in Appendix B for the simulation of ICET #1 conditions at 148 hours. The output file lists the choice of user options; the input data; attempted and successful iterations of the problem, and the final solution composition, aqueous speciation, solids removed, and final saturation indexes for solid and gas phases. The phases that were suppressed in the simulation included diaspore, dolomite, and mesolite, which had been allowed as reactants in the first set of blind predictions. With these phases suppressed, the solution equilibrated with different oversaturated phases, notably a sodium-aluminum carbonate mineral, dawsonite, and a magnesium carbonate mineral, magnesite (Table 3-4). Dissolved copper, iron, and zinc again were removed almost completely by the precipitation of simple metal oxides. In this simulation, no silicate phases precipitated, so there was no change in the dissolved silica concentration. Compared to the first trial, the total mass of solids removed by precipitation was approximately twice as large, due mainly to the formation of additional carbonates in the second trial.

The results of the two EQ3/6 simulations are compared in Figure 4-1 with ICET #1 analytical data for dissolved calcium, silicon, and aluminum that were obtained at equivalent exposure times during the experiment (Dallman, et al., 2005a). Figure 4-1 also includes results for a third EQ3/6 simulation, a trial case in which dissolved carbon dioxide was omitted from the starting solution. In this third simulation, no carbonate minerals could form.

As indicated by Figure 4-1, the final aluminum concentration measured in ICET #1 was greater than the starting estimated source-term concentration used for the modeling simulations, even though the estimated source term concentration was also large. This suggested that the aluminum source-term contribution rate in Table 3-2 needed to be reevaluated. All of the EQ3/6 simulations predicted that the precipitation of secondary phases would remove virtually all of the aluminum from the solution. These predictions were contrary to the measured aluminum concentration in ICET #1, which remained high (Figure 4-1), but the predictions were substantiated by particle-size analyses of the ICET #1 solution which indicated that a finely

Table 4-1. Blind Predictions for ICET* #1

	Source-Term (Input) Aqueous Starting Compositions						Baseline Predictions Complete Equilibrium (No Suppressed Phases)						Blind Prediction With Suppressed Precipitation (-X-) of Some Phases																	
	0.5		32		148		360		0.5		32		148		360		0.5		32		148		360							
	9.8		9.8		9.8		9.8		9.8		9.8		9.8		9.8		9.8		9.8		9.8		9.8		10.0					
Time (hours)	(mol/L)†																													
pH																														
							Percent Removed by Precipitation						Percent Removed by Precipitation						Percent Removed by Precipitation											
Aluminum	2.3×10^{-5}	6.8×10^{-4}	3.1×10^{-3}	7.5×10^{-3}	29.0	95.1	98.9	99.5	0	85.4	96.0	97.4																		
Boron	2.6×10^{-1}	2.6×10^{-1}	2.6×10^{-1}	2.6×10^{-1}	0	0	0	0	0	0	0	0	0	0	0	0	0	0	0	0	0	0	0	0	0	0	0			
Calcium	6.3×10^{-5}	9.8×10^{-5}	2.2×10^{-4}	4.1×10^{-4}	84.3	89.9	95.5	97.6	84.3	89.9	95.5	97.6	84.3	89.9	95.5	97.6	84.3	89.9	95.5	97.6	84.3	89.9	95.5	97.6	84.3	89.9	97.6			
Chlorine	2.7×10^{-3}	2.7×10^{-3}	2.7×10^{-3}	2.7×10^{-3}	0	0	0	0	0	0	0	0	0	0	0	0	0	0	0	0	0	0	0	0	0	0	0			
Copper	1.8×10^{-7}	1.2×10^{-5}	5.5×10^{-5}	1.3×10^{-4}	16.1	98.7	99.7	99.9	16.1	98.7	99.7	99.9	16.1	98.7	99.8	99.8	99.9	16.1	98.7	99.8	99.8	99.8	99.8	99.9	99.9	99.9	99.9			
Iron	2.1×10^{-8}	1.3×10^{-6}	6.1×10^{-6}	1.5×10^{-5}	100	100	100	100	100	100	100	100	100	100	100	100	100	100	100	100	100	100	100	100	100	100	100			
Carbon	6.4×10^{-2}	6.4×10^{-2}	6.4×10^{-2}	6.4×10^{-2}	0.1	0.1	0.3	0.6	0.1	0.1	0.3	0.6	0.1	0.1	0.3	0.6	0.1	0.1	0.3	0.6	0.1	0.1	0.3	0.6	0.1	0.1	12.1			
Lithium	1.0×10^{-4}	1.0×10^{-4}	1.0×10^{-4}	1.0×10^{-4}	0	0	0	0	0	0	0	0	0	0	0	0	0	0	0	0	0	0	0	0	0	0	0			
Magnesium	1.1×10^{-5}	1.5×10^{-5}	2.4×10^{-5}	2.4×10^{-5}	98.0	98.4	99.1	99.1	98.0	98.4	99.1	99.1	43.6	56.7	73.6	73.7	43.6	56.7	73.6	73.7	43.6	56.7	73.6	73.7	43.6	56.7	73.7			
Sodium	2.2×10^{-1}	2.2×10^{-1}	2.2×10^{-1}	2.2×10^{-1}	0	0	0	0	0	0	0	0	0	0	0	0	0	0	0	0	0	0	0	0	0	0	3.3			
Silicon	2.7×10^{-4}	3.2×10^{-4}	4.5×10^{-4}	4.6×10^{-4}	3.7	48.7	63.0	62.6	3.7	48.7	63.0	62.6	0	0	0	0	0	0	0	0	0	0	0	0	0	0	0			
Zinc	3.6×10^{-7}	2.3×10^{-5}	1.1×10^{-4}	2.6×10^{-4}	96.9	100	100	100	96.9	100	100	100	96.9	100	100	100	96.9	100	100	100	96.9	100	100	100	96.9	100	100			
Precipitates	Chemical Formula						Precipitate Removed (mol) per Liter†						Precipitate Removed (mol) per Liter†						Precipitate Removed (mol) per Liter†											
Calcite	CaCO ₃						4.0×10^{-5}						3.9×10^{-5}						1.2×10^{-4}						3.2×10^{-4}					
Dawsonite	NaAlCO ₃ (OH) ₂						0						0						0						0					
Diaspore	AlHO ₂						0						5.5×10^{-4}						2.9×10^{-3}						7.3×10^{-3}					
Dolomite	CaMg(CO ₃) ₂						1.1×10^{-5}						1.4×10^{-5}						2.4×10^{-5}						2.4×10^{-5}					
Hematite	Fe ₂ O ₃						1.0×10^{-8}						6.6×10^{-7}						3.0×10^{-6}						7.4×10^{-6}					
Magnesite	MgCO ₃						0						0						0						0					
Mesolite	Na _{0.767} Ca _{0.657} Al _{1.99} Si _{3.01} O ₁₀ •2.647H ₂ O						3.3×10^{-6}						5.1×10^{-5}						9.4×10^{-5}						9.6×10^{-5}					

Table 4-1. Blind Predictions for ICET* #1 (continued)												
Source-Term (Input) Aqueous Starting Compositions			Baseline Prediction Complete Equilibrium (No suppressed Phases)				Blind prediction With Suppressed Precipitation (-X-) of Some Phases					
Time (hours)	0.5	32	148	360	0.5	32	148	360	0.5	32	148	360
pH	9.8	9.8	9.8	9.8	9.8	9.8	9.8	9.9	9.8	9.8	9.9	10.0
Precipitates	Chemical Formula											
Tenorite	CuO											
Zincite	ZnO											
	Precipitate Removed (mol) per Liter†				Precipitate Removed (mol) per Liter†				Total Solids Removed (mg)‡ per Liter§			
	3.0 × 10 ⁻⁸				3.0 × 10 ⁻⁸				3.0 × 10 ⁻⁸			
	3.5 × 10 ⁻⁷				3.5 × 10 ⁻⁷				3.5 × 10 ⁻⁷			
	62				240				544			
	7				6				1,132			

*ICET = Integrated Chemical Effects Test

†mol/L = mol/0.26 gal

‡1 mg = 2.2 × 10⁻⁶ lb

§1L = 0.26 gal

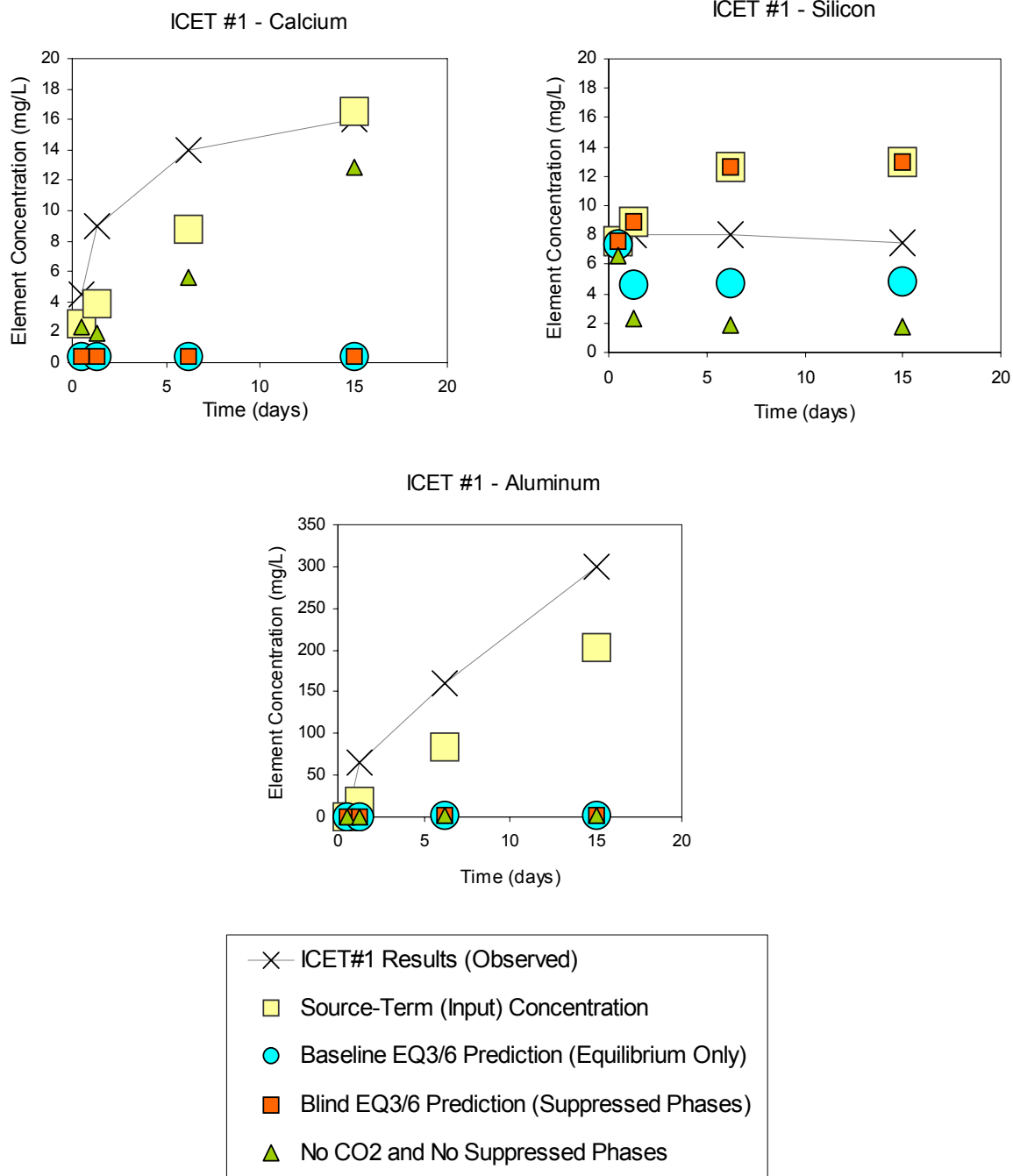


Figure 4-1. Comparison of Blind Predictions With Results of Experiment ICET #1

dispersed colloidal aluminum-bearing solid had formed during the experiment. The colloids were smaller than the 0.7 micrometer [28 microinches] pore size used to filter the sampled water, so they were included as “dissolved” aluminum in the ICET #1 solution analyses.

The measured calcium concentrations in ICET #1 also were slightly higher than the simulated input source-term concentrations and were notably higher than simulations where precipitation of carbonate minerals removed most of the calcium from the solution. Results for the trial case in which it was assumed that there was no dissolved carbon dioxide in the starting solution, corresponded more closely to the observed calcium concentration because under these conditions no calcium carbonate was removed from solution, but applying this assumption broadly was not supported by the experimental data. Chemical analysis of a precipitate that was observed upon cooling of water samples from the ICET #1 experiment indicated that it contained carbonate, as well as aluminum, boron, and sodium (Dallman, et al., 2005a).

4.2 Blind Predictions for ICET #2

ICET #2 was a 720-hour pilot-scale test at 60 °C [140 °F] in which bags of Nukon low-density fiber insulation and coupons of aluminum, copper, galvanized steel, carbon steel, and concrete were added to 949 L [250 gal] of borated containment water. The pH was controlled at near-neutral conditions of about 7.0 by adding trisodium phosphate. The containment water additives consisted of boric acid, lithium hydroxide, hydrochloric acid, and trisodium phosphate (Table 3-2). The results of ICET #2 are documented in the experiment report (Dallman, et al., 2005b).

Table 4-2 summarizes the estimated starting concentrations used for the EQ3/6 simulations of ICET #2 and the results of both sets of blind predictions. Compared to the starting source-term concentrations estimated for ICET #1 (Table 4-1), concentrations of aluminum and dissolved carbonate were lower under the near-neutral pH conditions of ICET #2, and calcium, iron, and magnesium concentrations were slightly higher. For the baseline blind predictions (complete thermodynamic equilibrium simulations), the code predicted that precipitation of diaspore and of the copper oxide mineral tenorite would remove nearly all aluminum and copper, respectively, from the solution. At low concentrations, iron was removed entirely from the solution by the precipitation of iron oxide. At longer exposure times, the estimated source-term iron concentration was larger, as were concentrations of other elements such as silicon and aluminum. In those cases, iron was removed entirely by the precipitation of iron-bearing clay minerals.

The high concentration of dissolved phosphorous in the ICET #2 containment water, due to trisodium phosphate added for pH control, was predicted by EQ3/6 to promote the formation of a calcium phosphate mineral, hydroxylapatite, and the zinc phosphate mineral hopeite, which removed most of the calcium and zinc from the solution. As exposure time increased, the starting source-term concentrations were increasingly oversaturated with respect to quartz so that proportionately larger amounts of silicon (up to 90 percent of the total input starting concentration) were removed in the simulations. The concentration of magnesium in the starting source-term solutions was slightly higher in ICET #2 compared to ICET #1, but magnesium was less affected by the formation of solubility-limiting solid phases under the conditions of ICET #2. Magnesium concentration was affected only slightly by the precipitation of a minor amount of the clay mineral nontronite at 360 hours of exposure in the baseline blind predictions.

For the second set of blind predictions for ICET #2, the input files were modified on a case-by-case basis to suppress precipitation of up to 40 solid phases that had been predicted by EQ3 to be

Table 4-2. Blind Predictions for ICET* #2

	Source-Term (Input) Aqueous Starting Compositions				Baseline Prediction Complete Equilibrium (No Suppressed Phases)				Blind Prediction With Suppressed Precipitation (-X-) of Some Phases					
	0.5		7.0		0.5		7.0		0.5		7.0			
	32	148	360	7.0	32	148	360	7.0	32	148	360	7.0		
Time (hours)	0.5	7.0	32	148	360	7.0	7.0	7.0	7.0	7.0	7.0	7.0		
pH	7.0	7.0	7.0	7.0	7.0	7.0	7.0	7.0	7.0	7.0	7.0	7.0		
Disolved	(mol/L)†													
Aluminum	4.2×10^{-6}	2.3×10^{-5}	9.0×10^{-5}	2.1×10^{-4}	2.1×10^{-4}	98.9	99.8	100	100	94.3	99.6	99.9	100	
Boron	2.6×10^{-1}	2.6×10^{-1}	2.6×10^{-1}	2.6×10^{-1}	2.6×10^{-1}	0	0	0	0	0	0	0	0	
Calcium	4.4×10^{-5}	1.1×10^{-4}	3.3×10^{-4}	7.5×10^{-4}	7.5×10^{-4}	70.8	87.7	96.0	98.1	70.8	87.7	96.0	98.1	
Chlorine	2.7×10^{-3}	2.7×10^{-3}	2.7×10^{-3}	2.7×10^{-3}	2.7×10^{-3}	0	0	0	0	0	0	0	0	
Copper	1.8×10^{-7}	1.2×10^{-5}	5.5×10^{-5}	1.3×10^{-4}	1.3×10^{-4}	0	61.7	91.7	96.5	100	100	100	100	
Iron	1.9×10^{-7}	1.2×10^{-5}	5.7×10^{-5}	1.4×10^{-4}	1.4×10^{-4}	100	100	100	100	100	100	100	100	
Carbon	3.9×10^{-5}	3.9×10^{-5}	4.0×10^{-5}	4.0×10^{-5}	4.0×10^{-5}	0	0	0	0	0	0	0	0	
Lithium	1.0×10^{-4}	1.0×10^{-4}	1.0×10^{-4}	1.0×10^{-4}	1.0×10^{-4}	0	0	0	0	0	0	0	0	
Magnesium	3.0×10^{-7}	1.9×10^{-5}	9.0×10^{-5}	2.2×10^{-4}	2.2×10^{-4}	0	0	0	5.2	0	0	5.2	25.8	
Sodium	3.6×10^{-2}	3.6×10^{-2}	3.7×10^{-2}	3.7×10^{-2}	3.7×10^{-2}	0	0	0	0	0	0	0	0	
Silicon	1.2×10^{-4}	3.8×10^{-4}	1.3×10^{-3}	3.0×10^{-3}	3.0×10^{-3}	0	11.2	74.4	88.9	3.2	5.9	63.4	84.1	
Zinc	3.6×10^{-7}	2.3×10^{-5}	1.1×10^{-4}	2.6×10^{-4}	2.6×10^{-4}	0	88.0	97.4	98.9	0	88.0	97.4	98.9	
Phosphorous	1.2×10^{-2}	1.2×10^{-2}	1.2×10^{-2}	1.2×10^{-2}	1.2×10^{-2}	0.2	0.6	2.2	5.1	0.2	0.6	2.2	5.1	
Precipitates	Chemical Formula													
Diaspore	AlOHO ₂													
Hematite	Fe ₂ O ₃													
Hopeite	Zn ₃ (PO ₄) ₂ •4H ₂ O													
Hydroxylapatite	Ca ₅ (OH)(PO ₄) ₃													
Kaolinite	Al ₂ Si ₂ O ₅ (OH) ₄													
	Precipitate Removed [mol] per Liter†				Precipitate Removed [mol] per Liter†				Precipitate Removed [mol] per Liter†					
	4.2×10^{-6}		2.1×10^{-5}		8.1×10^{-5}		1.9×10^{-4}		-X-		-X-		-X-	
	9.7×10^{-8}		0		0		0		9.7×10^{-8}		6.2×10^{-6}		0	
	0		6.7×10^{-6}		3.4×10^{-5}		8.5×10^{-5}		0		6.7×10^{-6}		3.4×10^{-5}	
	6.3×10^{-6}		1.9×10^{-5}		6.4×10^{-5}		1.5×10^{-4}		6.3×10^{-6}		1.9×10^{-5}		6.4×10^{-5}	
	0		0		0		0		2.0×10^{-6}		1.1×10^{-5}		4.0×10^{-5}	

Table 4-2. Blind Predictions for ICET* #2 (continued)

	Source-Term (Input) Aqueous Starting Compositions			Baseline Prediction Complete Equilibrium (No Suppressed Phases)			Blind Prediction With Suppressed Precipitation (-X-) of Some Phases					
	0.5	32	148	360	0.5	32	148	360	0.5	32	148	360
Time (hours)	0.5	32	148	360	0.5	32	148	360	0.5	32	148	360
pH	7.0	7.0	7.0	7.0	7.0	7.0	7.0	7.0	7.0	7.0	7.0	7.0
Precipitates	Chemical Formula											
Nontronite-Mg	Mg _{1.65} Fe ₂ Al _{0.33} Si _{3.67} H ₂ O ₁₂											
Nontronite-Na	Na _{0.33} Fe ₂ Al _{0.33} Si _{3.67} H ₂ O ₁₂											
Quartz	SiO ₂											
Tenorite	CuO											
	Total Solids Removed (mg)† per Liter‡			3	Total Solids Removed (mg)† per Liter‡			311	Total Solids Removed (mg)† per Liter‡			305
	18	122	17	4	114	17	114	17	4	114	17	305

*ICET = Integrated Chemical Effects Test

† mol/L = mol/0.26 gal

‡ 1 mg = 2.2 x 10⁻⁶ lb

§ 1L = 0.26 gal

oversaturated in the starting solutions, but that were also unlikely to precipitate under the experiment conditions. The phases that were suppressed included diaspore and one of the iron-bearing clay minerals that precipitated in the first set of simulations (Table 3-5). With these phases suppressed, the solution equilibrated with other silicates, notably the clay mineral kaolinite. Quartz, the most common silicon dioxide mineral, was suppressed from precipitating for kinetic reasons. The dissolved silica concentration instead was controlled by the precipitation of tridymite, another high-temperature form of silicon dioxide. Amorphous silicon dioxide, which potentially would be a realistic low-temperature phase, remained undersaturated in all the ICET #2 simulations.

The results of the two EQ3/6 simulations are contrasted in Figure 4-2 with ICET #2 analytical data for dissolved calcium, silicon, and aluminum that were obtained at equivalent exposure times during the experiment (Dallman, et al., 2005b). The concentration of aluminum in the experiment was below detection limits, so it is represented as a uniform value of zero in the graphs. In this respect, the predicted concentration of aluminum conforms with the experiment results. The predicted final concentrations of calcium and silicon are less than the measured results. In contrast, the source-term concentration of silicon corresponds closely to the measured value, suggesting that the modeled precipitation of tridymite in the second set of simulations was unrealistic.

4.3 Blind Predictions for ICET #3

ICET #3 was conducted under conditions nearly identical to those of ICET #2, except that the samples in ICET #3 included calcium silicate insulation as well as Nukon low-density glass fiber insulation in the proportions 80:20 by mass. ICET #3 was a 720-hour pilot-scale test at 60 °C [140 °F] in which bags of calcium silicate and Nukon low-density fiber insulation and coupons of aluminum, copper, galvanized steel, carbon steel, and concrete and were added to 949 L [250 gal] of borated containment water. As stated in the test plan, the pH was controlled at near-neutral conditions of about 7.0 by adding trisodium phosphate. The containment water additives consisted of boric acid, lithium hydroxide, hydrochloric acid, and trisodium phosphate in the concentrations shown in Table 3-2. The results of ICET #3 are documented in the experiment report (Dallman, et al., 2005c).

Table 4-3 summarizes the source-term water compositions used for the ICET #3 simulations and the results of both sets of blind predictions. Although the experiment was similar to ICET #2 in terms of the physical and chemical environment, the dissolution of calcium silicate insulation was assumed to result in much higher estimated starting concentrations of calcium and silicon in ICET #3 and in much larger predicted total amounts of precipitates in the simulations. In both sets of blind predictions for ICET #3, the final solution chemistry was strongly affected by the precipitation of a substantial amount of the calcium phosphate mineral hydroxylapatite, which had the effect of reducing the concentration of phosphorous in the solution by roughly 50 percent (Table 4-3).

For the second set of EQ3/6 blind predictions, the input files were modified on a case-by-case basis to suppress precipitation of up to 40 solid phases that had been predicted by EQ3 to be oversaturated in the starting solutions, but that were also unlikely to precipitate under the experiment conditions. In the baseline set of blind predictions, the precipitation of quartz removed most of the silicon from the solution. No precipitates of copper or zinc were predicted to form. In the second set of simulations, the suppression of precipitation for specified phases such as diaspore and nontronite had little effect on the overall results. Precipitation of quartz was suppressed, and in the example for an exposure time of 0.5 hours, tridymite also was suppressed, which caused silicon concentration to be controlled largely by equilibrium with a third form of silicon dioxide, chalcedony. For the remaining three examples, quartz

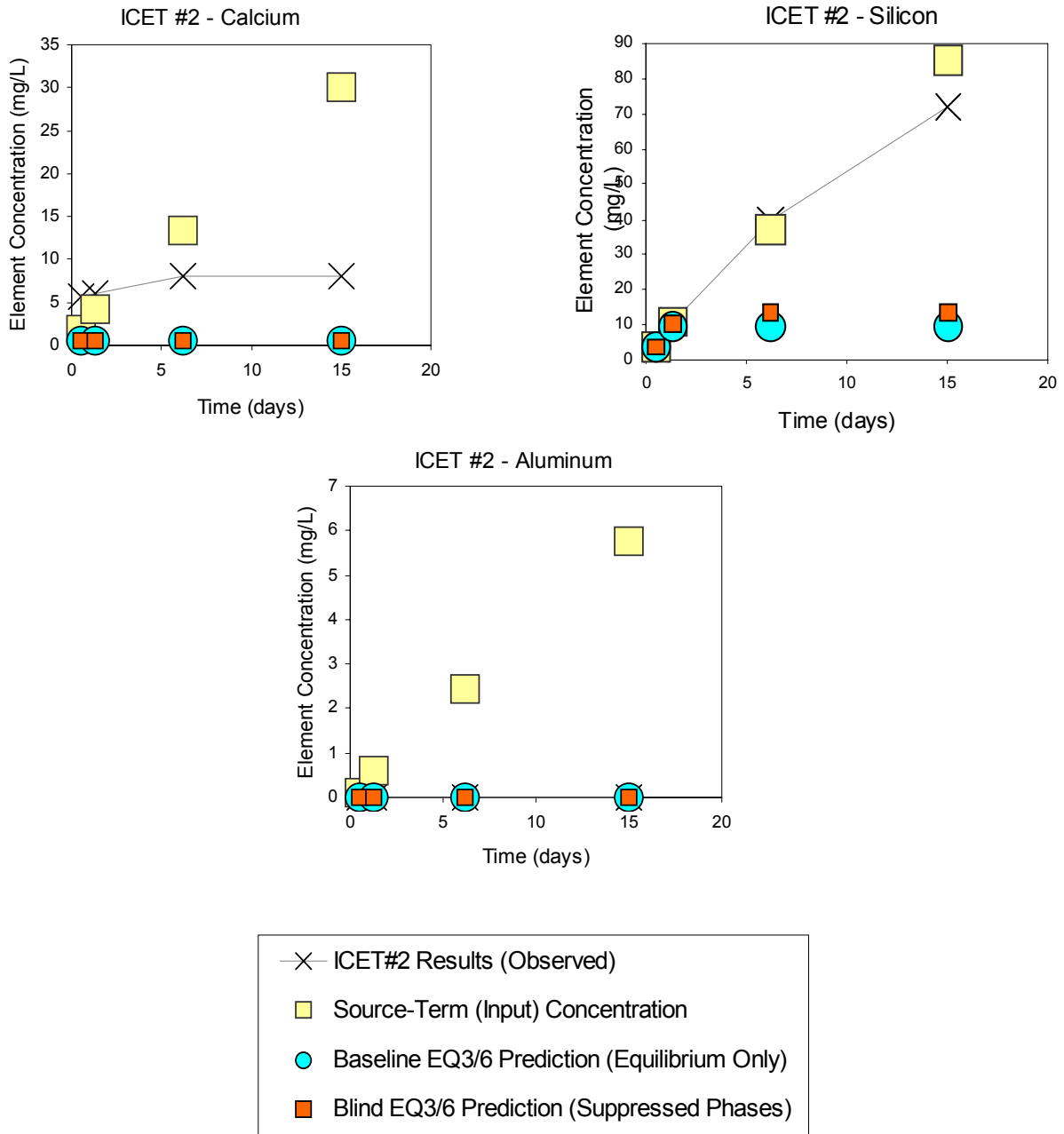


Figure 4-2. Comparison of Blind Predictions With Results of Experiment ICET #2

Table 4-3. Blind Predictions for ICET* #3

	Source-Term (Input) Aqueous Starting Compositions				Baseline Prediction Complete Equilibrium (No Suppressed Phases)				Blind Prediction With Suppressed Precipitation (-X-) of Some Phases							
	0.5		7.0		0.5		7.0		0.5		7.0		0.5		7.0	
	Time (hours)	pH	32	148	360	360	148	360	148	360	148	360	148	360	148	360
Dissolved	(mol/L)†															
Aluminum	4.0×10^{-6}	1.1×10^{-5}	3.8×10^{-5}	8.6×10^{-5}	8.6×10^{-5}	90.2	96.3	98.8	99.4	90.0	96.3	98.8	99.4	90.0	96.3	98.8
Boron	2.6×10^{-1}	2.6×10^{-1}	2.6×10^{-1}	2.6×10^{-1}	2.6×10^{-1}	0	0	0	0	0	0	0	0	0	0	0
Calcium	1.8×10^{-2}	1.8×10^{-2}	2.0×10^{-2}	2.2×10^{-2}	2.2×10^{-2}	53.0	52.2	49.5	45.5	53.0	52.2	49.5	45.4	53.0	52.2	49.5
Chlorine	2.7×10^{-3}	2.7×10^{-3}	2.7×10^{-3}	2.7×10^{-3}	2.7×10^{-3}	0	0	0	0	0	0	0	0	0	0	0
Copper	1.8×10^{-7}	1.2×10^{-5}	5.5×10^{-5}	1.3×10^{-4}	1.3×10^{-4}	0	0	0	0	0	0	0	0	0	0	0
Iron	1.9×10^{-7}	1.2×10^{-5}	5.7×10^{-5}	1.4×10^{-4}	1.4×10^{-4}	100.0	100.0	100.0	100.0	99.9	100.0	100.0	100.0	99.9	100.0	100.0
Carbon	4.4×10^{-5}	4.4×10^{-5}	4.4×10^{-5}	4.5×10^{-5}	4.5×10^{-5}	0	0	0	0	0	0	0	0	0	0	0
Lithium	1.0×10^{-4}	1.0×10^{-4}	1.0×10^{-4}	1.0×10^{-4}	1.0×10^{-4}	0	0	0	0	0	0	0	0	0	0	0
Magnesium	6.1×10^{-8}	3.9×10^{-6}	1.8×10^{-5}	4.4×10^{-5}	4.4×10^{-5}	0	0	0	0	0	0	0	0	0	0	26.2
Sodium	3.6×10^{-2}	3.6×10^{-2}	3.6×10^{-2}	3.6×10^{-2}	3.6×10^{-2}	0	0	0	0	0	0	0	0	0	0	0
Silicon	1.8×10^{-2}	1.9×10^{-2}	2.0×10^{-2}	2.3×10^{-2}	2.3×10^{-2}	98.1	98.2	98.3	98.5	96.8	97.4	97.6	97.9	96.8	97.4	97.6
Zinc	3.6×10^{-7}	2.3×10^{-5}	1.1×10^{-4}	2.6×10^{-4}	2.6×10^{-4}	0	0	0	0	0	0	0	0	0	0	0
Phosphorous	1.2×10^{-2}	1.2×10^{-2}	1.2×10^{-2}	1.2×10^{-2}	1.2×10^{-2}	47.8	48.1	49.3	51.3	47.8	48.2	49.3	51.3	47.8	48.2	49.3
Precipitates	Chemical Formula															
Berillite	AlPO ₄															
Chalcedony	SiO ₂															
Diaspore	AlHO ₂															
Hydroxylapatite	Ca ₅ (OH)(PO ₄) ₃															
Nontronite-Ca	Ca _{1.165} Fe ₂ Al _{3.33} Si _{3.67} H ₂ O ₁₂															
Nontronite-H	H _{3.33} Fe ₂ Al _{3.33} Si _{3.67} H ₂ O ₁₂															
						0	0	2.8×10^{-5}	6.2×10^{-5}	3.6×10^{-6}	8.7×10^{-6}	2.8×10^{-5}	6.2×10^{-5}	3.6×10^{-6}	8.7×10^{-6}	2.8×10^{-5}
						0	0	0	0	1.8×10^{-2}	0	0	0	1.8×10^{-2}	0	0
						3.6×10^{-6}	8.7×10^{-6}	0	0	-X-	-X-	-X-	-X-	-X-	-X-	-X-
						1.9×10^{-3}	1.9×10^{-3}	2.0×10^{-3}	2.0×10^{-3}	1.9×10^{-3}	1.9×10^{-3}	2.0×10^{-3}	2.0×10^{-3}	1.9×10^{-3}	1.9×10^{-3}	2.0×10^{-3}
						9.7×10^{-8}	6.2×10^{-6}	2.9×10^{-5}	7.0×10^{-5}	9.7×10^{-8}	-X-	-X-	-X-	9.7×10^{-8}	-X-	-X-
						0	0	0	0	9.7×10^{-8}	6.2×10^{-6}	2.9×10^{-5}	7.0×10^{-5}	9.7×10^{-8}	6.2×10^{-6}	2.9×10^{-5}

Table 4-3. Blind Prediction for ICET* #3 (continued)

	Source-Term (Input) Aqueous Starting Compositions			Baseline Prediction Complete Equilibrium (No Suppressed Phases)			Blind Prediction With Suppressed Precipitation (-X-) of Some Phases					
	0.5	32	148	360	0.5	32	148	360	0.5	32	148	360
Time (hours)	0.5	32	148	360	0.5	32	148	360	0.5	32	148	360
pH	7.0	7.0	7.0	7.0	4.8	4.8	4.7	4.7	4.8	4.8	4.7	4.7
Precipitates	Chemical Formula											
Nontronite-Mg	$Mg_{.165}Fe_2Al_{.33}Si_{3.67}H_2O_{12}$											
Quartz	SiO_2											
Tridymite	SiO_2											
	Precipitate Removed (mol) per Liter†			Precipitate Removed (mol) per Liter†			Precipitate Removed (mol) per Liter†					
	0			0			0					
	1.8×10^{-2}			1.8×10^{-2}			2.0×10^{-2}					
	0			0			0					
	Total Solids Removed (mg)‡ per Liter§			Total Solids Removed (mg)‡ per Liter§			Total Solids Removed (mg)‡ per Liter§					
	2,029			2,060			2,176					
	2,015			2,052			2,167					
	2,374			2,383			2,374					

*ICET = Integrated Chemical Effects Test

†mol/L = mol/0.26 gal

‡1 mg = 2.2×10^{-6} lb

§1L = 0.26 gal

was suppressed, but tridymite was not, and precipitation of tridymite largely controlled the silicon concentration. As in the first set of simulations, precipitation of hydroxylapatite had a pronounced effect on solution chemistry and pH. Aluminum, initially present in low concentrations, was predicted to be removed from the solution almost completely by precipitation of an aluminum phosphate mineral, berlinite, in the second set of simulations, and by diaspore and berlinite in the first set (Table 4-3). No precipitates of copper or zinc were predicted to form.

The results of the blind predictions for ICET #3 are compared in Figure 4-3 with data for dissolved calcium, silicon, aluminum, and phosphorous that were obtained by chemical analysis at equivalent exposure times during the experiment (Dallman, et al., 2005c). The concentration of aluminum in the experiment was similar to that predicted by the simulations, but the results for calcium and silicon were disparate. The predicted final concentrations of calcium were much higher than the measured values, and the predicted final concentrations of silicon were distinctly lower than the measured values.

Reactions involving phosphorous in ICET #3 were of particular interest for the blind prediction simulations because the dissolved phosphorous concentration in solution had been measured throughout ICET #3 and, unlike the source-term concentrations of most other elements in solution, the starting or source-term concentration was known with confidence. A specified quantity of highly soluble trisodium phosphate was added to the initial containment water for pH adjustment (Table 3-2), and there was no other source for it in the system. Changes in the concentration of phosphorous over time in the experiment consequently served as a good benchmark to which the blind predictions could be compared.

In the ICET #3 experiment, the observed phosphorous concentration dropped rapidly to values near zero at the beginning of the test. In contrast, both sets of the blind predictions indicated that precipitation of hydroxylapatite would reduce the phosphorous concentration by roughly half, at most, at any point in the experiment (Figure 4-3). Both sets of predictions also indicated that the precipitation of hydroxylapatite would lower the system pH from values of around 7 to values between 4.7 and 4.8. In contrast, measured pH values in ICET #3 remained fairly constant at values between about 7.5 and 8.0 (Dallman, et al., 2005c). These anomalies resulted from an oversight in the way that the EQ3/6 input files had been constructed for the blind predictions. The initial solution composition was not allowed to achieve electrical charge balance by adding hydroxide anions to balance the concentrations of cations in the input file, and as a result the system was poorly poised with respect to pH. This discrepancy was a significant factor only in the ICET #3 simulations, because in those calculations the precipitation of a relatively large amount of hydroxylapatite was predicted to cause a sharp drop in pH. At the lower pH values, the solubility of hydroxylapatite increased, and precipitation halted before all of the phosphorous in solution could be consumed by precipitation, contrary to what was observed experimentally. If the pH of the initial solution had been adjusted for charge balance in the EQ3/6 simulations, the pH would have remained buffered at values similar to those observed in ICET #3, and the predicted precipitation of hydroxylapatite would have continued until all phosphorous was removed from solution.

4.4 Blind Predictions for ICET #4

ICET #4 was a 720-hour pilot-scale test at 60 °C [140 °F] that was similar to ICET #3 in that the set of sample materials tested included an 80:20 combination (by mass) of calcium silicate insulation and Nukon low-density glass fiber, but in ICET #4 the experiment was conducted at a pH of about 10 in alkaline borated containment water, similar to the pH conditions of ICET #1. The containment water

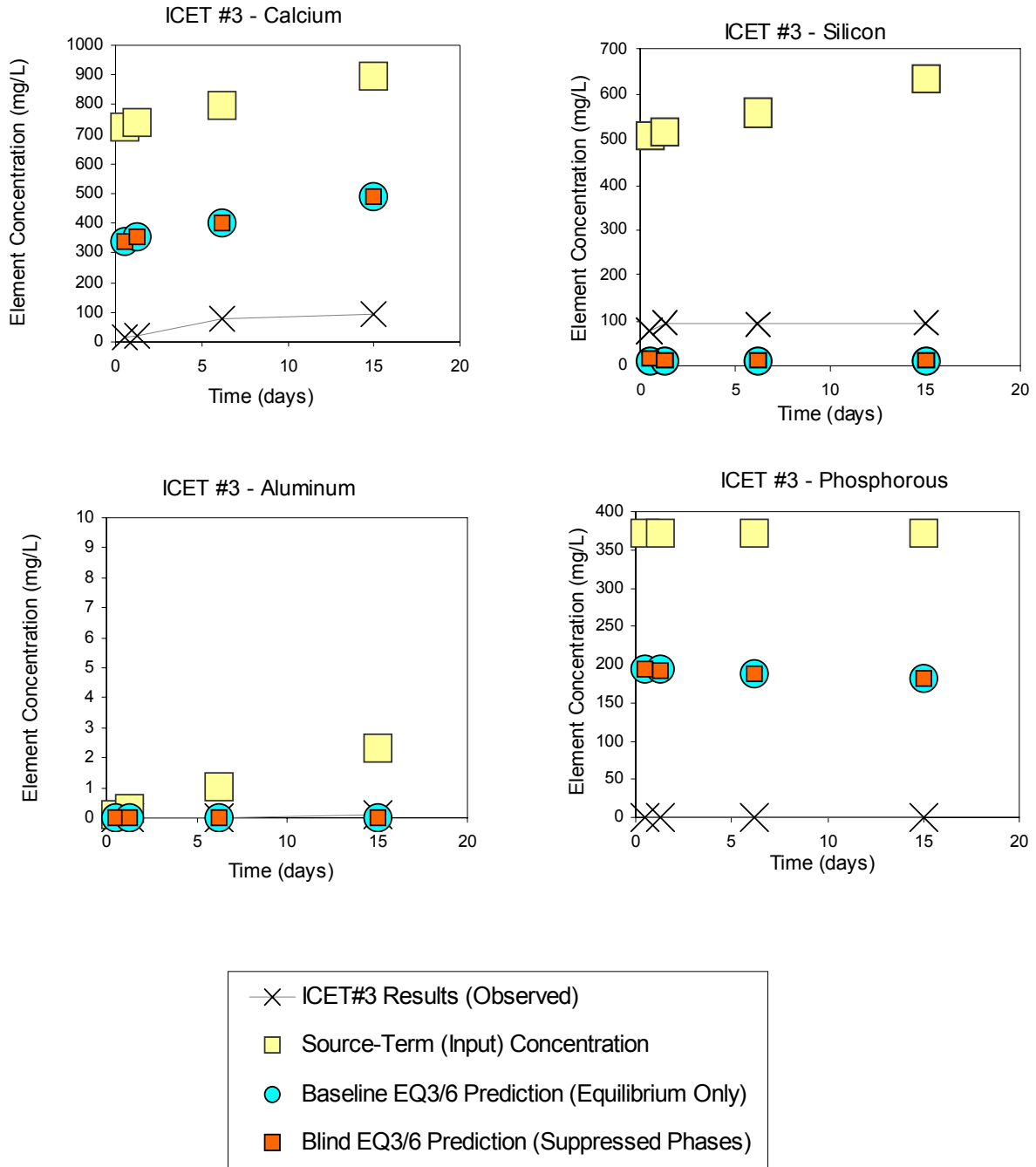


Figure 4-3. Comparison of Blind Predictions With Results of Experiment ICET #3

additives were boric acid, lithium hydroxide, hydrochloric acid, and sodium hydroxide (Table 3-2). In this test, based on the exposed surface area for debris components defined in the NRC test plan (NRC, 2005), coupons of aluminum, copper, galvanized steel, carbon steel and concrete, and bags of calcium-silicate insulation and Nukon low-density fiber insulation were added to 949 L [250 gal] of alkaline borated containment solution. The results of ICET #4 were documented in the experiment report (Dallman, et al., 2005d).

Table 4-4 summarizes the starting concentrations used for the ICET #4 blind predictions and the results of both sets of blind predictions. An initial pH value of 9.8 was used for the starting composition. As a result of the assumed high dissolution rate of calcium silicate insulation (Table 3-8), the initial input source-term concentrations of calcium and silica were high compared to the source-term concentrations in the similar alkaline conditions of ICET #1 (Table 4-1). The starting aluminum concentration under the conditions for ICET #4 was similar to that for ICET #1.

In the baseline set of blind predictions (complete thermodynamic equilibrium), the precipitation of the zeolite mineral mesolite was predicted to remove virtually all aluminum from the solution, in addition to a significant amount of calcium, silicon, and some sodium (Table 3-7). Most of the rest of the calcium in the solution and some of the carbonate was removed by the precipitation of calcite. In the two datasets with highest initial silicon concentrations (at exposure times of 148 and 360 hours) the precipitation of quartz also consumed a large proportion of the silicon in solution. Copper and zinc were removed from solution by precipitation of the oxides tenorite and zincite. Iron and magnesium, both initially present in low concentrations, were removed from the solution by the formation of several varieties of the clay mineral nontronite.

For the second set of ICET #4 blind predictions, the EQ6 input files were modified on a case-by-case basis to suppress precipitation of up to 40 solid phases that had been identified as oversaturated in the starting solutions, but that were also unlikely to precipitate under the experiment conditions. The suppressed phases included mesolite and a clay mineral, saponite, from the first set of simulations. In the second set of simulations, the concentrations of aluminum and silicon were diminished mainly by the precipitation of the clay mineral kaolinite, but precipitation of tridymite also influenced the concentration of silicon. Precipitation of calcite again controlled the calcium concentration, and concentrations of copper and zinc were limited by the solubilities of the oxide minerals tenorite and zincite.

The results of the blind predictions for ICET #4 are contrasted in Figure 4-4 with data for dissolved calcium, silicon, and aluminum that were obtained by chemical analysis at equivalent exposure times during the experiment (Dallman, et al., 2005d). Good agreement was obtained in the comparison for all three elements. The correspondence between measured and predicted concentrations of silicon was particularly good, given the large estimated initial silicon concentration.

In all of the ICET experiments, the containment water included specified concentrations of a sodium-bearing additive, either sodium hydroxide or trisodium phosphate, that maintained sodium concentrations at very high levels compared to most other elements in the solution. Despite this fact, the measured sodium concentration in ICETs #3 and #4 water samples increased throughout the experiments (Dallman, et al., 2005c,d). In fact, the concentration of dissolved sodium nearly doubled in ICET #4 (Dallman, et al., 2005d). This increase is attributed to continued dissolution of the calcium silicate insulation, which contained minor amounts of sodium, titanium, magnesium, and iron (Table 3-3).

Table 4-4. Blind Predictions for ICET* #4

	Source-Term (Input) Aqueous Starting Compositions				Baseline Prediction Complete Equilibrium (No Suppressed Phases)				Blind Prediction With Suppressed Precipitation (-X-) of Some Phases			
	0.5		9.8		0.5		9.8		0.5		9.8	
	32	148	360	9.8	32	148	360	10.0	32	148	360	10.1
Time (hours)	0.5	32	148	360	0.5	32	148	360	0.5	32	148	360
pH	9.8	9.8	9.8	9.8	9.8	9.8	9.9	10.0	9.8	9.8	9.9	10.1
Dissolved	(mol/L)†											
Aluminum	1.6×10^{-5}	6.7×10^{-4}	3.1×10^{-3}	7.5×10^{-3}	95.0	99.9	100	100	0	86.1	97.6	98.5
Boron	2.6×10^{-1}	2.6×10^{-1}	2.6×10^{-1}	2.6×10^{-1}	0	0	0	0	0	0	0	0
Calcium	1.8×10^{-3}	3.5×10^{-3}	9.8×10^{-3}	2.1×10^{-2}	99.4	99.7	99.9	100	99.4	99.7	99.9	100
Chlorine	2.7×10^{-3}	2.7×10^{-3}	2.7×10^{-3}	2.7×10^{-3}	0	0	0	0	0	0	0	0
Copper	1.8×10^{-7}	1.2×10^{-5}	5.5×10^{-5}	1.3×10^{-4}	16.8	98.7	99.8	99.9	16.7	98.8	99.8	99.9
Iron	2.1×10^{-8}	1.3×10^{-6}	6.1×10^{-6}	1.5×10^{-5}	100	100	100	100	100	100	100	100
Carbon	6.5×10^{-2}	6.6×10^{-2}	7.1×10^{-2}	8.0×10^{-2}	2.7	4.9	12.3	23.4	2.7	5.3	13.7	26.5
Lithium	1.0×10^{-4}	1.0×10^{-4}	1.0×10^{-4}	1.0×10^{-4}	0	0	0	0	0	91.2	97.6	0
Magnesium	2.3×10^{-6}	2.9×10^{-6}	5.4×10^{-6}	1.0×10^{-5}	98.5	99.2	99.8	99.9	0	98.4	99.9	100
Sodium	2.2×10^{-1}	2.2×10^{-1}	2.2×10^{-1}	2.2×10^{-1}	0	0.1	0.5	1.2	0	0	0	0
Silicon	1.9×10^{-3}	3.6×10^{-3}	9.8×10^{-3}	2.1×10^{-2}	1.3	28.6	56.2	74.3	3.9	27.1	38.6	60.3
Zinc	3.6×10^{-7}	2.3×10^{-5}	1.1×10^{-4}	2.6×10^{-4}	96.9	100	100	100	96.9	100	100	100
Precipitates	Chemical Formula											
Calcite	CaCO_3											
Hematite	Fe_2O_3											
Kaolinite	$\text{Al}_2\text{Si}_2\text{O}_5(\text{OH})_4$											
Mesolite	$\text{Na}_{.767}\text{Ca}_{.657}\text{Al}_{1.99}\text{Si}_{3.01}\text{O}_{10} \cdot 2.647\text{H}_2\text{O}$											
Montmor-Mg	$\text{Mg}_{.495}\text{Al}_{1.67}\text{Si}_4\text{O}_{10}(\text{OH})_2$											
Nontronite-Mg	$\text{Mg}_{.165}\text{Fe}_2\text{Al}_{.33}\text{Si}_{3.67}\text{H}_2\text{O}_{12}$											
Nontronite-Na	$\text{Na}_{.33}\text{Fe}_2\text{Al}_{.33}\text{Si}_{3.67}\text{H}_2\text{O}_{12}$											
	1.8×10^{-3}	3.3×10^{-3}	8.7×10^{-3}	1.9×10^{-2}	1.8×10^{-3}	3.5×10^{-3}	9.8×10^{-3}	2.1×10^{-2}	1.8×10^{-3}	3.5×10^{-3}	9.8×10^{-3}	2.1×10^{-2}
	0	0	0	0	1.0×10^{-8}	0	0	0	1.0×10^{-8}	0	0	0
	0	0	0	0	0	2.4×10^{-4}	1.5×10^{-3}	3.7×10^{-3}	0	2.4×10^{-4}	1.5×10^{-3}	3.7×10^{-3}
	7.5×10^{-6}	3.4×10^{-4}	1.6×10^{-3}	3.8×10^{-3}	-X-	-X-	-X-	-X-	-X-	-X-	-X-	-X-
	0	0	0	0	0	0	0	0	0	0	0	0
	0	0	0	0	-X-	6.6×10^{-7}	3.0×10^{-6}	7.4×10^{-6}	-X-	6.6×10^{-7}	3.0×10^{-6}	7.4×10^{-6}
	1.0×10^{-8}	6.6×10^{-7}	3.0×10^{-6}	7.4×10^{-6}	-X-	-X-	-X-	-X-	-X-	-X-	-X-	-X-

Table 4-4. Baseline Predictions for ICET* #4 (continued)												
	Source-Term (Input) Aqueous Starting Compositions				Baseline Prediction Complete Equilibrium (No Suppressed Phases)				Blind Prediction With Suppressed Precipitation (-X-) of Some Phases			
	0.5	32	148	360	0.5	32	148	360	0.5	32	148	360
Time (hours)	0.5	32	148	360	0.5	32	148	360	0.5	32	148	360
pH	9.8	9.8	9.8	9.8	9.8	9.8	9.9	10.0	9.8	9.8	9.9	10.1
Precipitates	Chemical Formula											
Petalite	LiAlSi ₄ O ₁₀											
Quartz	SiO ₂											
Saponite-Na	Na ₃₃ Fe ₂ Al ₃₃ Si _{3,67} O ₁₀ (OH) ₂											
Talc	Mg ₃ Si ₄ O ₁₀ (OH) ₂											
Tenonite	CuO											
Tridymite	SiO ₂											
Zincite	ZnO											
	Total Solids Removed (mg)† per Liter§				Precipitate Removed (mol) per Liter†				Precipitate Removed (mol) per Liter†			
	181	461	1,540	3,633	178	443	1,411	3,415	0	9.2 × 10 ⁻⁵	1.0 × 10 ⁻⁴	-X-
	0	0	0	0	0	0	7.9 × 10 ⁻⁴	4.3 × 10 ⁻³	0	0	-X-	-X-
	7.4 × 10 ⁻⁷	9.7 × 10 ⁻⁷	1.8 × 10 ⁻⁶	3.3 × 10 ⁻⁶	-X-	-X-	9.3 × 10 ⁻⁷	0	0	0	0	0
	3.1 × 10 ⁻⁸	1.2 × 10 ⁻⁵	5.4 × 10 ⁻⁵	1.3 × 10 ⁻⁴	3.1 × 10 ⁻⁸	1.2 × 10 ⁻⁵	5.4 × 10 ⁻⁵	1.3 × 10 ⁻⁴	3.1 × 10 ⁻⁸	1.2 × 10 ⁻⁵	5.4 × 10 ⁻⁵	1.3 × 10 ⁻⁴
	0	0	0	0	0	0	0	0	0	0	1.4 × 10 ⁻⁴	4.9 × 10 ⁻³
	3.5 × 10 ⁻⁷	2.3 × 10 ⁻⁵	1.1 × 10 ⁻⁴	2.6 × 10 ⁻⁴	3.5 × 10 ⁻⁷	2.3 × 10 ⁻⁵	1.1 × 10 ⁻⁴	2.6 × 10 ⁻⁴	3.5 × 10 ⁻⁷	2.3 × 10 ⁻⁵	1.1 × 10 ⁻⁴	2.6 × 10 ⁻⁴
	Total Solids Removed (mg)† per Liter§				Total Solids Removed (mg)† per Liter§				Total Solids Removed (mg)† per Liter§			
	181	461	1,540	3,633	178	443	1,411	3,415	0	9.2 × 10 ⁻⁵	1.0 × 10 ⁻⁴	-X-

*ICET = Integrated Chemical Effects Test

† mol/L = mol/0.26 gal

‡ 1 mg = 2.2 × 10⁻⁶ lb

§ 1L = 0.26 gal

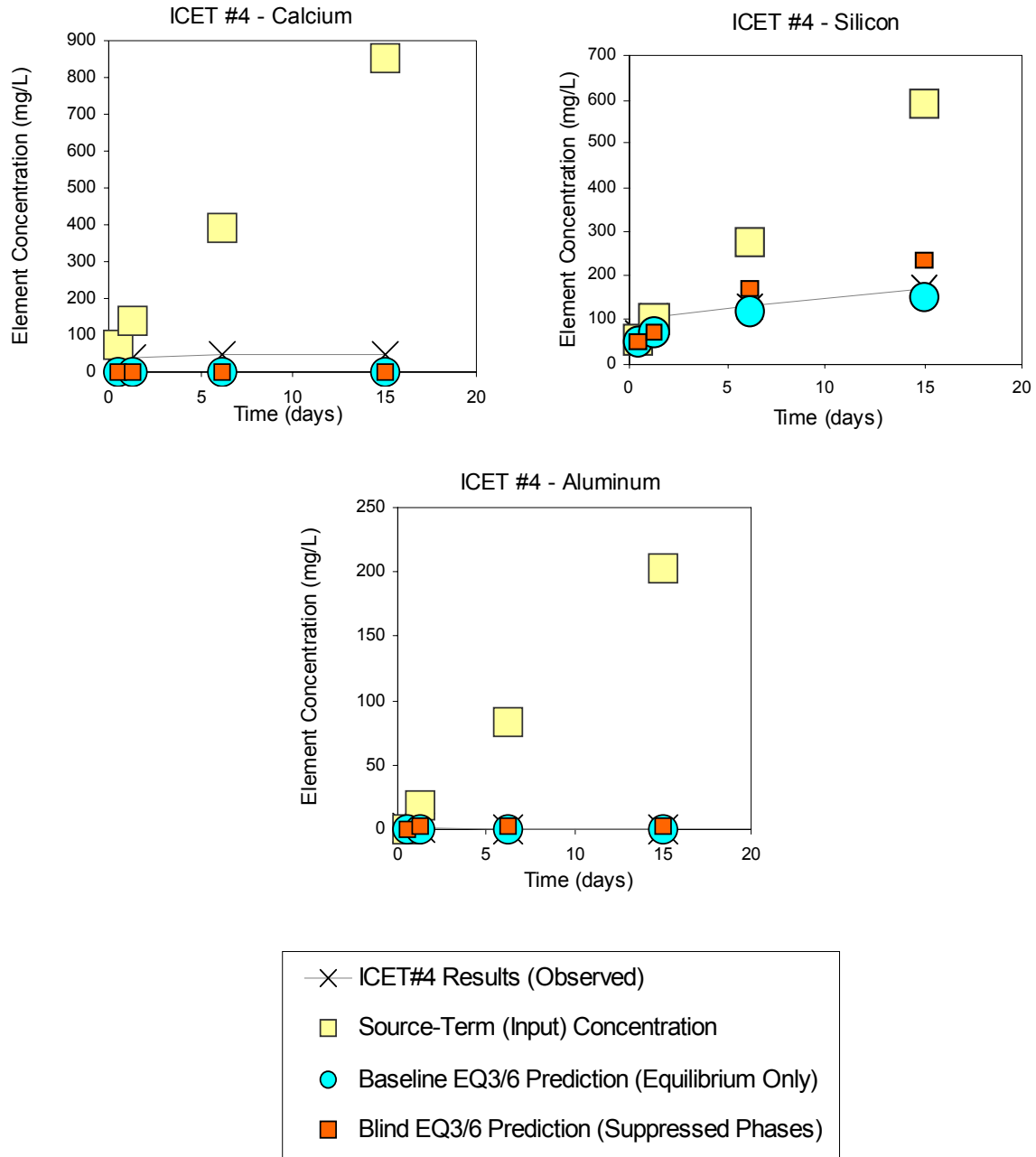


Figure 4-4. Comparison of Blind Predictions With Results of Experiment ICET #4

4.5 Blind Predictions for ICET #5

ICET #5 was a 720-hour pilot-scale test at 60 °C [140 °F] that simulated LOCA conditions in sodium borate containment water with a pH value of between 8.2 and 8.4. Test #5 had a lower boron concentration than the other four ICET experiments and included sodium tetraborate (borax) instead of sodium hydroxide as the main pH-buffering agent (Table 3-2). Except for the buffering agent and difference in pH, the experiment conditions for ICET #5 were identical to ICET #1. The set of materials tested was the same assortment as those in ICETs #1 and #2, in which bags of Nukon low-density fiber insulation and coupons of aluminum, copper, galvanized steel, carbon steel, and concrete were added to 949 L [250 gal] of sodium borated containment water. More details about ICET #5 are documented in the experiment report (Dallman, et al., 2005e).

Table 4-5 summarizes the starting concentrations used for the blind predictions for ICET #5 and the results of both sets of blind predictions. In the baseline of simulations (complete thermodynamic equilibrium), most of the silicon and some calcium, aluminum, and sodium were removed from the solution by the formation of the zeolite mineral mesolite. The remainder of the aluminum was removed from the solution by precipitation of the aluminum hydroxide mineral diaspore. Given their low initial concentrations, virtually all of the copper, iron, and zinc were removed from the solution by the precipitation of small amounts of metal oxides.

In the second set of simulations, the precipitation of mesolite and most of the clay minerals was suppressed. Under these conditions, aluminum concentrations were controlled mainly by precipitation of the aluminum hydroxide mineral gibbsite. The precipitation of kaolinite also affected the aluminum concentrations, as well as the concentration of silicon. The calcium concentration was unaffected by precipitation in the second set of simulations because mesolite was not allowed to form and calcite was slightly undersaturated in the initial water compositions. The concentration of copper, iron, and zinc continued to be controlled by precipitation of small amounts of metal oxides.

The results of the ICET #5 blind predictions are compared in Figure 4-5 with data for dissolved calcium, silicon, and aluminum that were obtained by chemical analysis at equivalent exposure times during the experiment (Dallman, et al., 2005e). Predicted concentrations were slightly less than measured values for all three elements. The estimated initial source-term concentrations of calcium also were less than the measured values. The reported concentrations of copper, iron, and zinc were present only in trace amounts, as predicted by the simulations.

4.6 Assessment of Blind Predictions Results

The blind predictions involved two approaches in simulating the ICET experiments. The baseline set of blind predictions, which were similar to the approach used in the code comparison exercise, ignored any kinetic constraints on the formation of solid phases and allowed the modeling program to precipitate any oversaturated solid phase that was listed in the database. The second set of blind predictions was a modification of this approach, in which precipitation was suppressed for up to forty oversaturated mineral phases from a user-specified list. The suppressed phases were solids from the database file that the user considered unlikely to form either for kinetic reasons at the temperature and timescale of the experiments or because these minerals are not expected to crystallize from an aqueous solution at or near conditions similar to the earth's surface environment.

Table 4-5. Blind Predictions for ICET* #5

	Source-Term (Input) Aqueous Starting Compositions				Baseline Prediction Complete Equilibrium (No Suppressed Phases)				Blind Prediction With Suppressed Precipitation (-X-) of Some Phases			
	0.5	32	148	360	0.5	32	148	360	0.5	32	148	360
	8.2	8.2	8.2	8.2	8.2	8.3	8.3	8.3	8.2	8.3	8.3	8.3
Dissolved	(mol/L)†											
Aluminum	2.3×10^{-5}	6.8×10^{-4}	3.1×10^{-3}	7.5×10^{-3}	99.3	99.9	100	100	90.1	99.4	99.8	99.9
Boron	2.2×10^{-1}	2.2×10^{-1}	2.2×10^{-1}	2.2×10^{-1}	0	0	0	0	0	0	0	0
Calcium	6.3×10^{-5}	9.8×10^{-5}	2.2×10^{-4}	4.1×10^{-4}	11.5	51.6	37.8	21.7	0	0	0	0
Chlorine	1.1×10^{-3}	1.1×10^{-3}	1.1×10^{-3}	1.1×10^{-3}	0	0	0	0	0	0	0	0
Copper	1.8×10^{-7}	1.2×10^{-5}	5.5×10^{-5}	1.3×10^{-4}	97.3	100	100	100	97.3	100	100	100
Iron	2.1×10^{-8}	1.3×10^{-6}	6.1×10^{-6}	1.5×10^{-5}	100	100	100	100	100	100	100	100
Carbon	6.3×10^{-4}	6.4×10^{-4}	6.8×10^{-4}	7.4×10^{-4}	0	0	0	0	0	0	0	0
Lithium	4.1×10^{-5}	4.1×10^{-5}	4.1×10^{-5}	4.1×10^{-5}	0	0	0	0	0	0	0	0
Magnesium	1.1×10^{-5}	1.5×10^{-5}	2.4×10^{-5}	2.4×10^{-5}	41.6	0	6.9	0	0	28.6	11.7	43.9
Sodium	5.7×10^{-2}	5.7×10^{-2}	5.7×10^{-2}	5.7×10^{-2}	0	0.1	0.2	0.2	0	0	0	0
Silicon	2.7×10^{-4}	3.2×10^{-4}	4.5×10^{-4}	4.6×10^{-4}	14.4	72.6	85.1	88.6	7.5	58.9	70.7	71.1
Zinc	3.6×10^{-7}	2.3×10^{-5}	1.1×10^{-4}	2.6×10^{-4}	0	97.5	99.5	99.8	0	97.5	99.5	99.8
Precipitates	Chemical Formula											
Clinchlore-14A	$Mg_5Al_2Si_3O_{10}(OH)_8$											
Diaspore	$AlHO_2$											
Gibbsite	$Al(OH)_3$											
Hematite	Fe_2O_3											
Kaolinite	$Al_2Si_2O_5(OH)_4$											
Mesolite	$Na_{.767}Ca_{.657}Al_{1.99}Si_{3.01}O_{10} \cdot 2.647H_2O$											
Nontronite-Na	$Na_{.33}Fe_2Al_{.33}Si_{3.67}H_2O_{12}$											
					Precipitate Removed (mol) per Liter†				Precipitate Removed (mol) per Liter†			
					0	5.3×10^{-4}	2.9×10^{-3}	7.3×10^{-3}	-X-	-X-	-X-	2.1×10^{-6}
					0	0	0	0	-X-	-X-	-X-	-X-
					0	6.6×10^{-7}	3.0×10^{-6}	7.4×10^{-6}	0	5.0×10^{-4}	2.8×10^{-3}	7.2×10^{-3}
					0	0	0	0	1.0×10^{-8}	6.6×10^{-7}	3.0×10^{-6}	7.4×10^{-6}
					0	0	0	0	1.0×10^{-5}	9.1×10^{-5}	1.6×10^{-4}	1.6×10^{-4}
					1.1×10^{-5}	7.7×10^{-5}	1.3×10^{-4}	1.4×10^{-4}	-X-	-X-	-X-	-X-
					1.0×10^{-8}	0	0	0	-X-	-X-	-X-	-X-

Table 4-5. Blind Predictions for ICET* #5 (continued)

	Source-Term (Input) Aqueous Starting Compositions			Baseline Prediction Complete Equilibrium (No Suppressed Phases)			Blind Prediction With Suppressed Precipitation (-X-) of Some Phases					
	0.5	32	148	360	0.5	32	148	360	0.5	32	148	360
Time (hours)	0.5	32	148	360	0.5	32	148	360	0.5	32	148	360
pH	8.2	8.2	8.2	8.2	8.2	8.3	8.3	8.3	8.2	8.3	8.3	8.3
Precipitates	Chemical Formula											
Saponite-Mg	Mg _{3.165} Al _{3.33} Si _{3.67} O ₁₀ (OH) ₂											
Saponite-Na	Na _{3.33} Mg ₃ Al _{3.33} Si _{3.67} O ₁₀ (OH) ₂											
Talc	Mg ₃ Si ₄ O ₁₀ (OH) ₂											
Tenorite	CuO											
Zincite	ZnO											
	Total Solids Removed (mg)† per Liter‡				Total Solids Removed (mol) per Liter†				Total Solids Removed (mg)‡ per Liter§			
	5	64	234	521	0	0	0	0	3	66	272	637

*ICET = Integrated Chemical Effects Test

†mol/L = mol/0.26 gal

‡1 mg = 2.2 x 10⁻⁶ lb

§1L = 0.26 gal

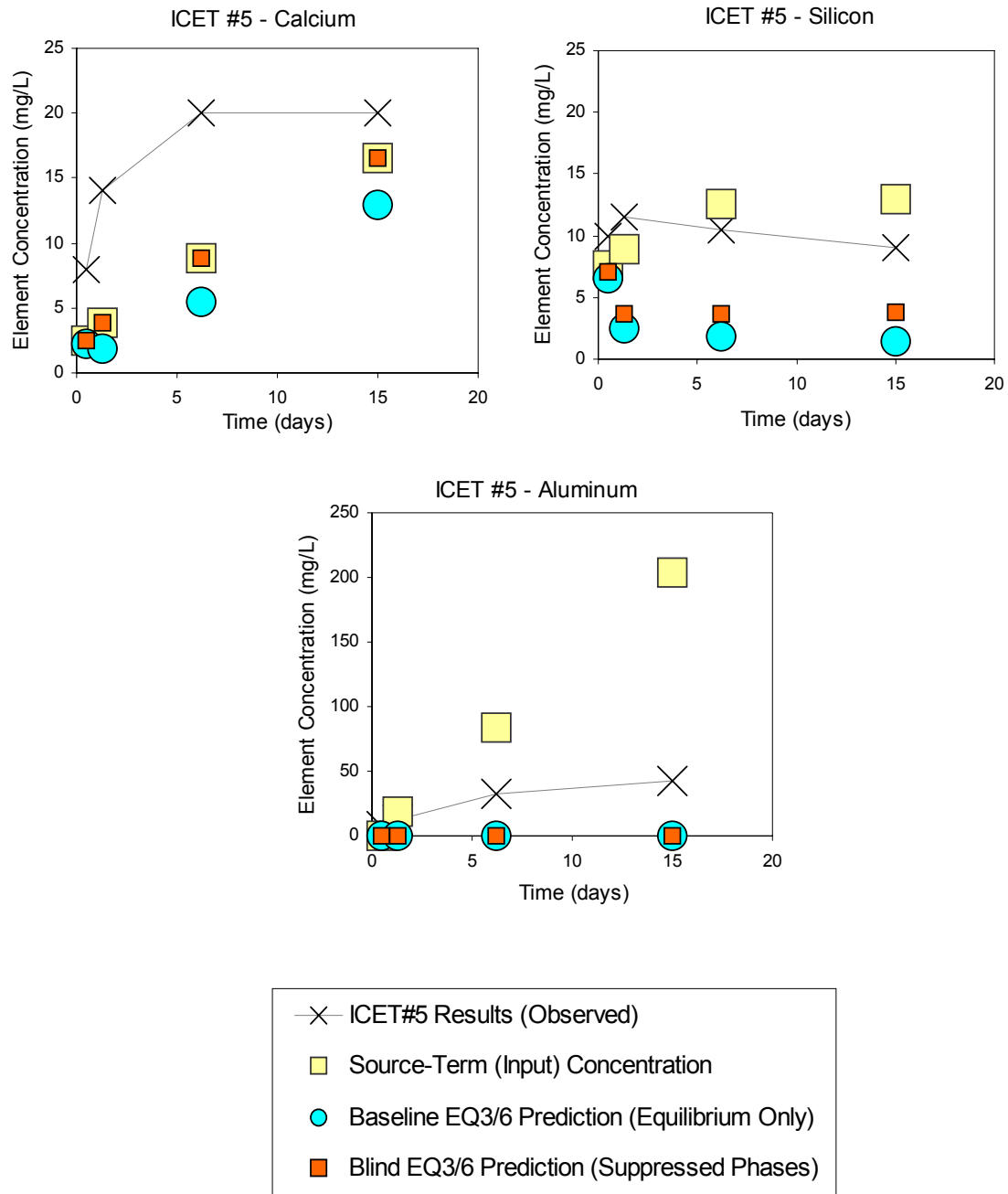


Figure 4-5. Comparison of Blind Predictions With Results of Experiment ICET #5

For these two approaches, in most cases the precipitation of different solid phases controlled the final solution chemistry, but ultimately the total mass of solids removed was similar for both sets of blind predictions. For example, Figure 4-6 compares the total masses of precipitates predicted to form in each of the ICET experiments for the source-term containment water representative of the post-LOCA conditions after 360 hours [15 days] of exposure. With the exception of the results for ICET#1, both blind prediction approaches predicted roughly similar total masses of precipitated solids.

Both of the simulations predicted that ICETs #3 and #4 would be expected to have the greatest total amount of precipitation, a result that was due mainly to the large source-term contribution from dissolved calcium silicate insulation material in these two experiments. In the actual experiments, it was not possible to quantify total amounts of precipitates because any new solids that formed tended to become mixed in with debris components in the tank and could not be separated. It was also difficult to discriminate between precipitates that formed during the experiment and precipitates that formed upon drying of other sample materials after the experiment. The general descriptions of particulate materials from test reports (Dallman, et al., 2005a–e) did indicate qualitatively, however, that more secondary solids were observed in experiments ICETs #2 and ICET #3 than in any of the other tests. These were the two experiments in which trisodium phosphate was added to the starting test solution for pH adjustment, and a calcium phosphate precipitate was observed to form in the water. In addition, the surfaces of the submerged metal plates in ICETs #2 and #3 acquired more patchy white and gray deposits than was observed in any of the other experiments.

Although the blind predictions agreed with the observed large amount of precipitation for ICET #3, the predictions did not agree closely with observations for ICET #2. The low predicted totals for ICET #2 (Figure 4-6) result partly from the lack of pH buffering in the simulations due to an input error in the EQ3/6 simulations. If more hydroxylapatite had been allowed to precipitate in these simulations, the total predicted amount for ICET #2 would have been higher. Even so, the predicted amount of

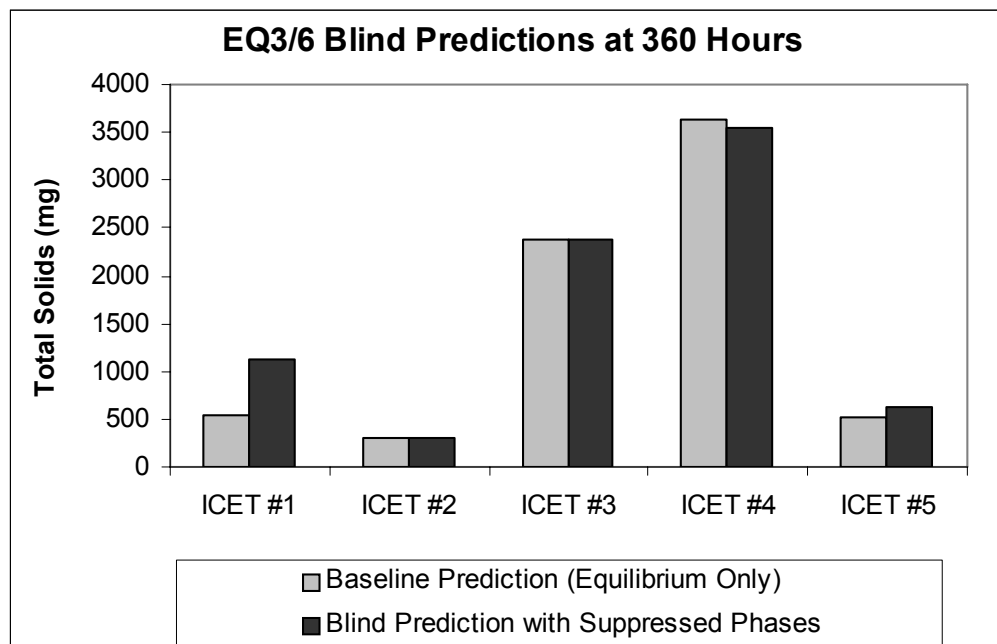


Figure 4-6. Predicted Total Masses of Precipitated Solids in ICETs #1–#5

hydroxylapatite precipitation would have been limited in ICET #2 by the total dissolved calcium, for which the source-term concentrations were relatively low (Table 4-5).

The largest discrepancy between blind predictions and observed results is for ICET #4. The blind predictions indicated that substantially more precipitation would occur under these conditions than for any of the other experiments. In the ICET #4 experiment, few particulates were observed to form, compared to amounts in ICET #2 and #3, and only minor deposits of secondary phases were observed on any of the submerged metal plates (Dallman, et al., 2005d). The source-term contribution from calcium silicate insulation was overestimated in ICET #4, which resulted in large overpredictions for precipitation of calcite and quartz or amorphous silica (Table 4-4).

Some of the discrepancies between the blind predictions and experimental results could be attributed to the development of the source-term compositions, which served as the input water composition for each simulation. The comparison between the blind predictions and the ICET results indicated that source terms used to develop starting water compositions for the simulations had underestimated the contributions of some of the materials. For example, in ICET #1 the measured aluminum concentration was consistently higher than the estimated source-term value (Figure 4-1), so the blind prediction final aluminum concentration by definition was too low compared to the measured results. In order to represent the conditions of the ICET experiments more accurately, additional leaching experiments were performed at the Center for Nuclear Waste Regulatory Analyses to better quantify the actual dissolution rates for calcium silicate insulation in ICETs #2 and #3 and to determine a more representative corrosion rate for aluminum metal in the presence of Nukon glass fiber insulation (Appendix A). These data were used to modify the source terms for subsequent modeling of the ICET experiments.

The database file that accompanies EQ3/6 is deliberately comprehensive in order to allow users to model a wide range of rock and water interactions. Many of the mineral phases that are listed form in igneous or metamorphic geologic environments. They are included in the database mainly for simulations in which these minerals, the constituents of rocks, slowly react with and control the chemistry of groundwater. The modeling approach used for the blind predictions was cumbersome to implement largely because so many of these potentially oversaturated phases were listed, but these phases would not realistically be expected to precipitate for kinetic reasons in the ICET experiments.

In the baseline blind predictions and in the code comparison exercise described in Section 2, both of which were based on the assumption of complete thermodynamic equilibrium with any oversaturated solid phases, EQ3/6 accessed the large database file and performed efficiently to automatically identify the oversaturated solid phases and allow them to precipitate until the selected solids were in equilibrium with the final water composition. In the second set of blind predictions, however, many of these strongly oversaturated solids had to be suppressed from precipitating for kinetic reasons in order to allow EQ3/6 to consider the other solids in the database file that were more likely to form under the conditions of the ICET experiments. In each input file, EQ3/6 allows the user to suppress the precipitation of as many as forty solids by name (Appendix B). In most of the ICET simulations for long time exposures, though, the starting source-term water composition had a high concentration of dissolved elements, and the list of strongly oversaturated phases in the database was greater than the maximum number that could be suppressed individually. Even by suppressing as many as forty phases, the remaining list of oversaturated phases for EQ3/6 to consider contained many other solids that still were not likely to form for kinetic reasons. As a result, in some of the simulations it was not possible, by suppressing phases, to restrict the list of precipitates to the desired small group of realistic candidates for precipitation. Developing the list of phases to suppress in each simulation was also

cumbersome because the saturation index of each phase varied depending on the source-term water composition of the specific simulation. To construct each input file, it was necessary to run EQ3/6 twice, first to calculate the saturation index of all relevant solids in the database in order to revise the EQ6 input file to add the list of phases to suppress in the actual simulation.

Other modeling approaches could be implemented with EQ3/6 to restrict the number of solid phases that were considered in the simulations, such as editing and recompiling the database file to limit the number of solid phases it contained, or specifying a list of “allowed” solids instead of “suppressed” solids for each simulation. Rather than repeat EQ3/6 simulations with another of these approaches, however, one of the other modeling codes from the code comparison exercise (Section 2) was used to perform a set of informed predictions taking advantage of observations and analytical data from the ICET experiments. Details of those simulations are provided in the next section.

5 INFORMED PREDICTIONS OF INTEGRATED CHEMICAL EFFECTS TEST RESULTS

The objective of the informed modeling predictions was to simulate the conditions and results of the Integrated Chemical Effects Test (ICET) experiments by using data and observations from the experiments to refine the modeling approach. The informed simulations were performed using the modeling code StreamAnalyzer, Version 2.0, developed by OLI Systems, Inc., for evaluating aqueous chemical processes in industrial and environmental applications. This version of StreamAnalyzer was one of the four modeling codes compared in the modeling exercise described in Section 2. The OLI thermodynamic database file, Public.dbb, was used with the modeling code for the informed simulations.

The first step in conducting simulations that would correspond more closely than blind predictions to the actual conditions of the ICET experiments was to modify several of the source terms that had been used to develop starting (input) water compositions for the modeling. These changes affected the source-term contribution of aluminum in simulations of ICETs #1, #3, #4, and #5 (Table 3-3) and the source-term concentrations of calcium and silicon in ICETs #3 and #4 (Table 3-8). Corrosion rates for aluminum metal and calcium silicate insulation were revised on the basis of Center for Nuclear Waste Regulatory Analyses (CNWRA) measurements described in Appendix A. The revised aluminum corrosion rate used for the simulations of ICETs #1 and #5 was based on weight-loss measurements in solutions that contained glass fiber insulation in addition to aluminum metal. The revised aluminum corrosion rates for simulations of ICETs #3 and #4 were based on corrosion rate measurements in borated solutions at pH 7 and pH 10 in the presence of calcium silicate insulation. The leaching tests for calcium silicate insulation material were performed using a sample-to-solution ratio equivalent to the ICET test plan (NRC, 2005) so the sample surface area did not have to be determined directly. The source-term contribution of the insulation was determined for calcium and silicon by measuring the concentration of these elements in solution at regular intervals during the leaching tests. In leaching tests at pH 7 with trisodium phosphate as an additive, the dissolved calcium and phosphate ions rapidly reacted to form a calcium phosphate precipitate, so the source-term calcium concentration was corrected to include the amount initially consumed by precipitation.

The general modeling approach in the informed predictions was similar to the approach used for the blind predictions in Section 4. Each ICET experiment was represented by a set of source-term water compositions at different times of exposure, estimated from the initial composition of the containment water and the corrosion rates of sample materials in the tests as described in Section 3. Simulations were performed for solutions at 0.5, 32, 148, and 360 hours of exposure, as was done for the blind predictions, and also at 720 hours [30 days] of exposure, which was the end point in all of the ICET experiments. Each modeling simulation assumed that the source-term water composition at the time of interest had not been modified by prior precipitation of secondary phases, regardless of the time of exposure.

On the basis of the results of the ICET experiments, in which no silica-bearing precipitates were conclusively identified, the precipitation of all silicate solid phases except amorphous silica was suppressed in the informed predictions by blocking the supplemental OLI database that contained the thermodynamic data for these minerals. Similarly, the precipitation of all carbonate solid phases was blocked by assuming that the source-term water did not equilibrate with atmospheric carbon dioxide. If dissolved carbon dioxide was included in the simulations,

the precipitation of calcite removed virtually all calcium from solution, contrary to what was observed in most of the ICET experiments. The precipitation of one other potentially oversaturated phase, aluminum hydroxide (gibbsite), was suppressed by excluding it individually in the input files.

5.1 Informed Predictions for ICET #1

ICET #1 was a 720-hour pilot-scale test at 60 °C [140 °F] to simulate post-loss-of-coolant accident (LOCA) conditions in an alkaline borated containment water using sodium hydroxide to control the pH at around 10. The water also contained boric acid, lithium hydroxide, and hydrochloric acid as additives. In this test, bags of Nukon low-density glass fiber insulation and samples of aluminum, copper, galvanized steel, carbon steel, and concrete were added to 949 L [250 gal] of alkaline borated containment water. The results of ICET #1 are documented in the experiment data report (Dallman, et al., 2005a).

Table 5-1 summarizes the source-term water composition for the modeled solutions at 0.5, 32, 148, 360, and 720 hours. The differences between the input starting compositions listed in Table 5-1 and the equivalent input data for ICET #1 in Table 4-1 are due to adjustments in source-term contributions based on the additional dissolution test data reported in Appendix A. (Similar differences exist for the other paired tables corresponding to input starting compositions for experiments ICETs #2 through #5.) The inputs as listed in Table 5-1 represent the “stream inflow” input file format used for StreamAnalyzer simulations. Note that in several cases, more than one sample material from the experiment has contributed to the source term concentration. For example, the aluminum concentration in the containment water is derived from reactions with aluminum metal (scaffolding, insulation jackets), glass fiber insulation, and concrete. The input files suppressed precipitation of aluminum hydroxide, $\text{Al}(\text{OH})_3$, because X-ray diffraction analysis of the ICET #1 debris indicated that a different phase, aluminum oxyhydroxide (AlOOH), precipitated in cooled samples during the test run.

The detailed results of an informed simulation are presented in Appendix C for the example at the exposure time of 148 hours, corresponding to the blind prediction example in Appendix B for the same set of conditions. The OLI StreamAnalyzer output file lists the input amounts of reactants; the amounts of reactants and products for the relevant aqueous species, vapor phases, and solid phases after the system has achieved chemical equilibrium; and supporting details about the calculations and relevant thermodynamic data for the simulation.

Table 5-2 lists the solid phases predicted to form in the borated alkaline containment water as a function of time at 60 °C [140 °F] under the conditions representative of ICET #1. Only two solid phases were predicted to form, an iron oxyhydroxide and a zinc oxyhydroxide. The predicted amounts in Table 5-2 are based on thermodynamic data for crystalline phases of these solids. Amorphous forms of these solids, which have higher solubilities, are more likely to form under the experiment conditions, so the predicted values are conservative estimates of the amounts expected to precipitate. The amounts formed are larger at increasing times of exposure because the source-term concentrations of iron and zinc in solution increase with time (Table 5-1).

Table 5-3 summarizes the dominant aqueous species for each element. No aqueous species of copper are listed because copper was considered thermodynamically stable as a solid (metal) by the modeling code and did not participate in speciation reactions.

Table 5-1. Source-Term Water Compositions in Borated Alkaline Containment Water at 60 °C [140 °F] for StreamAnalyzer Simulations of ICET* #1 Experiment Conditions

Inputs	Source Material	Amount Released [Mol] Per Liter of Alkaline Borated Containment Water				
		At 30 Minutes	At 32 Hours	At 148 Hours	At 360 Hours	At 720 Hours
Al	Scaffolding, Insulation Jackets	1.38×10^{-5}	8.85×10^{-4}	4.09×10^{-3}	9.96×10^{-3}	1.99×10^{-2}
Zn	Galvanized Steel	3.58×10^{-7}	2.99×10^{-5}	1.06×10^{-4}	2.57×10^{-4}	5.15×10^{-4}
Fe	Carbon and Stainless Steel	2.06×10^{-8}	1.32×10^{-6}	6.09×10^{-6}	1.48×10^{-5}	2.96×10^{-5}
Cu	Heat Exchanger, Fan Coolers	1.84×10^{-7}	1.18×10^{-5}	5.46×10^{-5}	1.33×10^{-4}	2.66×10^{-4}
SiO ₂	Nukon® Insulation, Concrete	2.70×10^{-4}	3.17×10^{-4}	4.49×10^{-4}	4.64×10^{-4}	4.88×10^{-4}
Al(OH) ₃	Nukon Insulation, Concrete	1.22×10^{-5}	1.65×10^{-5}	2.98×10^{-5}	4.16×10^{-5}	6.17×10^{-5}
Ca(OH) ₂	Nukon Insulation, Concrete	6.30×10^{-5}	9.76×10^{-5}	2.14×10^{-4}	4.12×10^{-4}	7.40×10^{-4}
Mg(OH) ₂	Nukon Insulation	1.13×10^{-5}	1.47×10^{-5}	2.40×10^{-5}	2.40×10^{-5}	2.40×10^{-5}
H ₃ BO ₃	Containment Water, Nukon Insulation	0.259	0.259	0.259	0.259	0.259
NaOH	Containment Water, Nukon Insulation	0.22	0.22	0.22	0.22	0.22
HCl	Containment Water	2.74×10^{-3}	2.74×10^{-3}	2.74×10^{-3}	2.74×10^{-3}	2.74×10^{-3}
LiOH	Containment Water	1.01×10^{-4}	1.01×10^{-4}	1.01×10^{-4}	1.01×10^{-4}	1.01×10^{-4}

*ICET = Integrated Chemical Effects Test

Table 5-2. Predicted Amount (mol) of Solid Phases Formed at 60 °C [140 °F], ICET* #1 Environment		
Time (h)	Fe(OH)₂	Zn(OH)₂
0.5	0	0
32	0	3.1×10^{-7}
148	1.2×10^{-6}	7.7×10^{-5}
360	1.0×10^{-5}	2.3×10^{-4}
720	2.4×10^{-5}	4.9×10^{-4}

*ICET = Integrated Chemical Effects Test

Table 5-3. Main Aqueous Species Predicted in the Alkaline Borated Containment Water at 60 °C [140 °F], ICET* #1 Environment (StreamAnalyzer Simulations)	
Element	Aqueous Species
Si	SiO ₂ , NaHSiO ₃ , H ₃ SiO ₄ ⁻¹
Ca	Ca ⁺² , CaHSiO ₃ ⁺¹
Al	Al(OH) ₄ ⁻¹
B	B(OH) ₃ , B(OH) ₄ ⁻¹ , B ₂ O(OH) ₅ ⁻¹ , B ₃ O ₃ (OH) ₄ ⁻¹ , B ₄ O ₅ (OH) ₄ ⁻²
Fe	Fe(OH) ₂ , Fe ⁺² , Fe(OH) ₃ ⁻¹ , FeOH ⁺¹
Mg	Mg ⁺² , MgOH ⁺¹
Na	Na ⁺¹
Zn	Zn(OH) ₂ , Zn ⁺² , ZnOH ⁺¹ , Zn(OH) ₃ ⁻¹

*ICET = Integrated Chemical Effects Test

Figures 5-1 through 5-3 show the concentrations of aluminum, calcium, and silicon, respectively, in the containment water as a function of time at 60 °C [140 °F]. Each figure shows data from three sources: the ICET #1 dataset represents measured concentrations from the ICET #1 experiment; the OLI Simulations dataset shows the solution concentrations from the informed prediction; and the Dissolution Test dataset provides, for comparison, the measured solution concentrations from Appendix A for the CNWRA dissolution test of Nukon low-density glass fiber insulation in the presence of aluminum in borated alkaline containment water.

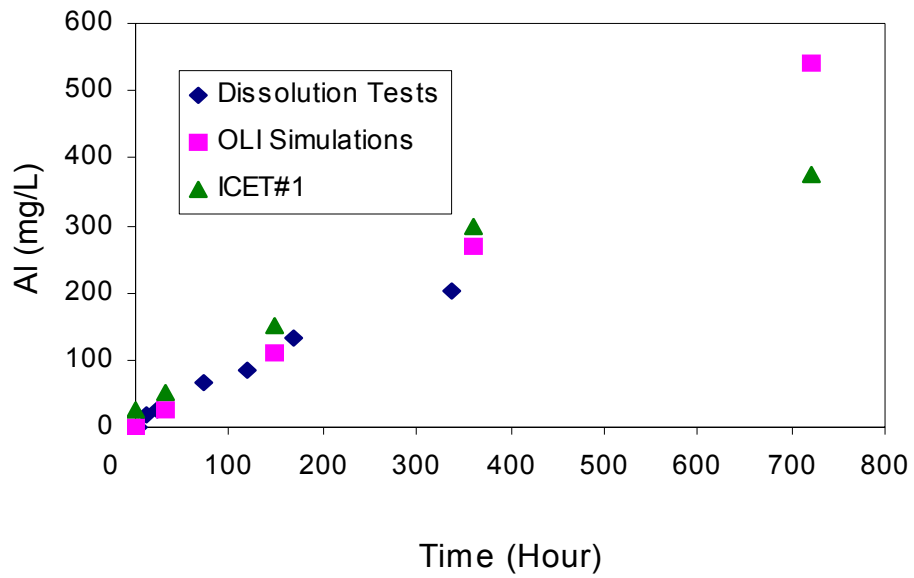


Figure 5-1. Aluminum Concentration From Informed Predictions (OLI) Compared With Data From ICET #1 and CNWRA Glass Fiber Dissolution Tests in the Presence of Aluminum Metal in Alkaline Borated Containment Water at 60 °C [140 °F]

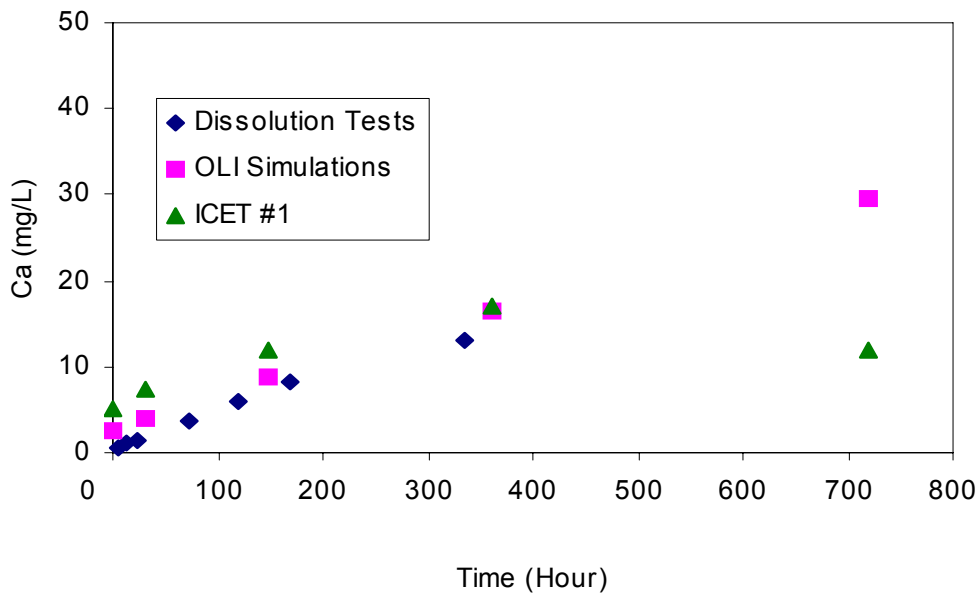


Figure 5-2. Calcium Concentration From Informed Predictions (OLI) Compared With Data From ICET #1 and CNWRA Glass Fiber Dissolution Tests in Alkaline Borated Containment Water at 60 °C [140 °F]

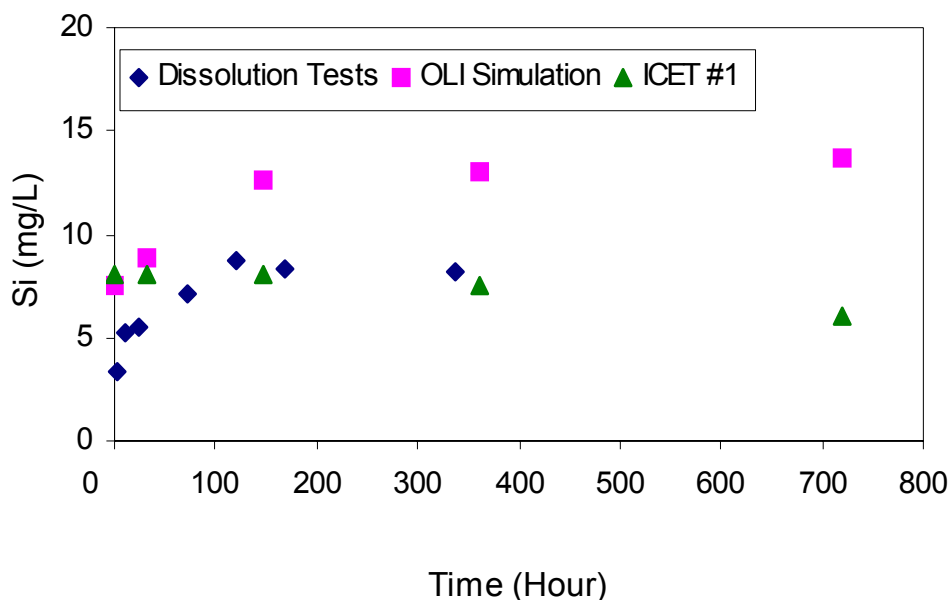


Figure 5-3. Silicon Concentration From Informed Predictions (OLI) Compared With Data From ICET #1 and CNWRA Glass Fiber Dissolution Tests in Alkaline Borated Containment Water at 60 °F [140 °F]

As indicated by Figure 5-4, the pH values predicted by the StreamAnalyzer simulations compare well with pH values as measured in ICET #1. In both cases, the pH remained between 9.6 and 9.8 for the time period ranging from 0.5 to 720 hours.

The informed predictions for calcium concentration provide good agreement with measured results for ICET #1 except that the simulated concentration is overpredicted at 720 hours (Figure 5-2). The concentration of silicon is overpredicted for the entire time period (Figure 5-3).

In contrast to the blind predictions, the formation of secondary aluminum solids in the informed simulations was suppressed by blocking the precipitation of aluminum hydroxide, and so the aluminum concentration in the informed predictions did not decrease due to precipitation. As noted in Section 4.1, a colloidal aluminum-bearing solid phase did form in the actual experiment, but it was not filtered out of the sampled water prior to analysis. In Figure 5-1, the predicted and measured dissolved aluminum concentrations are still comparable to each other, but in this case both datasets indicate total aluminum concentration, not the removal of precipitates. There is good general agreement between the predicted aluminum concentration and measured values through the first half of the experiment, but the aluminum concentration is overpredicted at 720 hours. This effect is attributed to an unaddressed change in the calculated source-term concentration of aluminum prior to this point in time. The estimated source-term contribution was based mainly on the corrosion rate for aluminum metal as determined by weight loss measurements up to 336 hours. These measurements indicated a linear increase in aluminum concentration with time (Figure A-9). However, this estimate did not account for passivity of aluminum at later times, as was observed in ICET #1 at or after 360 hours (Dallman, et al., 2005a). A change in the corrosion rate due to passivity, rather than removal of aluminum

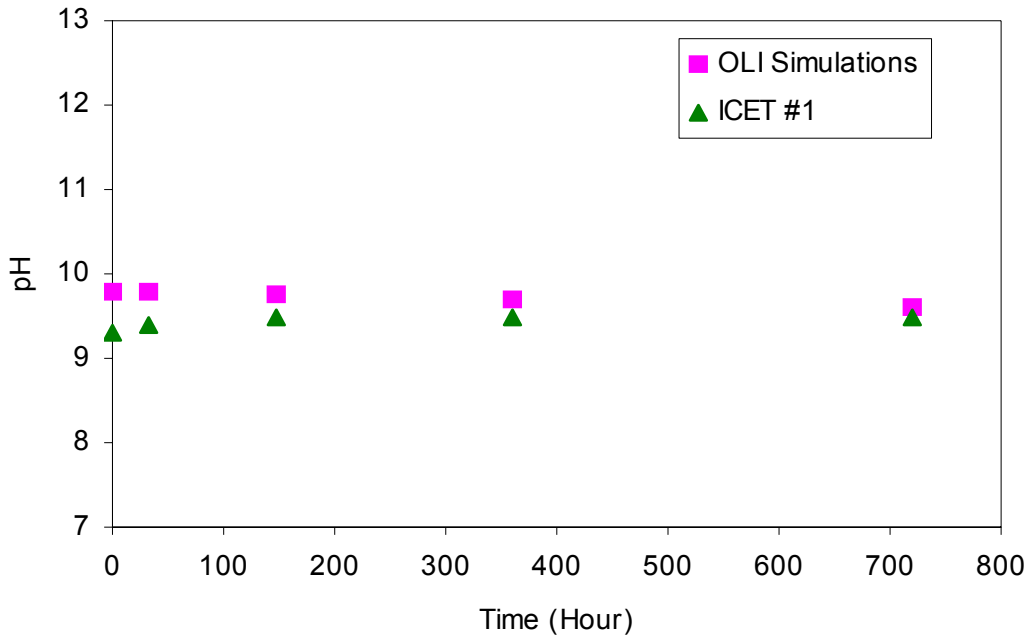


Figure 5-4. pH Values From Informed Predictions (OLI) Compared With the pH Measured in ICET #1

by precipitation of a secondary phase, is indicated by weight loss measurements of the aluminum coupons in ICET #1. These measurements indicated that the aluminum concentration in the solution after 360 hours was in good agreement with the total weight loss from the coupon after 720 hours. If the amount of aluminum contributed to the solution by the corrosion of aluminum metal is adjusted deliberately by the user for passivity at or after 360 hours, the thermodynamic simulations would predict the aluminum concentration to be closer to the measured aluminum concentration.

If the assumption is correct that no silicate or calcium carbonate solids would be removed from solution under the conditions modeled, then the overprediction of silicon and calcium concentrations is attributed to the use of conservative (high) dissolution rates for calculating releases from concrete.

5.2 Informed Predictions for ICET #2

ICET #2 was a 720-hour pilot-scale test at 60 °C [140 °F] to simulate LOCA conditions in borated containment water using trisodium phosphate to control the pH at near-neutral conditions. The initial test solution contained boric acid, lithium hydroxide, and hydrochloric acid, in addition to the trisodium phosphate. In this test, bags of Nukon low-density glass fiber insulation and samples of aluminum, copper, galvanized steel, carbon steel, and concrete were added to 949 L [250 gal] of trisodium phosphate borated containment water. The results of ICET #2 are documented in the experiment data report (Dallman, et al., 2005b).

Table 5-4 summarizes the source-term compositions for the modeled solutions at 60 °C [140 °F] for 0.5, 32, 148, 360, and 720 hours. The inputs as listed in Table 4-4 represent the “stream

Table 5-4. Source-Term Water Compositions in Borated Trisodium Phosphate Containment Water at 60 °C [140 °F] for Stream/Analyzer Simulations of ICET* #2 Experiment Conditions

Inputs	Source Material	Amount Released [Mol] Per Liter of Trisodium Phosphate Borated Containment Water					
		At 30 Minutes	At 32 Hours	At 148 Hours	At 360 Hours	At 720 Hours	
Al	Scaffolding, Insulation Jackets	4.12 x 10 ⁻⁸	2.63 x 10 ⁻⁶	1.22 x 10 ⁻⁵	2.96 x 10 ⁻⁵	5.93 x 10 ⁻⁵	
Zn	Galvanized steel	3.58 x 10 ⁻⁷	2.29 x 10 ⁻⁵	1.06 x 10 ⁻⁴	2.57 x 10 ⁻⁴	5.15 x 10 ⁻⁴	
Fe	Carbon and Stainless Steel	1.93 x 10 ⁻⁷	1.24 x 10 ⁻⁵	5.73 x 10 ⁻⁵	1.39 x 10 ⁻⁴	2.79 x 10 ⁻⁵	
Cu	Heat Exchanger, Fan Coolers	1.84 x 10 ⁻⁷	1.18 x 10 ⁻⁵	5.46 x 10 ⁻⁵	1.33 x 10 ⁻⁴	2.66 x 10 ⁻⁴	
SiO ₂	Nukon [®] Insulation, Concrete	1.25 x 10 ⁻⁴	3.81 x 10 ⁻⁴	1.32 x 10 ⁻³	3.05 x 10 ⁻³	5.98 x 10 ⁻³	
Al(OH) ₃	Nukon Insulation, Concrete	4.17 x 10 ⁻⁶	2.00 x 10 ⁻⁵	7.81 x 10 ⁻⁵	1.84 x 10 ⁻⁴	3.65 x 10 ⁻⁴	
Ca(OH) ₂	Nukon Insulation, Concrete	4.42 x 10 ⁻⁵	1.06 x 10 ⁻⁴	3.33 x 10 ⁻⁴	7.48 x 10 ⁻⁴	1.45 x 10 ⁻³	
Mg(OH) ₂	Nukon Insulation	3.05 x 10 ⁻⁷	1.95 x 10 ⁻⁵	9.02 x 10 ⁻⁵	2.19 x 10 ⁻⁴	4.39 x 10 ⁻⁴	
NaOH	Nukon Insulation	2.00 x 10 ⁻⁶	1.28 x 10 ⁻⁴	5.91 x 10 ⁻⁴	1.44 x 10 ⁻³	2.87 x 10 ⁻³	
H ₃ BO ₃	Containment Water, Nukon Insulation	0.259	0.259	0.259	0.259	0.259	
Na ₃ PO ₄	Containment Water	0.012	0.012	0.012	0.012	0.012	
HCl	Containment Water	2.74 x 10 ⁻³	2.74 x 10 ⁻³	2.74 x 10 ⁻³	2.74 x 10 ⁻³	2.74 x 10 ⁻³	
LiOH	Containment Water	1.01 x 10 ⁻⁴	1.01 x 10 ⁻⁴	1.01 x 10 ⁻⁴	1.01 x 10 ⁻⁴	1.01 x 10 ⁻⁴	

*ICET = Integrated Chemical Effects Test

inflow” format used for StreamAnalyzer simulations. Note that in several cases, more than one sample material from the experiment has contributed to the starting water composition. For example, the aluminum concentration is derived from reactions with aluminum metal (scaffolding, insulation jackets), glass fiber insulation, and concrete.

X-ray diffraction analysis of solids present at the end of ICET #2 indicated the potential formation of aluminum oxyhydroxide, AlOOH, and calcium phosphate, Ca₃(PO₄)₂, during the 720-hour test run. In the StreamAnalyzer simulation, precipitation of aluminum hydroxide, Al(OH)₃, and calcium oxyhydroxide phases was suppressed in order to allow aluminum oxyhydroxide or calcium phosphate to precipitate if they were oversaturated in the modeled containment water.

Table 5-5 lists the solid phases predicted to form in the borated trisodium phosphate containment water as a function of time at 60 °C [140 °F] under conditions representative of ICET #2. With the exception of SiO₂, which was predicted to be oversaturated at 720 hours, all of the solids that were predicted by StreamAnalyzer to form under these conditions were phosphorous-bearing phases. Even for low concentrations at low exposure times (0.5 hours), calcium phosphate was removed by precipitation from the starting solution. At later times, three additional phosphates were predicted to form as precipitates—a hydrated iron phosphate (vivianite), Fe₃(PO₄)₂•8H₂O, a hydrated zinc phosphate (hopeite), Zn₃(PO₄)₂•8H₂O, and an aluminum phosphate (berlinite), AlPO₄. The amounts removed from the solution for each phase increased at longer exposure times because the concentration of iron, zinc, and aluminum increased in the source-term solutions. Final aqueous concentrations for zinc, iron, and aluminum at 720 hours were low—0.1, 0.6, and 1.3 ppm, respectively— indicating that most of the initially dissolved portions of these metals were precipitated as phosphates, as indicated previously. At 720 hours, the code also predicted that a small amount of amorphous silicon dioxide would precipitate.

Table 5-6 summarizes the dominant aqueous species for each element. No aqueous species of copper are listed because copper was considered thermodynamically stable as a native metal by the modeling code and did not participate in subsequent speciation reactions.

Table 5-5. Predicted Amount (mol) of Solid Phases Formed in Trisodium Phosphate Borated Containment Water at 60 °C [140 °F], ICET* #2 Environment (StreamAnalyzer Simulations)					
Time (h)	SiO₂	Ca₃(PO₄)₂	Fe₃(PO₄)₂·8H₂O	Zn₃(PO₄)₂·8H₂O	AlPO₄
0.5	0	7.86 × 10 ⁻⁶	0	0	0
32	0	2.85 × 10 ⁻⁵	0	6.94 × 10 ⁻⁶	7.78 × 10 ⁻⁶
148	0	1.04 × 10 ⁻⁴	1.45 × 10 ⁻⁵	3.47 × 10 ⁻⁵	7.31 × 10 ⁻⁵
360	0	2.43 × 10 ⁻⁴	4.21 × 10 ⁻⁵	8.50 × 10 ⁻⁵	1.88 × 10 ⁻⁴
720	2.45 × 10 ⁻³	4.77 × 10 ⁻⁴	8.87 × 10 ⁻⁵	1.71 × 10 ⁻⁴	3.93 × 10 ⁻⁴
*ICET = Integrated Chemical Effects Test					

Table 5-6. Main Aqueous Species Predicted in the Trisodium Phosphate Borated Containment Water at 60 °C [140 °F], ICET* #2 Environment	
Element	Aqueous Species
Si	SiO ₂ , NaHSiO ₃ , H ₃ SiO ₄ ⁻¹
Ca	Ca ⁺² , CaHPO ₄ , CaPO ₄ ⁻¹ , CaHB ₂ O ₃ ⁺¹
Al	Al(OH) ₄ ⁻¹
B	B(OH) ₃ , B(OH) ₄ ⁻¹ , B ₂ O(OH) ₅ ⁻¹ , B ₃ O ₃ (OH) ₄ ⁻¹ , B ₄ O ₅ (OH) ₄ ⁻²
Fe	FeHPO ₄ , Fe(OH) ₂ , Fe ⁺² , FeOH ⁺¹
Mg	MgHPO ₄ , Mg ⁺² , MgOH ⁺¹ , MgPO ₄ ⁻¹ , MgP ₂ O ₇ ⁻²
Na	NaB(OH) ₄ , Na ⁺¹
Zn	ZnHPO ₄ , Zn(OH) ₂ , Zn ⁺² , ZnOH ⁺¹ , Zn(OH) ₃ ⁻¹ , ZnH ₂ PO ₄ ⁺¹
P	PO ₄ ⁻³ , P ₂ O ₇ ⁻⁴ , HPO ₄ ⁻² , HP ₂ O ₇ ⁻³ , H ₂ PO ₄ ⁻¹
*ICET = Integrated Chemical Effects Test	

Figures 5-5 through 5-7 show the concentrations of silicon, magnesium, and calcium, respectively, in the aqueous phase as a function of time at 60 °C [140 °F]. Each figure shows three data sets: the ICET #2 dataset represents measured concentrations from the ICET #2 experiment; the OLI Simulations dataset shows the solution concentrations from the informed prediction; and the Dissolution Test data set provides, for comparison, the measured solution concentrations from Appendix A for the CNWRA dissolution test of Nukon low-density glass fiber insulation in borated trisodium phosphate containment water. Results from all three datasets are in good agreement with respect to silicon concentration (Figure 5-5)—as is also the case for magnesium concentration except at 720 hours of exposure, where the measured value has decreased compared to the value at 360 hours of exposure (Figure 5-6). The observed calcium concentration in ICET #2 initially increases to values of about 8 ppm then levels off and decreases slightly at or after about 200 hours of exposure (Figure 5-7). The initial increase in calcium concentration is mirrored by the results of the dissolution test, but even at longer exposure times (336 hours), a linear increase in calcium concentration was indicated by the dissolution test results. In contrast to both sets of experiment data, the modeled concentration of calcium remains near zero through the simulation due to the predicted precipitation of calcium phosphate. The calculated pH varied from 7.05 at 30 minutes to 7.24 at 720 hours, a slight increase which corresponds to observation in ICET #2, in which the pH remained at values between 7.3 and 7.4 for most of the test (Dallman, et al., 2005b).

5.3 Informed Predictions for ICET #3

ICET #3 was a 720-hour pilot-scale test at 60 °C [140 °F] to simulate LOCA conditions in borated containment water using trisodium phosphate to control the pH at near neutral conditions. Except for adding calcium silicate insulation in ICET #3 as one of the tested sample materials, the experiment conditions for ICET #3 were basically identical to those for ICET #2.

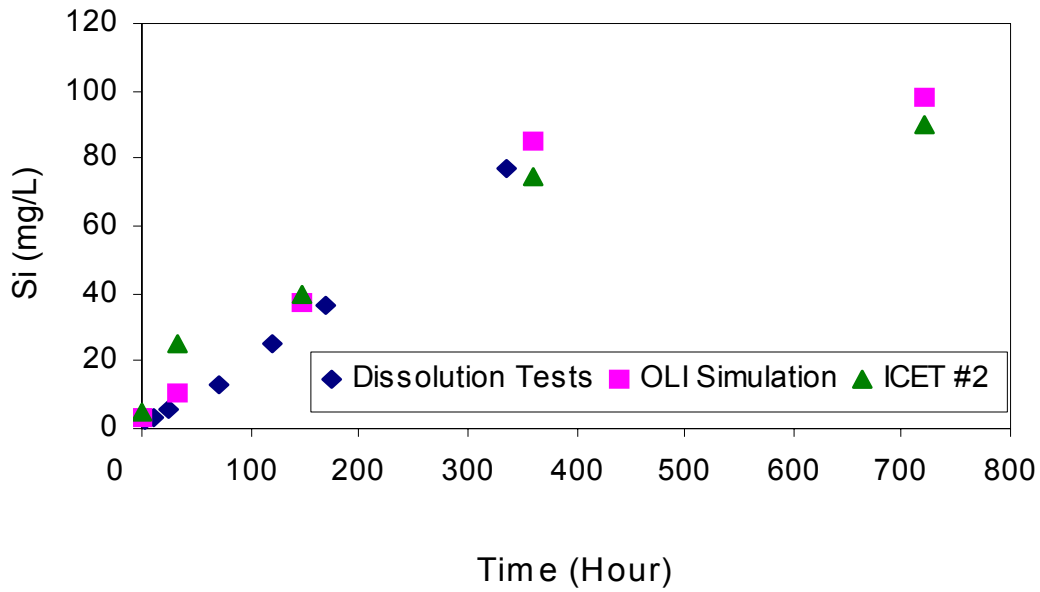


Figure 5-5. Silicon Concentration From Informed Predictions (OLI) Compared With Data From ICET #2 and CNWRA Glass Fiber Dissolution Tests in Trisodium Phosphate Borated Containment Water at 60 °C [140 °F]

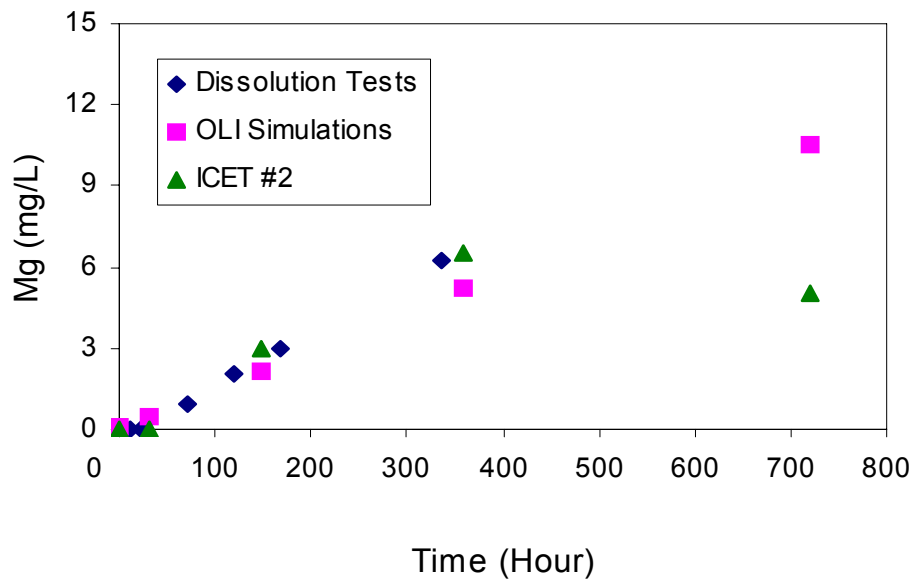


Figure 5-6. Magnesium Concentration From Informed Predictions (OLI) Compared With Data From ICET #2 and CNWRA Glass Fiber Dissolution Tests in Trisodium Phosphate Borated Containment Water at 60 °FC [140 °F]

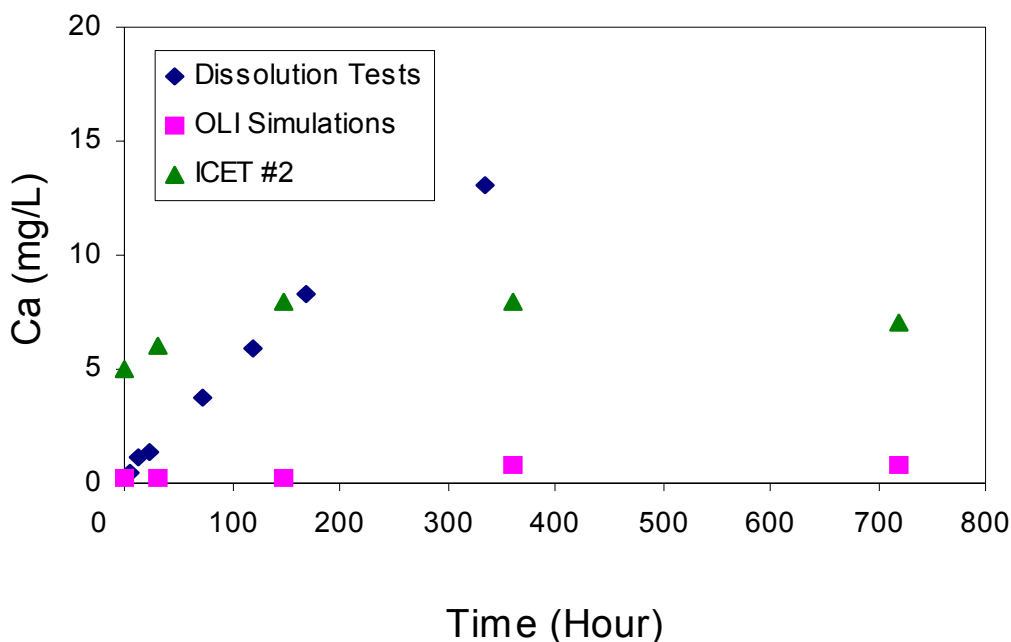


Figure 5-7. Calcium Concentration From Informed Predictions (OLI) Compared With Data From ICET #2 and CNWRA Glass Fiber Dissolution Tests in Trisodium Phosphate Borated Containment Water at 60 °C [140 °F]

The initial test solution contained boric acid, lithium hydroxide, and hydrochloric acid, in addition to the trisodium phosphate (Table 3-2). In this test, bags of calcium silicate insulation and Nukon low-density glass fiber insulation, in the proportion of 80:20 by volume, and samples of aluminum, copper, galvanized steel, carbon steel, and concrete were added to 949 L [250 gal] of trisodium phosphate borated containment water. The results of ICET #3 are documented in the experiment data report (Dallman, et al., 2005c).

Table 5-7 summarizes the source-term composition for the modeled solutions at 60 °C [140 °F] for 0.5, 32, 148, 360, and 720 hours. The inputs as listed in Table 5-7 represent the “stream inflow” format used for StreamAnalyzer simulations. Note that several sample materials in the experiment contributed certain elements to the starting water composition. For example, the silicon concentration is derived from reactions with calcium silicate insulation, glass fiber insulation, and concrete. The concentrations of calcium and silicon released to solution from the insulation material were estimated from the dissolution rate for calcium silicate (solid sample) that is listed in Table 3-8.

Given the similarity in experimental conditions for ICETs #2 and #3, the same set of solid phases was suppressed from precipitation, namely, aluminum hydroxide, $Al(OH)_3$, calcium oxyhydroxide, and all silicate phases except amorphous silicon dioxide, SiO_2 .

Table 5-8 shows the amount of solid phases predicted to form in ICET #3 as a function of time at 60 °C [140 °F]. Due to the large amount of silicon released to solution by the dissolution of calcium silicate insulation, the main precipitate predicted to form is amorphous SiO_2 . The

Table 5-7. Source-Term Water Compositions in Borated Trisodium Phosphate Containment Water at 60 °C [140 °F] for Stream Analyzer Simulations of ICET* #3 Experiment Conditions						
Inputs	Source Material	Amount Released (mol) Per Liter of Trisodium Phosphate Borated Containment Water				
		At 30 Minutes	At 32 Hours	At 148 Hours	At 360 Hours	At 720 Hours
Al	Scaffolding, Insulation Jackets	2.96 x 10 ⁻⁷	1.89 x 10 ⁻⁵	8.75 x 10 ⁻⁵	2.13 x 10 ⁻⁴	4.26 x 10 ⁻⁴
Zn	Galvanized Steel	3.58 x 10 ⁻⁷	2.29 x 10 ⁻⁵	1.06 x 10 ⁻⁴	2.57 x 10 ⁻⁴	5.15 x 10 ⁻⁴
Fe	Carbon and Stainless Steel	1.93 x 10 ⁻⁷	1.24 x 10 ⁻⁵	5.73 x 10 ⁻⁵	1.39 x 10 ⁻⁴	2.79 x 10 ⁻⁵
Cu	Heat Exchanger, Fan Coolers	1.84 x 10 ⁻⁷	1.18 x 10 ⁻⁵	5.46 x 10 ⁻⁵	1.33 x 10 ⁻⁴	2.66 x 10 ⁻⁴
SiO ₂	Nukon® Insulation, Concrete, Calcium Silicate Insulation	1.81 x 10 ⁻²	1.90 x 10 ⁻²	2.22 x 10 ⁻²	2.81 x 10 ⁻²	2.87 x 10 ⁻²
Al(OH) ₃	Nukon Insulation, Concrete	3.99 x 10 ⁻⁶	8.56 x 10 ⁻⁶	2.54 x 10 ⁻⁵	5.61 x 10 ⁻⁵	1.08 x 10 ⁻⁴
Ca(OH) ₂	Nukon Insulation, Concrete, Calcium Silicate Insulation	1.81 x 10 ⁻²	1.89 x 10 ⁻²	2.21 x 10 ⁻²	2.78 x 10 ⁻²	2.82 x 10 ⁻²
Mg(OH) ₂	Nukon Insulation	6.09 x 10 ⁻⁸	3.90 x 10 ⁻⁶	1.80 x 10 ⁻⁵	4.39 x 10 ⁻⁵	8.77 x 10 ⁻⁵
NaOH	Nukon Insulation	3.99 x 10 ⁻⁷	2.55 x 10 ⁻⁵	1.18 x 10 ⁻⁴	2.87 x 10 ⁻⁴	5.75 x 10 ⁻⁴
H ₃ BO ₃	Containment Water, Nukon Insulation	0.259	0.259	0.259	0.259	0.259
Na ₃ PO ₄	Containment Water	0.012	0.012	0.012	0.012	0.012
HCl	Containment Water	2.74 x 10 ⁻³	2.74 x 10 ⁻³	2.74 x 10 ⁻³	2.74 x 10 ⁻³	2.74 x 10 ⁻³
LiOH	Containment Water	1.01 x 10 ⁻⁴	1.01 x 10 ⁻⁴	1.01 x 10 ⁻⁴	1.01 x 10 ⁻⁴	1.01 x 10 ⁻⁴

*ICET = Integrated Chemical Effects Test

Time (h)	SiO ₂	Ca ₃ (PO ₄) ₂	Zn(OH) ₂
0.5	0.014	6.00 × 10 ⁻³	0
32	0.015	6.00 × 10 ⁻³	0
148	0.018	6.00 × 10 ⁻³	0
360	0.024	6.00 × 10 ⁻³	1.43 × 10 ⁻⁴
720	0.025	6.00 × 10 ⁻³	4.05 × 10 ⁻⁴

*ICET = Integrated Chemical Effects Test

starting containment water solutions at all times of exposure also were oversaturated with respect to calcium phosphate, Ca₃(PO₄)₂, which is predicted to precipitate in much greater amounts than in ICET #2. At long exposure times (360 and 720 hours), sufficient zinc was present in the starting solutions that a small amount of a third phase, zinc hydroxide, was predicted to form.

Table 5-9 summarizes the dominant aqueous species for each element. No aqueous species of copper are listed because copper was considered thermodynamically stable as a native metal by the modeling code and did not participate in subsequent speciation reactions.

Figures 5-8 through 5-11 show the concentrations of silicon, calcium, phosphorous, and magnesium, respectively, in the aqueous phase as a function of time at 60 °C [140 °F]. Each figure shows three datasets: the ICET #3 dataset represents measured concentrations from the experiment; the OLI Simulations dataset shows the solution concentrations from the informed prediction; and the Dissolution Test dataset provides, for comparison, the measured solution concentrations from Appendix A for the CNWRA dissolution test of calcium silicate insulation (solid sample) in borated trisodium phosphate containment water.

The silicon concentrations for all three data sets show good agreement (Figure 5-8), although predicted results are consistently higher than the measured values from ICET #3 and from the dissolution tests. In the insulation dissolution test, measured calcium concentrations increased initially to values of about 120 mg/L [0.001 lb/gal] and then began to level off (Figure 5-9). A similar, but lower, trend was noted for calcium concentrations in ICET #3. In contrast, the StreamAnalyzer simulations greatly overpredicted the dissolved calcium concentration, even with a large amount of calcium being removed from the solution in each simulation by the precipitation of calcium phosphate. As a result of the precipitation reaction, the StreamAnalyzer simulations also predicted that almost all of the phosphorous would be removed from solution by this reaction, as indicated in Figure 5-10. There is good agreement between this prediction and the results of ICET #3 and the dissolution tests, in which phosphorous concentration was observed to decrease almost immediately to values near zero. In addition, the experimenters noted during ICET #3 that the solution in the tank, which was already in contact with submerged calcium silicate insulation material, became turbid and cloudy as soon as trisodium phosphate

Table 5-9. Main Aqueous Species Predicted in the Trisodium Phosphate Borated Containment Water at 60 °C [140 °F], ICET* #3 Environment (StreamAnalyzer Simulations)	
Element	Aqueous Species
Si	SiO ₂ , NaHSiO ₃ , H ₃ SiO ₄ ⁻¹
Ca	Ca ⁺² , CaOH ⁺¹ , CaHSiO ₃ ⁺¹ , CaHPO ₄ , CaPO ₄ ⁻¹ , CaHB ₂ O ₃ ⁺¹
Al	Al(OH) ₄ ⁻¹
B	B(OH) ₃ , B(OH) ₄ ⁻¹ , B ₂ O(OH) ₅ ⁻¹ , B ₃ O ₃ (OH) ₄ ⁻¹ , B ₄ O ₅ (OH) ₄ ⁻²
Fe	FeHPO ₄ , Fe(OH) ₂ , Fe ⁺² , FeOH ⁺¹
Mg	MgHPO ₄ , Mg ⁺² , MgOH ⁺¹ , MgPO ₄ ⁻¹ , MgP ₂ O ₇ ⁻²
Na	NaB(OH) ₄ , Na ⁺¹
Zn	ZnHPO ₄ , Zn(OH) ₂ , Zn ⁺² , ZnOH ⁺¹ , Zn(OH) ₃ ⁻¹ , ZnH ₂ PO ₄ ⁺¹
P	PO ₄ ⁻³ , P ₂ O ₇ ⁻⁴ , HPO ₄ ⁻² , HP ₂ O ₇ ⁻³ , H ₂ PO ₄ ⁻¹

*ICET = Integrated Chemical Effects Test

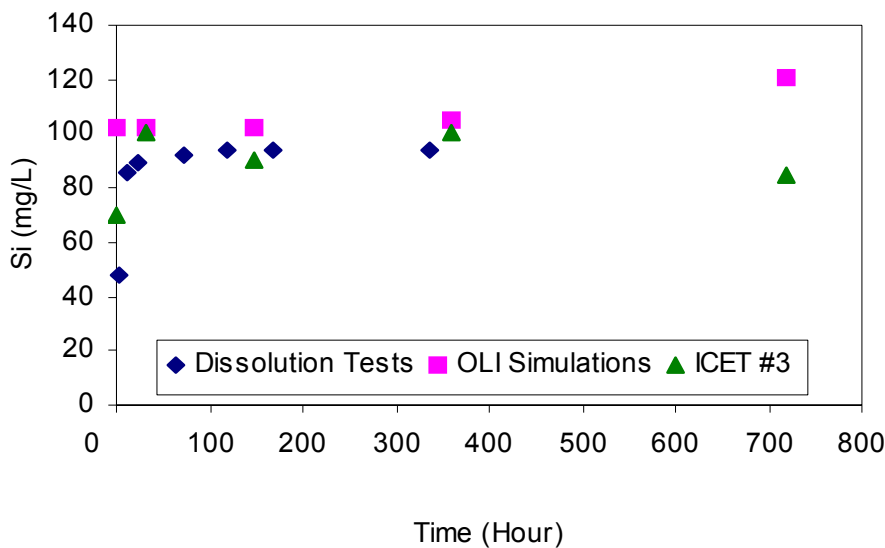


Figure 5-8. Silicon Concentration From Informed Predictions (OLI) Compared With Data From ICET #3 and CNWRA Calcium Silicate Dissolution Tests in Trisodium Phosphate Borated Containment Water at 60 °C [140 °F]

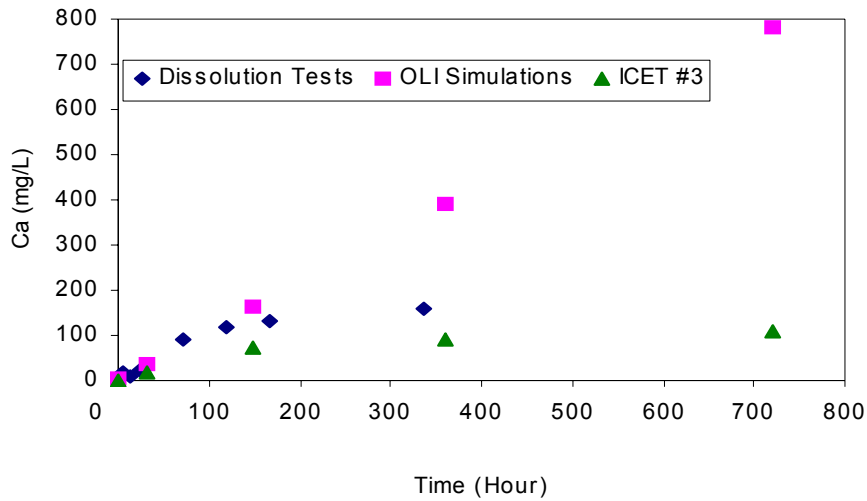


Figure 5-9. Calcium Concentration From Informed Predictions (OLI) Compared With Data From ICET #3 and CNWRA Calcium Silicate Dissolution Tests in Trisodium Phosphate Borated Containment Water at 60 °C [140°F]

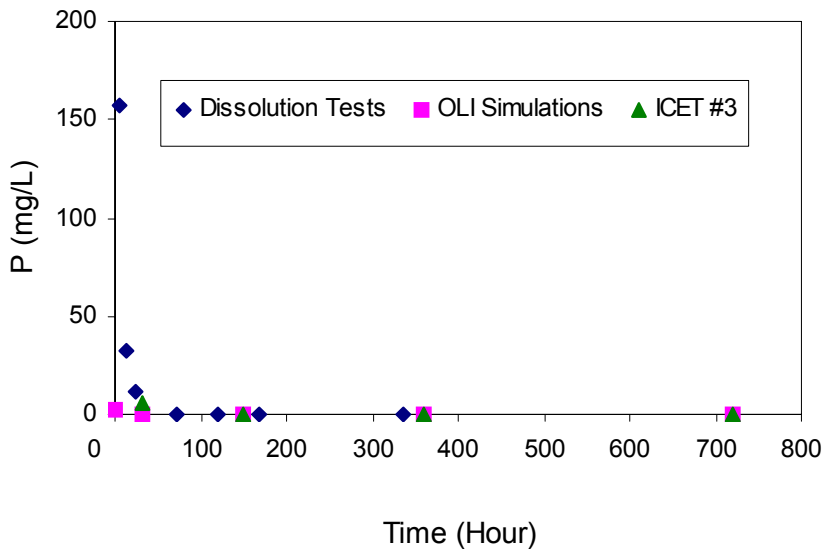


Figure 5-10. Phosphorous Concentration From Informed Predictions (OLI) Compared With Data From ICET #3 and CNWRA Calcium Silicate Dissolution Tests in Trisodium Phosphate Borated Containment Water at 60 °C [140 °F]

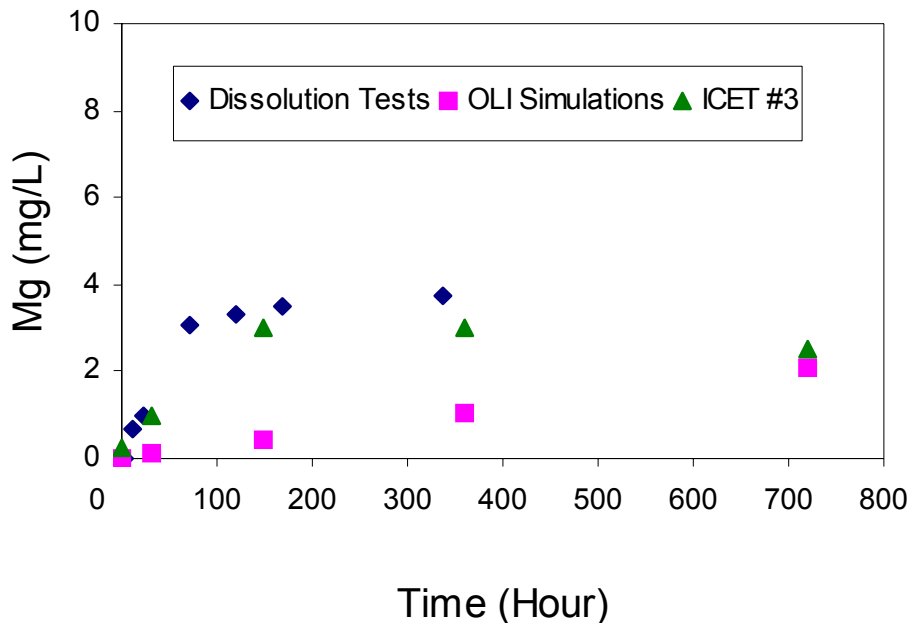


Figure 5-11. Magnesium Concentration From Informed Predictions (OLI) Compared With Data From ICET #3 and CNWRA Calcium Silicate Dissolution Tests in Trisodium Phosphate Borated Containment Water at 60 °C [140 °F]

was added to the water (Dallman, et al., 2005c). The predictions do not account for the observed decrease in calcium and silicon at later times.

The measured concentration of magnesium in ICET #3 is small, but it is similar to the result of the corresponding dissolution test (Figure 5-11). The measured concentrations are greater than the predicted concentrations (Figure 5-11). Because the modeling code does not predict that magnesium would be removed from solution by precipitation, the low predicted concentration indicates that the source-term concentration was slightly underestimated.

Though not shown in the figures, the predicted aqueous concentrations for zinc, iron, and aluminum reached maximum values of 7.2, 15.6, and 14.5 ppm, respectively, at 720 hours. However, in ICET #3, zinc, iron, and aluminum were not detected analytically in the aqueous phase.

Figure 5-12 compares the predicted pH from the thermodynamic simulations with the pH measured in ICET #3. At 60 °C [140 °F], the predicted and the measured pH values showed similar trends. The pH increased from near neutral to 7.8 within two days and remained constant at around 8 thereafter. The initial increase in the predicted and measured pH is attributed to the consumption of trisodium phosphate, which otherwise would have acted as a buffering agent.

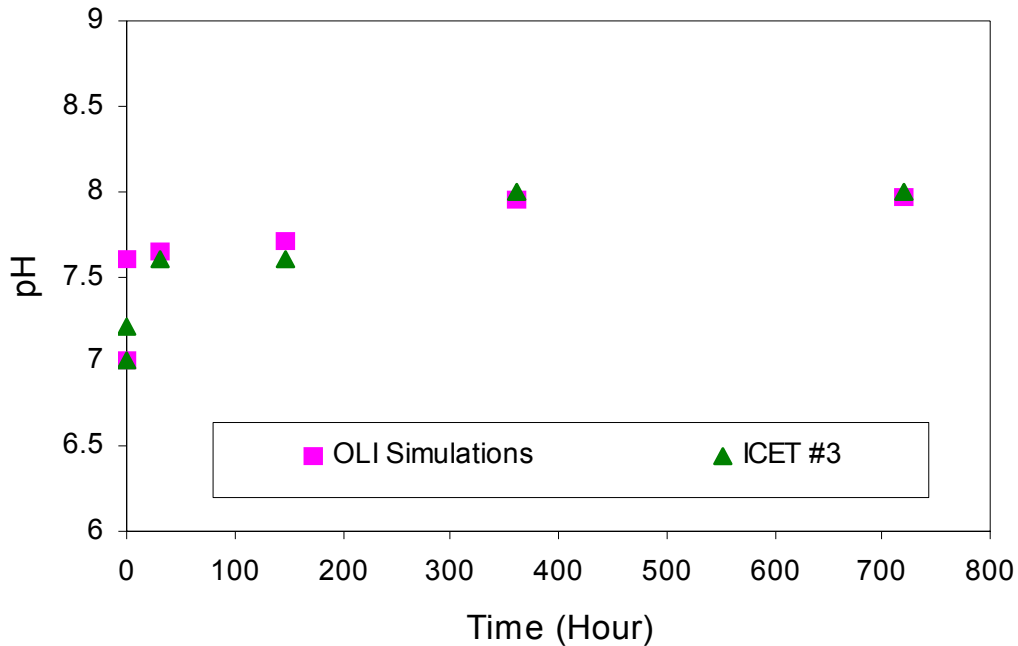


Figure 5-12. pH Values From Informed Predictions (OLI) Compared With the Measured pH in ICET #3

5.4 Informed Predictions for ICET #4

ICET #4 was a 720-hour pilot-scale test at 60 °C [140 °F] to simulate LOCA conditions in alkaline borated containment water using sodium hydroxide to control the pH at a value of about 10. Except for adding calcium silicate insulation as one of the tested sample materials, the experiment conditions for ICET #4 were the same as those for ICET #1. The initial test solution contained boric acid, lithium hydroxide, and hydrochloric acid, in addition to the sodium hydroxide (Table 3-2). In this test, bags of calcium silicate insulation and Nukon low-density glass fiber insulation, in the proportion 80:20 by volume, and samples of aluminum, copper, galvanized steel, carbon steel and concrete were added to 949 L [250 gal] of alkaline borated containment water. The results of ICET #4 are documented in the experiment data report (Dallman, et al., 2005d).

Table 5-10 summarizes the source-term water composition for the modeled solutions at 60 °C [140 °F] for 0.5, 32, 148, 360, and 720 hours. The inputs as listed in Table 5-10 represent the “stream inflow” format used for StreamAnalyzer simulations. Note that several sample materials in the experiment contributed to the concentration of certain elements to the starting water composition. For example, the dissolved silicon is derived from reactions with calcium silicate insulation, glass fiber insulation, and concrete. The source-term concentrations of calcium and silicon released to the solution from the insulation material were estimated mainly from the dissolution rate for calcium silicate (solid sample) in alkaline borated containment water as listed in Table 3-8. Note that the source-term concentrations of calcium and silicon are considerably larger than those for ICET #1 due to the presence of calcium silicate insulation in ICET #4. The source-term contribution of aluminum to the solution due to corrosion of aluminum metal for

Table 5-10. Source-Term Water Compositions in Borated Alkaline Containment Water at 60 °C [140 °F] for StreamAnalyzer Simulations of ICET* #4 Experiment Conditions						
Inputs	Source Material	Amount Released (mol) Per Liter of Alkaline Borated Containment Water				
		At 30 Minutes	At 32 Hours	At 148 Hours	At 360 Hours	At 720 Hours
Al	Scaffolding, Insulation Jackets	1.04×10^{-5}	5.40×10^{-4}	2.50×10^{-3}	6.08×10^{-3}	1.22×10^{-2}
Zn	Galvanized steel	3.58×10^{-7}	2.99×10^{-5}	1.06×10^{-4}	2.57×10^{-4}	5.15×10^{-4}
Fe	Carbon and Stainless Steel	2.06×10^{-8}	1.32×10^{-6}	6.09×10^{-6}	1.48×10^{-5}	2.96×10^{-5}
Cu	Heat Exchanger, Fan Coolers	1.84×10^{-7}	1.18×10^{-5}	5.46×10^{-5}	1.33×10^{-4}	2.66×10^{-4}
SiO ₂	Nukon® Insulation, Concrete, Calcium Silicate Insulation	2.01×10^{-3}	3.00×10^{-3}	6.64×10^{-3}	1.33×10^{-2}	2.46×10^{-2}
Al(OH) ₃	Nukon Insulation, Concrete	5.60×10^{-6}	7.86×10^{-6}	1.62×10^{-5}	3.14×10^{-5}	5.72×10^{-5}
Ca(OH) ₂	Nukon Insulation, Concrete, Calcium Silicate Insulation	8.57×10^{-4}	9.89×10^{-4}	1.48×10^{-3}	2.37×10^{-3}	3.88×10^{-3}
Mg(OH) ₂	Nukon Insulation	2.26×10^{-6}	2.94×10^{-6}	5.45×10^{-6}	1.00×10^{-5}	1.78×10^{-5}
H ₃ BO ₃	Containment Water, Nukon Insulation	0.259	0.259	0.259	0.259	0.259
NaOH	Containment Water, Nukon Insulation	0.22	0.22	0.22	0.22	0.22
HCl	Containment Water	2.74×10^{-3}	2.74×10^{-3}	2.74×10^{-3}	2.74×10^{-3}	2.74×10^{-3}
LiOH	Containment Water	1.01×10^{-4}	1.01×10^{-4}	1.01×10^{-4}	1.01×10^{-4}	1.01×10^{-4}

*ICET = Integrated Chemical Effects Test

conditions representative of ICET #4 is slightly less than the amount estimated for ICET #1 (Table 4-1). To conform to the same assumptions that were made for the simulations for ICET #1, silicate phases (with the exception of amorphous silicon dioxide) and aluminum hydroxide [Al(OH)₃] were not allowed to precipitate.

Table 5-11 shows the predicted amount of solid phases formed in the alkaline borated containment water as a function of time at 60 °C [140 °F]. Results are almost identical to those predicted for the simulations of ICET #1 (Table 5-2), with zinc hydroxide precipitating in the solution at 32 hours of exposure and with zinc hydroxide and ferrous oxyhydroxide forming in the solutions at later exposure times. No aluminum-bearing phases are predicted to precipitate.

Table 5-12 summarizes the dominant aqueous species for each element. No aqueous species of copper are listed because copper was considered thermodynamically stable by the modeling code and did not participate in subsequent speciation reactions.

Table 5-11. Predicted Amount (mol) of Solid Phases Formed at 60 °C [140 °F], ICET* #4 Environment		
Time (h)	Fe(OH)₂	Zn(OH)₂
0.5	0	0
32	0	5.1×10^{-7}
148	1.1×10^{-6}	7.8×10^{-5}
360	9.2×10^{-6}	2.3×10^{-4}
720	2.2×10^{-5}	4.9×10^{-4}

*ICET = Integrated Chemical Effects Test

Table 5-12. Main Aqueous Species Predicted in the Trisodium Phosphate Borated Containment Water at 60 °C [140 °F], ICET* #4 Environment (StreamAnalyzer Simulations)	
Element	Aqueous Species
Si	SiO ₂ , NaHSiO ₃ , H ₃ SiO ₄ ⁻¹
Ca	Ca ⁺² , CaOH ⁺¹ , CaHSiO ₃ ⁺¹ , CaHB ₂ O ₃ ⁺¹
Al	Al(OH) ₄ ⁻¹
B	B(OH) ₃ , B(OH) ₄ ⁻¹ , B ₂ O(OH) ₅ ⁻¹ , B ₃ O ₃ (OH) ₄ ⁻¹ , B ₄ O ₅ (OH) ₄ ⁻²
Fe	Fe(OH) ₂ , Fe ⁺² , FeOH ⁺¹
Mg	Mg ⁺² , MgOH ⁺¹
Na	NaB(OH) ₄ , Na ⁺¹
Zn	Zn(OH) ₂ , Zn ⁺² , ZnOH ⁺¹ , Zn(OH) ₃ ⁻¹

*ICET = Integrated Chemical Effects Test

Figures 5-13 through 5-15 show the concentrations of silicon, calcium, and aluminum, respectively, in the aqueous phase as a function of time at 60 °C [140 °F]. Each figure shows three datasets: the ICET #4 dataset represents measured concentrations from the experiment; the OLI Simulations dataset shows the final solution concentrations at each time of exposure in the informed predictions; and the Dissolution Test dataset provides, for comparison, the measured solution concentrations from Appendix A for the CNWRA dissolution test of calcium silicate insulation (solid sample) in borated alkaline containment water. Though not shown in the figures, the maximum predicted final concentrations for zinc, iron, and magnesium are 1.6, 0.4, and 0.4 ppm, respectively, at 720 hours, values that conform to the trace amounts reported for ICET #4 (Dallman, et al., 2005d).

The measured silicon concentrations from the dissolution tests conform closely to the measured values from ICET #4 (Figure 5-13). Silicon concentrations as predicted by StreamAnalyzer are in good agreement with these values up to exposure times of about 148 hours, after which the silicon concentrations are considerably overpredicted compared to the measured data. Similarly, good agreement was obtained for the predicted concentrations of calcium, compared to measured values, for times up to 148 hours, after which the measured rates leveled off but predicted values increased (Figure 5-14).

The measured and simulated results for ICET #1 and the corresponding dissolution tests all indicated a steady and substantial increase in dissolved aluminum over time in borated alkaline

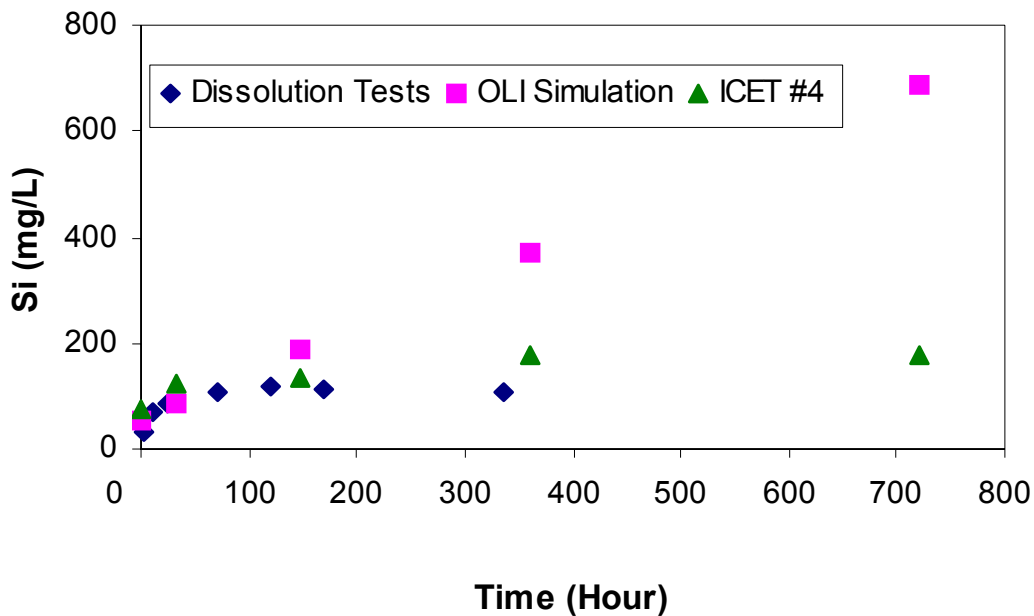


Figure 5-13. Silicon Concentration From Informed Predictions (OLI) Compared With Data From ICET #4 and CNWRA Calcium Silicate Dissolution Tests in Alkaline Borated Containment Water at 60 °C [140 °F]

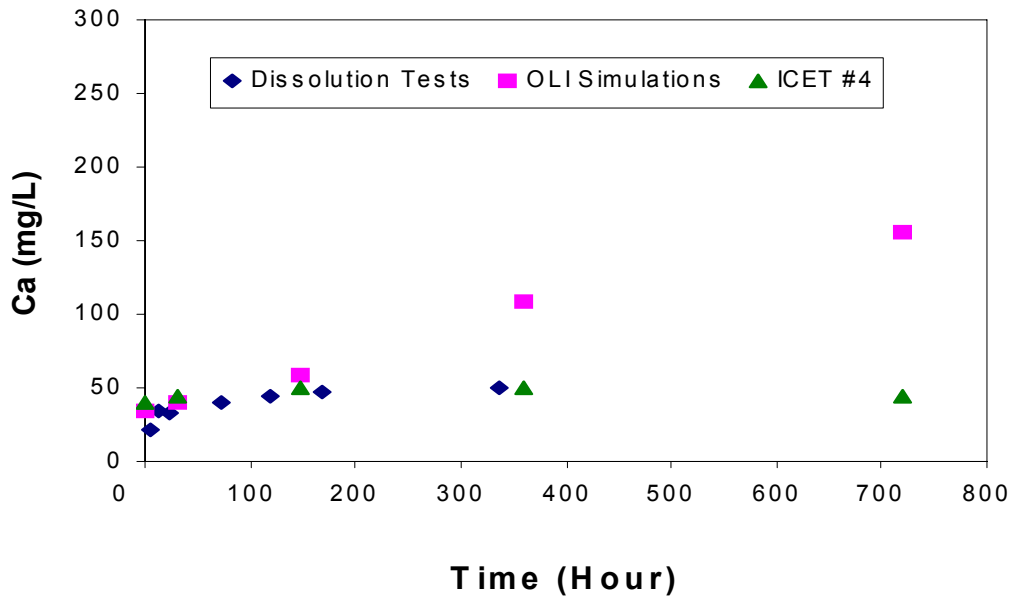


Figure 5-14. Calcium Concentration From Informed Predictions (OLI) Compared With Data From ICET #4 and CNWRA Calcium Silicate Dissolution Tests in Alkaline Borated Containment Water at 60 °C [140 °F]

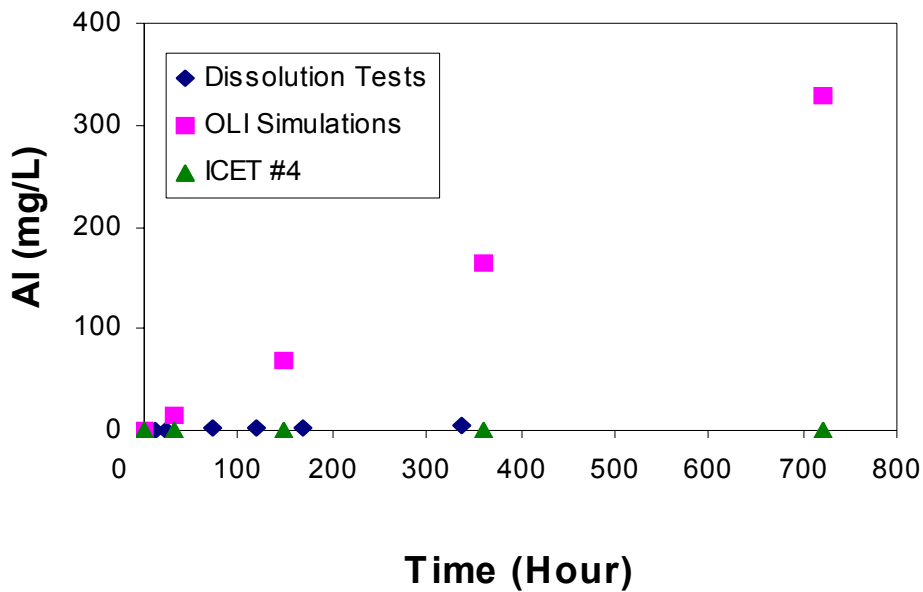


Figure 5-15. Aluminum Concentration From Informed Predictions (OLI) Compared With Data From ICET #4 and CNWRA Calcium Silicate Dissolution Tests in Alkaline Borated Containment Water at 60 °C [140 °F]

containment water (Figure 5-2). In distinct contrast, the measured results for ICET #4 and the corresponding dissolution tests indicated that little or no aluminum was present in solution throughout the experiment. The StreamAnalyzer simulations for ICET #4 were based on the same source-term contributions and solubility constraints assumptions as for ICET #1, but for ICET #4 the aluminum concentrations were greatly overpredicted at and beyond 148 hours of exposure (Figure 5-15).

The predicted pH from the thermodynamic simulations decreased slightly over time (from 9.8 to 9.5) and was slightly lower compared to the pH measured in ICET #4 in the alkaline borated containment water, which varied between 9.7 and 9.9 at 60 °C [140 °F]. The slightly higher observed pH in ICET #4 could be attributed to the release of sodium from the dissolution of sodium silicate, which is present as an impurity in the calcium silicate insulation. The source-term calculations ignored the presence of sodium silicate as a possible reactant.

Predictions based on the thermodynamic calculations provided good agreement for silicon and calcium release in the aqueous phase, as compared with ICET #4 data and the corresponding CNWRA dissolution measurements up to 148 hours. However, beyond this timeframe, the concentrations of calcium and silicon were significantly overpredicted. The discrepancy can be attributed to two possibilities: either the dissolution of calcium silicate insulation was inhibited by the formation of a passive film as the exposure time increased, or calcium and silicon precipitated in solids that were not included in the modeling simulations. Although a cloudy particulate phase and some secondary deposits were observed to form during ICET #4 (Dallman, et al., 2005d), no definitive calcium-bearing or silicon-bearing precipitates were identified. Also, it would be unusual for a calcium-bearing solid and a silicon-bearing solid to precipitate independently of each other in proportions that would result in trends for calcium and silicon that are essentially parallel to each other, as indicated in Figures 5-13 and 5-14. A more likely explanation is that the dissolution was physically inhibited after 148 hours in some way, such as by the formation of a surface coating.

The informed predictions for ICET #4 also significantly overpredicted the final aluminum concentration. Weight loss measurement for aluminum coupons at the conclusion of ICET #4 indicated no measurable loss of aluminum (Dallman, et al., 2005d), suggesting the passivity of aluminum metal in the presence of calcium-silicate insulation.

5.5 Informed Predictions for ICET #5

ICET #5 was a 720-hour pilot-scale test at 60 °C [140 °F] to simulate LOCA conditions in a sodium borate containment water using sodium tetraborate to adjust the pH to values between 8.2 and 8.4. The initial test solution contained boric acid, lithium hydroxide, and hydrochloric acid, in addition to the sodium tetraborate (Table 3-2). With the exception of the changes in buffering additives to obtain a lower initial pH, test conditions were identical to ICET #1 and included bags of Nukon low-density glass fiber insulation and samples of aluminum, copper, galvanized steel, carbon steel, and concrete, which were added to 949 L [250 gal] of sodium borated containment water. The results of ICET #5 are documented in the experiment report (Dallman, et al., 2005e).

The source-term concentrations for simulations of ICET #5 were based on the conservative assumption that the corrosion rates in a pH 8 environment could be represented by using the same rates as for a pH 10 environment (ICET #1 conditions). Table 5-13 summarizes the input

Table 5-13. Source-Term Water Compositions in Borated Slightly Alkaline Containment Water at 60 °C [140 °F] for Stream/Analyzer Simulations of ICET* #5 Experiment Conditions

Input	Source Material	Amount Released (mol) Per Liter of Sodium Borate Containment Water				
		At 30 Minutes	At 32 Hours	At 148 Hours	At 360 Hours	At 720 Hours
Al	Scaffolding, Insulation Jackets	1.38×10^{-5}	8.85×10^{-4}	4.09×10^{-3}	9.96×10^{-3}	1.99×10^{-2}
Zn	Galvanized steel	3.58×10^{-7}	2.99×10^{-5}	1.06×10^{-4}	2.57×10^{-4}	5.15×10^{-4}
Fe	Carbon and Stainless Steel	2.06×10^{-8}	1.32×10^{-6}	6.09×10^{-6}	1.48×10^{-5}	2.96×10^{-5}
Cu	Heat Exchanger, Fan Coolers	1.84×10^{-7}	1.18×10^{-5}	5.46×10^{-5}	1.33×10^{-4}	2.66×10^{-4}
SiO ₂	Nukon® Insulation, Concrete	2.70×10^{-4}	3.17×10^{-4}	4.49×10^{-4}	4.64×10^{-4}	4.88×10^{-4}
Al(OH) ₃	Nukon Insulation, Concrete	1.22×10^{-5}	1.65×10^{-5}	2.98×10^{-5}	4.16×10^{-5}	6.17×10^{-5}
Ca(OH) ₂	Nukon Insulation, Concrete	6.30×10^{-5}	9.76×10^{-5}	2.14×10^{-4}	4.12×10^{-4}	7.40×10^{-4}
Mg(OH) ₂	Nukon Insulation	1.13×10^{-5}	1.47×10^{-5}	2.40×10^{-5}	2.40×10^{-5}	2.40×10^{-5}
H ₃ BO ₃	Containment Water, Nukon Insulation	0.217	0.217	0.217	0.217	0.217
NaOH	Containment Water, Nukon Insulation	0.057	0.057	0.057	0.057	0.057
HCl	Containment Water	2.74×10^{-3}	2.74×10^{-3}	2.74×10^{-3}	2.74×10^{-3}	2.74×10^{-3}
LiOH	Containment Water	1.01×10^{-4}	1.01×10^{-4}	1.01×10^{-4}	1.01×10^{-4}	1.01×10^{-4}

*ICET = Integrated Chemical Effects Test

starting composition, or source term, for the modeled solutions at 60 °C [140 °F] for 0.5, 32, 148, 360, and 720 hours. The inputs as listed in Table 5-13 represent the “stream inflow” format used for StreamAnalyzer simulations. Note that several sample materials in the experiment contributed to the concentration of certain elements to the starting water composition. The concentration of silicon in solution was limited by the assumption that the dissolution of Nukon low-density fiber insulation dissolution was inhibited in the presence of aluminum, as documented by dissolution tests in Appendix A. Except for different concentrations of sodium and boron, the overall source terms in Table 5-13 are identical to the values at equivalent exposure times for ICET #1 in Table 5-1.

Table 5-14 shows the amount of solid phases predicted to form in the ICET #5 sodium borate containment water as a function of time at 60 °C [140 °F]. To conform to the same assumptions that were made for the ICET #1 simulations, silicate phases (with the exception of amorphous silicon dioxide) and aluminum hydroxide [Al(OH)₃] were not allowed to precipitate. The solid phases predicted to form were the same as for ICET #1, minor amounts of zinc hydroxide and ferrous oxyhydroxide.

Table 5-15 summarizes the dominant aqueous species for each element. No aqueous species of copper are listed because copper was considered thermodynamically stable as a native metal by the modeling code and did not participate in subsequent speciation reactions.

Figures 5-16 through 5-18 show the concentrations of silicon, calcium, and aluminum, respectively, in the aqueous phase as a function of time at 60 °C [140 °F]. Each figure shows three datasets: the ICET #5 dataset represents measured aqueous concentrations from the experiment; the OLI Simulations dataset shows the final solution concentrations at each time of exposure in the informed predictions; and the CNWRA dissolution test dataset provides, for comparison, the measured solution concentrations from Appendix A for the CNWRA dissolution test of Nukon low-density glass fiber insulation in the presence of aluminum in borated alkaline containment water at pH 10. Although not shown in the figures, the predicted final concentrations for magnesium, iron, and zinc were 0.6, 1.7, and 9.4 ppm, respectively, at 720 hours, conforming to low concentrations reported in ICET #5 (Dallman, et al., 2005e). Although the absence of measurable iron or zinc is attributed to precipitation in the simulations, the low concentrations also could be due to the passivity of metal surfaces with time or to the

Table 5-14. Predicted Amount (mol) of Solid Phases Formed at 60 °C [140 °F], ICET* #5 Environment	
Time (h)	Zn(OH)₂
0.5	0
32	0
148	3.4×10^{-5}
360	1.7×10^{-4}
720	3.7×10^{-4}

*ICET = Integrated Chemical Effects Test

Table 5-15. Main Aqueous Species Predicted in the Slightly Alkaline Borated Containment Water at 60 °C [140 °F], ICET* #5 Environment (StreamAnalyzer Simulations)	
Element	Aqueous Species
Si	SiO ₂ , NaHSiO ₃ , H ₃ SiO ₄ ⁻¹
Ca	Ca ⁺² , CaHSiO ₃ ⁺¹
Al	Al(OH) ₄ ⁻¹
B	B(OH) ₃ , B(OH) ₄ ⁻¹ , B ₂ O(OH) ₅ ⁻¹ , B ₃ O ₃ (OH) ₄ ⁻¹ , B ₄ O ₅ (OH) ₄ ⁻²
Fe	Fe(OH) ₂ , Fe ⁺² , Fe(OH) ₃ ⁻¹ , FeOH ⁺¹
Mg	Mg ⁺² , MgOH ⁺¹
Na	Na ⁺¹
Zn	Zn(OH) ₂ , Zn ⁺² , ZnOH ⁺¹ , Zn(OH) ₃ ⁻¹

*ICET = Integrated Chemical Effects Test

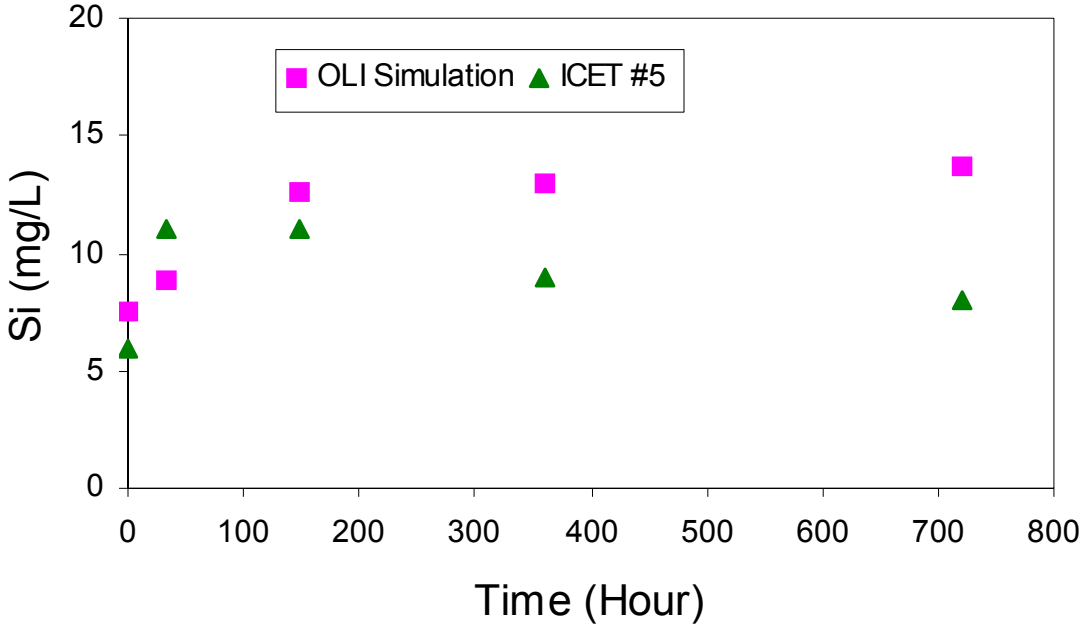


Figure 5-16. Silicon Concentration From Informed Predictions (OLI) Compared With Data From ICET #5 in Sodium Borate Containment Water at 60°C [140 °F]

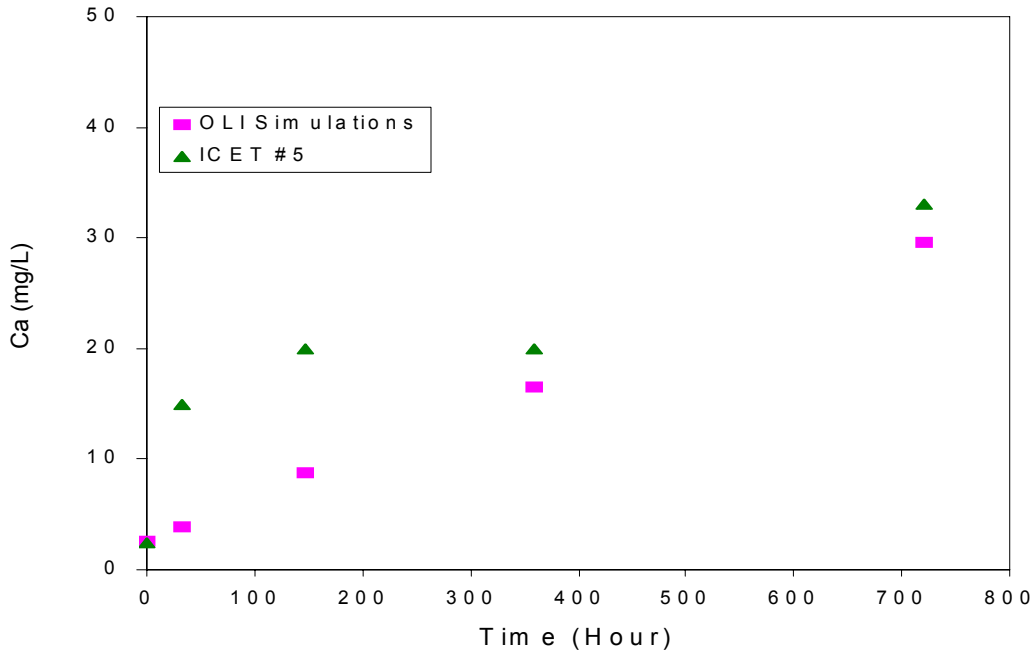


Figure 5-17. Calcium Concentration From Informed Predictions (OLI) Compared With Data From ICET #5 in Sodium Borate Containment Water at 60 °C [140 °F]

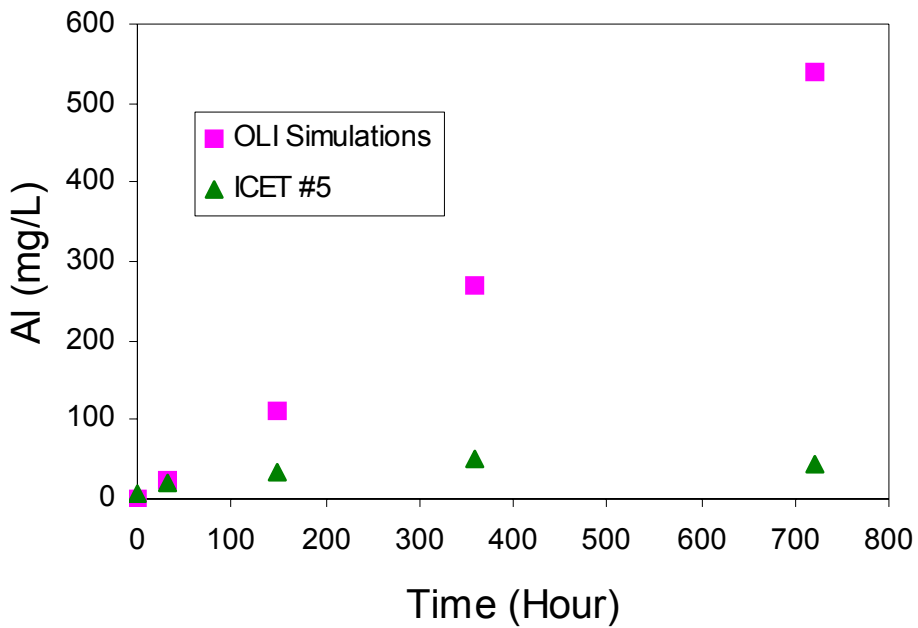


Figure 5-18. Aluminum Concentration From Informed Predictions (OLI) Compared With Data From ICET #5 in Sodium Borate Containment Water at 60 °C [140 °F]

uncertainty in the assumed corrosion rates at pH 10, which may have overestimated the actual source-term contributions at pH 8.

Figure 5-19 compares the predicted pH from thermodynamic simulations with the pH measured in ICET #5 in the sodium borate containment water. At 60 °C [140 °F], the predicted pH in the sodium borate containment water was slightly lower compared to the measured pH in ICET #5. The predicted pH remained between 7.9 and 8.2, while measured pH in ICET #5 remained between 8.2 and 8.4 over the time period of 0.5 to 720 hours. The pH in both cases showed a slight decrease with time.

With the exception of aluminum, the informed predictions provided good agreement with the dataset for ICET #5. The overprediction of final aluminum concentration is attributed in part to the fact that the source-term estimate ignored the passivity of aluminum metal at or after 360 hours. The passivity of aluminum in ICET #5 was confirmed by weight loss measurements of the aluminum coupons at the end of the experiment, which indicated a good agreement between aluminum concentration in solution at 360 hours and the total weight loss after 720 hours (Dallman, et al., 2005e). However, even if the source-term contribution of aluminum is adjusted to account for passivity at or after 360 hours, the predicted aluminum concentration for ICET #5 at 720 hours would still be significantly higher compared to the measured concentration. Lower source-term aluminum concentrations would be calculated by using a lower corrosion rate at pH 8. In fact, the aluminum corrosion rate at pH 7 is almost negligible. However, to estimate the corrosion rate at pH 8 with more confidence, additional measurements would be necessary using ICET #5 conditions and sample proportions.

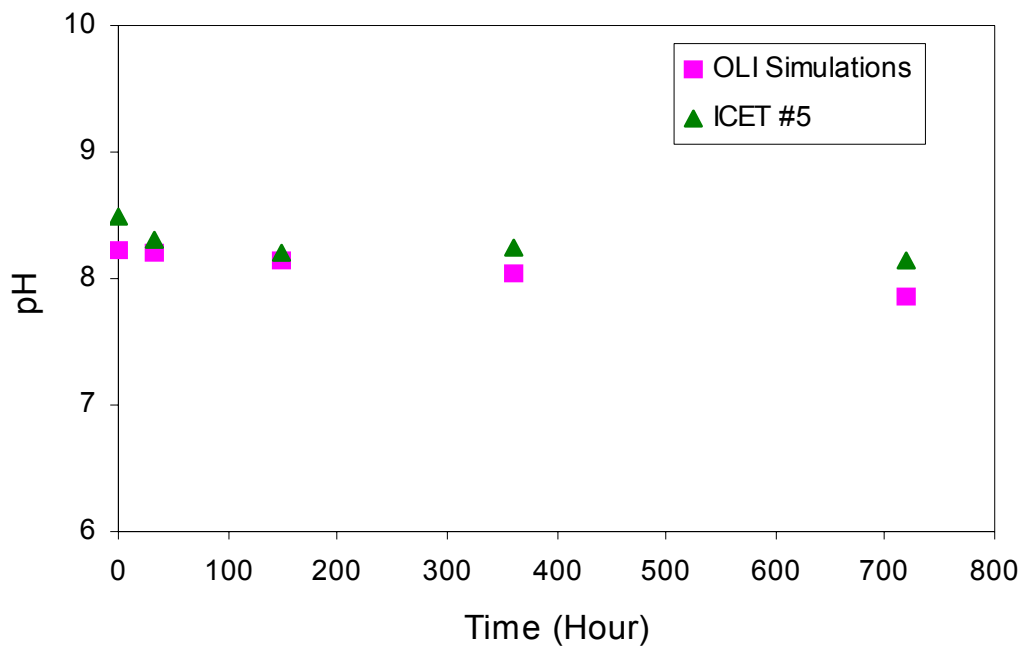


Figure 5-19. pH Values From the Informed Predictions (OLI) Simulation Compared With Measured pH in ICET #5 in Sodium Borate Containment Water at 60 °C [140 °F]

5.6 Assessment of Informed Prediction Results

The informed predictions used the data and observations from the completed ICET experiments to improve the estimated source-term water compositions that were used as starting values for the simulation input files. A revised corrosion rate for aluminum metal provided different source-term concentrations of aluminum in all of the simulations except those for ICET #2. Dissolution rates for calcium silicate insulation were measured in separate experiments, and those results were used to modify the source-term concentrations of calcium and silicon in simulations of ICETs #3 and #4.

One important difference between the blind predictions and the informed predictions was that no aluminum-bearing solids were predicted to form in the informed simulations. Because the revised source-term aluminum concentration in ICET #1 was similar to the measured aluminum concentrations in the experiment, the informed prediction gave a closer match to the observed conditions than the blind prediction. The low aluminum corrosion rate that corresponded to conditions in ICET #2 was not modified, and predictions corresponded with observed low concentrations of aluminum in the experiment. In the simulations of ICETs #3, #4, and #5, the revised source-term concentrations of aluminum were high and remained unaffected by the precipitation of any secondary aluminum phases. In contrast, the measured aluminum concentrations in ICETs #3 and #4 were at or near detection limits. On the basis of post-experiment weight loss measurements, which indicated very little corrosion of aluminum in ICETs #3 and #4, with slightly more in ICET #5, the aluminum corrosion rate in the experiments appears to have been affected by another process, such as passivation of the metal surface, that was not considered in the source-term estimates. The blind predictions, which included precipitation of secondary aluminum-bearing solids, were more similar in this case to the measured aluminum concentrations. Except for an aluminum phosphate precipitate that was predicted in ICET #2, no secondary aluminum-bearing solids were predicted in the informed simulations. One solid, $\text{Al}(\text{OH})_3$ (aluminum hydroxide), was not allowed to precipitate during the simulations because it was not observed as a precipitate in the experiments. Although aluminum oxyhydroxide (AlOOH) was identified by X-ray diffraction analysis as a possible precipitate in ICET #1, it was not predicted to form in the simulation because it was not listed as a stable phase at or below 60 °C [140 °F] in the OLI database file.

With the exception of calcium phosphate, which was predicted to precipitate in the simulations of ICETs #2 and #3 and which was identified as a precipitate in the actual experiments, no calcium-bearing solids were predicted to form in any of the informed predictions. High source-term concentrations of calcium for long exposure times lead to overestimated final concentrations in ICET #3 and #4, but the predicted results corresponded well to the measured results for low exposure times of exposure and at all times in simulations of ICETs #1, #2, and #5. The formation of calcite, CaCO_3 , or a similar phase may have limited calcium concentrations in some of the ICET experiments, but the informed predictions were unable to consider precipitation of carbonate minerals because the simulations did not include equilibration with atmospheric carbon dioxide. These conditions were modeled in a separate set of simulations using PHREEQC (Section 6).

The only silicate phase that was allowed to precipitate in the informed simulations was amorphous silicon dioxide, which was predicted to be an important oversaturated phase in ICET #3. In this case, there was excellent agreement between the informed prediction and the experiment results. In the other simulations, the source-term concentration of silicon

corresponded well with the experiment results at exposure times to about 360 hours, and so in these cases the informed predictions also provided reasonable simulations of the experiment conditions.

6 ADDITIONAL SIMULATIONS OF INTEGRATED CHEMICAL EFFECTS TEST CONDITIONS

Compared to the blind predictions of the Integrated Chemical Effects Test (ICET) experiments in Section 4, the informed predictions reported in Section 5 were improved by modifications to the source-term concentrations. However, the informed predictions did not address other conditions of interest such as the potential precipitation of carbonate minerals or aluminum oxyhydroxide under post-loss-of-coolant accident post-(LOCA) conditions. Additional sets of blind and informed simulations subsequently were performed using PHREEQC, another of the modeling codes evaluated in Section 2, to consider some of these additional modeling options. One set of blind predictions used the original estimated source-term concentrations. A second set of blind predictions, called the modified blind predictions, used the same modified source terms as were developed for the informed predictions. In all of the simulations, it was assumed that the solutions modeled remained in equilibrium with atmospheric carbon dioxide throughout the experiment. To facilitate comparison of results between blind and informed predictions, the same thermodynamic database was used for both sets of simulations. An example of a more detailed PHREEQC simulation was also performed for one experiment, ICET #4, to model how the composition of the containment water would change over time as it was affected by dissolution and precipitation reactions simultaneously.

6.1 PHREEQC Database Modifications

The PHREEQC thermodynamic database file used in the simulations was `lnl.dat`, which was the same database used in the code comparison exercise (Section 2). This file contains solubility constants for more than a thousand potential solid phases, few of which would be realistically expected to form under the relatively low-temperature, short-term conditions associated with the ICET experiments. To facilitate the PHREEQC chemical effect simulations, the `lnl.dat` database file was edited to shorten the list of solids to about thirty phases (Table 6-1). These solids included carbonate and phosphate minerals as well as common metal oxides, some of which had been observed to form in the ICET experiments. The edited list also included the mineral tobermorite, an important constituent of the calcium silicate insulation samples, in order to assess its solubility under ICET conditions.

The main silicate phase in the revised database was amorphous SiO_2 , which was included on the assumption that its precipitation would be favored kinetically over more structurally complex crystalline silicates. Similarly, most of the sodium-bearing minerals in the `lnl.dat` database file were either silicate minerals or highly soluble evaporite minerals that would be unlikely precipitates under ICET conditions. For this reason, sodium tetraborate (borax) was the only sodium-bearing phase included in the abbreviated database list. It was retained to assess its saturation index with respect to the high concentrations of sodium and boron in some of the ICET experiment solutions. An amorphous form of AlOOH (pseudoboehmite) was observed in the ICET experiments, so the two most similar AlOOH polymorphs, boehmite and diaspore, were included in the edited database file, as was the aluminum hydroxide mineral gibbsite, $\text{Al}(\text{OH})_3$. The numerous other aluminum-bearing solids in the `lnl.dat` database file were more structurally complex (e.g., clay minerals) and were assumed to be unlikely to form under the temperatures and timeframes of interest in the tests.

In the PHREEQC blind predictions, any solid phase in the database file was allowed to precipitate if it was calculated to be oversaturated in the source-term water. Because the edited

Table 6-1. Modified PHREEQC Database of Solid Phases for Integrated Chemical Effects Test (ICET) Simulations		
Formula	Database Name	Comments
Al(OH) ₃	Gibbsite	—
AlOOH	Boehmite	Proxy for pseudoboehmite observed in ICET #1
AlOOH	Diaspore	—
B(OH) ₃	Boric acid	—
B ₂ O ₃	B2O3	—
Ca ₃ (PO ₄) ₂	Whitlockite	Proxy for gel formed in ICET #2 and #3
Ca ₅ (OH)(PO ₄) ₃	Hydroxylapatite	—
Ca ₅ Si ₆ H ₂₁ O _{27.5}	Tobermorite-14A	Major constituent of calcium silicate insulation
Ca ₆ Si ₆ O ₁₇ (OH) ₂	Xonotlite	—
CaCO ₃	Calcite	—
CaCO ₃ •H ₂ O	Monohydrocalcite	Metastable precursor of calcite
CaHPO ₄ •2H ₂ O	Brushite	—
CaMg ₃ (CO ₃) ₄	Huntite	—
Cu ₂ CO ₃ (OH) ₂	Malachite	—
CuO	Cuprite	—
Fe(OH) ₃	Fe(OH)3	—
FeCO ₃	Siderite	—
Mg(OH) ₂	Brucite	—
Mg ₂ CO ₃ (OH) ₂ •3H ₂ O	Artinite	—
MgCaB ₆ O ₁₁ •6H ₂ O	Hydroboracite	—
MgCO ₃	Magnesite	—
MgCO ₃ •3H ₂ O	Nesquehonite	—
MgCO ₃ •5H ₂ O	Lansfordite	—
Na ₂ B ₄ O ₅ (OH) ₄ •8H ₂ O	Borax	—
SiO ₂ (am)	Amorphous SiO2	Metastable precursor of crystalline silicon dioxide
Zn(OH) ₂	Zn(OH)2 (gamma)	—
Zn ₃ (PO ₄) ₂ •4H ₂ O	Hopeite	—
ZnCO ₃	Smithsonite	—
ZnCO ₃ •H ₂ O	ZnCO3:H2O	Metastable precursor of smithsonite

database file contained thermodynamic data for the most relevant solids, this approach provided a reasonable approximation of the reactions expected under the conditions of interest.

For the informed predictions, the list of solids allowed to precipitate upon oversaturation was shortened by the user, based on observations from each ICET experiment. An example of this approach is illustrated in the PHREEQC output file reproduced in Appendix D, which represents an informed simulation for ICET #1 at an exposure time of 148 hours.

6.2 Source-Term Water Compositions

The source-term water compositions for each simulation, compiled mainly from the input values used in the previous blind predictions (Section 4) and informed predictions (Section 5), are listed in Tables 6-2 through 6-6. In addition, in the PHREEQC simulations the pH of each starting solution was adjusted slightly by the program at the start of the simulation to achieve electrical charge balance. The solutions were then equilibrated with atmospheric carbon dioxide to produce a source-term concentration for inorganic carbon and a further small adjustment of initial pH.

In Tables 6-2 through 6-6, the same source-term concentrations that corresponded to the input values used in the EQ3/6 blind predictions (Section 4) are indicated as the “original source terms,” except for a few minor differences related to carbon and lithium concentrations. Because the pH of the starting solutions in the EQ3/6 blind predictions was not adjusted for charge balance, the equilibration of the solutions with atmospheric carbon dioxide produced different dissolved carbon concentrations. In Tables 6-2 through 6-6, lithium concentrations were revised minimally to represent the amount of lithium hydroxide that was actually added in the ICET experiments rather than the amount that had been specified as an additive in the test plan (NRC, 2005).

The modified source-term concentrations for aluminum and in some cases for calcium and silicon that were used by the OLI StreamAnalyzer informed predictions in Section 5 were based on data obtained from specific dissolution rate experiments or observations from the ICET experiments. Where these concentrations differed from the blind prediction input values, the revised concentrations are indicated in Tables 6-2 through 6-6 as “modified source terms.” For all other elements, the source-term concentrations used for the PHREEQC simulations were the same values as listed for the original source terms in Tables 6-2 through 6-6.

6.3 Results of Blind and Informed Predictions

Two sets of blind predictions were performed using PHREEQC. The first blind predictions used the original source-term concentrations (Tables 6-2 through 6-6) as input values and allowed any oversaturated phases in the database to precipitate automatically. The second set of blind predictions, called modified blind predictions, used the modified source-term concentrations (Tables 6-2 through 6-6), and again allowed any oversaturated phases in the database to precipitate automatically. Because the database had been edited in advance to comprise only the solid phases that were considered likely to be relevant under the conditions modeled, this approach provided a simple but reasonable initial overview of chemical effects in the system. Two sets of blind predictions were completed to examine how precipitation was affected by changes in the source term.

Table 6-2. Source-Term Water Compositions for Integrated Chemical Effects Test (ICET) #1 Simulations

mol/kgw*	0.5 Hours		32 Hours		148 Hours		360 Hours		720 Hours	
	Original Source Term	Modified Source Term	Original Source Term	Modified Source Term	Original Source Term	Modified Source Term	Original Source Term	Modified Source Term	Original Source Term	Modified Source Term
Al	2.26×10^{-5}	2.60×10^{-5}	6.83×10^{-4}	9.02×10^{-4}	3.11×10^{-3}	4.12×10^{-3}	7.54×10^{-3}	1.00×10^{-2}	—	2.00×10^{-2}
B	2.59×10^{-1}	same	2.59×10^{-1}	same	2.59×10^{-1}	same	2.59×10^{-1}	same	—	2.59×10^{-1}
C	1.31×10^{-2}	same	1.30×10^{-2}	same	1.26×10^{-2}	same	1.19×10^{-2}	same	—	9.85×10^{-3}
Ca	6.31×10^{-5}	same	9.76×10^{-5}	same	2.19×10^{-4}	same	4.13×10^{-4}	same	—	7.40×10^{-4}
Cl	2.74×10^{-3}	same	2.74×10^{-3}	same	2.74×10^{-3}	same	2.74×10^{-3}	same	—	2.74×10^{-3}
Cu	1.85×10^{-7}	same	1.18×10^{-5}	same	5.46×10^{-5}	same	1.33×10^{-4}	same	—	2.66×10^{-4}
Fe	2.06×10^{-8}	same	1.32×10^{-6}	same	6.09×10^{-6}	same	1.48×10^{-5}	same	—	2.96×10^{-5}
Li	2.93×10^{-5}	same	2.93×10^{-5}	same	2.93×10^{-5}	same	2.93×10^{-5}	same	—	2.93×10^{-5}
Mg	1.13×10^{-5}	same	1.47×10^{-5}	same	2.41×10^{-5}	same	2.41×10^{-5}	same	—	2.40×10^{-5}
Na	2.20×10^{-1}	same	2.20×10^{-1}	same	2.20×10^{-1}	same	2.20×10^{-1}	same	—	2.20×10^{-1}
Si	2.70×10^{-4}	same	3.18×10^{-4}	same	4.49×10^{-4}	same	4.64×10^{-4}	same	—	4.88×10^{-4}
Zn	3.58×10^{-7}	same	2.29×10^{-5}	same	1.06×10^{-4}	same	2.58×10^{-4}	same	—	5.15×10^{-4}
pH	9.33	same	9.33	same	9.31	same	9.29	9.27	—	9.21

* mol/kgw = moles/2.2 pounds of water

Table 6-3. Source-Term Water Compositions for Integrated Chemical Effects Test (ICET) #2 Simulations

mol/kgw*	0.5 Hours		32 Hours		148 Hours		360 Hours		720 Hours	
	Original Source Term	Modified Source Term	Original Source Term	Modified Source Term	Original Source Term	Modified Source Term	Original Source Term	Modified Source Term	Original Source Term	Modified Source Term
Al	4.21×10^{-6}	same	2.26×10^{-5}	same	9.03×10^{-5}	same	2.14×10^{-4}	same	—	4.24×10^{-4}
B	2.59×10^{-1}	same	2.59×10^{-1}	same	2.59×10^{-1}	same	2.60×10^{-1}	same	—	2.59×10^{-1}
C	1.34×10^{-4}	same	1.38×10^{-4}	same	1.50×10^{-4}	same	1.72×10^{-4}	same	—	2.08×10^{-4}
Ca	4.42×10^{-5}	same	1.06×10^{-4}	same	3.33×10^{-4}	same	7.48×10^{-4}	same	—	1.45×10^{-3}
Cl	2.74×10^{-3}	same	2.74×10^{-3}	same	2.74×10^{-3}	same	2.74×10^{-3}	same	—	2.74×10^{-3}
Cu	1.84×10^{-7}	same	1.18×10^{-5}	same	5.46×10^{-5}	same	1.33×10^{-4}	same	—	2.66×10^{-4}
Fe	1.94×10^{-7}	same	1.24×10^{-5}	same	5.73×10^{-5}	same	1.39×10^{-4}	same	—	2.79×10^{-5}
Li	2.93×10^{-5}	same	2.93×10^{-5}	same	2.93×10^{-5}	same	2.93×10^{-5}	same	—	2.93×10^{-5}
Mg	3.05×10^{-7}	same	1.95×10^{-5}	same	9.02×10^{-5}	same	2.19×10^{-4}	same	—	4.39×10^{-4}
Na	3.60×10^{-2}	same	3.61×10^{-2}	same	3.66×10^{-2}	same	3.74×10^{-2}	same	—	3.89×10^{-2}
P	1.20×10^{-2}	same	1.20×10^{-2}	same	1.20×10^{-2}	same	1.20×10^{-2}	same	—	1.20×10^{-2}
Si	1.25×10^{-4}	same	3.81×10^{-4}	same	1.32×10^{-3}	same	3.05×10^{-3}	same	—	5.98×10^{-3}
Zn	3.58×10^{-7}	same	2.29×10^{-5}	same	1.06×10^{-4}	same	2.57×10^{-4}	same	—	5.15×10^{-4}
pH	7.56	same	7.57	same	7.60	same	7.66	same	—	7.74

*mol/kgw = moles/2.2 pounds of water

Table 6-4. Source-Term Water Compositions for Integrated Chemical Effects Test (ICET) #3 Simulations

mol/kgw*	0.5 Hours		32 Hours		148 Hours		360 Hours		720 Hours	
	Original Source Term	Modified Source Term	Original Source Term	Modified Source Term	Original Source Term	Modified Source Term	Original Source Term	Modified Source Term	Original Source Term	Modified Source Term
Al	4.04×10^{-6}	4.29×10^{-6}	1.12×10^{-5}	2.75×10^{-5}	3.76×10^{-5}	1.13×10^{-4}	8.58×10^{-5}	2.69×10^{-04}	—	5.34×10^{-4}
B	2.59×10^{-1}	same	2.59×10^{-1}	same	2.59×10^{-1}	same	2.59×10^{-1}	same	—	2.59×10^{-1}
C	5.82×10^{-4}	same	5.93×10^{-4}	same	6.43×10^{-4}	same	7.42×10^{-4}	same	—	9.72×10^{-4}
Ca	1.81×10^{-2}	1.81×10^{-2}	1.84×10^{-2}	1.89×10^{-2}	1.98×10^{-2}	2.21×10^{-2}	2.24×10^{-2}	2.78×10^{-02}	—	2.82×10^{-2}
Cl	2.74×10^{-3}	same	2.74×10^{-3}	same	2.74×10^{-3}	same	2.74×10^{-3}	same	—	2.74×10^{-3}
Cu	1.84×10^{-7}	same	1.18×10^{-5}	same	5.46×10^{-5}	same	1.33×10^{-4}	same	—	2.66×10^{-4}
Fe	1.93×10^{-7}	same	1.24×10^{-5}	same	5.73×10^{-5}	same	1.39×10^{-4}	same	—	2.79×10^{-5}
Li	2.92×10^{-5}	same	2.93×10^{-5}	same	2.93×10^{-5}	same	2.93×10^{-5}	same	—	2.92×10^{-5}
Mg	6.09×10^{-8}	same	3.90×10^{-6}	same	1.80×10^{-5}	same	4.39×10^{-5}	same	—	8.77×10^{-5}
Na	3.60×10^{-2}	same	3.60×10^{-2}	same	3.61×10^{-2}	same	3.63×10^{-2}	same	—	3.66×10^{-2}
P	1.20×10^{-2}	same	1.20×10^{-2}	same	1.20×10^{-2}	same	1.20×10^{-2}	same	—	1.20×10^{-2}
Si	1.81×10^{-2}	1.81×10^{-2}	1.85×10^{-2}	1.90×10^{-2}	2.00×10^{-2}	2.22×10^{-2}	2.27×10^{-2}	2.81×10^{-02}	—	2.87×10^{-2}
Zn	3.58×10^{-7}	same	2.29×10^{-5}	same	1.06×10^{-4}	same	2.57×10^{-4}	same	—	5.15×10^{-4}
pH	8.12	same	8.12	8.13	8.15	8.19	8.19	8.26	8.27	8.27

*mol/kgw = moles/2.2 pounds of water

Table 6-5. Source-Term Water Compositions for Integrated Chemical Effects Test (ICET) #4 Simulations

mol/kgw*	0.5 Hours		32 Hours		148 Hours		360 Hours		720 Hours	
	Original Source Term	Modified Source Term	Original Source Term	Modified Source Term	Original Source Term	Modified Source Term	Original Source Term	Modified Source Term	Original Source Term	Modified Source Term
Al	1.60×10^{-5}	1.60×10^{-5}	6.74×10^{-4}	5.48×10^{-4}	3.10×10^{-3}	2.52×10^{-3}	7.53×10^{-3}	6.11×10^{-3}	—	1.23×10^{-2}
B	2.59×10^{-1}	same	2.59×10^{-1}	same	2.59×10^{-1}	same	2.60×10^{-1}	same	—	2.59×10^{-1}
C	1.39×10^{-2}	same	1.45×10^{-2}	same	1.68×10^{-2}	same	2.12×10^{-2}	same	—	9.73×10^{-3}
Ca	1.79×10^{-3}	8.57×10^{-4}	3.50×10^{-3}	9.90×10^{-4}	9.77×10^{-3}	1.48×10^{-3}	2.12×10^{-2}	2.37×10^{-3}	—	3.88×10^{-3}
Cl	2.74×10^{-3}	same	2.74×10^{-3}	same	2.74×10^{-3}	same	2.74×10^{-3}	same	—	2.74×10^{-3}
Cu	1.85×10^{-7}	same	1.18×10^{-5}	same	5.46×10^{-5}	same	1.33×10^{-4}	same	—	2.66×10^{-4}
Fe	2.06×10^{-8}	same	1.32×10^{-6}	same	6.09×10^{-6}	same	1.48×10^{-5}	same	—	2.96×10^{-5}
Li	2.93×10^{-5}	same	2.93×10^{-5}	same	2.93×10^{-5}	same	2.93×10^{-5}	same	—	2.93×10^{-5}
Mg	2.26×10^{-6}	same	2.94×10^{-6}	same	5.45×10^{-6}	same	1.01×10^{-5}	same	—	1.78×10^{-5}
Na	2.20×10^{-1}	same	2.20×10^{-1}	same	2.20×10^{-1}	same	2.20×10^{-1}	same	—	2.20×10^{-1}
Si	1.90×10^{-3}	2.01×10^{-3}	3.58×10^{-3}	3.00×10^{-3}	9.79×10^{-3}	6.64×10^{-3}	2.11×10^{-2}	1.33×10^{-2}	—	2.46×10^{-2}
Zn	3.58×10^{-7}	same	2.29×10^{-5}	same	1.06×10^{-4}	same	2.58×10^{-4}	same	—	5.15×10^{-4}
pH	9.34	9.33	9.34	9.32	9.34	9.30	9.34	9.26	9.19	9.19

* mol/kgw = moles/2.2 pounds of water

Table 6-6. Source-Term Water Compositions for Integrated Chemical Effects Test (ICET) #5 Simulations

mol/kgw*	0.5 Hours		32 Hours		148 Hours		360 Hours		720 Hours	
	Original Source Term	Modified Source Term	Original Source Term	Modified Source Term	Original Source Term	Modified Source Term	Original Source Term	Modified Source Term	Original Source Term	Modified Source Term
Al	$2.20.6 \times 10^{-5}$	2.60×10^{-5}	6.83×10^{-4}	9.02×10^{-4}	3.11×10^{-3}	4.12×10^{-3}	7.54×10^{-3}	1.00×10^{-2}	—	2.00×10^{-2}
B	2.17×10^{-1}	same	2.17×10^{-1}	same	2.17×10^{-1}	same	2.17×10^{-1}	same	—	2.17×10^{-1}
C	9.84×10^{-4}	same	9.77×10^{-4}	same	9.49×10^{-4}	same	8.92×10^{-4}	same	—	6.90×10^{-4}
Ca	6.31×10^{-5}	same	9.76×10^{-5}	same	2.19×10^{-4}	same	4.12×10^{-4}	same	—	7.40×10^{-4}
Cl	1.10×10^{-3}	same	1.10×10^{-3}	same	1.10×10^{-3}	same	1.10×10^{-3}	same	—	1.10×10^{-3}
Cu	1.84×10^{-7}	same	1.18×10^{-5}	same	5.46×10^{-5}	same	1.33×10^{-4}	same	—	2.66×10^{-4}
Fe	2.06×10^{-8}	same	1.32×10^{-6}	same	6.09×10^{-6}	same	1.48×10^{-5}	same	—	2.96×10^{-5}
Li	1.25×10^{-5}	same	1.25×10^{-5}	same	1.25×10^{-5}	same	1.25×10^{-5}	same	—	1.25×10^{-5}
Mg	1.13×10^{-5}	same	1.47×10^{-5}	same	2.40×10^{-5}	same	2.40×10^{-5}	same	—	2.40×10^{-5}
Na	5.67×10^{-2}	same	5.67×10^{-2}	same	5.68×10^{-2}	same	5.68×10^{-2}	same	—	5.70×10^{-2}
Si	2.70×10^{-4}	same	3.18×10^{-4}	same	4.49×10^{-4}	same	4.64×10^{-4}	same	—	4.88×10^{-4}
Zn	3.58×10^{-7}	same	2.29×10^{-5}	same	1.06×10^{-4}	same	2.57×10^{-4}	same	—	5.15×10^{-4}
pH	8.41	same	8.41	same	8.38	8.37	8.34	8.32	—	8.20

*mol/kgw = moles/2.2 pounds of water

The informed PHREEQC predictions used the modified source-term concentrations (Tables 6-2 through 6-6) as input values and selectively blocked the precipitation of certain oversaturated phases to produce results that conformed more closely to observations from the ICET experiments.

6.3.1 PHREEQC Simulations for ICET #1

ICET #1 was a test of chemical effects produced by a set of various sample materials submerged in an alkaline borated solution at 60 °C [140 °F] in which pH buffering was provided by sodium hydroxide (Table 3-1). The sample insulation material used in this test was glass fiber (Nukon). Water samples were collected and analyzed at regular intervals over the 30-day duration of the experiment. The modeled chemical effects simulations were based on estimated source-term water compositions at exposure times of 0.5, 32, 148, 360, and 720 hours (0.02, 1.3, 6.2, 15, and 30 days, respectively), as shown in Table 6-2, assuming in each case that no precipitation had occurred prior to this time to affect the solution composition. After modeling the precipitation of oversaturated solid phases, the resulting final solution composition was compared to the chemical analysis of the ICET #1 solution that had been sampled at approximately the same time period.

In the original and modified blind predictions, the main oversaturated phase was predicted to be the AIOOH polymorph diaspore, as indicated by results in Figure 6-1 for simulations at 360 hours of exposure. The increase in dissolved aluminum in the modified source term (Table 6-2) resulted in the precipitation of proportionally more diaspore, but no other changes. Other precipitates in the blind predictions consisted of minor amounts of calcite (CaCO_3), tenorite (CuO), and smithsonite (ZnCO_3) as well as trace amounts of $\text{Fe}(\text{OH})_3$ and cuprite (Cu_2O). Because the source-term concentrations of copper, zinc, and iron were small, the precipitation removed virtually all of the dissolved metals from solution.

In the informed predictions, the precipitation of any aluminum-bearing solids (Table 6-1) was blocked to better represent the measured ICET #1 aluminum concentration. However, the measured values later were determined to have included a finely dispersed colloidal aluminum phase that was not separated prior to analysis, and a visible precipitate thought to be pseudoboehmite was observed to form in some of the sample solutions upon cooling (Dallman, et al., 2005a). The precipitation of calcite was also blocked, on the assumption that a less stable phase might be expected to form instead. This resulted in the precipitation of a small amount of monohydrocalcite instead of calcite (Figure 6-1) and no aluminum-bearing solids. All other precipitates, and amounts, were the same as had been predicted in the blind simulations.

Changes in aqueous composition during the ICET #1 experiment are compared in Figure 6-2 with the modeled variations for the original set of blind predictions and for the informed predictions. The informed predictions used a modified source term for aluminum and provided an additional simulation at 30 days (720 hours). The source-term concentration of calcium, derived mainly from the leaching of concrete in the ICET #1 simulations, was calculated to increase linearly over time. In the blind prediction, the precipitation of calcite removed virtually all calcium from solution, contrary to observed results. However, the precipitation of the hydrated phase, monohydrocalcite, in the informed prediction resulted in calcium concentrations that corresponded well to the observed values.

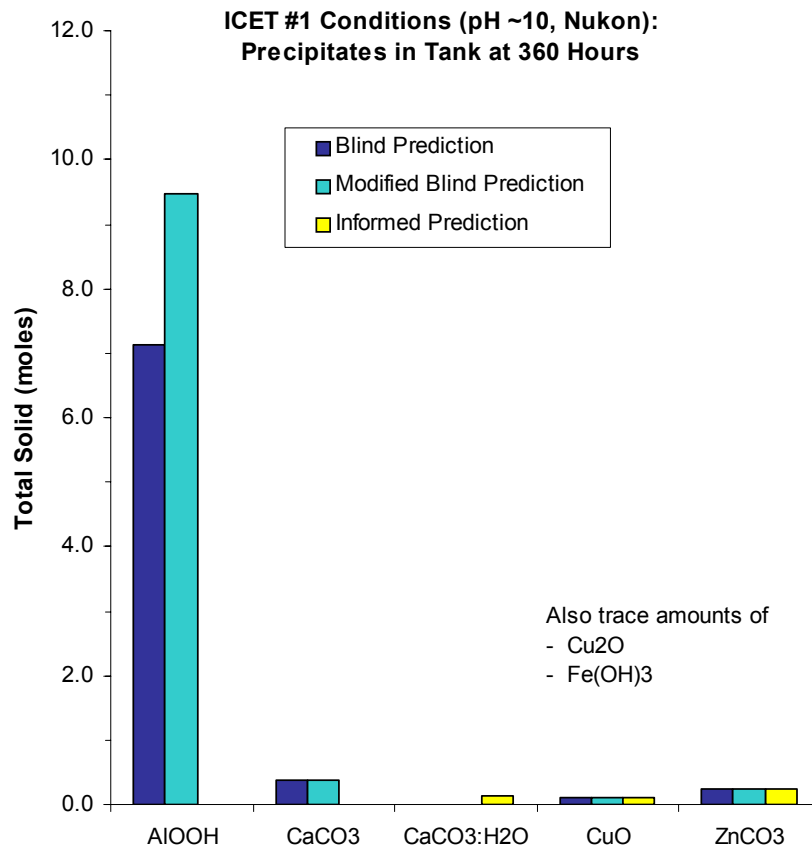


Figure 6-1. Predicted Precipitates in ICET #1 Simulations

The estimated source-term concentration of silicon for the ICET #1 simulations was derived from the leaching of Nukon glass fiber insulation and concrete. There was no oversaturated silica-bearing phase in any of the simulations, so the final dissolved silicon concentration and the source-term concentrations were equal. Compared to the experiment results, the estimated source-term concentration of silicon was initially similar to the observed values in ICET #1, but it was greater than the observed values throughout most of the experiment. Given that no silica-bearing precipitates were predicted or observed, the source-term calculations appear to have overestimated the amount of dissolved silicon in the system.

In the blind predictions for ICET #1, the source-term concentrations for aluminum were lower than the observed final concentrations, indicating that the source-term calculations had underestimated the release rate of aluminum. The measured aluminum concentration in ICET #1, which included colloidal aluminum as well as dissolved aluminum, corresponded well with the calculated source-term concentration for aluminum (Figure 6-2) except that the calculated source-term concentration at 30 days (720 hours) was too high. As discussed in Section 5.1, the source-term calculations did not account for a change in the aluminum corrosion rate due to passivity at later times.

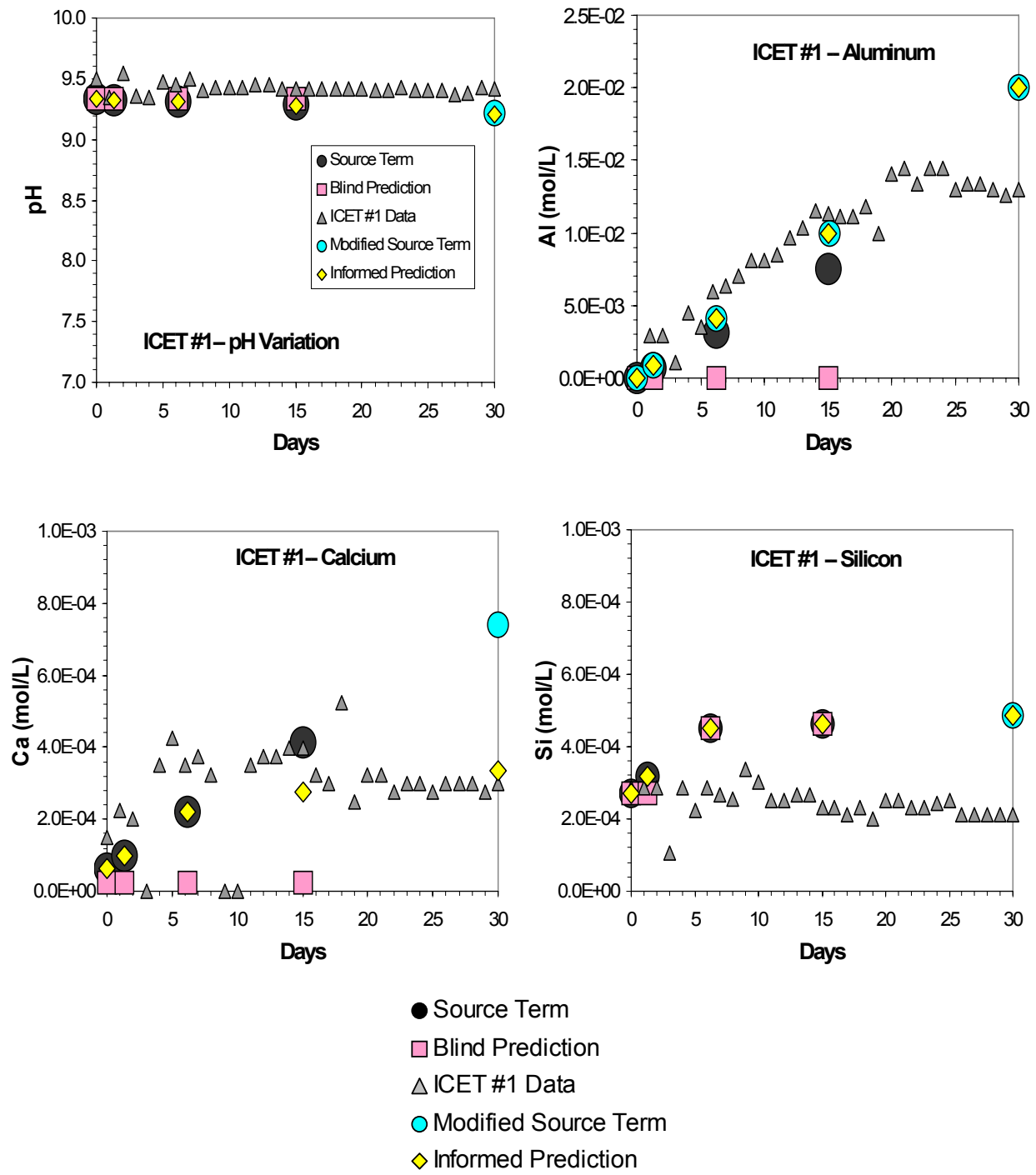


Figure 6-2. Predicted and Observed Variations in ICET #1 Water Chemistry [mol/L = mol/0.26 gal or mol/1.06 quart]

Throughout the simulations, the predicted pH values corresponded well with the observed values. A slight decrease in pH over time was predicted in the simulations, but this effect was not observed in the experiment (Figure 6-2).

6.3.2 PHREEQC Simulations for ICET #2

ICET #2 was a test of chemical effects produced by a set of sample materials submerged in a near-neutral borated solution at 60 °C [140 °F] in which pH buffering was provided by trisodium phosphate (Table 3-1). The sample insulation material used in this test was glass fiber (Nukon). Water samples were collected and analyzed at regular intervals over the 30-day duration of the experiment. The modeled chemical effects simulations were based on estimated source-term water compositions at exposure times of 0.5, 32, 148, 360, and 720 hours (0.02, 1.3, 6.2, 15, and 30 days, respectively), as shown in Table 6-3, assuming in each case that no precipitation had occurred prior to this time to affect the solution composition. After modeling the precipitation of oversaturated solid phases, the resulting final solution composition was compared to the chemical analysis of the ICET #2 solution that had been sampled at approximately the same time period.

The original source-term compositions for simulations of ICET #2 were not modified for later simulations (Table 6-3), so a second set of blind predictions was not performed. The only differences between the blind predictions and the informed predictions were the addition of a simulated source-term composition at 720 hours and restrictions on precipitation in the informed predictions.

For the conditions and sample materials represented by ICET #2, the total concentrations of most of the dissolved materials were very low compared to the other ICET experiments. Several secondary solid phases nevertheless were predicted to be oversaturated, and their precipitation removed virtually all dissolved calcium, aluminum, copper, iron, and zinc from solution. At 720 hours of exposure (30 days), the source-term concentration of silicon was high enough that amorphous silicon dioxide was predicted to precipitate from solution.

As indicated by the results in Figure 6-3 for simulations at 360 hours of exposure, calcium phosphate was the main solid that was predicted to precipitate. The amount of calcium phosphate formed in each simulation was limited by the amount of dissolved calcium in the source-term water at the time of exposure. In the blind predictions, some of the remaining dissolved phosphorous was consumed by precipitation of zinc phosphate, and dissolved aluminum was removed from solution by precipitation of diaspore, a polymorph of AlOOH. In the informed prediction, the precipitation of zinc phosphate was blocked deliberately. Precipitation of diaspore and gibbsite were also blocked in the informed predictions, but boehmite, the other AlOOH polymorph, was allowed. Because the solubility of boehmite was only slightly greater than that of diaspore, the amount of AlOOH that precipitated in the informed predictions was roughly equivalent to the amount formed in the blind predictions (Figure 6-3).

Changes in the solution composition during the ICET #2 experiment are compared with modeled results in Figure 6-4. The simulated pH values were comparable to, but slightly higher than, the measured values in ICET #2. The only difference in source-term compositions between the blind and informed predictions was an additional informed simulation at 30 days (720 hours). As indicated in Figure 6-4, the source-term concentrations of calcium, silicon, and aluminum increased at linear rates according to the duration of exposure. The source-term concentration of phosphorous was constant throughout the simulations because the only source

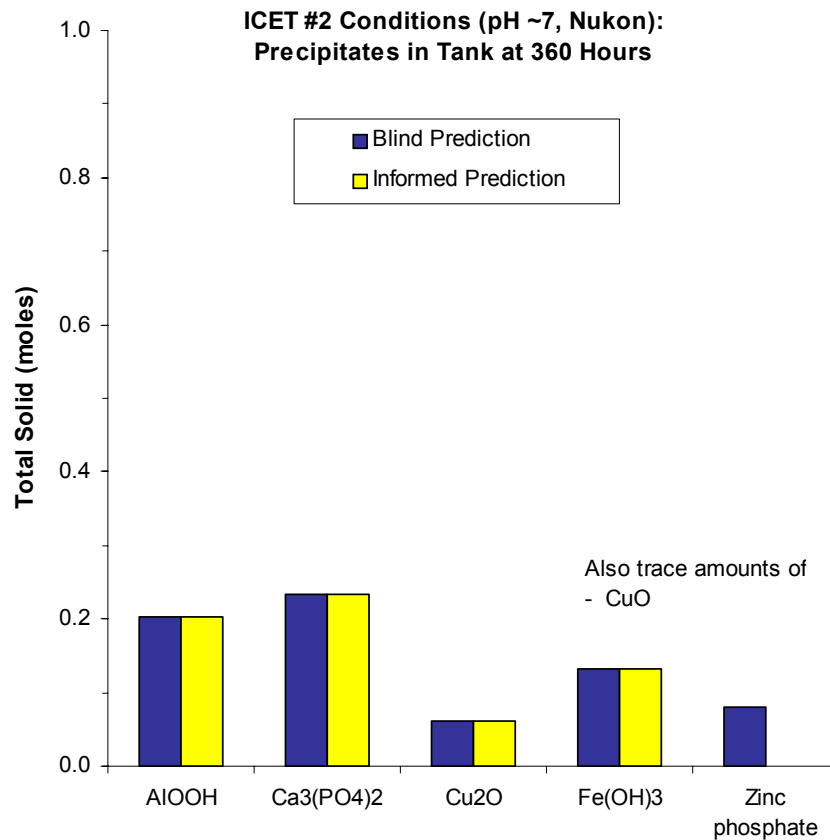


Figure 6-3. Predicted Precipitates in ICET #2 Simulations

of phosphorous was a fixed amount of trisodium phosphate dissolved in the water at the beginning of the experiment. No analytical data for phosphorous were reported for ICET #2 (Dallman, et al., 2005b), but the initial concentration in the experiment was the same as the source-term concentration (Table 6-3). The changes in phosphorous concentration in Figure 6-4 are shown mainly to illustrate that the simulated precipitation of calcium phosphate in ICET #2 removed virtually all calcium from solution but only slightly decreased the amount of phosphorous in solution.

Aluminum, copper, and iron concentrations were below detection limits in the ICET #2 experiments (Dallman, et al., 2005b) and no visible precipitates were noted although a small accumulation of aluminum oxyhydroxide precipitate was predicted by the blind and informed simulations. Whether minor precipitation occurred or the source-term release of aluminum was lower in the experiment than estimated in the calculated source-term compositions, the end result in both cases was a very low aqueous concentration of aluminum.

The source-term and measured silicon concentrations corresponded closely to each other up to about 15 days, at which point the measured concentrations leveled off and the source-term concentration continued to increase. The source-term solution at 30 days (720 hours) was oversaturated with respect to amorphous silicon dioxide. In the simulation, precipitation of this

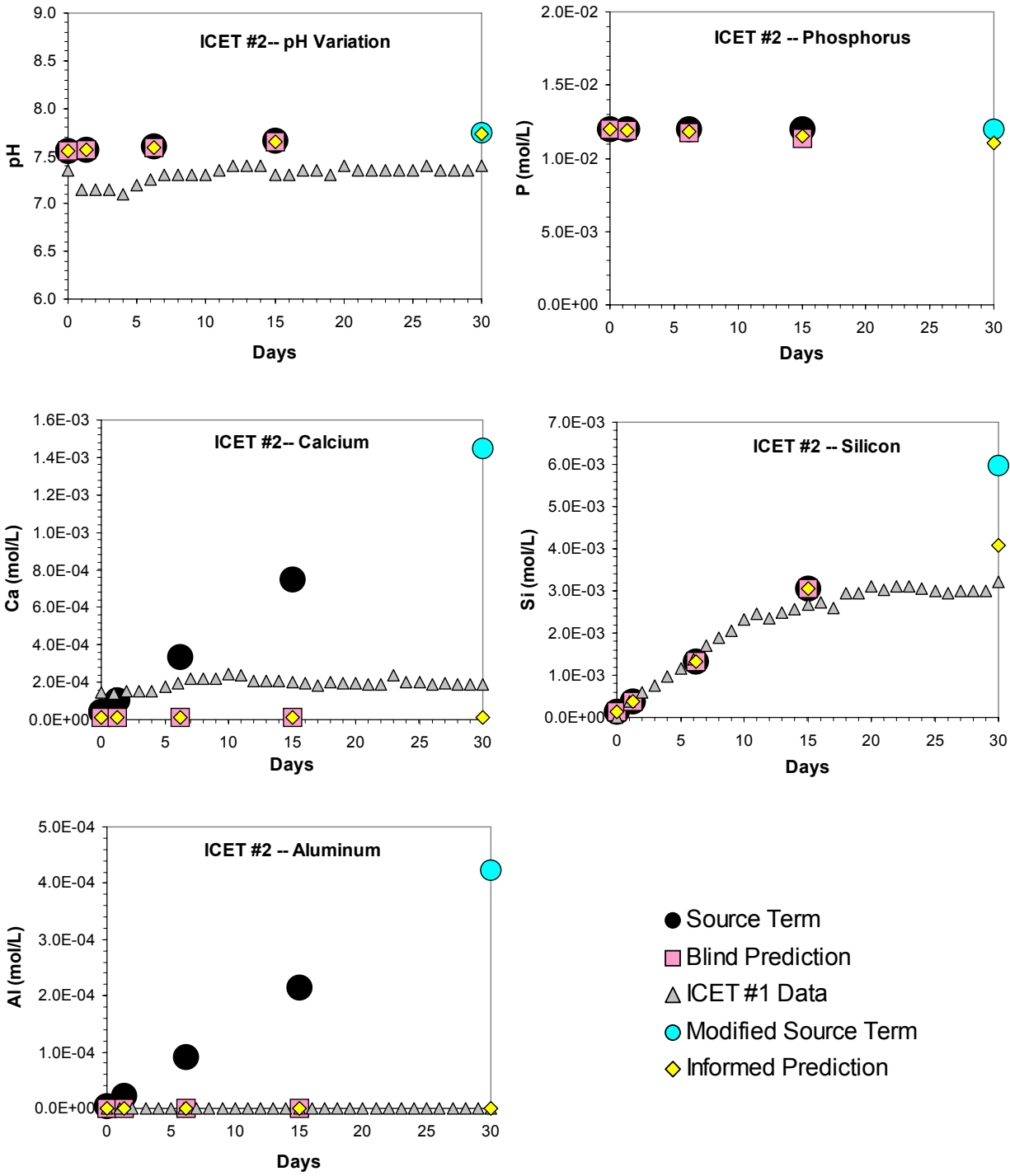


Figure 6-4. Predicted and Observed Variations in ICET #2 Water Chemistry [mol/L = mol/0.264 gal or mol/1.06 quart]

solid lowered the predicted silicon concentration to a value similar to the measured results. This solubility relationship, and an examination of the modeled saturation index of amorphous silicon dioxide in the other simulations, suggests that the ICET #2 experiment solution reached equilibrium with respect to amorphous silicon dioxide in the second half of the test. The saturation index, which is calculated automatically for each solid phase in a PHREEQC simulation, is a measure of the approach to equilibrium for a given phase relative to a given solution composition. If the system is not affected by kinetic restrictions, a negative saturation index for a particular solid indicates that the solid phase is undersaturated with respect to the solution, and if that phase is in contact with the water it would be expected to dissolve. A positive saturation index indicates that the solid phase is oversaturated and would be expected to precipitate. A saturation index of zero indicates that the solution and the solid are in equilibrium with each other, and neither precipitation nor dissolution of the solid would occur.

Figure 6-5 shows how the calculated saturation index for amorphous silicon dioxide changed in the ICET #2 simulations as the source-term waters became more enriched in dissolved silicon with increasing time of exposure to the sample materials. The silicon concentration in the source-term water at 15 days is high enough that the source-term water is nearly in equilibrium with respect to amorphous silicon dioxide, and over the remainder of the test period the source-term silicon concentration would be great enough that amorphous silicon dioxide would begin to precipitate from solution, which in turn would maintain the observed aqueous concentration of silicon at a fixed level by maintaining equilibrium with the solid phase. Another interpretation of the data is that the glass fiber insulation material, which was composed mainly of amorphous silicon dioxide, reached equilibrium with the test solution after about 15 days and stopped dissolving, thereby stabilizing the silicon concentration.

6.3.3 PHREEQC Simulations for ICET #3

ICET #3 was a test of chemical effects produced by a set of sample materials submerged in a near-neutral borated solution at 60 °C [140 °F] in which pH buffering was provided by trisodium phosphate (Table 3-1). The main difference between ICETs #2 and #3 was that the sample insulation material tested in ICET #3 was a combination of calcium silicate insulation and glass fiber insulation (Nukon) in the proportion 80:20 by mass. Water samples were collected from the tank and analyzed at regular intervals over the 30-day duration of the experiment. The modeled chemical effects simulations were based on estimated source-term water compositions at exposure times of 0.5, 32, 148, 360, and 720 hours (0.02, 1.3, 6.2, 15, and 30 days, respectively), as shown in Table 6-4, assuming in each case that no precipitation had occurred prior to this time to affect the solution composition. After modeling the precipitation of oversaturated solid phases, each simulated final solution composition was compared to the chemical analysis of the ICET #3 solution that had been sampled at approximately the same time period.

The dissolution of calcium silicate insulation in the trisodium phosphate-buffered solution promoted precipitation of secondary solids in the modeling predictions, an effect that was also noted as the formation of a calcium phosphate gel in ICET #3 (Dallman, et al., 2005c). The most abundant phase predicted to precipitate was amorphous silicon dioxide, as shown in Figure 6-6 for simulations using the source-term water composition at 360 hours of exposure.

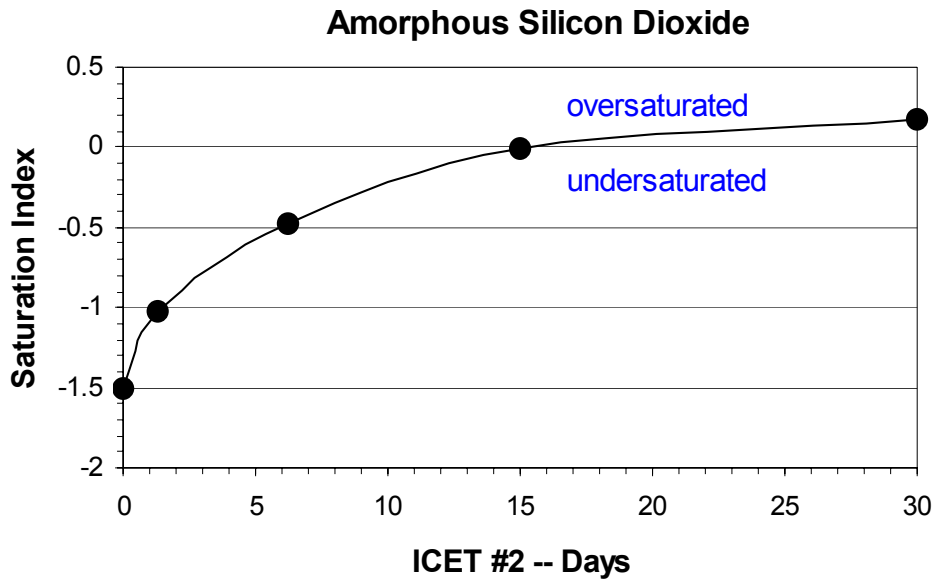


Figure 6-5. Predicted Changes in Saturation in ICET #2

Another important predicted precipitate was the calcium phosphate phase. A third abundant precipitate in the two sets of blind predictions was the calcium carbonate mineral calcite. Note that the amount of predicted calcite was greater in the modified blind prediction, as was the amount of amorphous silicon dioxide, because the release rate of calcium and silicon in the calcium silicate insulation had been increased in the modified source-term calculations. In the informed prediction, calcite was blocked from precipitating and a small amount of monohydrocalcite formed instead (Figure 6-6). The simulations also predicted that small amounts of aluminum oxyhydroxide (AlOOH), copper and iron oxides, and zinc carbonate would precipitate from the source-term solution. The informed predictions also indicated that a trace amount of a magnesium-calcium borate mineral, hydroboracite, would precipitate from the ICET #3 source-term waters represented by compositions at 148 hours, 360 hours and 720 hours. These three cases were the only examples in all of the ICET simulations in which a boron-bearing solid phase was calculated to be oversaturated in the borated containment waters.

Changes in the solution composition during the ICET #3 experiment are compared with modeled results in Figure 6-7. The predicted pH values were comparable to, though slightly higher than, the measured values in ICET #3, but the precipitation of calcite in the blind predictions lowered the simulated pH to values close to the measured values.

In contrast to simulations of ICET #2, where the predicted precipitation of calcium phosphate slightly reduced the concentration of dissolved phosphorous (Figure 6-4), the predicted precipitation of calcium phosphate in the ICET #3 simulations completely removed dissolved phosphorous from solution (Figure 6-7). These results conformed to the analytical data for phosphorous concentrations in the experiment. The source-term concentration of calcium also was depleted in the simulations, but not consumed entirely, by the precipitation of calcium phosphate. In the blind predictions the remainder of the dissolved calcium was removed from solution by the precipitation of calcite. The observed calcium concentration in ICET #3 was similar to the final concentration in the blind predictions. In the informed predictions, a more

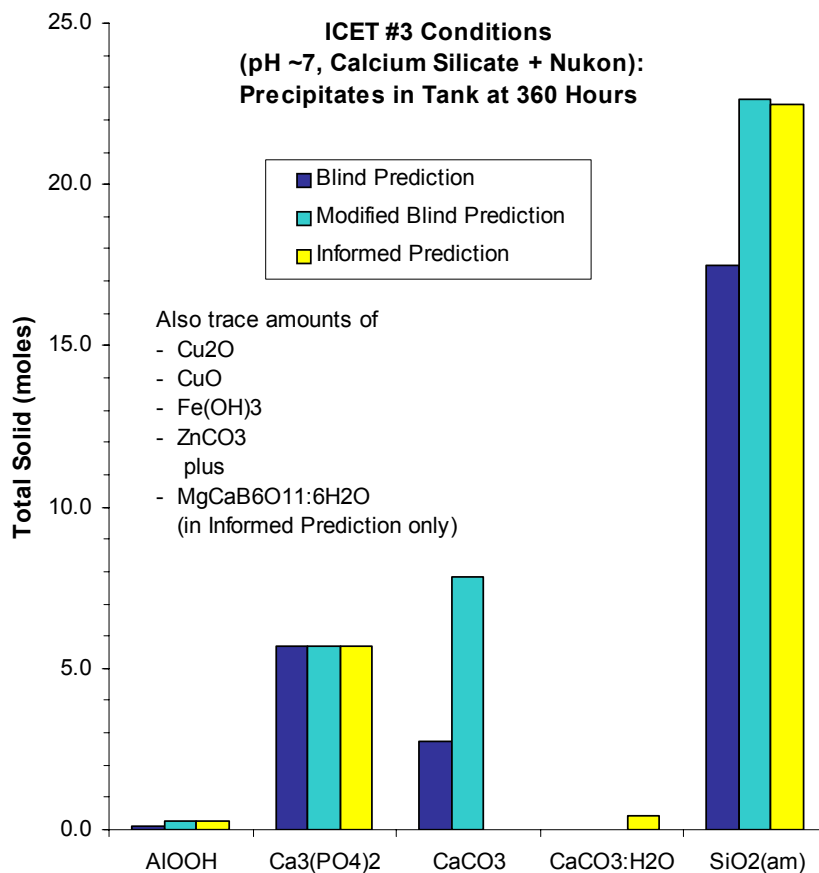


Figure 6-6. Predicted Precipitates in ICET #3 Simulations

soluble calcium carbonate phase, monohydrocalcite, was oversaturated instead of calcite, and it equilibrated with the water in the simulation before all dissolved calcium was consumed (Figure 6-7). In this case, the blind prediction corresponded more closely to observed results than the informed prediction did.

The observed concentration of silicon in ICET #3 was relatively uniform throughout the duration of the experiment. The blind and informed simulations indicated that the ICET #3 solution was in equilibrium with amorphous silicon dioxide, which was predicted to be oversaturated in all of the source-term water compositions. Given that the high source-term concentrations of silicon resulted mainly from the dissolution of calcium silicate insulation, not from glass fiber insulation as in ICET #2, the modeled results suggest that the uniform dissolved silicon concentration observed in ICET #3 was controlled by the precipitation of amorphous silicon dioxide.

6.3.4 PHREEQC Simulations for ICET #4

ICET #4 was a test of chemical effects produced by a set of sample materials submerged in an alkaline borated solution at 60 °C [140 °F] in which pH buffering was provided by sodium hydroxide (Table 3-1). The main difference between ICETs #1 and #4 was that the sample insulation material tested in ICET #4 was a combination of calcium silicate insulation and glass

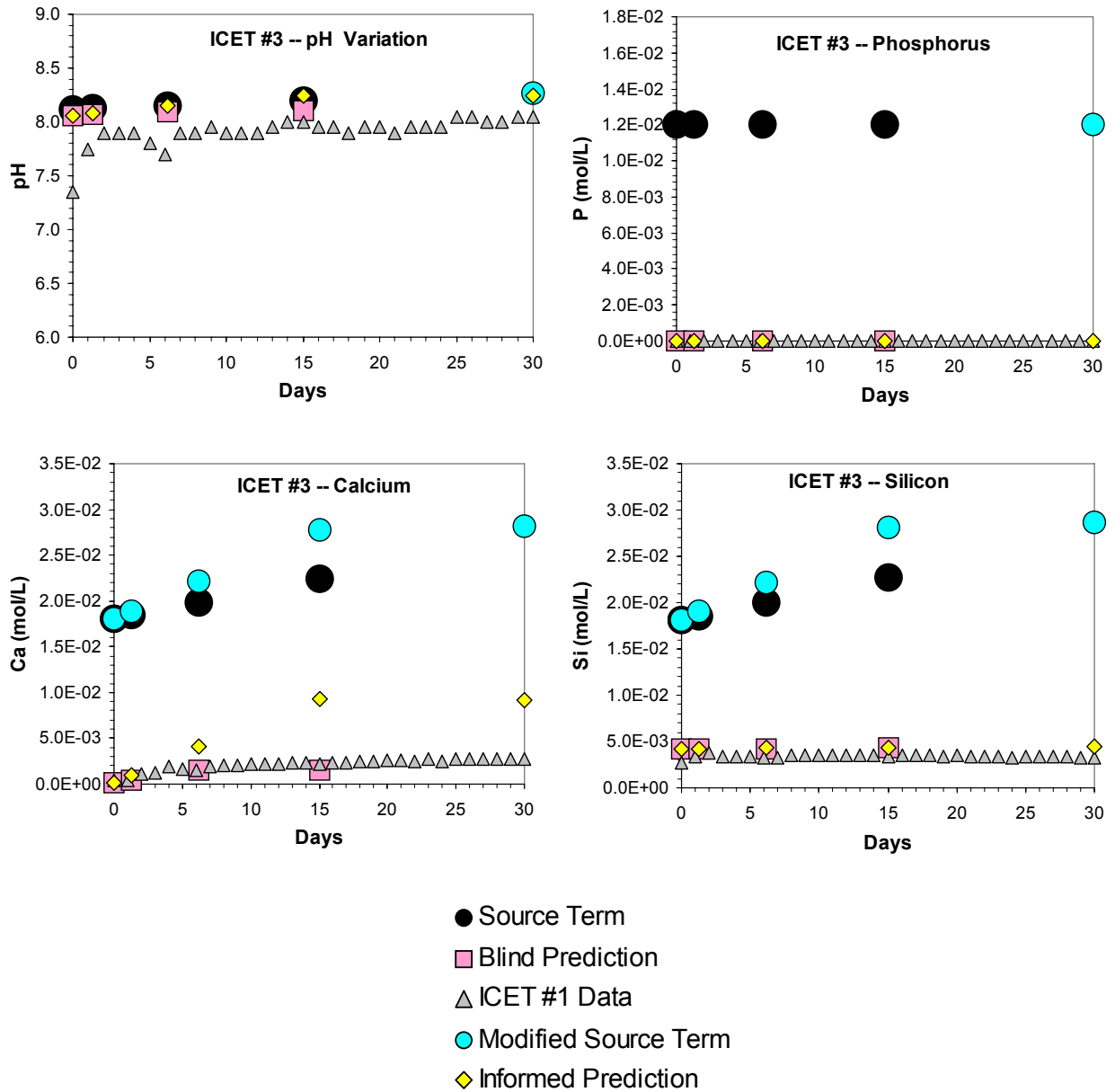


Figure 6-7. Predicted and Observed Variations in ICET #3 Water Chemistry [mol/l = mol/0.264 gal or mol/1.06 quart]

fiber insulation (Nukon) in the proportion 80:20 by mass. Water samples were collected from the tank and analyzed at regular intervals over the 30-day duration of the experiment. The modeled chemical effects simulations were based on estimated source-term water compositions at exposure times of 0.5, 32, 148, 360, and 720 hours (0.02, 1.3, 6.2, 15, and 30 days, respectively), as shown in Table 6-5, assuming in each case that no precipitation had occurred prior to this time to affect the solution composition. After modeling the precipitation of oversaturated solid phases, each simulated final solution composition was compared to the chemical analysis of the ICET #4 solution that had been sampled at approximately the same time period.

The original source-term concentrations of calcium and silicon in Table 6-5 were based on high estimates of the dissolution rate of calcium silicate insulation material that were demonstrated by experiments to be overly conservative (Appendix A). The modified source-term concentrations were more realistic and were based on the rates from dissolution experiments. Due to the anomalously high original source-term calcium concentration in the blind predictions, a large amount of the calcium carbonate mineral calcite was predicted to form in the blind predictions for ICET #4, as indicated by the comparison of precipitates in Figure 6-8 based on simulations using the source-term water composition at 360 hours of exposure. The modified blind prediction, using the lower modified source-term calcium concentration, indicated that a

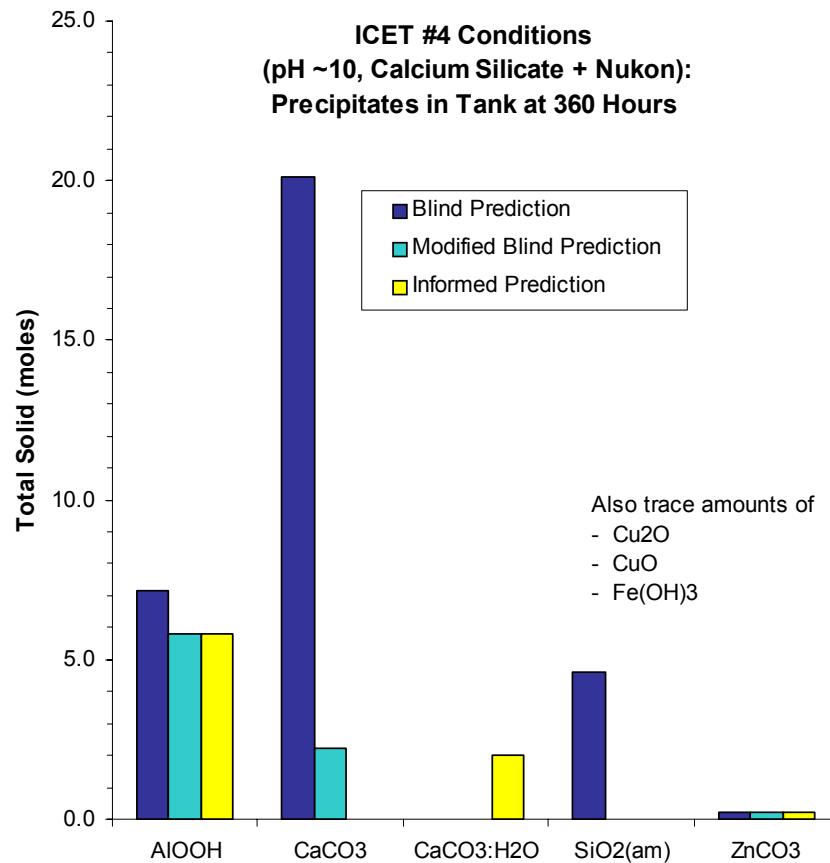


Figure 6-8. Predicted Precipitates in ICET #4 Simulations

significantly smaller amount of calcite would be expected to precipitate under these conditions. In the informed prediction, the precipitation of calcite was blocked by the user for kinetic reasons, but a comparable amount of monohydrocalcite precipitated in its place. Similarly, the anomalously high silicon concentration in the original blind prediction resulted in the precipitation of some amorphous silicon dioxide, but this phase was undersaturated where modeled using the modified source terms. Small amounts of aluminum oxyhydroxide (AlOOH), zinc carbonate, and copper and iron oxides also were predicted to form precipitates in the modeled solutions.

Changes in the modeled solution compositions are compared with the ICET #4 experimental data in Figure 6-9. The predicted pH values are uniform but about 0.5 pH units lower than the measured values. Compared to the results from the simulations of the other ICET experiments, this is the largest discrepancy between observed and predicted pH values that was produced by the simulations.

Figure 6-9 also illustrates the conspicuous difference between the original and modified source-term estimates of calcium concentration. Even without precipitation of calcium-bearing phases, the modified source-term concentration of dissolved calcium would be similar to that observed analytically in ICET #4. The agreement between predicted and observed silicon concentrations was not as close, with respect to either source-term values or predicted changes in concentration.

The source-term estimates for aluminum concentration indicated in Figure 6-9 assumed a steady and substantial increase over time due to the dissolution of aluminum metal in borated alkaline water. The simulations indicated that the resulting source-term solutions would be strongly oversaturated with respect to aluminum oxyhydroxide phases (AlOOH), either diaspore or boehmite. Precipitation of either of these phases (Figure 6-8) would lower the aluminum concentration to values comparable to those observed experimentally in ICET #4, in which dissolved aluminum was present only in trace amounts throughout the test. Observations of the submerged aluminum metal samples at the conclusion of the experiment indicated that the post-test appearance was very similar to the pre-test appearance (Dallman, et al., 2005c), so the low observed aluminum concentrations likely were due to passivation of the aluminum metal surface rather than to a steady release and precipitation of aluminum as predicted in the simulations.

6.3.5 PHREEQC Simulations for ICET #5

ICET #5 was a test of chemical effects produced by a set of sample materials submerged in a slightly alkaline (pH ~8) borated solution at 60 °C [140 °F] in which pH buffering was provided by sodium tetraborate (Table 3-1). The sample insulation material tested in ICET #5 was glass fiber insulation (Nukon). Water samples were collected from the tank and analyzed at regular intervals over the 30-day duration of the experiment. The modeled chemical effects simulations were based on estimated source-term water compositions at exposure times of 0.5, 32, 148, 360, and 720 hours (0.02, 1.3, 6.2, 15, and 30 days, respectively), as shown in Table 6-6, assuming in each case that no precipitation had occurred prior to this time to affect the solution composition. After modeling the precipitation of oversaturated solid phases, each simulated final solution composition was compared to the chemical analysis of the ICET #4 solution that had been sampled at approximately the same time period.

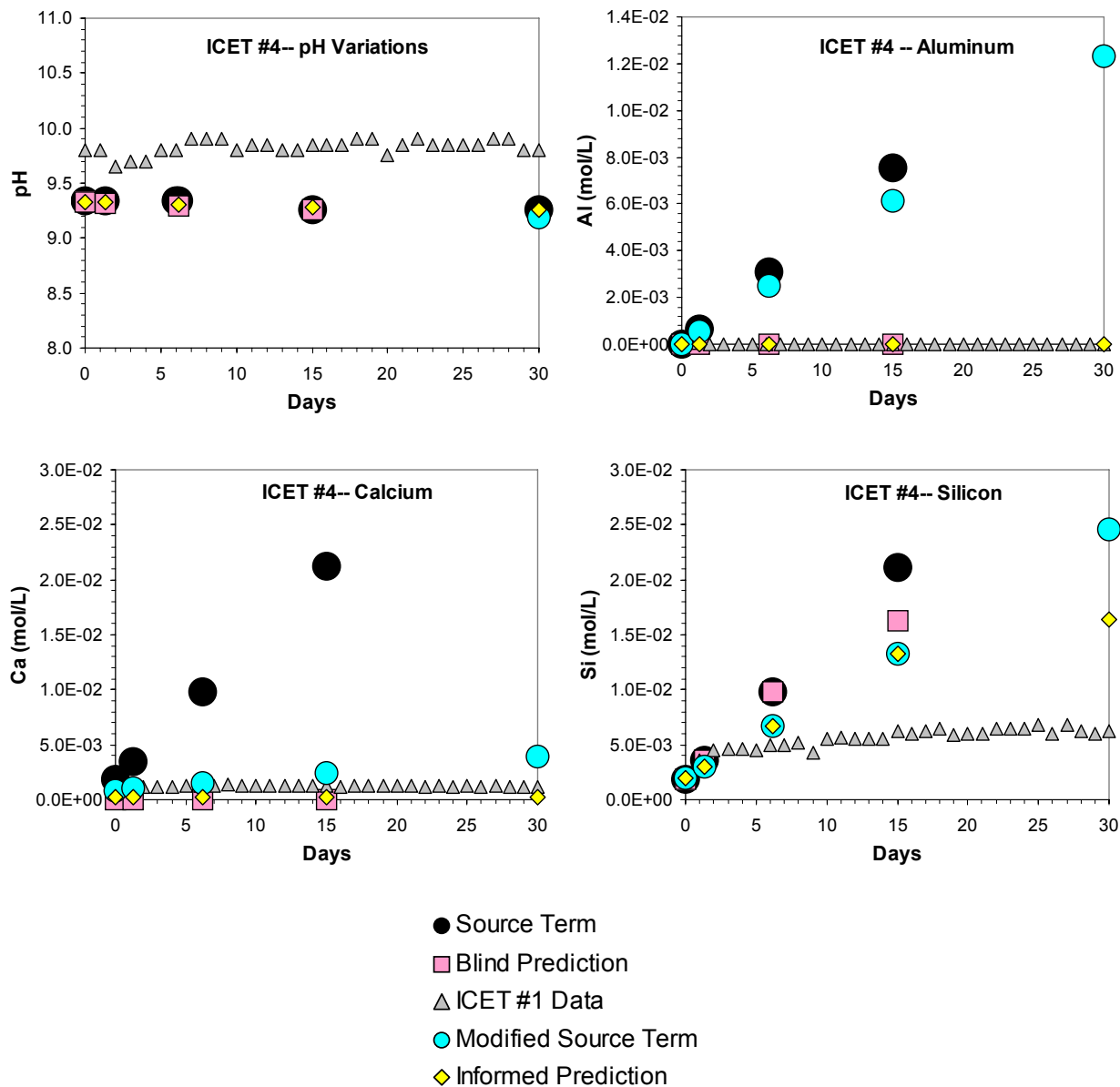


Figure 6-9. Predicted and Observed Variations in ICET #4 Water Chemistry [mol/L = mol/0.264 gal or mol/1.06 quart]

The source-term compositions in the ICET #5 simulations were calculated from the same dissolution and corrosion rates that had been used for the ICET #1 simulations, so the starting compositions for the blind and informed predictions were identical to the source-term concentrations listed for ICET #1 in Table 6-2 except for differences related to the initial proportions of containment water additives (Table 3-2). Both sets of blind predictions for ICET #5 indicated that aluminum oxyhydroxide would precipitate from solution, due to the high estimated concentrations of aluminum in both the original and modified source terms (Figure 6-10). In the informed predictions for ICET #5, aluminum oxyhydroxide was again indicated as a precipitate. Other predicted precipitates consisted of minor amounts of smithsonite ($ZnCO_3$) as well as trace amounts of iron and copper oxides.

Changes in aqueous composition during the ICET #5 experiment are compared in Figure 6-11 with the modeled variations for the original set of blind predictions and for the informed predictions. The simulated pH values were approximately equal to the pH values measured in ICET #5. The measured concentration of dissolved aluminum was slightly higher than was predicted by the precipitation of secondary aluminum-bearing solids. Because no calcium-bearing or silicon-bearing phases were predicted to precipitate in the ICET #5 simulations, the source-term and final predicted concentrations of calcium and silicon were unchanged in each case. The measured calcium concentrations were greater than the predicted values except at long times of exposure (Figure 6-11), indicating that the release rate for calcium had been underestimated in the source-term calculations. Predicted silicon concentrations were roughly

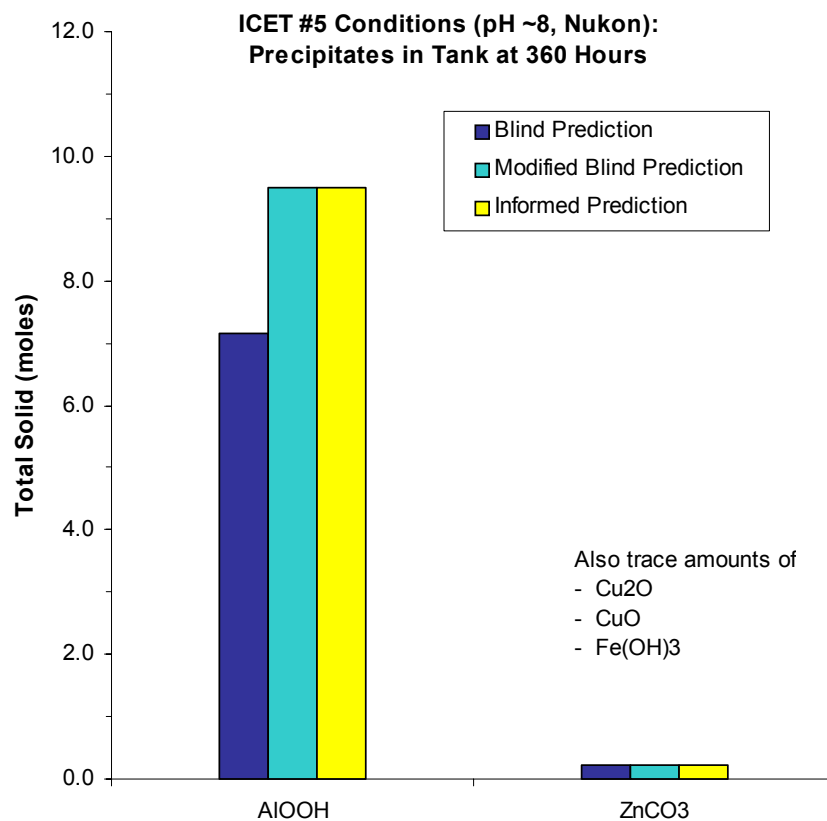


Figure 6-10. Predicted Precipitates in ICET #5 Simulations

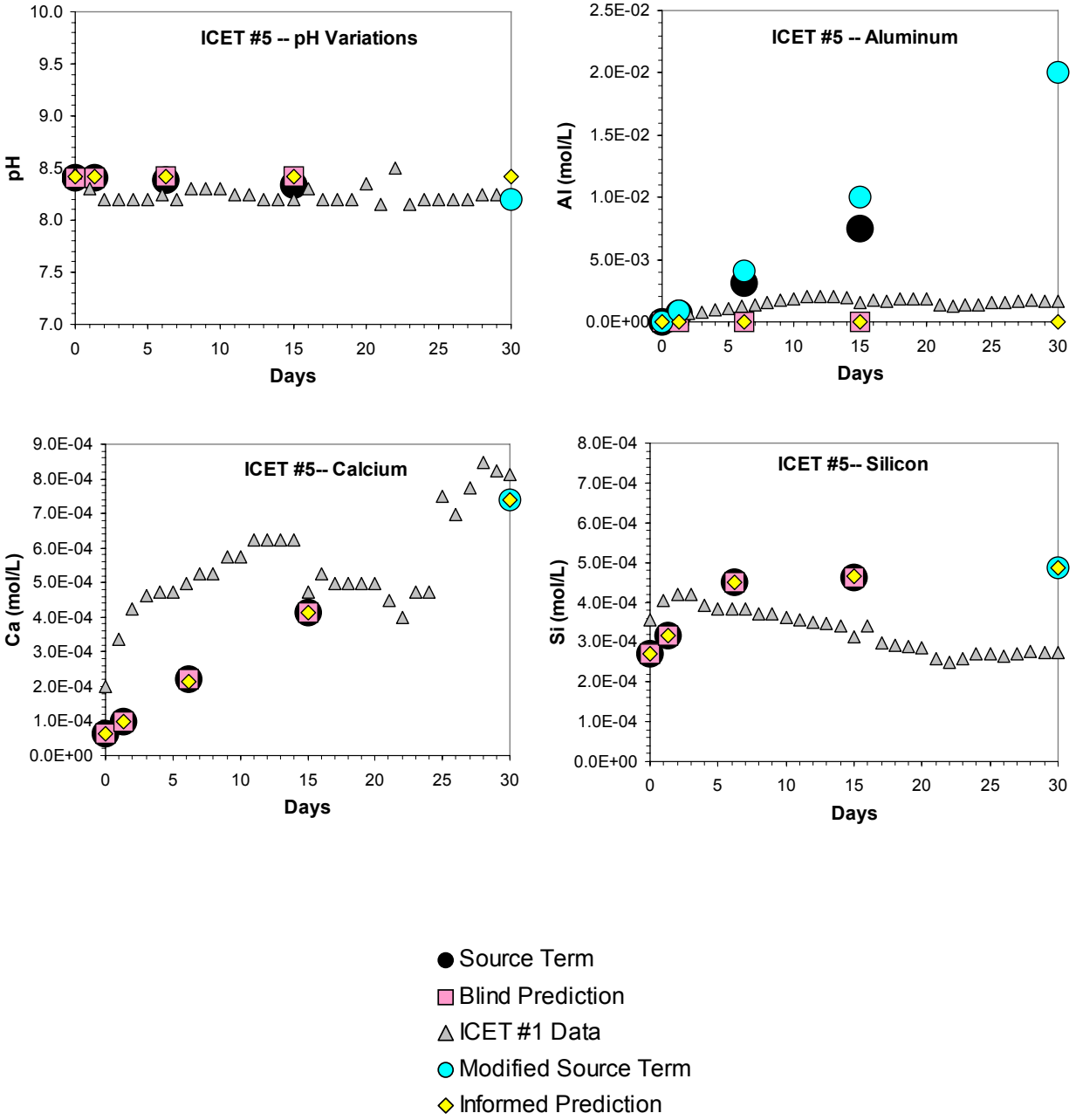


Figure 6-11. Predicted and Observed Variations in ICET #5 Water Chemistry [mol/L = mol/0.264 gal or mol/1.06 quart]

comparable to measured values, but the predictions did not account for an observed gradual decrease in silicon concentration.

6.3.6 Assessment of Blind and Informed PHREEQC Simulations

The blind and informed PHREEQC simulations were adapted to the same conceptual models as were used for the ICET simulations reported in Sections 4 and 5. Because the PHREEQC simulations used the same original and modified source-term compositions, the results in many cases were similar to those of the previous simulations. Comparisons between the PHREEQC blind and informed predictions were facilitated, however, because the same modeling code and the same thermodynamic database were used in all of the simulations. In addition, in the PHREEQC simulations an initial charge-balancing adjustment was made in all of the input files that compensated for pH-buffering discrepancies noted in some of the previous blind predictions in Section 4. A shortened and customized PHREEQC database of relevant low-temperature solid phases simplified and strengthened the applicability of the blind predictions and provided more flexibility in carrying out the informed predictions. The source-term solutions were equilibrated with atmospheric carbon dioxide, so the potential oversaturation of secondary carbonate minerals could be evaluated.

In the informed predictions in which the solution chemistry was affected by precipitation, good agreement between predicted and observed results was obtained for calcium concentration in ICET #1 (precipitation of monohydrocalcite), silicon concentration in ICETs #2 and #3 (precipitation of amorphous silicon dioxide), and phosphorous concentration in ICET #3 (precipitation of calcium phosphate). In ICET #3, better results for calcium concentration were obtained in the blind prediction, which considered the combined precipitation of calcite and calcium phosphate, than in the informed prediction, in which monohydrocalcite was predicted instead of calcite.

An interesting result of the PHREEQC simulations was the observation that the uniform dissolved silicon concentrations that were measured in the latter half of the ICET #2 experiment could be attributed to the equilibration of the water with the glass fiber insulation material. In contrast, the modeling for ICET #3 suggested that the measured uniform silicon concentrations more likely resulted from the precipitation of amorphous silicon dioxide as a secondary phase. This phase was not identified in the ICET #3 experiments, but it is plausible that such a precipitate could have formed as a coating on fibers of the insulation material, where it would have been difficult to detect.

The predicted changes in solution chemistry for ICETs #4 and #5 were uneven, as they were for the same predictions for the equivalent simulations reported in Sections 4 and 5. Additional refinement of the estimated source-term compositions probably would be necessary to improve the simulated results for these cases.

6.4 Example Simulation of Evolving Chemical Conditions in ICET #4

The development of source-term compositions for the chemical effects simulations was based on the simplifying assumption that the water chemistry represented interactions with the sample materials over a specified interval of time, but it did not include any prior precipitation. For long times of exposure, in some cases this assumption resulted in unrealistically large source terms and strongly oversaturated solids. A more detailed modeling approach was applied, using

ICET #4 conditions as an example, to provide a more realistic simulation that addressed precipitation as well as dissolution or corrosion reactions at each timestep. This simulation is described as an “evolved prediction” to indicate that it represents how the initial water composition would be expected to evolve gradually over a 30-day period in response to interactions with the solids in the system. The evolved prediction was performed using PHREEQC Version 2.8 and the same edited version of the lnl.dat database file that was used for the other PHREEQC simulations.

6.4.1 Source-Term Composition for the Evolved Prediction

The modeled example was based on the same values and release rates for modified source-term concentrations for ICET #4 as were used for the previous informed predictions (Sections 5 and 6), but the initial source-term composition was configured a bit differently. The evolved prediction assumed that the composition of the ICET #4 source-term water at the beginning of the simulation included the initial containment water additives (Table 3-2) and the amount of concrete dust, glass fiber insulation, and calcium silicate insulation that was assumed to be released instantaneously upon contact with water (Tables 3-4, 3-6, and 3-8). All of the other source-term contributions to the water were time-dependent. Based on the size of the timestep, these concentrations were calculated offline from the release rates supplied in Tables 3-3, 3-4, 3-6, and 3-8 and were supplied separately to the input file as added reactants. The source-term calculations, with all concentration units standardized to moles per liter, are summarized in Tables 6-7 and 6-8.

	Initial Contributors (mol/kgw)				Total Concentration (mol/L)
	Water Conditioners	Concrete (Dust)	Nukon Glass Fiber (Instant Release)	Calcium Silicate Insulation (Instant Release)	
Al	—	7.80×10^{-6}	1.64×10^{-6}	—	9.44×10^{-6}
B	0.259	—	3.29×10^{-6}	—	0.259
Ca	—	1.20×10^{-4}	3.85×10^{-6}	8.03×10^{-4}	9.27×10^{-4}
Cl	2.74×10^{-3}	—	—	—	2.74×10^{-3}
Li	2.93×10^{-5}	—	—	—	2.93×10^{-5}
Mg	—	—	2.25×10^{-6}	—	2.25×10^{-6}
Na	0.220	—	1.47×10^{-5}	—	0.220
Si	—	4.30×10^{-5}	2.96×10^{-5}	1.84×10^{-3}	1.91×10^{-3}

Table 6-8. Source-Term Release Rates for Integrated Chemical Effects Test (ICET) #4 Example Evolved Prediction					
	Release Rate Contributions (Moles per Liter per Hour)				
	Metals	Concrete (Solid)	Nukon Glass Fiber	Calcium Silicate Insulation	Total Release Rate per Hour (mol/L)
Al	1.69×10^{-5}	5.59×10^{-8}	1.58×10^{-8}	—	1.70×10^{-5}
B	—	—	3.17×10^{-8}	—	3.17×10^{-8}
Ca	—	8.92×10^{-7}	3.71×10^{-8}	3.24×10^{-6}	4.17×10^{-6}
Cu	3.70×10^{-7}	—	—	—	3.70×10^{-7}
Fe	4.26×10^{-8}	—	—	—	4.26×10^{-8}
Mg	—	—	2.17×10^{-8}	—	2.17×10^{-8}
Na	—	—	1.42×10^{-7}	—	1.42×10^{-7}
Si	—	6.74×10^{-8}	2.86×10^{-7}	3.10×10^{-5}	3.14×10^{-5}
Zn	7.21×10^{-7}	—	—	—	7.21×10^{-7}

In the first step of the simulation, the input water composition at time zero was allowed to equilibrate with atmospheric carbon dioxide, and the pH was adjusted for electrical charge balance. Any secondary phases that were oversaturated in the initial water were allowed to precipitate, and the resulting solution chemistry was calculated and saved.

The simulation was divided into 32 timesteps, initially at 4, 12, and 24 hours to represent the first day of the simulation, and then at every subsequent 24 hours, to correspond to the 30-day length of the ICET #4 experiment. At each timestep, the saved final solution composition from the previous step was introduced as the new input solution composition, and any source-term contributions based on corrosion or dissolution release rates within that timestep were added. Any resulting oversaturated secondary phases were allowed to precipitate from the water. The modified solution then was used as the new input value for the next timestep.

6.4.2 Results

Although the conceptual models in the evolved prediction and the informed predictions were based on several different assumptions, the results in terms of total source-term contributions and the solids identified as potential precipitates were the same. More detail was provided by the evolved prediction, however. For example, Figure 6-12 compares the variation in aluminum concentration for the evolved prediction and the informed prediction. For each timestep in the evolved prediction, the amount of aluminum added to the solution is small, but the additional aluminum is sufficient to oversaturate the water slightly with respect to AlOOH. The

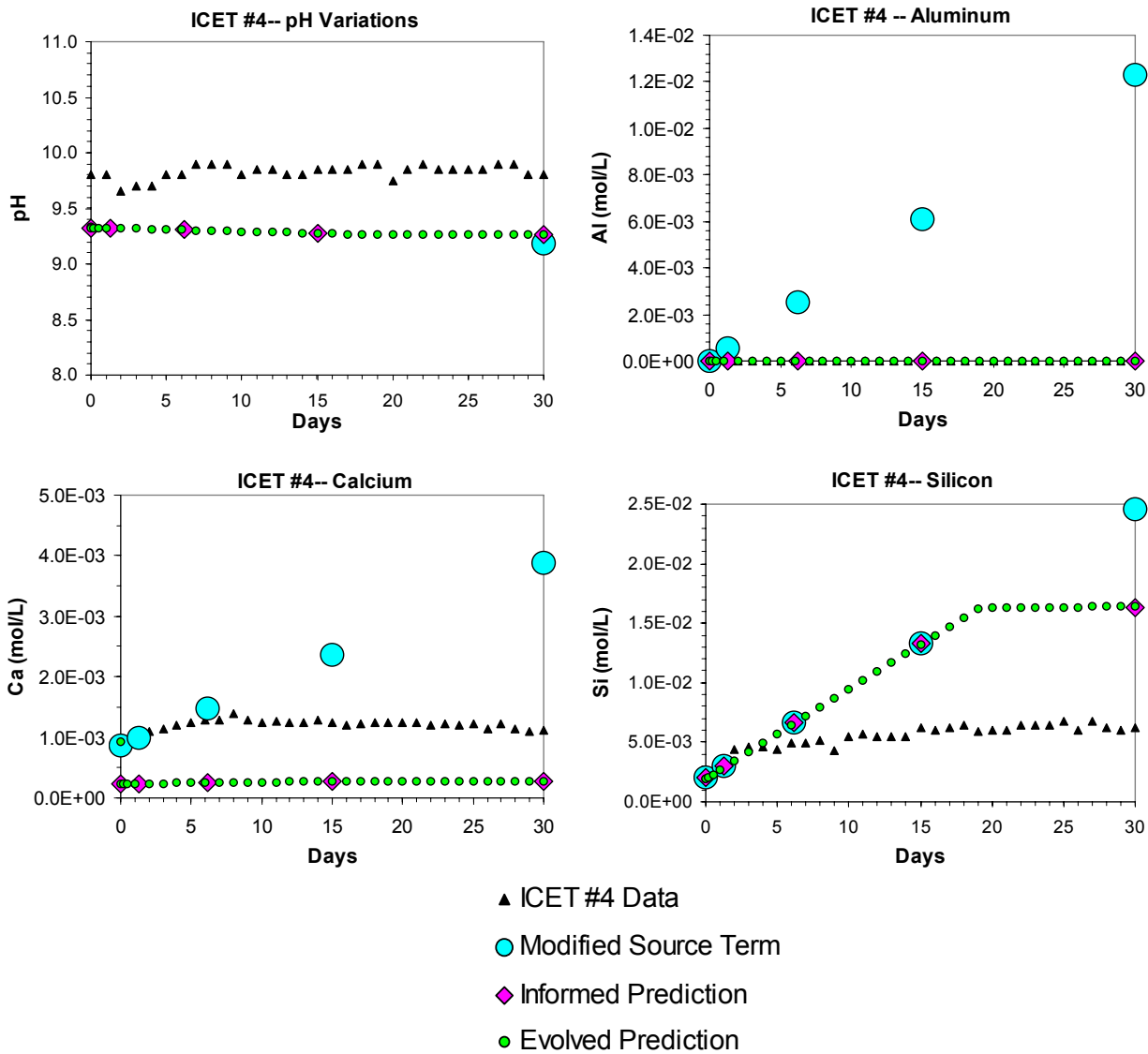


Figure 6-12. Modeled Evolution of Solution Chemistry in ICET #4, Contrasted With Source-Term Calculations and Informed Predictions at Specified Times

precipitation of a minor amount of this phase at each timestep maintains the dissolved aluminum concentration at low levels throughout the simulation. This corresponds to observed trace levels of aluminum in the ICET #4 test solution (Dallman, et al., 2005d). In the informed simulations, no prior precipitation of secondary solids had been assumed, so source-term aluminum concentrations were high for each time of exposure that was modeled, but the total amount of AlOOH that was precipitated over a 30-day period was the same in the informed and evolved predictions.

The precipitation of monohydrocalcite, a metastable precursor of calcite, was predicted to maintain calcium concentrations throughout the simulation at much lower levels than were observed in ICET #4. In contrast to calcium concentrations, during the first 15 days of the simulation silicon concentrations increased steadily until the solution eventually became oversaturated with amorphous silicon dioxide. Precipitation of this phase, beginning on day 16, then maintained dissolved silicon at a fixed concentration for the remainder of the simulation. Note that this leveling off in silicon concentration due to the precipitation of amorphous silicon dioxide was also indicated, but more abruptly, by the informed prediction at day 30.

If the precipitation of monohydrocalcite were suppressed in the evolved prediction, the modeled calcium concentration would increase as indicated by the alternate prediction in Figure 6-13, corresponding at first to the observed calcium concentrations in ICET #4 but surpassing the observed concentration at about day 6. The modeled calcium concentration would increase until day 16, at which point the solution would be oversaturated with respect to the mineral tobermorite, the main constituent of calcium silicate insulation. Subsequent precipitation of tobermorite, accompanied at day 21 and thereafter by precipitation of amorphous silicon dioxide, would then maintain calcium and silicon at fixed concentrations. Although the alternate prediction also corresponds poorly with the ICET #4 experiment data, the example is included here to illustrate a scenario in which the containment water eventually (after about 2 weeks) equilibrates with calcium silicate insulation material (tobermorite) and Nukon glass fiber insulation (amorphous silicon dioxide), and the net dissolution of these materials ceases. In the ICET #4 experiment, the release rate of calcium and silica from the insulation materials appears to have leveled off much sooner and at much lower concentrations, indicating that some other factor suppressed the dissolution of the insulation material before they became saturated in the water.

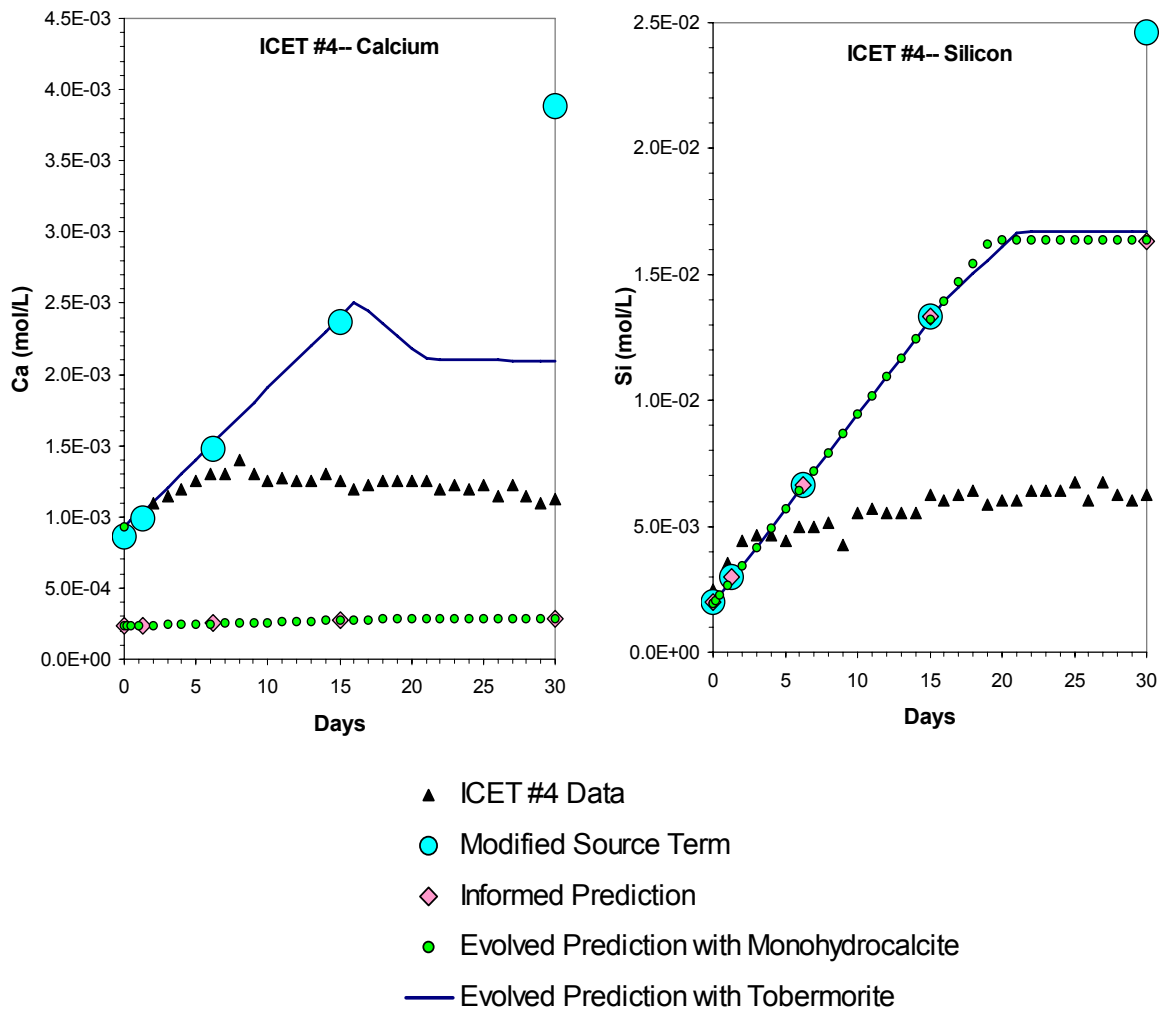


Figure 6-13. Change in Evolution of Calcium and Silicon Concentrations if Precipitation of Monohydrocalcite Is Suppressed and Equilibration With Tobermorite, the Main Component of Calcium Silicate Insulation, Is Allowed

7 CONCLUSIONS

This section assesses the results of the modeling simulations with respect to the general range of physical and chemical conditions that may be expected to occur in potential post-loss-of-coolant accident (LOCA) environments. The discussion includes insights obtained from experiments such as the Integrated Chemical Effects Test (ICET) and related Center for Nuclear Waste Regulatory Analyses (CNWRA) corrosion and dissolution tests, and an assessment of the limitations in estimating chemical effects by the use of chemical equilibration software.

7.1 Post-LOCA Interactions Involving Metals

In the modeled simulations of the ICET experiments, the quantity of secondary precipitates contributed by zinc, copper and carbon steel corrosion under post-LOCA conditions was minimal. Moreover, the patchy secondary deposits on sample metal coupon surfaces in the ICET experiments suggest that in many cases the corrosion products formed directly on the metal surfaces. Such attached solids might not easily be transported as particulates through the cooling system to sump screens. For a larger system, such as a containment building, the total mass of metal-bearing precipitates in a larger volume of water could be more significant. For the range of conditions considered in ICET experiments, however, interactions between the containment water and the exposed metal surfaces effectively were of minor importance.

The observed interactions between aluminum metal and containment water were more pronounced, at least in environments similar to the alkaline conditions of the ICET #1 experiment in which sodium hydroxide was used as a buffering agent in the presence of Nukon glass fiber insulation (Table A-4). The high aluminum concentrations observed in ICET #1 resulted in the formation of colloidal aluminum solids and, upon cooling of the sampled waters, visible precipitation of aluminum oxyhydroxide (Klasky, et al., 2006). In contrast, observed aluminum concentrations were significantly lower in ICETs #4 and #5, which were the other two experiments that had alkaline containment water conditions. In ICET #4, the main difference relative to ICET #1 was the inclusion of calcium silicate insulation material in addition to Nukon glass fiber insulation (Dallman, et al., 2005d). In ICET #5, the main difference relative to ICET #1 was the use of a different buffering agent, sodium tetraborate, which also resulted in a slightly lower pH. No corrosion rate data were available for conditions conforming to ICET #5, but short-term electrochemical tests indicated that the aluminum corrosion rate in the ICET #1 and ICET #4 environments was comparable (A-4). However, the ICET #4 experiment results indicated passivation of aluminum metal in the presence of calcium-silicate insulation, an unmodeled effect that would limit the source-term contribution of aluminum metal in terms of secondary chemical effects under ICET #4 conditions.

Given the differences noted for chemical effects of aluminum in alkaline borated waters and sodium borate waters, it is important to include these effects in the evaluation of post-LOCA conditions for plant-specific environments.

7.2 Post-LOCA Interactions Involving Insulation Materials

7.2.1 Nukon Low-Density Glass Fiber Insulation

The ICETs and separate experiments performed at CNWRA to examine the dissolution of insulation materials under alkaline conditions have indicated that secondary chemical effects likely would not be significant for Nukon low-density glass fiber insulation at either pH 10 (sodium hydroxide buffer solution) or 8.2 (sodium tetraborate buffer solution). Under the conditions represented by ICETs #1, #4, and #5, the dissolution rate measurement experiments indicated that the dissolution of the glass fiber insulation (Figures A-5 and A-6) is inhibited by the presence of aluminum in the system. However, if the dissolved aluminum concentration in the containment pool (from corrosion of metallic aluminum components) is insufficient to impede the dissolution of glass fiber insulation, the source-term contributions from the glass could be significantly higher. For example, Table 7-1 contrasts the difference in aqueous concentration of silicon, calcium, magnesium, and aluminum (all of which are components of the Nukon insulation) that would be produced by the dissolution of the Nukon in a system comparable to the ICET #1 environment (aluminum metal present) with the same system except without aluminum metal present. Even using the higher concentrations as input values, chemical simulations indicate that no additional precipitates would form. Such simulations suggest that even without the inhibiting effect of interactions with aluminum metal in alkaline borated containment water, secondary chemical effects attributed to the dissolution of glass fiber insulation would be minimal.

In the ICET #2 experiment, in which the water was buffered to near-neutral pH values by addition of trisodium phosphate, the dissolution of glass fiber insulation released some calcium to solution, which reacted with some of the dissolved trisodium phosphate to form a minor quantity of calcium phosphate. Although loose precipitates were not observed in the ICET #2 experiment, secondary phosphorous-containing solid phases were noted as coatings on components of the test apparatus (Dallman, et al., 2005b). The glass fiber insulation material is a source for aluminum and calcium that could react with the phosphate under these conditions.

7.2.2 Calcium-Silicate Insulation

Of all the post-LOCA environments considered in this study, the one in which the formation of secondary precipitates was most likely a concern for sump performance was the environment represented by ICET #3, in which a trisodium phosphate borated containment water interacts with calcium-silicate insulation material. The calcium silicate insulation releases a large amount of calcium to solution, which is then available to react with all of the phosphorous from the containment water additive (Table 4-7). This result was predicted by the modeling simulations and was observed in the ICET #3 experiment as a finely dispersed calcium phosphate precipitate (Dallman, et al., 2005c). The effect of interactions between phosphate and the insulation material is more pronounced for calcium silicate insulation than for the Nukon low-density glass fiber insulation because the dissolution of calcium silicate insulation provides abundant calcium to react with the phosphorous, even at early times of exposure.

The chemical effects of interactions between the containment water and calcium silicate insulation are much less significant for conditions in which sodium hydroxide is used to buffer the pH to alkaline conditions, as represented by the ICET #4 environment, compared to the ICET #3 environment which used trisodium phosphate as a buffering agent. The modeled

Table 7-1. Comparison of Aqueous Concentrations for ICET* #1 Environment With and Without Aluminum in Borated Alkaline Containment Water at 60 °C [140 °F]

Element	Test Condition	Predicted Concentration (mmol/L)† of Aqueous Ions in Alkaline Borated Containment Water				
		At 30 Minutes	At 32 Hours	At 148 Hours	At 360 Hours	At 720 Hours
Si	ICET #1 Environment	0.27	0.32	0.45	0.46	0.49
	ICET #1 Environment without aluminum and higher Nukon dissolution rate	0.54	0.75	1.7	3.3	6.2
Ca	ICET #1 Environment	0.06	0.10	0.22	0.41	0.74
	ICET #1 Environment without aluminum and higher Nukon dissolution rate	0.09	0.15	0.38	0.79	1.5
Mg	ICET #1 Environment	0.01	0.02	0.02	0.02	0.02
	ICET #1 Environment without aluminum and higher Nukon dissolution rate	0.03	0.05	0.05	0.05	0.005
Al	ICET #1 Environment	0.03	0.90	4.1	10.0	20.0
	ICET #1 Environment without aluminum and higher Nukon dissolution rate	0.01	0.04	0.10	0.20	0.38

*ICET = Integrated Chemical Effects Test
†mmol/L = mmol/0.26 gal

simulations for ICET #4 that included carbonate chemistry predicted that a secondary calcium carbonate phase would precipitate under ICET #4 conditions, but the resulting predicted dissolved calcium concentrations were significantly lower than the observed concentrations, indicating that this precipitation did not occur during the experiment. The modeled simulations for ICET #4 overpredicted the measured final concentrations of silicon and aluminum in solution, and calcium concentrations were overpredicted at exposure times greater than 148 hours if precipitation did not occur.

7.3 Post-LOCA Interactions Involving Concrete

The chemical effects associated with interactions between containment water and concrete are expected to be minimal under all the conditions that were considered for plant-specific environments. Each of the modeled simulations of the ICET experiments assumed complete dissolution of concrete particulates at the beginning of post-LOCA conditions. Under this assumption, the total amount released from the insulation and concrete particulates dominated the amount released from concrete walls, providing a conservative upper bound for total release from concrete walls over a 720-hour period. The elements released (calcium, silicon, and aluminum) from the concrete are similar to those released from insulation materials, and the potential chemical effects of source-term releases from concrete were addressed by the same modeling simulations.

7.4 Limitations of the Modeling Predictions

The main objective of this study was to evaluate the use of chemical modeling software in predicting the chemical effects of post-LOCA interactions between the containment water and reactive solids in the system. The results of the modeling exercises indicated that the limitations in the use of software are not likely to come from the capability of a particular modeling code to deal with a specific range of expected conditions, such as extremes of temperature, pH, ionic strength, or redox conditions. Rather, the limitations are more generic and relate to the importance of detailed characterization of the systems being modeled.

7.4.1 Estimating Source-Term Concentrations for Modeling

One of the key influences on the simulations, which was clearly demonstrated by the comparison of modeled and measured results for the ICET experiments, is the uncertainty in quantifying how reactions between containment water and the various materials in the containment system—metals, insulation, and concrete—would affect the composition of the water over time. Even if corrosion/dissolution rates for the individual materials are known with some confidence, there are numerous complications in estimating the changes in composition over time. For example, a calculation based on a linear corrosion rate for aluminum in alkaline containment water successfully estimated the release of aluminum to solution at short exposure times but did not account for the observed passivation of the metal surfaces at longer times or in the presence of calcium silicate insulation material. The measured release of silicon by dissolution of Nukon low-density glass fiber insulation is different from the release measured for the same material in the presence of aluminum, which inhibits the dissolution rate. Compared to most other elements, sodium was present in solution in high concentrations because it was a major component of the containment water additives. Because sodium was not indicated to be a reactant in most of the modeled precipitation reactions, its simulated concentration remained almost constant. Nevertheless, the measured sodium concentration varied considerably in some of the ICET experiments and tended to increase over time to values greater than the starting concentration. The most likely contributor of additional sodium to the solution is calcium silicate insulation (Table 3-7), indicating that more detailed characterization of the source-term contribution of the insulation material would improve the chemical effects simulations.

The source-term concentrations that were estimated from experimentally measured release rates for single materials and combinations of materials agreed well with observed concentrations in the ICET experiments in most cases, particularly at early times, but the

release rates in those cases were determined for specific conditions that corresponded closely to the ICET conditions. Extrapolating the source-term release rates for different pH conditions (e.g., ICET #5), for different combinations of reactive solids, or for different proportions of materials, as would be the case in different plant-specific environments, would introduce additional uncertainties into the source-term concentrations to be used for chemical effects predictions. Because interactions between containment water and the insulation materials caused the greatest changes in the starting water compositions, it is particularly important to be able to estimate their source term contributions reliably. For example, in the modeling study, the starting water compositions that were used for the initial blind predictions in ICETs #3 and #4 assumed that calcium silicate insulation dissolved congruently and contributed equal molar proportions of calcium and silicon to the water. For the subsequent informed predictions, the estimated source-term releases of silicon and calcium were revised on the basis of additional dissolution tests conducted separately with Nukon insulation and calcium silicate insulation for conditions specific to the ICET experiments (Tables 3-6 and 3-8). Even with the measured dissolution rates, the simulations tended to overpredict the ICET results, particularly at longer exposure times. This could be attributed to the inhibited release due to the formation of passive films, or to the attainment of the solubility limit for the insulation material, effectively inhibiting its further dissolution. In order to extend the source term estimates to plant-specific conditions for other nuclear power reactors, it may be necessary to conduct additional experiments relevant to the expected conditions to understand the passivity of metals and inhibition of dissolution for insulation materials.

7.4.2 Limitations of Thermodynamic Data

Another potential limitation of the chemical effects simulations is the sufficiency of the thermodynamic database file used for the modeling calculations. The prediction of oversaturated solid phases depends on the concentration of elements in solution and also on the speciation of those elements. For example, the measured concentration of aluminum in borated alkaline containment water in experiments ICETs #1 and #4 was higher than predicted. In ICET #1, the high concentration can be attributed in part to a colloidal aluminum phase that was not filtered from the water effectively before analysis, but the high observed concentrations may also be due in part to aqueous complexation reactions between aluminum and borate ions (e.g., Tagirov, et al., 2004). This possibility could not be assessed because no thermodynamic data for alumino-borate species were available in the database files used by the modeling codes in this study.

The database files that accompanied the chemical modeling programs evaluated in this study contained thermodynamic data for many igneous and metamorphic minerals that form at high temperatures and high pressures. Although these phases, which are the main constituents of the Earth's crust, are thermodynamically stable solids, and equilibrium calculations may indicate that they are oversaturated in a post-LOCA coolant system, they would not precipitate for kinetic reasons.

The database files also contain thermodynamic data for minerals that originate under lower-temperature conditions at or near the Earth's surface. These are more reasonable representations of the solids that would be likely to form secondary phases in an aqueous post-LOCA environment. But in most cases, even these minerals are at best approximations of the phases that would actually precipitate. For kinetic reasons, the oversaturated solid that is most likely to nucleate typically is not the crystalline phase but a more soluble, commonly amorphous, metastable phase. Recrystallization to a more stable crystalline phase eventually

occurs, but generally this is on timescales much longer than those covered by potential post-LOCA conditions. Some of the database files that were used in this study included a few such phases that were amorphous or metastable predecessors of more crystalline solids, and the precipitation of the metastable phase could be modeled by deliberately suppressing the precipitation of the more crystalline solid.

The modeling codes and their accompanying database files were tested without amendment in this study to establish the extent of their “off-the-shelf” suitability without special modifications. The size and complexity of the database files nevertheless required many specific decisions about which solid phases to suppress in the modeled reactions. A widely supported program such as PHREEQC has modeling advantages in terms of its flexibility in suppressing the precipitation of specified phases and the ease with which its thermodynamic database files can be modified to more realistically represent the system being studied. The use of any of the modeling codes evaluated in this study, however, would be facilitated by a customized database file that had only the solid phases that would be realistically expected to form at the conditions of interest. The modeling results would be more meaningful, in particular, if the database incorporated thermodynamic data, developed or estimated from published studies, for the candidate metastable, amorphous, or colloidal phases that would be considered likely to occur in borated containment waters under post-LOCA conditions.

7.5 Assessment of Modeling Approach for Plant-Specific Conditions

The usefulness of the chemical effect simulations conducted in this study depended on two main factors—a realistic estimate of the various source-term contributions to the water composition and an appropriate set of thermodynamic data for the relevant solids and aqueous species at the conditions of interest. The informed predictions, which were calibrated on the basis of observations from the experiments being simulated, corresponded reasonably well to the experiment data for hours to days after the initiating event. The ability to predict the chemical effects on this timescale is important because it is the timeframe that would be common to almost all post-LOCA conditions. In the simulations of ICET #1 conditions, for example, the rapid release of aluminum to solution was predicted to oversaturate the alkaline containment water almost immediately with respect to an aluminum hydroxide or oxyhydroxide phase such as gibbsite or boehmite. Although no visible precipitate was noted during the ICET #1 experiment, the concentration of dissolved aluminum remained high throughout the test and was later determined to be due at least in part to the presence of a colloidal aluminum phase, too small to be seen or removed by the micropore filter prior to analysis. To the extent that such a precipitate, even in its colloidal form, might result in head loss in a sump pool environment, the simulation provided important information about the expected behavior of the system under post-LOCA conditions that was not initially apparent in the experiment itself.

At longer timeframes in the simulations, on the scale of several days or more, the dissolved concentrations of elements were overestimated because the corrosion and dissolution rates of the sample materials had slowed with time but these changes were not included in the source-term water composition. In several of the ICET experiments, the dissolution rates of sample materials also were affected by the co-dissolution of other materials in the system. In order to represent the source-term contributions accurately for different plant-specific containment systems, the effect of multiple materials on release rates needs to be characterized separately. In addition, the dissolution behavior of calcium silicate insulation needs to be

examined in more detail to improve source-term release rates because it is an important influence on water chemistry in the systems where it is present.

Chemical modeling software can be a broadly useful tool in assessing the potential effects of post-LOCA interaction on sump screen blockage. In order to apply the technique to different plant-specific environments, the composition and the dissolution rates of the contributing structural and insulation materials must be carefully characterized, including the effects of co-dissolving materials on solution composition. This important step is separate from, but critical to, the success of any plant-specific modeling simulations. If the estimated source-term release rates are appropriate to the conditions modeled, the evolution of the solution chemistry can be represented in a series of timesteps that indicate when and to what extent precipitates would be expected to form. The predictive capability of post-LOCA chemical effects simulations software depends on the geochemistry experience of the analyst and on the development of thermodynamic data for a set of solids and aqueous species that are appropriate to the relatively short timeframe and comparatively low temperatures of an emergency core cooling system.

8 REFERENCES

- Bickmore, B.R., K.L. Nagy, A.K. Gray, and A.R. Brinkerhoff. "The Effect of $\text{Al}(\text{OH})_4^-$ on the Dissolution Rate of Quartz." *Geochimica Cosmochimica Acta*. Vol. 70. pp. 290–305. 2006.
- Dallman, J., J. Garcia, M. Klasky, B. Letellier, and K. Howe. NUREG/CR–6914, "Integrated Chemical Effects Test Project: Test #1 Data Report." Vol. 2. Los Alamos, New Mexico: Los Alamos National Laboratory. 2005a.
- Dallman, J., B. Letellier, J. Garcia, M. Klasky, W. Roesch, J. Madrid, K. Howe, and D. Chen. NUREG/CR–6914, "Integrated Chemical Effects Test Project: Test #2 Data Report." Vol. 3. Los Alamos, New Mexico: Los Alamos National Laboratory. 2005b.
- Dallman, J., B. Letellier, J. Garcia, J. Madrid, W. Roesch, D. Chen, K. Howe, L. Archuleta, and F. Sciacca. NUREG/CR–6914, "Integrated Chemical Effects Test Project: Test #3 Data Report." Vol. 4. Los Alamos, New Mexico: Los Alamos National Laboratory. 2005c.
- . NUREG/CR–6914, "Integrated Chemical Effects Test Project: Test #4 Data Report." Vol. 5. Los Alamos, New Mexico: Los Alamos National Laboratory. 2005d.
- . NUREG/CR–6914, "Integrated Chemical Effects Test Project: Test #5 Data Report." Vol. 6. Los Alamos, New Mexico: Los Alamos National Laboratory. 2005e.
- Garrels, R.M. and M.E. Thompson. "A Chemical Model for Seawater at 25 °C and One Atmosphere Total Pressure." *American Journal of Science*. Vol. 260. pp. 57–66. 1962.
- Helgeson, H.C., T.H. Brown, and R.H. Leeper. *Handbook of Theoretical Activity Diagrams*. San Francisco, California: Freeman, Cooper, and Co. 1969.
- Helgeson, H.C., T.H. Brown, A. Nigrini, and T.A. Jones. "Calculation of Mass Transfer in Geochemical Processes Involving Aqueous Solutions." *Geochimica Cosmochimica Acta*. Vol 34. pp. 569–592. 1970.
- Jain, V., X. He., and Y. -M. Pan. NUREG/CR–6873, "Corrosion Rate Measurements and Chemical Speciation of Corrosion Products Using Thermodynamic Modeling of Debris Components to Support GSI–191." Washington, DC: NRC. 2005.
- Johns, R.C., B.C. Letellier, K.J. Howe, and A.K. Ghosh. "Small-Scale Experiments: Effects of Chemical Reactions on Debris-Bed Head Loss." LA–UR–03–6415. Los Alamos, New Mexico: Los Alamos National Laboratory. 2003.
- Klasky, M., J. Zhang, M. Ding, B. Letellier, D. Chen, and K. Howe. NUREG/CR–6915. "Aluminum Chemistry in Prototypical Post-LOCA PWR Containment Environment." Washington, DC: NRC. 2006.
- Lawrence Livermore National Laboratory. "EQ3/6." Version 7.2b. Livermore, California: Lawrence Livermore National Laboratory. 1995.

Nordstrom, D.K. and J.L. Munoz. *Geochemical Thermodynamics*. Palo Alto, California: Blackwell Scientific Publications. 1986

Nordstrom, D.K., L.N. Plummer, T.M.L. Wigley, T.J. Wolery, and J.W. Ball. "A Comparison of Computerized Chemical Models for Equilibrium Calculations in Aqueous Systems." *Chemical Modeling in Aqueous Systems Symposium Series 93*. E.A. Jenne, ed. Washington, DC: American Chemical Society. pp. 857–892. 1979.

NRC. "Test Plan: Characterization of Chemical and Corrosion Effects Potentially Occurring During a Pressurized Water Reactor LOCA." Rev. 12b. ML050450478. Washington, DC: NRC. <www.nrc.gov/reading-rm/adams.html> 2005.

———. "Potential Plugging of Emergency Core Cooling Suction Strainers by Debris in Boiling-Water Reactors." NRC Bulletin 96-03. ML 12970261. Washington, DC: NRC. 1996.

OLI Systems, Inc. "StreamAnalyzer." Version 2.0. Morris Plains, New Jersey: OLI Systems, Inc. 2005.

RockWare, Inc. "The Geochemist's Workbench®." Version 5.0. Golden, Colorado: RockWare, Inc. 2004.

Tagirov, B., J. Schott, J.-C. Harrichoury, and J. Escalier. "Experimental Study of the Stability of Aluminate-Borate Complexes in Hydrothermal Solutions." *Geochimica Cosmochimica Acta*. Vol. 68. pp. 1,333–1,345. 2004.

U.S. Geological Survey. "PHREEQC." Version 2.8. Reston, Virginia: U.S. Geological Survey. 2003.

Wolery, T.J. "Some chemical aspects of hydrothermal processes at mid-oceanic ridges B a theoretical study." Ph.D. thesis. Northwestern University. Evanston, Illinois. 1978.

Wolery, T.J. and S.A. Daveler. "EQ6, A Computer Program for Reaction Path Modeling of Aqueous Geochemical Systems: Theoretical Manual, User's Guide, and Related Documentation (Version 7.0)." UCRL-MA-110662 PT IV. Livermore, California: Lawrence Livermore National Laboratory. 1992.

Zhu, C. and G. Anderson. *Environmental Applications of Geochemical Modeling*. Cambridge, England: Cambridge University Press. 2002.

APPENDIX A

DISSOLUTION RATE MEASUREMENTS FOR INSULATION MATERIALS

The sample materials tested in the Integrated Chemical Effects Test experiments (ICETs #1–#5), which were conducted at the University of New Mexico, included two types of pipe insulation material, Nukon® low-density glass fiber insulation and calcium silicate particulate insulation. Dissolution rates for these materials have been measured separately at the Center for Nuclear Waste Regulatory Analyses (CNWRA) in borated containment waters at 60 °C [140 °F] at pH values of 7 and 10. The dissolution rates for Nukon low-density glass fiber insulation also were measured in the presence of aluminum metal in the borated containment waters at pH values of 7 and 10. The dissolution rates for calcium silicate particulate insulation were determined using bulk (solid) samples of calcium-silicate insulation and disaggregated (particulate) samples. The borated waters in all the dissolution rate tests contained 0.259 M [2,800 ppm B] boric acid (H_3BO_3), conforming to the composition of most of the containment waters used in the ICETs. The borated solution was either adjusted to a pH of 7 by adding trisodium phosphate ($\text{Na}_3\text{PO}_4 \cdot 12\text{H}_2\text{O}$) or to a pH of 10 by adding sodium hydroxide (NaOH).

Experimental Methods

Samples of Nukon low-density glass fiber insulation (with and without coupons of aluminum metal) and solid and particulate samples of calcium silicate insulation were used in this study. Starting amounts of insulation materials and aluminum were estimated from the U.S. Nuclear Regulatory Commission (NRC) Test Plan (NRC, 2005). Using a maximum immersed volume of insulation and a minimum volume of available containment water and assuming an immersed insulation fraction of 0.75, the test plan estimated that the ratio of the mass of Nukon insulation to the volume of containment water would be 3.9 kg/m^3 [0.25 lb/ft^3]. Similarly, for calcium silicate insulation, the ratio of the sample mass to the volume of containment water was estimated as 31.68 kg/m^3 [1.98 lb/ft^3]. In the ICETs experiments that used calcium silicate insulation, Nukon glass fiber insulation also was present in a ratio of 80-percent calcium silicate to 20-percent Nukon glass fiber insulation by volume. The adjusted ratio of the calcium silicate sample mass to the volume of containment water was reduced to 25.3 kg/m^3 [1.58 lb/ft^3] for the CNWRA dissolution tests.

The density of Nukon low-density glass fiber insulation is 38.1 kg/m^3 [2.4 lb/ft^3], and the density of calcium silicate insulation is 307.5 kg/m^3 [19.2 lb/ft^3]. This study conservatively assumed that 100 percent of the insulation in each case was contacted by borated containment water. Similarly, the ratio of surface area to volume for the aluminum metal was estimated as $11.5 \text{ m}^2/\text{m}^3$ [$3.5 \text{ ft}^2/\text{ft}^3$], and the total immersed surface area-to-containment volume was estimated as $0.57 \text{ m}^2/\text{m}^3$ [$0.17 \text{ ft}^2/\text{ft}^3$], conservatively assuming an immersed fraction of 0.34 for aluminum.

Representative examples of Nukon low-density glass fiber insulation and calcium silicate test specimens are displayed in Figures A–1 and A–2. The calcium silicate particulate specimens had a particle size distribution between –100 and +120 mesh. Chemical compositions of Nukon low-density glass fiber insulation and calcium silicate particulates, analyzed by inductively coupled plasma atomic emission spectrometry, are provided in Tables A–1 and A–2. The chemical analysis for the calcium silicate insulation (Table A–2) indicates that the mass fraction of calcium oxide is almost twice that of silicon dioxide. The analysis indicates that calcium is associated with other phases in the insulation material besides calcium silicate. In addition,

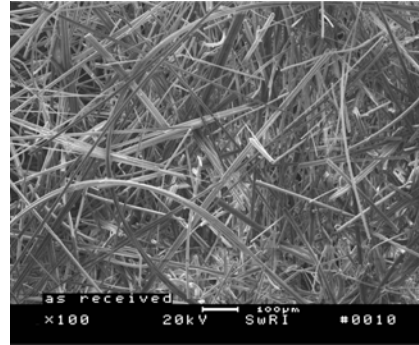
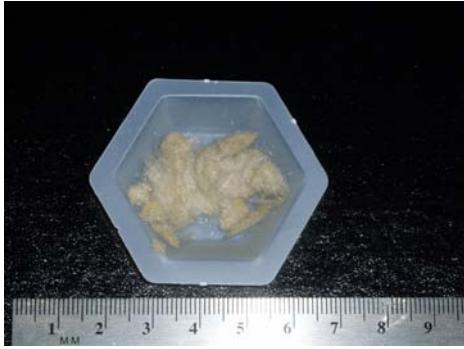


Figure A-1. Photograph (Left) and Scanning Electron Micrograph (Right) of the Representative Nukon® Glass Fiber Insulation Test Specimen. Scale of the Left Photograph in mm.

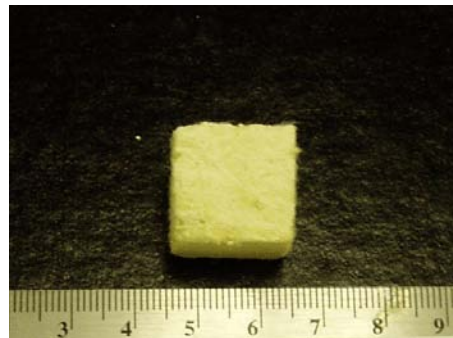


Figure A-2. Photographs of the Representative Calcium Silicate Insulation Test Specimens in Particulate (Left) and Bulk Solid (Right) Form. Scale in cm.

Component	Weight Percent	Molecular Weight	Mole Fraction
SiO ₂	62.5	60	0.637
Al ₂ O ₃	3.6	102	0.022
CaO	8.2	56	0.090
MgO	3.45	40	0.053
Na ₂ O	15.8	62	0.156
B ₂ O ₃	5.0	70	0.044

Oxide	Weight Percent
CaO	40.5
SiO ₂	18.5
Na ₂ O	2.7
TiO ₂	2.6
Al ₂ O ₃	1.1
K ₂ O	0.2
MgO	0.5
Fe ₂ O ₃	0.5
Loss on Ignition	35.2
Total	102.0

titanium and sodium are present in the insulation, as well as minor amounts of aluminum, potassium, magnesium, and iron.

The dissolution rates for samples of Nukon low-density glass fiber insulation and calcium silicate insulation were determined using the static leaching method provided in ASTM Standard C-1285 (ASTM International, 2003). Except for the use of sample-to-volume ratios that corresponded to those of the ICETs (NRC, 2005), the protocols in the ASTM C-1285 were followed.

Static leaching tests for Nukon low-density glass fiber insulation and calcium silicate insulation were conducted in 60-mL [2.0-oz] polytetrafluoroethylene vessels. The test vessels were cleaned and checked for pH and fluoride release to meet the requirements specified in the test method. In all tests, test specimens were placed in 50 mL [1.7 oz] of test solution. Test vessels were placed in ovens held at 60 °C [140 °F] and were withdrawn at time intervals of 1/6, 1/2, 1, 3, 5, 7, and 14 days. In addition, one blank control test that did not contain a test sample in the solution was subjected to the same procedures for 14 days for each pH value.

At the end of each test period, the vessels were removed from the ovens and allowed to cool. A small portion of the leachate was withdrawn to measure pH using a standard glass electrode and a calibrated pH meter. The leachate was then filtered with a 0.45- μ m [0.018-mil] syringe filter prior to cation analysis using inductively coupled plasma atomic emission spectrometry.

For Nukon low-density glass fiber insulation, the mass release, NR_i , from the insulation material, based on the leached component i from the sample, was calculated using Eq. (A-1)

$$NR_i = \frac{(C_i - B_i)}{F_i} \quad (A-1)$$

where

- NR_i — normalized insulation mass release, in units of mg/L
- C_i — concentration of element i in solution, in units of mg/L
- B_i — concentration of element i in the blank solution, in units of mg/L
- F_i — mass fraction of element i in the unleached specimen (dimensionless)

The dissolution rates were determined from the slopes of the normalized plots of insulation mass release versus time.

Linear polarization tests were conducted on test specimens of aluminum cut from plates of as-received metal. Specimen coupons had dimensions of ~2.5 cm [~1 in] (length), ~2.5 cm [~1 in] (width), and the same thickness as the as-received metal. Before the aluminum specimens were used, they were polished on successive grades of silicon carbide papers (320, 400, and 600 grit) and cleaned in deionized water and in acetone. An Alloy 825 wire sealed in glass was connected to the specimen for electrical conduction, and the contact area was coated with Microstop. The measurements were conducted in a three-electrode electrochemical cell in N_2 -deaerated solutions. The three electrodes consisted of a test specimen (or working electrode), a reference electrode, and a counter electrode. The measurements were conducted at 60 °C [140 °F] in a 250-mL [0.067-gal] test cell made of glass and Teflon. The test cell was fitted with a water-cooled condenser to minimize solution loss at elevated temperatures. A saturated calomel electrode was used as a reference electrode. It was connected to the solution through a water-cooled Luggin probe with a porous silica tip to maintain the reference electrode at room temperature. A platinum flag was used as the counter electrode. Polarization resistance measurements were conducted by measuring the current density while scanning the potential of the test specimens in the anodic direction over the range -10 to +10 mV or -20 to +10 mV with respect to the corrosion potential. The scan rate used was 0.01 mV/s.

The specimens were immersed in solution for 1 hour prior to the start of the tests. The value of the polarization resistance, R_p , was obtained by fitting a straight line to the data in the range of

-5 to +5 mV with respect to the corrosion potential. The corrosion current density was calculated using Eq. (A-2).

$$I_{\text{corr}} = \frac{0.12}{2 \times 2.303R_p} \quad (\text{A-2})$$

After I_{corr} was obtained, the corrosion rate, CR, based on Faraday's law, was calculated according to Eq. A-3

$$\text{CR} = K \frac{I_{\text{corr}} \text{EW}}{\rho} \quad (\text{A-3})$$

where K is the constant with values depending on the units of other parameters in the equation, and EW is the equivalent weight.

Results and Discussion

Nukon Low-Density Glass Fiber Insulation

The measured dissolution of Nukon low-density glass fiber insulation, calculated from silicon release as a function of time at 60 °C [140 °F], is shown in Figure A-3 for the test in borated trisodium phosphate containment water at pH 7 and in Figure A-4 for the equivalent test in the presence of aluminum metal. Figure A-5 shows results of the test for the dissolution of Nukon low-density glass fiber insulation as a function of time at 60 °C [140 °F] in alkaline containment water at pH 10. Figure A-6 shows results for the equivalent test in the presence of aluminum metal. Table A-3 shows the evolution of pH in each of the four tests as a function of time. In each case, the pH remained constant, which is indicative of the effectiveness of the buffering agents. In all of the tests, as illustrated in Figures A-3 to A-6, the amount of dissolution of the glass fiber insulation increased over time.

For the tests conducted at pH 7, the Nukon low-density glass fiber insulation dissolution showed linear increases as a function of increased time of exposure irrespective of the presence of aluminum (Figures A-3 and A-4). The leaching rate was provided by the slope of the best-fit line between fiber dissolution (mg/L) and time.

In contrast, the dissolution of Nukon low-density glass fiber insulation in alkaline borated containment water was strongly affected by the presence or absence of aluminum. Figure A-5 shows results for the dissolution of Nukon low-density glass fiber insulation at pH 10 in the absence of aluminum, calculated on the basis of silicon released to solution. The dissolution behavior has two distinct components. The intercept value indicates a finite amount of instantaneous dissolution at the starting time, followed by a linear increase in dissolution over time. The instantaneous release component is attributed to hydroxyl ion attack on the surface of the fibers. The slope for the linear increase in the remainder of the test is comparable to the slope for the previous tests at pH 7 (Figures A-3 and A-4), indicating that the dissolution rate at pH 10 for fibers in the absence of aluminum is similar under neutral and alkaline conditions. However, the dissolution behavior of the Nukon low-density glass fiber insulation at pH 10 in the presence of aluminum (Figure A-6) is markedly different from the observed behavior at pH 10 in the absence of aluminum (Figure A-5). In the presence of aluminum, the total amount of dissolution of the Nukon low-density glass fiber insulation after 14 days is almost an order of magnitude less than in the equivalent test without aluminum. The intercept in Figure A-6

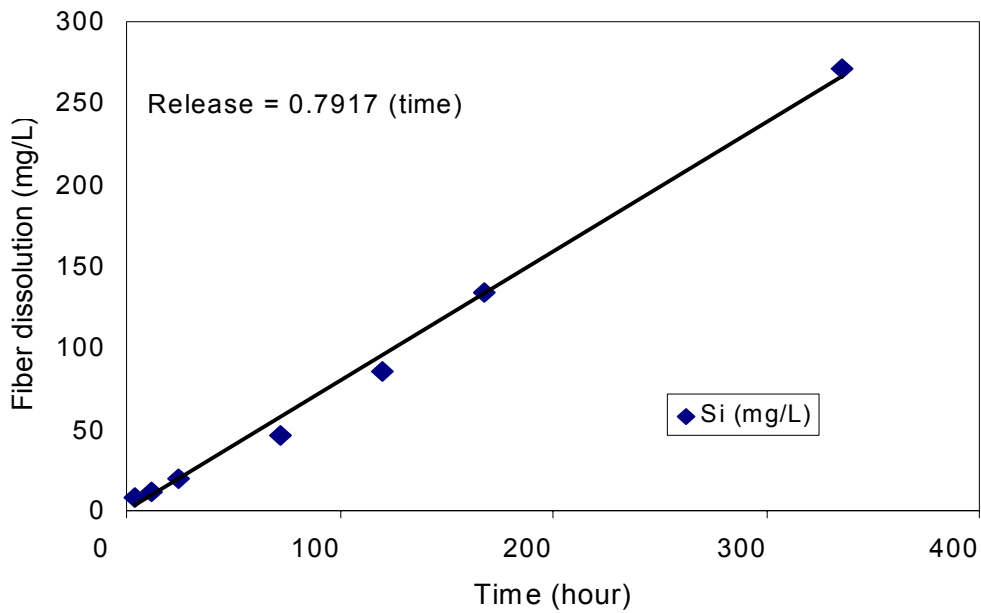


Figure A-3. Glass Fiber Dissolution in the Absence of Aluminum Metal, Based on Si Release, in Borated Trisodium Phosphate Containment Solution at pH 7 and 60 °C [140 °F]

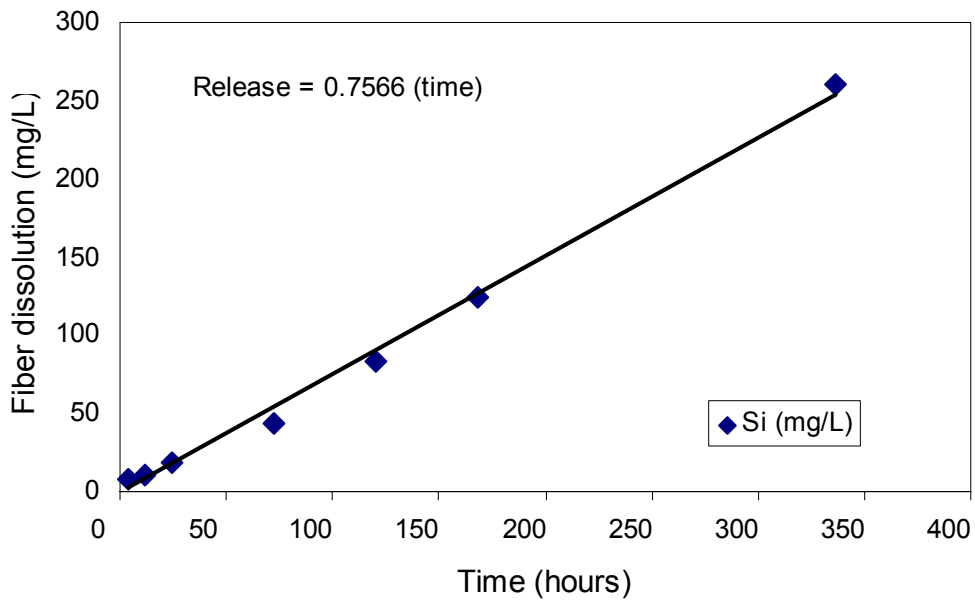


Figure A-4. Glass Fiber Dissolution in the Presence of Aluminum Metal, Based on Si Release, in Borated Trisodium Phosphate Solution at pH 7 and 60 °C [140 °F]

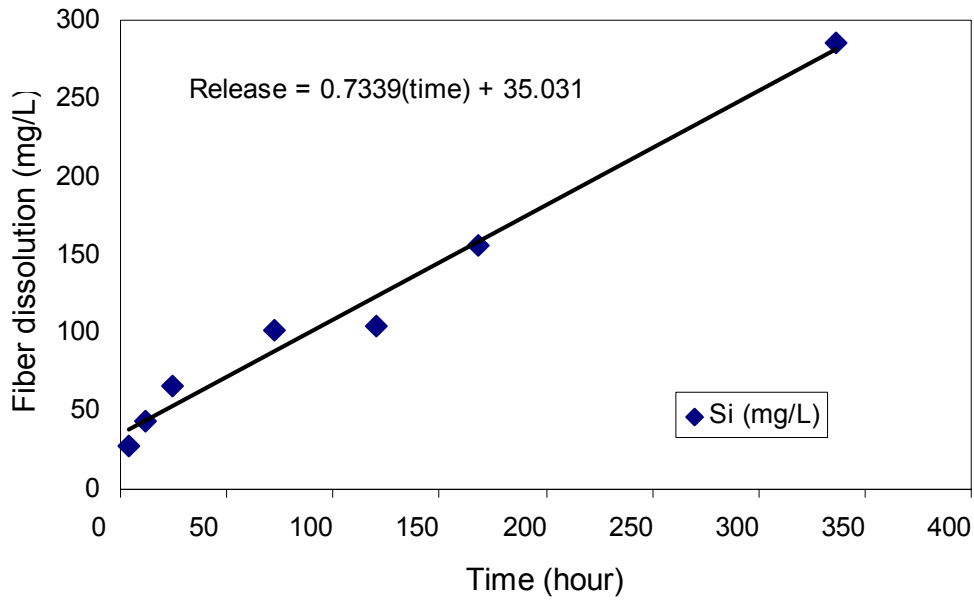


Figure A-5. Glass Fiber Dissolution in the Absence of Aluminum Metal, Based on Si Release, in Alkaline Borated Containment Water at pH 10 and 60 °C [140 °F]

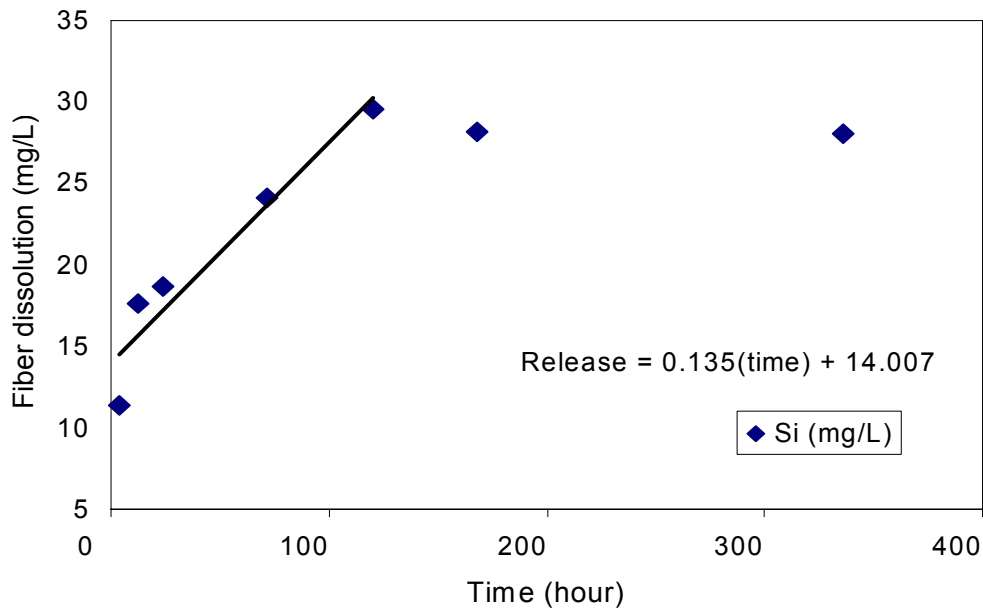


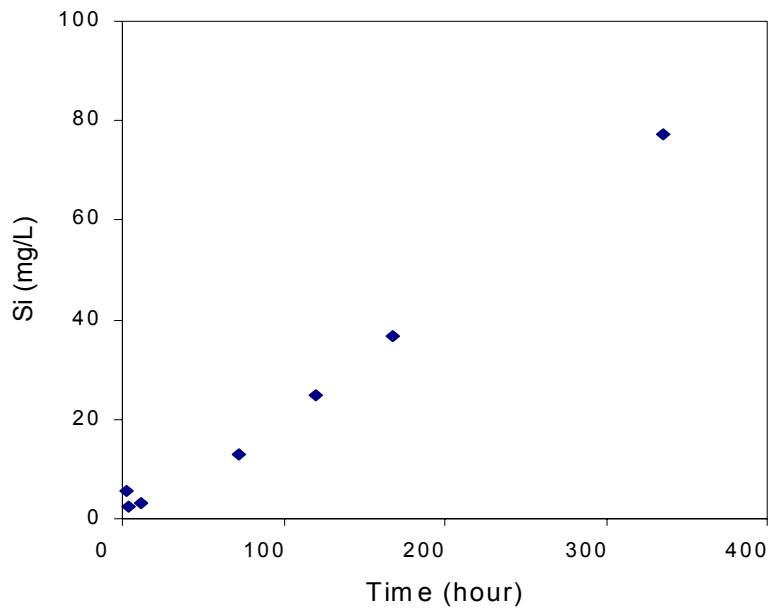
Figure A-6. Glass Fiber Dissolution in the Presence of Aluminum, Based on Si Release, in Alkaline Borated Containment Water at pH 10 at 60 °C [140 °F]

Time (days)	pH of the Borated Alkaline Containment Water With Glass Fiber and Aluminum	pH of the Borated Alkaline Containment Water With Glass Fiber	pH of the Borated Trisodium Phosphate Containment Water With Glass Fiber and Aluminum	pH of the Borated Trisodium Phosphate Containment Water With Glass Fiber
0	10.00	10.00	7.06	7.06
6	9.72	9.71	7.20	7.18
12	9.75	9.74	7.17	7.17
24	9.76	—	7.19	7.15
72	9.75	9.73	7.18	7.17
120	9.76	9.75	7.19	7.19
144	9.77	—	7.20	7.21
336	9.78	9.75	7.28	7.23

indicates an instant release by dissolution at starting time, followed by a linear increase in the amount of dissolution with increasing time up to 96 hours. Beyond 96 hours, the dissolution of the Nukon low-density glass fiber insulation was completely inhibited in the presence of aluminum.

The silicon concentrations in the Nukon low-density glass fiber insulation dissolution tests corresponded closely to the measured concentrations from tests #1 and #2 of the ICET Project (Dallman, et al., 2005a,b). Figure A-7 shows the silicon concentration over time for the dissolution test of Nukon low-density glass fiber insulation in borated trisodium phosphate containment water at pH 7, which represents conditions similar to those of ICET #2. In the dissolution test and in ICET #2, the silicon concentration was approximately 80 ppm after about 300 hours (Dallman, et al., 2005b). In the dissolution test in borated alkaline containment water at pH 10 (with aluminum present) the silicon concentration was much lower and stabilized in less than 100 hours to values of about 7 or 8 ppm (Figure A-8). Similar low concentrations were observed under similar test conditions in ICET #1 (Dallman, et al., 2005a).

High solution concentrations of aluminum in ICET #1, approximately 300 ppm after 14 days of exposure (Dallman, et al., 2005a), also were observed in the Nukon dissolution test at pH 10 in the presence of aluminum. Figure A-9 shows the concentration of aluminum in the dissolution test, as determined by chemical analysis of the test solution, as well as the aluminum release calculated by the linear polarization technique and by the electrochemical method. The calculated amount of aluminum released based on the electrochemical method was approximately 30 percent less than that of the weight loss method. The analyzed aluminum



A-7. Silicon Release (mg/L) From Glass Fiber Dissolution in a pH 7 Borated Containment Water at 60 °C [140 °F]

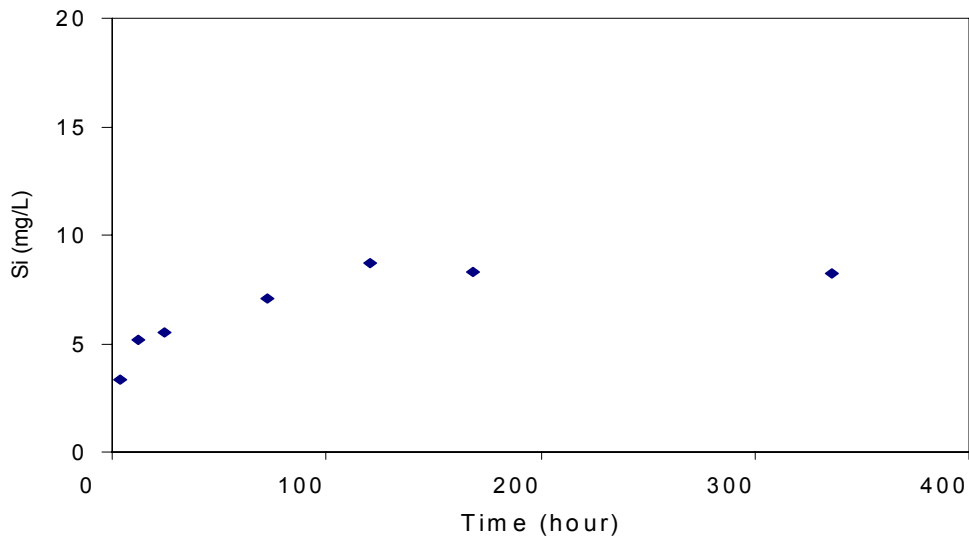


Figure A-8. Silicon Release (mg/L) From Glass Fiber Dissolution in a pH 10 Borated Containment Water at 60 °C [140 °F]

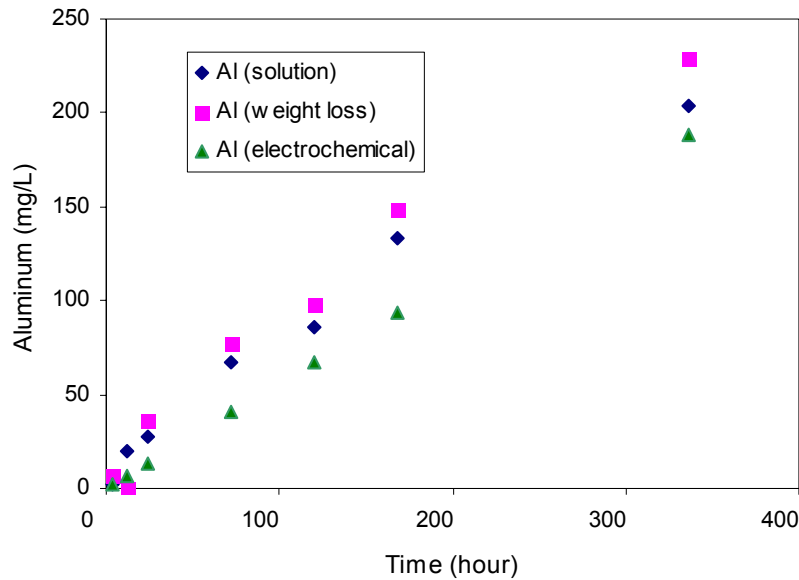


Figure A–9. Aluminum Release (mg/L), Based on Weight Loss, Solution Analysis, and Linear-Polarization Method in a pH 10 Borated Containment Water at 60 °C [140 °F]

concentration in the test solution, which after about 14 days was approximately 200 ppm, was slightly lower than the amount of aluminum released to solution as estimated by the weight loss method. Some of the aluminum released from the metal coupon may not have remained in solution, but formed a secondary precipitate.

In the dissolution test at pH 7 in the presence of aluminum, both the chemical analysis of the solution and the weight loss measurement method indicated that there was no detectable release of aluminum, and the corrosion rate for aluminum calculated from the linear polarization method was extremely low. These results are comparable to the results of ICET #2, conducted under similar conditions, for which aluminum was not detected by chemical analysis in the test solution (Dallman, et al., 2005b).

Table A–4 summarizes the aluminum corrosion rates that were calculated for the different Nukon glass fiber dissolution experiment conditions in the presence of aluminum. In borated water, the dissolution of aluminum is enhanced by several orders of magnitude under alkaline conditions as compared to neutral conditions. In contrast, as indicated by the differences between Figures A–5 and A–6, the dissolution of glass fiber insulation, which is significant in alkaline borated water, is greatly diminished under the same conditions if aluminum is included in the test materials.

At the conclusion of the dissolution tests for Nukon low-density glass fiber insulation, the leached insulation material from the dissolution test in alkaline water in the presence of aluminum was characterized by scanning electron microscope and energy dispersive X-ray spectroscopy to determine the morphology of the glass fibers and the chemical composition of

Table A-4. Measured Corrosion Rate of Aluminum in Borated Containment Test Solutions		
Test Conditions	Method	Corrosion Rate g/m²-h [mil/yr]
Borated alkaline containment water (pH 10)	Electrochemical	0.986 [126]
Borated alkaline containment water (pH 10) with Nukon glass fiber insulation	Weight loss	1.31 [168]
Borated alkaline containment water (pH 10) with Nukon glass fiber insulation	Chemical analysis	1.16 [148]
Borated trisodium phosphate containment water (pH 7)	Electrochemical	3.9×10^{-3} [0.5]
Borated trisodium phosphate containment water (pH 7) with calcium silicate insulation	Electrochemical	0.028 [3.61]
Borated alkaline containment water (pH 10) with calcium silicate insulation	Electrochemical	0.80 [103]

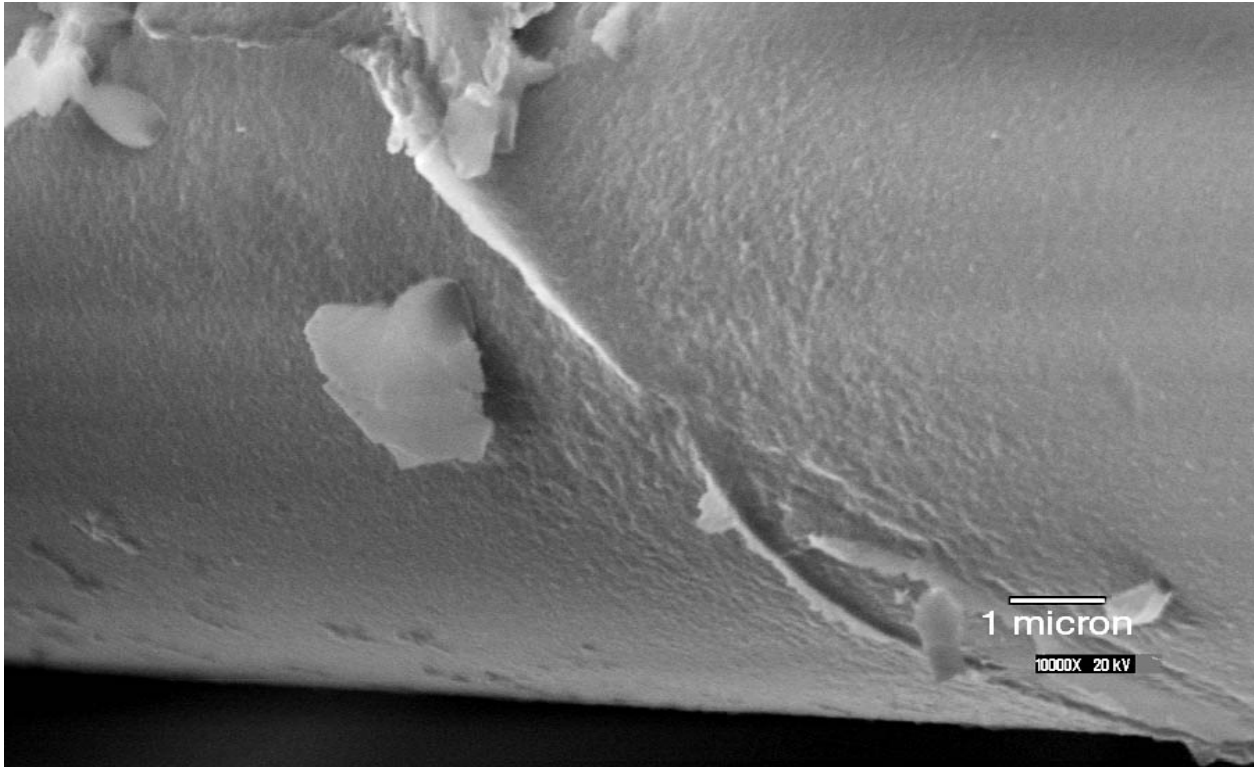


Figure A-10. Scanning Electron Micrograph Showing a Submicron Coating on the Surface of a Glass Fiber in a pH 10 Borated Alkaline Water Containing Aluminum at 60 °C [140 °F]

their surface layers. Figure A–10 is a scanning electron micrograph of one of the leached glass fibers, which appears to show a secondary surface coating on the fiber. The energy dispersive X-ray spectroscopy spectra for this sample did not detect any distinct changes in the surface composition, but the surface layer may have been so thin that the energy dispersive X-ray spectroscopy was unable to resolve differences in the bulk and surface composition. The apparent presence of a coating on the fibers is supportive of the test results, given that the dissolution of the glass fibers was strongly inhibited under alkaline conditions in the presence of aluminum.

Oka and Tomozawa (1980) studied the inhibition of glass dissolution in alkaline solutions in the presence of various cations. The study showed strong inhibition by alkaline earth ions and a weak inhibition by aluminum. The study demonstrated that small amounts {0.001 mol/L [8×10^{-9} mol/gal]} of alkaline earth ions led to the formation of metal-silicate hydrated layers on the glass surface, inhibiting glass dissolution. However, Oka and Tomozawa (1980) did not observe the formation of comparable layers on the glass surface when aluminum was introduced to the solution. Nevertheless, some inhibitive effect from aluminum was observed in the dissolution tests reported here for Nukon glass fiber. It is possible that the pH of the test solution was not sufficient to hydrolyze aluminum complexes in solution.

In a review paper, Grambow and Muller (2001) noted that observed decreases in glass dissolution rate with increasing time can be attributed to gradual saturation of major elements such as silica on the surface of the glass and condensation of surface silanol groups. A first-order dissolution rate law is widely used to predict the performance of nuclear waste glasses. However, precipitation of secondary mineral phases or formation of aqueous complexes containing major elements could continue to promote glass dissolution while maintaining element concentrations at or near saturated levels in the solution.

Ferrand, et al. (2004) studied alteration kinetics of French borosilicate glass SON 68 between 50 and 90 °C [122 and 194 °F] in a dynamic system enriched with silica, boron, and sodium and used analyses from a scanning transmission electron microscope to show that, except for pH < 4.8 at 90 °C [194 °F], an alteration layer was absent on the surfaces of the glass. Despite the absence of an alteration layer, the low dissolution rate was attributed to a reduction in glass dissolution affinity in silica-rich solutions.

In contrast to affinity-based explanations of glass dissolution, Gin (2001) theorized that glass alteration kinetics is not controlled by solution saturation, but by the protective properties of the alteration film. The formation of hydrated surface layers would act as a diffusion barrier for water molecules in the glass network and, hence, would reduce overall dissolution. The ability of protective layers to limit water diffusion depends on glass composition (Strachan and Croak, 2000). The low dissolution rate of glass fibers in alkaline solutions containing boron, sodium, and aluminum metal could be attributed to a combination of reduced glass dissolution affinity in the presence of aluminum and to the formation of a hydrated layer on fiber surfaces. For source-term conditions similar to those of the ICET experiments in which Nukon low-density glass fiber insulation and aluminum metal are exposed to alkaline or neutral borated containment water at a temperature of 60 °C [140 °F], the use of glass dissolution rates (indicated in Table A–5) is recommended to estimate the concentration of elements that would be contributed to a post-loss-of-coolant accident (LOCA) containment solution by the dissolution of glass fiber insulation material. For an alkaline borated containment water, the amount of glass dissolution was conservatively bound at 30 mg/L after 96 hours of exposure, based on

Table A-5. Summary of Dissolution Behavior of Insulation Materials in Borated Containment Water at 60 °C [140 °F]			
Insulation	Test Conditions	Dissolution (mg/L)	Remarks
Nukon low-density glass fiber insulation	Trisodium phosphate, pH 7	$0.79 \times \text{time}$	Linear increase with time. Used for estimating amount of Nukon for simulating ICET* #2.
Nukon low-density glass fiber insulation	Aluminum, trisodium phosphate, pH 7	$0.76 \times \text{time}$	No effect of aluminum on Nukon dissolution.
Nukon low-density glass fiber insulation	Sodium hydroxide, pH 10	$35 + 0.73 \times \text{time}$	Showed instantaneous release.
Nukon low-density glass fiber insulation	Aluminum, sodium hydroxide, pH 10	$14 + 0.14 \times \text{time}$	Strong inhibitive effect of aluminum on Nukon dissolution. Maximum release 30 mg/L. Used for estimating amount of Nukon for simulating ICET #1.
Calcium silicate insulation (particulate)	Trisodium phosphate, pH 7	$5.61 \times P + 1.27 \times \text{time}$	Calcium silicate reaction with trisodium phosphate.
Calcium silicate insulation (solid)	Trisodium phosphate, pH 7	$5.61 \times P + 3.02 \times \text{time}$	Behavior similar to calcium silicate particulate but higher calcium release. Used for estimating amount of Calcium silicate for simulating ICET #3.
Calcium silicate insulation (particulate/solid)	Sodium hydroxide, pH 10	Ca: $32.2 + 0.13 \times \text{time}$ Si: $51.6 + 0.87 \times \text{time}$	Used for estimating calcium and silicon amount from calcium silicate for simulating ICET #4.
*ICET = Integrated Chemical Effects Test			

observations from ICET #1 and from the glass fiber dissolution tests. This fixed amount was used to estimate the contribution from fiber insulation components released into the solution after 96 hours. For a borated containment water at pH 7, a linear dissolution rate of 0.79 mg [1.7×10^{-6} lb] of glass fiber per liter [0.26 gal] of solution per hour is recommended.

Calcium silicate insulation tests

Separate dissolution tests using calcium silicate insulation material were conducted for equal masses of bulk material (solid sample) and disaggregated material (particulate sample). Sets of tests were conducted using borated containment water at pH 10 and pH 7. Compared to the Nukon low-density glass fiber insulation, the calcium silicate insulation was generally more soluble under all conditions tested. Analysis of the sample material by X-ray diffraction indicated that its main crystalline components were a calcium silicate mineral, tobermorite, and a lesser amount of calcium oxide. For the dissolution rate calculations, it was assumed that the calcium silicate insulation had an idealized composition of equal molecular proportions of CaO and SiO₂.

The concentrations of silicon and calcium were measured as a function of time in borated containment water at pH 10 for dissolution of particulate and solid calcium silicate samples, as shown in Figures A-11 and A-12. The trends in concentration were similar for both elements. In the dissolution test with the solid sample, the concentration of calcium was slightly less than for that of the particulate sample (Figure A-12).

The dissolution of the calcium silicate insulation also released some potassium and sodium to the solution (Table A-6). If all of the sodium and potassium were released from a sample of

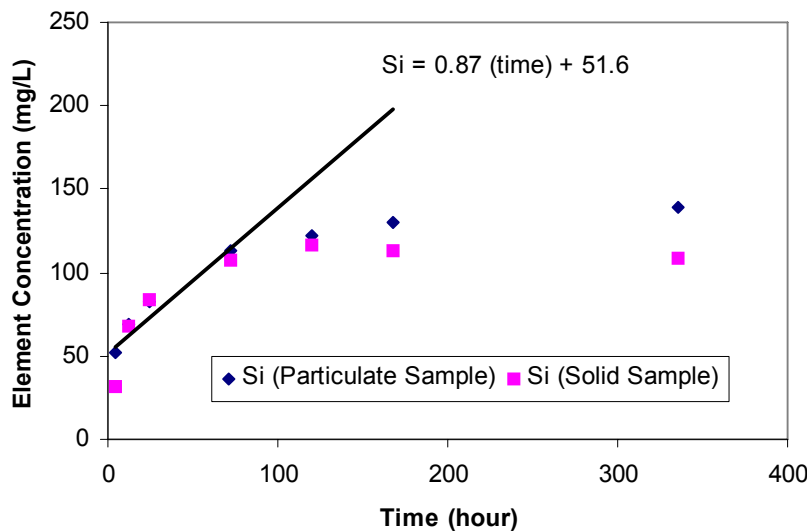


Figure A-11. Silicon Released From Calcium Silicate Particulate and Solid Insulation Samples at 60 °C [140 °F] in Borated Alkaline Containment Water

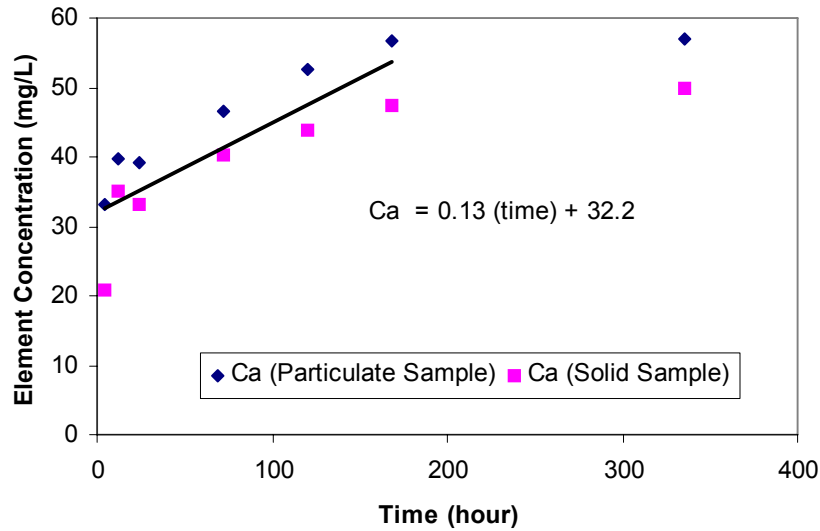


Figure A-12. Calcium Released From Calcium Silicate Particulate and Solid Insulation Samples at 60 °C [140 °F] in Borated Alkaline Containment Water

Time (hours)	Calcium Silicate (Particulate)		Calcium Silicate (Solid)	
	Sodium (mg/L)* (Calculated)	Potassium (mg/L)	Sodium (mg/L)† (Calculated)	Potassium (mg/L)
4	220	27.2	120	27.2
12	240	25.6	100	37.8
24	230	29.5	190	41.0
72	150	28.2	200	42.7
120	180	29.2	140	43.4
168	160	30.2	-70	39.3
336	120	30.3	-160	38.3

*Initial sodium concentration was 4,180 ppm
†Initial sodium concentration was 5,260 ppm

insulation material that had a mass-to-solution ratio of 25.3 kg/m³ [1.58 lb/ft³], the concentration of dissolved sodium would increase by about 500–600 ppm and that of potassium would increase by about 40 ppm. The measured potassium concentration in the test solutions ranged between about 30 and 40 ppm, and did not increase significantly over time. These observations suggest that the small amount of potassium in the insulation material (Table A–2) was associated with a highly soluble phase, possibly a potassium salt, that dissolved immediately upon contact with the containment water.

The release of additional sodium from the samples is attributed to an uncharacterized sodium-bearing phase in the insulation material, as indicated by bulk chemical analysis (Table A–2). If this phase is a sodium silicate, it would account for about 10 percent of the mass in the insulation material. The amount of sodium released from the insulation material in the tests was estimated as the difference between the measured sodium concentration in the sampled water at any given time and the initial sodium concentration in the borated containment water, prior to introducing the insulation material in the experiment. The starting sodium concentration in the borated alkaline containment water was very high (~ 4,000–5,000 ppm) because the water was adjusted to high pH conditions by adding sodium hydroxide. The amount of additional sodium released by dissolution of insulation material potentially would be underestimated by these calculations if sodium was also removed from solution by other chemical reactions. The removal of sodium by ion exchange or by precipitation in secondary phases also is indicated by the observation that the calculated amounts of sodium released from the insulation material became smaller over time, and in fact became negative after 7 days for the solid calcium silicate test samples (Table A–6).

Table A–7 shows the variation of pH with time for the calcium silicate insulation samples in the borated alkaline containment water. During the dissolution tests, the pH of the alkaline solution remained essentially constant, which is indicative of the effectiveness of the buffering agent. The difference in starting pH values between the test that used a calcium silicate particulate

Time (hours)	Calcium Silicate Particulate		Calcium Silicate Solid	
	pH of the Borated Alkaline Containment Water	pH of the Borated Trisodium Phosphate Containment Water	pH of the Borated Alkaline Containment Water	pH of the Borated Trisodium Phosphate Containment Water
0	9.74	7.13	10.09	7.52
4	9.73	7.73	10.09	7.52
12	9.75	7.79	10.12	7.62
24	9.76	7.81	10.12	7.82
72	9.77	7.89	10.13	7.87
120	9.76	7.91	10.11	7.89
168	9.77	7.93	10.15	7.93
334	9.78	7.92	10.11	7.94

sample (pH 9.74) and the test that used a solid sample (pH 10.09) is attributed to minor differences in the solution preparation process for the two tests.

Overall, the dissolution behavior of the calcium silicate insulation in borated alkaline containment water displays three distinct stages, as illustrated by the trends in Figures A-11 and A-12. In both graphs, the intercept value represents an instantaneous dissolution at initial contact between the sample material and the containment water, which is attributed to the hydroxyl attack in an alkaline solution and the release of silicon from the silicate minerals (e.g., tobermorite) in the insulation. This stage is followed by a linear increase in dissolution over time, which is more clearly defined for silicon (Figure A-11) than for calcium (Figure A-12), followed by a leveling off to a constant concentration, which represents a steady state. Differences in the stages of the concentration trends for silicon and calcium in Figures A-11 and A-12 are attributed to the assumption that the insulation consists of multiple solid phases, which release calcium and silicon at different rates.

For estimates of source-term conditions similar to those of ICET #4 (Dallman, et al., 2005a), in which calcium silicate insulation and Nukon low-density glass fiber insulation (in addition to other containment system components) were exposed to borated alkaline containment water at a temperature of 60 °C [140 °F] and at a pH of about 10, use of the relevant dissolution rates (shown in Table A-5) is recommended to estimate how much calcium and silicon would be released by the dissolution of calcium silicate insulation. In Table A-5, the release rate for calcium silicate insulation at a pH of 10 was based on an average of the measured results for particulate and solid samples. Figures A-11 and A-12 show the linear part of the curve for the calculated dissolution rate. The dissolution experiments indicate that the selected rate overestimates calcium and silicon release at longer exposure times. The calculation provides a conservative bound for estimating the source-term contribution of calcium silicate insulation material to the overall solution composition.

The second set of dissolution tests involved samples of calcium silicate insulation in borated containment water with the initial pH adjusted to a value of 7 by adding trisodium phosphate. Tests were performed using bulk (solid) calcium silicate samples and disaggregated (particulate) samples. Figures A-13 and A-14 compare the aqueous concentrations of silicon and calcium in dissolution tests for particulate and solid calcium silicate insulation samples. The type of sample tested (particulate or solid) made little difference in the concentration trends. However, the concentration over time for silicon in solution was slightly higher for the particulate insulation sample than for the solid sample (Figure A-13). In contrast, the concentration of calcium in solution was significantly higher for the solid insulation sample than for the particulate sample (Figure A-14).

Sodium and potassium from the calcium silicate insulation samples also were released to solution in the dissolution tests. Compared to the releases from tests at pH 10 (Table A-6), the concentration of potassium in solution was lower in the tests at pH 7 (Table A-8), with values between about 12 and 18 ppm. The release of sodium associated with dissolution of the solid calcium silicate insulation sample varied over time from about 160 to 240 ppm (Table A-8), a range similar to estimated sodium releases in the tests at pH 10 (Table A-6). In comparison, significantly higher sodium releases, on the order of 357 to 386 ppm, were calculated for the particulate calcium silicate insulation sample. The higher estimated releases from the

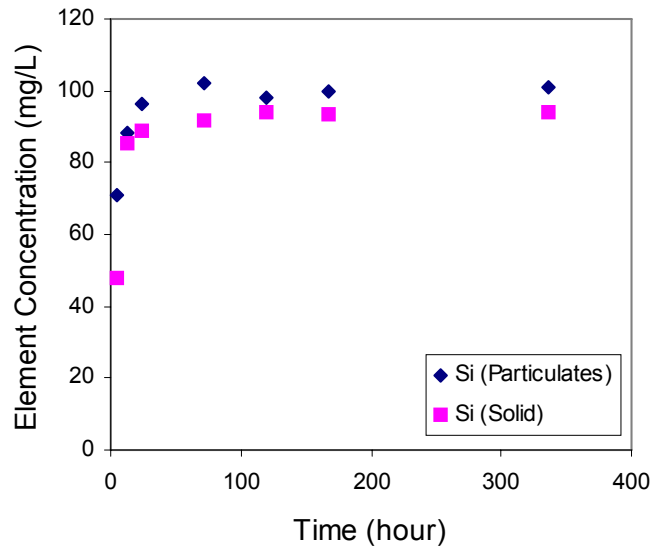


Figure A–13. Silicon Released From Calcium Silicate Particulate and Solid Insulation Samples in Borated Trisodium Phosphate Containment Water at 60 °C [140 °F]

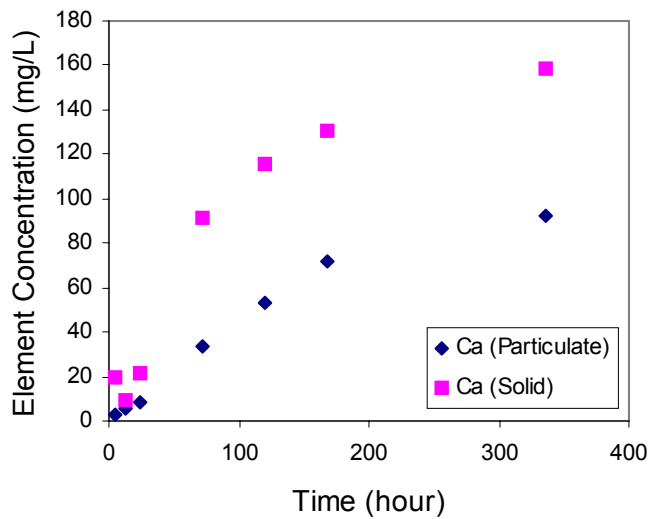


Figure A–14. Calcium Released From Calcium Silicate Particulate and Solid Insulation Samples in Borated Trisodium Phosphate Water at 60 °C [140 °F]

Table A–8. Concentration of Sodium and Potassium Released From Calcium Silicate Insulation in Borated Trisodium Phosphate Test Solutions				
Time (hours)	Calcium Silicate (Particulate)		Calcium Silicate (Solid)	
	Calculated Sodium (mg/L)*	Potassium (mg/L)	Calculated Sodium (mg/L)*	Potassium (mg/L)
4	363	13.8	174	11.8
12	361	16.1	158	14.3
24	361	14.4	281	16.2
72	357	18.6	181	16.8
120	383	15.8	189	17.8
168	386	16.3	225	18.0
336	363	16.3	241	17.8

*Initial sodium concentration was 518 ppm

particulate sample are likely due to the larger surface area accessible to the contacting solution in the particulate sample. Given sufficient time, the amount of sodium released would be expected to be equivalent for particulate and solid calcium silicate insulation samples. In contrast to the observations at pH 10 (Table A–6), the estimated sodium concentration in the dissolution tests initiated at pH 7 did not decrease significantly over time, suggesting that the excess sodium in this case was not being removed from solution by precipitation. No differences were observed between the particulate and solid samples for potassium releases, indicating that the potassium-bearing impurity in the insulation samples dissolved quickly and completely regardless of sample type.

Figure A–15 illustrates the changes in phosphorous concentration over time for solid and particulate samples of calcium silicate insulation. Although the insulation material did not contain phosphorous (Table A–2), the concentration of phosphorous in the borated containment water initially was high (about 240 ppm) due to the addition of trisodium phosphate to the starting solution for pH adjustment. As illustrated by Figure A–15, the phosphorous concentration in the test solution dropped sharply to values near zero soon after the dissolution tests commenced, indicating that phosphorous was being consumed by reaction with some component of the insulation material. The same rapid decrease in phosphorous concentration was noted in ICET #3 (Dallman, et al., 2005c), which was the ICET experiment conducted under conditions that were the most similar to these dissolution tests. Table A–7 shows the variation of pH with time for the calcium silicate insulation samples in the borated trisodium phosphate containment water. The pH increased from an initial value of about 7.1 for the particulate sample and 7.5 for the solid sample to a final value of about 7.9 at the end of both tests. The dissolved phosphorous served as a pH buffer, and the increase in pH during the test corresponded to the removal of most of the phosphorous from the test solution.

In the dissolution tests in which Nukon low-density glass fiber insulation was used as the sample material in borated trisodium phosphate containment water, no abrupt drop in phosphorous concentration and only a minor increase in pH (Table A–3) was noted. Also, no

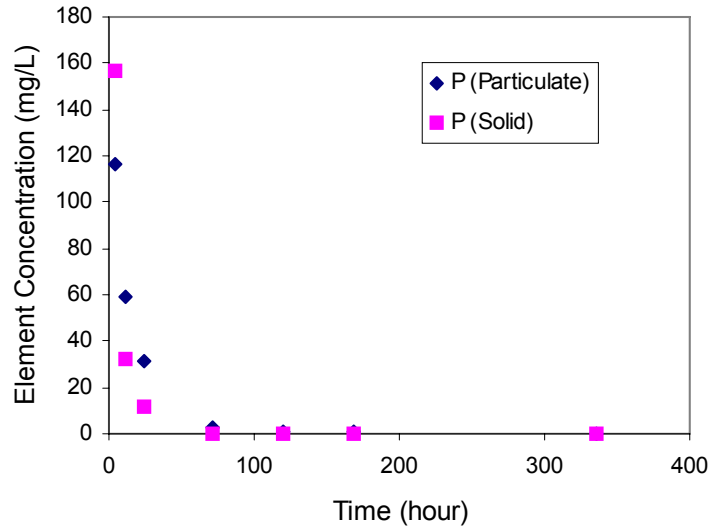
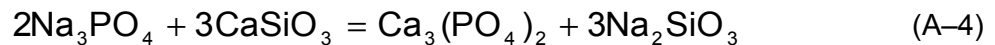


Figure A–15. Phosphorous Concentration in Dissolution Tests for Calcium Silicate Particulate and Solid Insulation Samples in Borated Trisodium Phosphate Containment Water at 60 °C [140 °F]

change in phosphorous concentration was reported for the related ICET experiment, ICET #2 (Dallman, et al., 2005b), that involved Nukon glass fiber insulation, but not calcium silicate insulation, in borated trisodium phosphate containment water. These observations suggest that the phosphorous is reacting with calcium released from the calcium silicate insulation material. A possible reaction between trisodium phosphate and calcium silicate is indicated by Eq. A–4.



The calcium silicate insulation dissolution behavior in the borated trisodium phosphate solution has three distinct parts, as indicated by the concentration trends for calcium, silicon, and phosphorous in Figure A–16 for the particulate insulation sample. In this test, the starting phosphorous concentration of 240 ppm dropped to 117 ppm in 4 hours, to 32 ppm in 24 hours, and to 3 ppm in 72 hours. For the reaction shown in Eq. A–4, it was assumed that 5.61 mg/L [4.8×10^{-5} lb/gal] of calcium silicate, represented simplistically as CaSiO_3 , reacts with 1 ppm of phosphorous. The amount of phosphorous removed from solution in the dissolution test would require the dissolution of 1,300 ppm of calcium silicate in 72 hours. To calculate the dissolution rate for calcium silicate insulation, it was conservatively assumed that the reaction between the insulation material and trisodium phosphate was immediate and consumed all calcium released by the dissolution of 1,300 ppm of the sample material. With continued dissolution, calcium concentration begins to increase linearly, as indicated by Figure A–16, at a rate of 0.437 ppm/h.

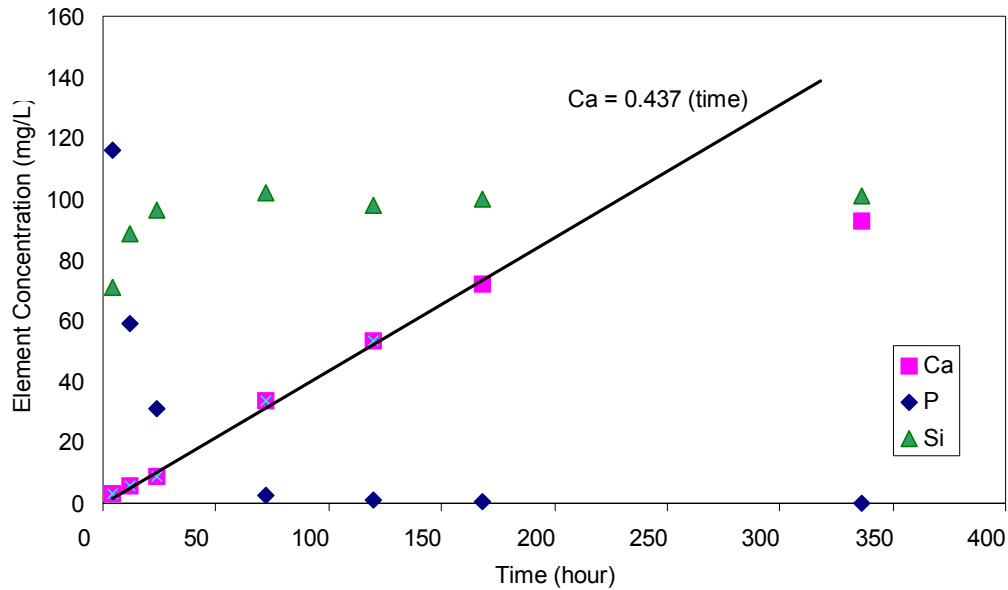


Figure A-16. Elements Associated With Dissolution of Calcium Silicate Insulation (Particulate Sample) as a Function of Time in Borated Trisodium Phosphate Containment Water at 60 °C [140 °F]

Based on these assumptions, the dissolution rate for calcium silicate is given by Eq. A-5

$$M = 5.61 \times P + 0.437 \times \frac{116}{40} \times t \quad (\text{A-5})$$

where M is the mass of calcium silicate in mg, reacted at any given time, t ; P is the concentration of phosphorous, mg/L; and $116/40$ is the mass ratio of calcium silicate to calcium in containment water.

In the dissolution test involving the solid calcium silicate insulation sample, the concentrations trends for calcium, silicon, and phosphorous were similar, but the observed calcium release was much higher. Using these data to calculate dissolution rates would result in a linear increase in calcium concentration with increasing time at a rate of 3.08 ppm/h.

Note that if calculations based on Eq. A-5 are compared with the experimentally measured calcium concentrations, the equation overpredicts the dissolved amount at times beyond 14 days. The change in slope for calcium concentration after this time may indicate that the insulation material has reached its solubility limit at this point, or that an alteration layer has formed on the surface of the sample material and has significantly reduced the transport of reactants (water) or cations (calcium, silicon). It is also possible that as the calcium concentration increased, the solution became oversaturated with respect to a secondary calcium-bearing phase. Precipitation of this phase would limit the calcium concentration to a fixed value, even as dissolution of the insulation material continued. A similar limit on concentration is indicated for silicon (Figure A-13), which stabilized at about 90 ppm soon after

the dissolution tests commenced although the sample material dissolution rate in Eq. A-5 indicates that the concentration should be greater.

By these calculations, approximately 5.3 percent of the insulation material, if present in the borated containment water as calcium silicate (CaSiO_3), would participate in the reaction shown by Eq. A-4, and approximately 7.0 percent of the total sample of particulate calcium silicate insulation material, or approximately 9.3 percent of the total sample of solid calcium silicate insulation material, would dissolve over a time period of 336 hours in the borated trisodium phosphate containment water. Comparison of these source-term estimates with the measured values for silicon and calcium in ICET #3 (Dallman, et al., 2005c) indicates that the results are similar.

Table A-5 provides a summary of the results and observations for the dissolution tests involving the insulation materials. Corrosion rates for other debris components related to the ICET are provided in Jain, et al. (2005).

REFERENCES

ASTM International. "Nuclear, Solar, and Geothermal Energy." *ASTM C1285-02: Standard Test Method for Static Leaching of Monolithic Waste Forms for the Disposal of Radioactive Waste. Volume 12.01: Nuclear Energy (I)*. Published on CD ROM. West Conshohocken, Pennsylvania: ASTM International. 2003.

Dallman, J., J. Garcia, M. Klasky, B. Letellier, and K. Howe. "Integrated Chemical Effects Test Project: Test #1 Data Report." LA-UR-05-0124. Los Alamos, New Mexico: Los Alamos National Laboratory. 2005a.

Dallman, J., B. Letellier, J. Garcia, M. Klasky, W. Roesch, J. Madrid, K. Howe, and D. Chen. "Integrated Chemical Effects Test Project: Test #3 Data Report." LA-UR-05-6146. Los Alamos, New Mexico: Los Alamos National Laboratory. 2005b.

Dallman, J., B. Letellier, J. Garcia, J. Madrid, W. Roesch, D. Chen, K. Howe, L. Archuleta, and F. Sciacca. "Integrated Chemical Effects Test Project: Test #3 Data Report." LA-UR-05-6996. Los Alamos, New Mexico: Los Alamos National Laboratory. 2005c.

Ferrand, K., A. Abdelouas, B. Grambow, and J. Crovisier. "The Role of Water Diffusion in the Corrosion of the French Nuclear Waste Glass SON 68 Under Solution Saturation Conditions." *Proceedings of the Materials Research Society Conference*. Vol. 807. Pittsburgh, Pennsylvania: Materials Research Society. pp. 193-198. 2004.

Gin, S. "Protective Effect of the Alteration Gel: A Key Mechanism in the Long-Term Behavior of Nuclear Waste Glass." *Proceedings of the Materials Research Society Conference*. Vol. 663. Pittsburgh, Pennsylvania: Materials Research Society. Vol. 663. pp. 207-215. 2001.

Grambow, B. and R. Muller. "First Order Dissolution Rate Law and The Role of Surface Layers in Glass Performance Assessment." *Journal of Nuclear Material*. Vol. 298. pp. 112-124. 2001.

Jain, V., X. He., and Y. -M. Pan. NUREG/CR-6873, "Corrosion Rate Measurements and Chemical Speciation of Corrosion Products Using Thermodynamic Modeling of Debris Components to Support GSI-191." Washington, DC: NRC. 2005.

NRC. "Test Plan: Characterization of Chemical and Corrosion Effects Potentially Occurring During a Pressurized Water Reactor LOCA." Rev. 12b. ML050450478. Washington, DC: NRC. <www.nrc.gov/reading-rm/adams.html> 2005.

Oka, Y. and M. Tomozawa. "Effect of Alkaline Earth Ion as an Inhibitor to Alkaline Attack on Silica Glass." *Journal of Non-Crystalline Solids*. Vol. 42. pp. 535-544. 1980.

Strachan, D. M. and T. L. Croak. "Compositional Effects on Long-Term Dissolution of Borosilicate Glass". *Journal of Non-Crystalline Solids*. Vol. 272. pp. 22-33. 2000.

APPENDIX B

SIMULATED OUTPUT FILE FOR INTEGRATED CHEMICAL EFFECTS TEST (ICET) #1 AT 60 °C [140 °F] AT 148 HOURS, USING EQ3/6 VERSION 7.2B

EQ3/6, Version 7.2b (EQ3/6-V7-REL-V7.2b-PC)
 EQ6 Reaction-Path Code (EQ3/6-V7-EQ6-EXE-R136-P5)
 Supported by the EQLIB library (EQ3/6-V7-EQLIB-LIB-R168-P5)

Copyright (c) 1987, 1990-1993, 1995 The Regents of the University of California, Lawrence Livermore National Laboratory. All rights reserved.

This work is subject to additional statements and disclaimers which may be found in the README.txt file included in the EQ3/6 software transmittal package.

Run 15:50:32 10/07/05

```
-----
EQ3NR input file name= icell1488.6i
Description= "T60H148 composition at pH 9.8 for calculations
of ICET #1 solution simulations. Mineral suppression."
Version level= 7.2
Created 10/07/05      Creator= D.A. Pickett - J.McMurry
```

Purpose: Assess the usefulness of commercially available modeling software to thermodynamically simulate reactions between borated containment water at pH 7 and 10 with debris components to form corrosion products during a postulated LOCA event in a PWR.

ICET #1 test solution simulation. 60 C after 148 hours. Data originated from spreadsheet "ICET#1 Revised EQ36 Input Data.xls," provided by J. McMurry. Fix pH. Suppress some minerals. Assume atmospheric control of redox (via oxygen) and aqueous carbon (via carbon dioxide).

```
-----
calculational mode  |*normal      | economy      | super economy
-----
model type         | titration   |*closed      | open
-----
temperature model  |*power       | fluid mixing
-----
```

```
c power model --> temp = tstart + tk1*zi + tk2*zi**2 + tk3*zi**3
c mixing model --> temp = (tstart * tk1 + zi*tk2) / (zi + tk1)
```

```
-----
c
| tstart(c) | 60.00 | tk1 | 0. | tk2 | 0. | tk3 | 0.
|-----|
| starting value of zi | 0. | max. value of zi | 1.0000
|-----|
| starting time (sec) | 0. | max. time (sec) | 1.00000E+38
|-----|
| max. steps | 400 | max. steps w/o print | 100
|-----|
| linear print interval | 1.0000 | log print interval | 1.0000
|-----|
```

```

-----
suppress mineral phases
-----
phases w/ elements |           |
phases except      |           |
-----
fixed fugacity phases- species, moles(per kg h2o), log fugacity(bars)
-----
none                |           |
-----
c
c          R A T E      L A W S
c 1 = relative          rate = rk1 + rk2*zi + (1/2)rk3*zi*zi
c 2 = transition state theory  rate = CHECK DOCUMENTATION
c 3 = specified rate
c 4 = activity term rate      rate = CHECK DOCUMENTATION
c
c          R E A C T A N T      T Y P E S
c mineral      solid solution      special      aqueous      gas
c
c          S U R F A C E      T Y P E
c 0 = fixed surface area      1 = fixed specific surface area
c
c          N O T E S
c status and jreac are normally not set by the user
-----
reactants      (ss) solid solution only      (sp) special reactant only
-----
REACTANT      | none                | status      |
-----
options
-----
- SOLID SOLUTIONS -
  * ignore solid solutions
  process solid solutions
- LOADING OF SPECIES INTO MEMORY -
  * don't print
  lists species loaded into memory
- LIST DERIVATIVES OF BASIS ELEMENTS AT EACH PRINT POINT -
  * don't print
  print
- LIST ALL SPECIES LOADED INTO MEMORY AND THEIR LOG K VALUES -
  * don't print
  print
- LIST DISTRIBUTION OF AQUEOUS SPECIES AT EACH PRINT POINT -
  only species > 10**-12 molal
  * all species
  don't print
- LIST CATION/H+ ACTIVITY RATIOS AT EACH PRINT POINT -
  * don't print
  print
- LIST BULK ELEMENT AND OXIDE COMPOSITION AT EACH PRINT POINT -
  * don't print
  print
- MINERAL SATURATION STATES -
  * print if affinity > -10 kcals
  print all
  don't print
- LIST GAS SPECIES SUMMARY AT EACH PRINT POINT -

```

```

    don't print
  * print
- PRINT AQUEOUS MASS AND CONCENTRATION TOTALS -
  * don't print
  print
- TAB FILES -
  * write
  append to previous tabx file
  don't write
- WRITE PICKUP FILE -
  * write pickup file at end of run
  don't write pickup file
  write pickup file for each print point
- PHYSICALLY REMOVED SUBSYSTEM -
  * does nothing
  transfer minerals but leave trivial mass in the system
  transfer minerals
- CLEAR INITIAL PHYSICALLY REMOVED SUBSYSTEM -
  * does nothing
  clear p.r.s. before first reaction progress advance
- PHASE BOUNDARY SEARCH -
  * step size constrained by predicted phase boundaries
  phase boundaries estimated from Taylor's series and printed
  locations of phase boundaries ignored
- AUTO BASIS SWITCHING -
  * off
  on
- SUPPRESS REDOX REACTIONS -
  * does nothing
  suppress all redox reactions
- LINEAR OR LOGARITHMIC TAYLOR'S SERIES -
  * linear for kcol = 1,kdim, logarithmic for kcol = 1,kbt
  logarithmic for kcol = 1,kbt
  linear for kcol = 1,kdim
- AZERO AND HYDRATION NUMBERS -
  * no change
  read in new azero and hydration numbers
- PRINT MEAN MOLAL ACTIVITY COEFFICIENTS FOR DISSOLVED SPECIES -
  * does nothing
  print
- PITZER DATABASE INFORMATION -
  * print only warnings
  print species in model and number of Pitzer coefficients
  print species in model and names of Pitzer coefficients
- PRINT DIAGNOSTIC MESSAGES -
  * don't print
  print level 1 messages
  print level 2 messages
- PRINT PRE-NEWTON-RAPHSON OPTIMIZATION -
  * don't print
  print summary information
  print detailed information
- PRINT STEP SIZE AND ORDER -
  * don't print
  print scale factor
  print orders and step size scaling factors
- CONTROL STEP SIZE AND ORDER PRINT -
  * does nothing

```

```

    print step size and order when delzi .le. dlzmx1
- NEWTON ITERATIONS -
  * don't print
    print summary of newton iterations
    print summary, residual functions and correction terms
    print summary, residual functions, correction terms and matrix
- PRINT SEARCH ITERATIONS -
  * don't print
    print
- PRINT HPSAT ITERATIONS -
  * don't print
    print
- PRINT FINITE DIFFERENCE AND DERIVATIVE DATA -
  * don't print
    print computations from RDERIV, and RTAYLR
    print computations from RDERIV, RTAYLR, DERIV and TAYLOR
- PRINT KINETICS DIAGNOSTIC MESSAGES -
  * don't print
    print level 1 diagnostics
    print level 1 and level 2 diagnostics
- PRINT AKMATR -
  * don't print
    print level 1 diagnostics
- KILL ITERATION VARIABLES -
  * does nothing
    allow selection of variables to remove

```

development options (used for code development)

```

    0 check finite difference and Taylor series expression
    0 check reaction rate finite difference and Taylor series

```

tolerances desired values - defaults info-only

number of N-R iterations	40	itermx
p.r.s. transfer interval	varies	dlzidp
residual magnitude	1.0e-06	tolbt
correction magnitude	1.0e-06	toldl
search/find tolerance	varies	tolx
supersaturation	varies	tolsat
supersaturation set size	varies	tolsst
max. size Taylor's series term	1.0e-04	screw1
max. initial value betamx	n/a	screw2
max. Taylor's series term (kin.)	1.0e-04	screw3
corrector iteration	1.0e-04	screw4
max. size of N-R correction term	4.0	screw5
step size (economy mode)	4.0	screw6
log mass of phases	varies	zklogu
decrement mass (p.r.s.)	2.0	zklogl
min. left after p.r.s.	.98	zkfac
initial step size	varies	dlzmx1
upper limit step size	varies	dlzmx2
maximum order	6	nordlm
num. attempted assemblages	25	ntrymx
slide -> over phase bound.	8	npslmx
slide -> over redox insta.	3	nsslmx
fo2 scan control	none	ioscan

c pickup file written by EQ3NR.7.2bR139

c supported by eqlib.7.2bR168

EQ3NR input file name= icell1484.3i

Description= "T60H148 composition at pH 9.8 for calculations of ICET #1 solution simulations."

Version level= 7.2

Created 09/15/05 Creator= D.A. Pickett

Purpose: Assess the usefulness of commercially available modeling software to thermodynamically simulate reactions between borated containment water at pH 7 and 10 with debris components to form corrosion products during a postulated LOCA event in a PWR.

ICET #1 test solution simulation. 60 C after 148 hours. Data originated from spreadsheet "ICET#1 Revised EQ36 Input Data.xls," provided by J. McMurry. Fix pH. No mineral suppression. Assume atmospheric control of redox (via oxygen) and aqueous carbon (via carbon dioxide).

temperature (C)			60.000
electrical imbalance			-1.236008767334290E-01
number of aqueous master species			15
position of last pure mineral			15
position of last solid solution			15
suppressed species	(suppress, replace, augmentk, augmentg)		value
Albite	mineral	suppress	0.
Albite low	mineral	suppress	0.
Amesite-14A	mineral	suppress	0.
Analcime	mineral	suppress	0.
Andradite	mineral	suppress	0.
Anthophyllite	mineral	suppress	0.
Antigorite	mineral	suppress	0.
Boehmite	mineral	suppress	0.
Chrysotile	mineral	suppress	0.
Clinochlore-14A	mineral	suppress	0.
Clinochlore-7A	mineral	suppress	0.
Clinozoisite	mineral	suppress	0.
Diaspore	mineral	suppress	0.
Dolomite	mineral	suppress	0.
Dolomite-dis	mineral	suppress	0.
Dolomite-ord	mineral	suppress	0.
Epidote	mineral	suppress	0.
Epidote-ord	mineral	suppress	0.
Ferrite-Cu	mineral	suppress	0.
Laumontite	mineral	suppress	0.
Lawsonite	mineral	suppress	0.
Margarite	mineral	suppress	0.
Mesolite	mineral	suppress	0.
Montmor-Na	mineral	suppress	0.
Natrolite	mineral	suppress	0.

Nontronite-Ca	mineral	suppress	0.
Nontronite-H	mineral	suppress	0.
Nontronite-Mg	mineral	suppress	0.
Nontronite-Na	mineral	suppress	0.
Paragonite	mineral	suppress	0.
Pargasite	mineral	suppress	0.
Prehnite	mineral	suppress	0.
Saponite-Ca	mineral	suppress	0.
Saponite-H	mineral	suppress	0.
Saponite-Mg	mineral	suppress	0.
Saponite-Na	mineral	suppress	0.
Scolecite	mineral	suppress	0.
Talc	mineral	suppress	0.
Tremolite	mineral	suppress	0.
Zoisite	mineral	suppress	0.

iopg options

- pH SCALE CONVENTION -
modified NBS
* internal
rational
- ACTIVITY COEFFICIENT OPTIONS -
* use B-dot equation
Davies' equation
Pitzer's equations

elements, moles and moles aqueous

O	5.629120836317404E+01	0.000000000000000E+00
Al	3.109999955620369E-03	0.000000000000000E+00
B	2.593000012063180E-01	0.000000000000000E+00
Ca	2.192999962994622E-04	0.000000000000000E+00
Cl	2.739999999394764E-03	0.000000000000000E+00
Cu	5.459000003075840E-05	0.000000000000000E+00
Fe	6.086999942152880E-06	0.000000000000000E+00
H	1.111949505259741E+02	0.000000000000000E+00
C	6.395166330525934E-02	0.000000000000000E+00
Li	1.013999999999046E-04	0.000000000000000E+00
Mg	2.403999976758425E-05	0.000000000000000E+00
Na	2.20199998915266E-01	0.000000000000000E+00
Si	4.49199996617276E-04	0.000000000000000E+00
Zn	1.057999989741578E-04	0.000000000000000E+00

master species and logarithmic basis variables

H2O	H2O	1.744358983526984E+00
Al+++	Al+++	-2.130221035124618E+01
B(OH)3(aq)	B(OH)3(aq)	-1.643947543002099E+00
Ca++	Ca++	-4.811750090244336E+00
Cl-	Cl-	-2.570847113555952E+00
Cu++	Cu++	-1.001906504400390E+01

Fe++	Fe++	-1.848918234393105E+01
H+	H+	-9.700467744170056E+00
HCO3-	HCO3-	-1.598192493612142E+00
Li+	Li+	-3.994027582768387E+00
Mg++	Mg++	-5.558407751686410E+00
Na+	Na+	-7.120543518224124E-01
SiO2 (aq)	SiO2 (aq)	-4.409346723272810E+00
Zn++	Zn++	-5.485662282424268E+00
O2 (g)	O2 (g)	-7.000000000000000E-01

physically removed subsystem (solid solution, mineral, moles)		

none		

--- Reading the data1 file ---

--- The data1 file has been successfully read ---

* note - (eq6/flgstz) This run involves at least one redox reaction. The code will therefore use a redox parameter and the charge balance constraint.

- The species Albite has been user-suppressed
- The species Albite low has been user-suppressed
- The species Amesite-14A has been user-suppressed
- The species Analcime has been user-suppressed
- The species Andradite has been user-suppressed
- The species Anthophyllite has been user-suppressed
- The species Antigorite has been user-suppressed
- The species Boehmite has been user-suppressed
- The species Chrysotile has been user-suppressed
- The species Clinochlore-14A has been user-suppressed
- The species Clinochlore-7A has been user-suppressed
- The species Clinozoisite has been user-suppressed
- The species Diaspore has been user-suppressed

The species Dolomite	has been user-suppressed
The species Dolomite-dis	has been user-suppressed
The species Dolomite-ord	has been user-suppressed
The species Epidote	has been user-suppressed
The species Epidote-ord	has been user-suppressed
The species Ferrite-Cu	has been user-suppressed
The species Laumontite	has been user-suppressed
The species Lawsonite	has been user-suppressed
The species Margarite	has been user-suppressed
The species Mesolite	has been user-suppressed
The species Montmor-Na	has been user-suppressed
The species Natrolite	has been user-suppressed
The species Nontronite-Ca	has been user-suppressed
The species Nontronite-H	has been user-suppressed
The species Nontronite-Mg	has been user-suppressed
The species Nontronite-Na	has been user-suppressed
The species Paragonite	has been user-suppressed
The species Pargasite	has been user-suppressed
The species Prehnite	has been user-suppressed
The species Saponite-Ca	has been user-suppressed
The species Saponite-H	has been user-suppressed
The species Saponite-Mg	has been user-suppressed
The species Saponite-Na	has been user-suppressed
The species Scolecite	has been user-suppressed
The species Talc	has been user-suppressed
The species Tremolite	has been user-suppressed
The species Zoisite	has been user-suppressed

* note - (eqlib/inbndot) The following aqueous species
have been assigned a default hard core diameter of
4.000 Angstroms-
CO(aq)

Ca (CH3COO) 2 (aq)
 CaCO3 (aq)
 CaCl2 (aq)
 Cu (CH3COO) 2 (aq)
 CuCH3COO (aq)
 Fe (CH3COO) 2 (aq)
 FeCl2 (aq)
 LiCH3COO (aq)
 LiCl (aq)
 Mg (CH3COO) 2 (aq)
 MgCO3 (aq)
 NaCH3COO (aq)
 NaHSiO3 (aq)
 Zn (CH3COO) 2 (aq)
 Zn (OH) 2 (aq)
 ZnCl2 (aq)

```

eeee qqq 666
e  q  q 6
eeee q  q 6666
e  q q q 6 6
eeee qqq 666
      q
  
```

EQ36, version 7.2b (R136)
 supported by EQLIB, version 7.2b (R168)

```

|EQ3NR input file name= icell488.6i
|Description= "T60H148 composition at pH 9.8 for calculations
|of ICET #1 solution simulations. Mineral suppression."
|Version level= 7.2
|Created 10/07/05      Creator= D.A. Pickett - J.McMurry
  
```

```

|  Purpose: Assess the usefulness of commercially available modeling
|software to thermodynamically simulate reactions between borated
|containment water at pH 7 and 10 with debris components to form
|corrosion products during a postulated LOCA event in a PWR.
  
```

```

|ICET #1 test solution simulation. 60 C after 148 hours. Data
|originated from spreadsheet "ICET#1 Revised EQ36 Input Data.xls,"
|provided by J. McMurry. Fix pH. Suppress some minerals. Assume
|atmospheric control of redox (via oxygen) and aqueous carbon (via
|carbon dioxide).
  
```

```

|EQ3NR input file name= icell484.3i
|Description= "T60H148 composition at pH 9.8 for calculations
|of ICET #1 solution simulations."
|Version level= 7.2
  
```

Created 09/15/05 Creator= D.A. Pickett

Purpose: Assess the usefulness of commercially available modeling software to thermodynamically simulate reactions between borated containment water at pH 7 and 10 with debris components to form corrosion products during a postulated LOCA event in a PWR.

ICET #1 test solution simulation. 60 C after 148 hours. Data originated from spreadsheet "ICET#1 Revised EQ36 Input Data.xls," provided by J. McMurry. Fix pH. No mineral suppression. Assume atmospheric control of redox (via oxygen) and aqueous carbon (via carbon dioxide).

data0.com.R2

CII: GEMBOCHS.V2-EQ8-DATA0.COM.R2

THERMODYNAMIC DATABASE

generated by GEMBOCHS.V2-JEWEL.SRC.R3 02-aug-1995 16:45:06

Output package: eq3

Data set: com

+-----

The activity coefficients of aqueous solute species and the activity of water are calculated according to the B-dot equation plus others

No. of elements in the data base = 79

No. of elements dimensioned for = 100

No. of active elements = 14

No. of aqueous species dimensioned for = 800

No. of aqueous species loaded = 341

No. of active aqueous species = 200

No. of aqueous reactions dimensioned for = 699

No. of aqueous reactions loaded = 261

No. of active aqueous reactions = 186

No. of pure minerals dimensioned for = 850

No. of pure minerals loaded = 216

No. of active pure minerals = 176

No. of gases dimensioned for = 80

No. of gases loaded = 19

No. of active gases = 19

No. of solid solutions in the data base = 12

No. of solid solutions dimensioned for = 50

No. of active solid solutions = 0

zistrt = 0.000000E+00 (initial value of zi)

zimax = 1.000000E+00 (maximum value of zi)

timemx = 1.000000E+38 (maximum value of time, sec)

kstpmax = 400 (maximum number of steps this run)

dzprnt = 1.000000E+00 (linear print interval)
dzprlg = 1.000000E+00 (logarithmic print interval)
dlzidp = 1.000000E+38 (P.R.S. transfer interval)

maximum permitted step sizes.....
dlzmx1 = 1.000000E-02 (nord=0)
dlzmx2 = 1.000000E+38 (nord.ge.1)
nordlm = 6 (maximum permitted order)

Temperature = 60.000 C

nmodl1 = 2 (physical system switch)
1 = titration, 2 = closed, 3 = flow-through)
nmodl2 = 0 (economy mode permission switch)
0 = normal, 1 = economy, 3 = super economy)

iopt1 = 0 (kinetic mode switch)
iopt2 = 0 (suppress phase boundary location)
iopt3 = 0 (interfacing output switch)
iopt4 = 0 (permit solid solutions switch)
iopt5 = 0 (remove initial solids switch)
iopt6 = 0 (clear P.R.S. at start switch)
iopt7 = 0 (auto basis switch mode switch)
iopt8 = 0 (linear vs. log Taylor's series)
iopt9 = 0 (not used)
iopt10 = 0 (not used)
iopt11 = 0 (suppress all redox reactions switch)
iopt12 = 0 (not used)
iopt13 = 0 (tab file output switch)
iopt14 = 0 (not used)
iopt15 = 0 (not used)
iopt16-20 (not used)
ifile = 0 (supplementary input file)

iopg1 = 0 (choice of act. coeff. equations)
iopg2 = -1 (choice of pH scale)
iopg3 = 0 (not used)
iopg4 = 0 (not used)
iopg5 = 0 (not used)
iopg6 = 0 (not used)
iopg7 = 0 (not used)
iopg8 = 0 (not used)
iopg9 = 0 (not used)
iopg10 = 0 (not used)

iopr1 = 0 (print loading of species from data1)
iopr2 = 0 (print derivatives of basis elements)
iopr3 = 0 (print loaded species and log K values)
iopr4 = 1 (print aqueous species distribution)
iopr5 = 0 (print cation/H+ activity ratios)
iopr6 = 0 (print element/oxide comp. of mineral assemblage)
iopr7 = 0 (print mineral affinity summary)
iopr8 = 1 (print gas fugacity summary)
iopr9 = 0 (print mean molal activity coefficient)
iopr10 = 0 (print tabulation of Pitzer coefficients)
iopr11 = 0 (print major species for each element)

iopr12-20 (not used)

iodb1 = 0 (enable comp. messages)
iodb2 = 0 (print pre-Newton-Raphson optimization)
iodb3 = 0 (print order/scaling info.)
iodb4 = 0 (print newton iteration info.)
iodb5 = 0 (print search iterations)
iodb6 = 0 (print hpsatz iterations)
iodb7 = 0 (print f.d. and t.s. calculations)
iodb8 = 0 (turns iodb3 on and off)
iodb9 = 0 (print kinetics info.)
iodb10 = 0 (check basis var. f.d. and t.s.)
iodb11 = 0 (check reac. rate f.d. and t.s.)
iodb12 = 0 (iteration variable killer option)
iodb13 = 0 (not used)
iodb14 = 0 (not used)
iodb15 = 0 (not used)
iodb16 = 0 (turn on akmatr prints)
iodb17-20 (not used)

tolbt = 1.000000E-06 (residual function convergence tolerance)
toldl = 1.000000E-06 (correction term convergence tolerance)
tolx = 1.000000E-06 (sol-sol reactant/product identity tolerance)
tolsat = 5.000000E-04 (lower supersaturation tolerance)
tolsst = 1.000000E-03 (upper supersaturation tolerance)

screw1 = 1.000E-04 (primary step-size parameter for basis variables)
screw2 = 0.00000 (not used)
screw3 = 1.000E-04 (step size parameter for rate functions)
screw4 = 1.000E-04 (corrector parameter for rate functions)
screw5 = 4.00000 (under-relaxation control for n-r iteration)
screw6 = 4.00000 (step size parameter for economy mode)

zklogu = -7.000 (threshold log mass for solids)
zklogl = 2.000 (log mass decrement for P.R.S shift)
zkfac = 0.800 (shift adjustment factor)
zklgmn = -7.097 (minimum log mass after a shift)

itermx= 90 (Newton-Raphson iteration limit)
ntrymx= 25 (phase assemblage try limit)
npslmx= 12 (critical phase instability slide limit)
nsslmx= 8 (critical redox instability slide limit)

--- Inactive Loaded Aqueous Species ---

Ag+	Am+++
Ar(aq)	Au+
Ba++	Be++
Br-	Cd++
Ce+++	Co++
CrO4--	Cs+
Dy+++	Er+++
Eu+++	F-

Ga+++	Gd+++
H2AsO4-	HPO4--
He (aq)	Hg++
Ho+++	I-
In+++	K+
Kr (aq)	La+++
Lu+++	Mn++
MoO4--	NH3 (aq)
Nd+++	Ne (aq)
Ni++	Np++++
Pb++	Pd++
Pr+++	Pu++++
Ra++	Rb+
ReO4-	Rn (aq)
RuO4--	SO4--
Sb (OH) 3 (aq)	Sc+++
SeO3--	Sm+++
Sn++	Sr++
Tb+++	TcO4-
Th++++	Ti (OH) 4 (aq)
Tl+	Tm+++
UO2++	VO++
WO4--	Xe (aq)
Y+++	Yb+++
Zr (OH) 2++	HS-
S2--	S2O3--
Ag++	Am++
Am++++	AmO2+
AmO2++	Au+++
Br3-	BrO-
BrO3-	BrO4-
CN-	Co+++
Cr++	Cr+++
CrO4---	Ethanamine (aq)
Eu++	Glycine (aq)
H2AsO3-	HSO5-
HSe-	Hg2++
I3-	IO-
IO3-	IO4-
Mn+++	MnO4--
N2 (aq)	N3-
NO2-	NO3-
Np+++	NpO2+
NpO2++	Pb++++
Pu+++	PuO2+
PuO2++	Ru (OH) 2++
Ru++	Ru+++
RuO4 (aq)	RuO4-
S2O4--	S2O6--
S2O8--	S3--
S3O6--	S4--
S4O6--	S5--
S5O6--	SCN-
SO3--	Se--
SeO4--	Sm++
Sn++++	Tc+++
TcO++	TcO4--
TcO4---	Tl+++

U+++	U++++
UO2+	V+++
VO2+	VO4---
Yb++	Zr++++

--- Inactive Loaded Minerals ---

Albite	Albite low
Amesite-14A	Analcime
Andradite	Anthophyllite
Antigorite	Boehmite
Chrysotile	Clinochlore-14A
Clinochlore-7A	Clinozoisite
Diaspore	Dolomite
Dolomite-dis	Dolomite-ord
Epidote	Epidote-ord
Ferrite-Cu	Laumontite
Lawsonite	Margarite
Mesolite	Montmor-Na
Natrolite	Nontronite-Ca
Nontronite-H	Nontronite-Mg
Nontronite-Na	Paragonite
Pargasite	Prehnite
Saponite-Ca	Saponite-H
Saponite-Mg	Saponite-Na
Scolecite	Talc
Tremolite	Zoisite

Stepping to zi= 0.0000E+00, delzi= 0.0000E+00, nord= 0

Attempted species assemblage no. 1

1	1	H2O
2	3	Al+++
3	7	B(OH)3(aq)
4	11	Ca++
5	14	Cl-
6	18	Cu++
7	23	Fe++
8	26	H+
9	28	HCO3-
10	38	Li+
11	40	Mg++
12	44	Na+
13	62	SiO2(aq)
14	78	Zn++
15	80	O2(g)

iter = 4
 35 supersaturated pure minerals
 0 supersaturated solid solutions

The most supersaturated phases			Affinity, kcal
1	102	Goethite	10.47987097
2	210	Zincite	6.06659534
3	73	Delafossite	10.58203864
4	194	Smithsonite	3.26833410
5	116	Hydrozincite	21.89948969
6	213	Zn(OH)2(epsilon)	5.11911117
7	199	Tenorite	3.88145948
8	212	Zn(OH)2(beta)	4.74516615

Attempted species assemblage no. 2

1	1	H2O
2	3	Al+++
3	7	B(OH)3(aq)
4	11	Ca++
5	14	Cl-
6	18	Cu++
7	23	Fe++
8	26	H+
9	28	HCO3-
10	38	Li+
11	40	Mg++
12	44	Na+
13	62	SiO2(aq)
14	78	Zn++
15	80	O2(g)
16	102	Goethite

iter = 13

30 supersaturated pure minerals
0 supersaturated solid solutions

The most supersaturated phases			Affinity, kcal
1	210	Zincite	6.06666624
2	194	Smithsonite	3.26828665
3	116	Hydrozincite	21.89960773
4	213	Zn(OH)2(epsilon)	5.11918215
5	199	Tenorite	3.88154187
6	212	Zn(OH)2(beta)	4.74523713
7	44	Calcite	2.05216103
8	16	Aragonite	1.83386129

Attempted species assemblage no. 3

1	1	H2O
2	3	Al+++
3	7	B(OH)3(aq)
4	11	Ca++
5	14	Cl-
6	18	Cu++
7	23	Fe++
8	26	H+
9	28	HCO3-

10	38	Li+
11	40	Mg++
12	44	Na+
13	62	SiO2 (aq)
14	78	Zn++
15	80	O2 (g)
16	102	Goethite
17	210	Zincite

iter = 13

24 supersaturated pure minerals
0 supersaturated solid solutions

The most supersaturated phases			Affinity, kcal
1	199	Tenorite	3.87959831
2	44	Calcite	2.05203151
3	16	Aragonite	1.83373177
4	131	Malachite	3.00363471
5	129	Magnesite	0.88027536
6	72	Dawsonite	2.31025155
7	100	Gibbsite	1.86874993
8	112	Huntite	2.63044334

Attempted species assemblage no. 4

1	1	H2O
2	3	Al+++
3	7	B(OH)3 (aq)
4	11	Ca++
5	14	Cl-
6	18	Cu++
7	23	Fe++
8	26	H+
9	28	HCO3-
10	38	Li+
11	40	Mg++
12	44	Na+
13	62	SiO2 (aq)
14	78	Zn++
15	80	O2 (g)
16	102	Goethite
17	199	Tenorite
18	210	Zincite

iter = 13

21 supersaturated pure minerals
0 supersaturated solid solutions

The most supersaturated phases			Affinity, kcal
1	44	Calcite	2.05218776
2	16	Aragonite	1.83388802
3	129	Magnesite	0.88060992
4	72	Dawsonite	2.31301979
5	100	Gibbsite	1.86981095
6	112	Huntite	2.63160325

7	119	Kaolinite	2.32326192
8	143	Monohydrocalcite	0.55941200

Attempted species assemblage no. 5

1	1	H2O
2	3	Al+++
3	7	B(OH)3(aq)
4	11	Ca++
5	14	Cl-
6	18	Cu++
7	23	Fe++
8	26	H+
9	28	HCO3-
10	38	Li+
11	40	Mg++
12	44	Na+
13	62	SiO2(aq)
14	78	Zn++
15	80	O2(g)
16	44	Calcite
17	102	Goethite
18	199	Tenorite
19	210	Zincite

iter = 12

17 supersaturated pure minerals
0 supersaturated solid solutions

The most supersaturated phases			Affinity, kcal
1	129	Magnesite	0.88032754
2	72	Dawsonite	2.31309122
3	100	Gibbsite	1.87012604
4	119	Kaolinite	2.32440110
5	63	Corundum	1.02885778
6	118	Jadeite	0.81519755
7	146	Montmor-Mg	1.17818796
8	25	Beidellite-Na	1.28945220

Attempted species assemblage no. 6

1	1	H2O
2	3	Al+++
3	7	B(OH)3(aq)
4	11	Ca++
5	14	Cl-
6	18	Cu++
7	23	Fe++
8	26	H+
9	28	HCO3-
10	38	Li+
11	40	Mg++
12	44	Na+
13	62	SiO2(aq)
14	78	Zn++

15	80	O2(g)
16	44	Calcite
17	102	Goethite
18	129	Magnesite
19	199	Tenorite
20	210	Zincite

iter = 11
 14 supersaturated pure minerals
 0 supersaturated solid solutions

The most supersaturated phases			Affinity, kcal
1	72	Dawsonite	2.31310173
2	100	Gibbsite	1.87018151
3	119	Kaolinite	2.32460319
4	63	Corundum	1.02896812
5	118	Jadeite	0.81529598
6	25	Beidellite-Na	1.28973272
7	163	Nepheline	0.58543786
8	146	Montmor-Mg	0.74269927

Attempted species assemblage no. 7

1	1	H2O
2	3	Al+++
3	7	B(OH)3(aq)
4	11	Ca++
5	14	Cl-
6	18	Cu++
7	23	Fe++
8	26	H+
9	28	HCO3-
10	38	Li+
11	40	Mg++
12	44	Na+
13	62	SiO2(aq)
14	78	Zn++
15	80	O2(g)
16	44	Calcite
17	72	Dawsonite
18	102	Goethite
19	129	Magnesite
20	199	Tenorite
21	210	Zincite

iter = 11
 2 supersaturated pure minerals
 0 supersaturated solid solutions

The most supersaturated phases			Affinity, kcal
1	109	Hematite	1.70960412
2	94	Ferrite-Zn	1.31370717

Attempted species assemblage no. 8

1	1	H2O
2	3	Al+++
3	7	B(OH)3(aq)
4	11	Ca++
5	14	Cl-
6	18	Cu++
7	23	Fe++
8	26	H+
9	28	HCO3-
10	38	Li+
11	40	Mg++
12	44	Na+
13	62	SiO2(aq)
14	78	Zn++
15	80	O2(g)
16	44	Calcite
17	72	Dawsonite
18	102	Goethite
19	109	Hematite
20	129	Magnesite
21	199	Tenorite
22	210	Zincite

--- Iteration has gone sour (iter= 16) ---
 The phase to be dropped is Goethite

(102)

Attempted species assemblage no. 9

1	1	H2O
2	3	Al+++
3	7	B(OH)3(aq)
4	11	Ca++
5	14	Cl-
6	18	Cu++
7	23	Fe++
8	26	H+
9	28	HCO3-
10	38	Li+
11	40	Mg++
12	44	Na+
13	62	SiO2(aq)
14	78	Zn++
15	80	O2(g)
16	44	Calcite
17	72	Dawsonite
18	109	Hematite
19	129	Magnesite
20	199	Tenorite
21	210	Zincite

iter = 12

Reaction progress = 0.000000000000000E+00
Log of reaction progress = -999.0000000

Temperature = 60.000 degrees C
total pressure = 1.013 bars

Change in the product phase assemblage

Start or re-start of run

--- Element Totals for the Aqueous Solution ---

Element	mg/kg soln.	Molality	Moles
O	8.817801E+05	5.627295E+01	5.627543E+01
Al	3.276307E+00	1.239827E-04	1.239881E-04
B	2.745403E+03	2.592886E-01	2.593000E-01
Ca	3.874037E-01	9.869630E-06	9.870064E-06
Cl	9.513441E+01	2.739880E-03	2.740000E-03
Cu	7.630049E-03	1.225977E-07	1.226031E-07
Fe	1.339372E-08	2.448750E-13	2.448858E-13
H	1.097575E+05	1.111841E+02	1.111890E+02
C	7.144654E+02	6.073586E-02	6.073853E-02
Li	6.892833E-01	1.013955E-04	1.014000E-04
Mg	1.510324E-01	6.344796E-06	6.345074E-06
Na	4.890578E+03	2.172044E-01	2.172140E-01
Si	1.235548E+01	4.491803E-04	4.492000E-04
Zn	6.276614E-04	9.800703E-09	9.801134E-09

Single ion activities and activity coefficients are here defined with respect to the internal pH scale

	pH	Eh	pe
internal pH scale	9.8566	0.5608	8.4835E+00
modified NBS pH scale	9.6788	0.5725	8.6613E+00
rational pH scale	9.7571	0.5673	8.5830E+00

pHCl = 12.6051

Oxygen fugacity = 1.99399E-01
Log oxygen fugacity = -0.70028

Activity of water = 0.99160
Log activity of water = -0.00366

Ionic strength = 2.865712E-01 molal
Sum of molalities = 0.5160217986635
Osmotic coefficient = 0.90754

Mass of solution = 1.021086 kg
 Mass of solutes = 0.021042 kg
 Conc. of solutes = 2.060732 per cent (w/w)

Moles of solvent H2O = 5.55109E+01
 Mass of solvent H2O = 1.00004E+00 kg

Species	Molality	Log molality	Log gamma	Log activity
BO2-	2.1878E-01	-0.6600	-0.1579	-0.8179
Na+	1.9140E-01	-0.7181	-0.1579	-0.8760
CO3--	3.3266E-02	-1.4780	-0.6048	-2.0828
HCO3-	2.2333E-02	-1.6511	-0.1579	-1.8089
NaB(OH)4(aq)	2.0321E-02	-1.6921	0.0000	-1.6921
B(OH)3(aq)	2.0183E-02	-1.6950	0.0000	-1.6950
NaCO3-	3.5177E-03	-2.4537	-0.1579	-2.6116
Cl-	2.6868E-03	-2.5708	-0.1777	-2.7485
NaHCO3(aq)	1.6044E-03	-2.7947	0.0000	-2.7947
OH-	1.0080E-03	-2.9965	-0.1777	-3.1743
NaHSiO3(aq)	2.9266E-04	-3.5336	0.0000	-3.5336
O2(aq)	1.6118E-04	-3.7927	0.0291	-3.7636
HSiO3-	1.2156E-04	-3.9152	-0.1579	-4.0731
AlO2-	1.2063E-04	-3.9185	-0.1579	-4.0764
Li+	1.0138E-04	-3.9941	-0.1579	-4.1519
NaCl(aq)	5.3045E-05	-4.2754	0.0000	-4.2754
SiO2(aq)	3.4866E-05	-4.4576	0.0000	-4.4576
NaOH(aq)	1.5016E-05	-4.8234	0.0000	-4.8234
CaCO3(aq)	7.6103E-06	-5.1186	0.0000	-5.1186
CO2(aq)	3.7795E-06	-5.4226	0.0291	-5.3935
NaAlO2(aq)	3.3436E-06	-5.4758	0.0000	-5.4758
MgCO3(aq)	3.2516E-06	-5.4879	0.0000	-5.4879
MgB(OH)4+	2.2896E-06	-5.6402	-0.1579	-5.7981
CaB(OH)4+	1.5099E-06	-5.8210	-0.1579	-5.9789
Mg++	7.2296E-07	-6.1409	-0.4684	-6.6093
Ca++	6.8685E-07	-6.1631	-0.5515	-6.7146
Cu(CO3)2--	1.1420E-07	-6.9423	-0.6692	-7.6115
H2SiO4--	9.0662E-08	-7.0426	-0.6692	-7.7118
MgHCO3+	8.0060E-08	-7.0966	-0.1579	-7.2545
CaHCO3+	6.2161E-08	-7.2065	-0.1579	-7.3644
LiOH(aq)	1.1507E-08	-7.9390	0.0000	-7.9390
ZnOH+	8.9067E-09	-8.0503	-0.1579	-8.2082
HALO2(aq)	8.1771E-09	-8.0874	0.0000	-8.0874
CuCO3(OH)2--	5.5919E-09	-8.2524	-0.6692	-8.9216
LiCl(aq)	5.2186E-09	-8.2824	0.0000	-8.2824
CuCO3(aq)	2.7736E-09	-8.5570	0.0000	-8.5570
Zn(OH)3-	5.6057E-10	-9.2514	-0.1579	-9.4093
MgCl+	5.5624E-10	-9.2547	-0.1579	-9.4126
CaOH+	2.7937E-10	-9.5538	-0.1579	-9.7117
Zn++	2.6327E-10	-9.5796	-0.5515	-10.1311
H+	1.7494E-10	-9.7571	-0.0994	-9.8566
CaCl+	1.2769E-10	-9.8938	-0.1579	-10.0517
ZnHCO3+	6.5745E-11	-10.1821	-0.1579	-10.3400
CuOH+	3.1061E-11	-10.5078	-0.1579	-10.6657
H6(H2SiO4)4--	7.6324E-12	-11.1173	-0.6692	-11.7865
ZnCl+	2.2187E-12	-11.6539	-0.1579	-11.8118
Zn(OH)4--	2.2108E-12	-11.6554	-0.6692	-12.3247
H4(H2SiO4)4----	2.1932E-12	-11.6589	-2.7145	-14.3734

B2O(OH) 5-	8.6963E-13	-12.0607	-0.1579	-12.2186
CuO2--	2.5549E-13	-12.5926	-0.6692	-13.2618
Cu++	2.0913E-13	-12.6796	-0.5515	-13.2311
Fe(OH) 4-	1.7636E-13	-12.7536	-0.1579	-12.9115
Al(OH) 2+	1.5614E-13	-12.8065	-0.1579	-12.9644
CaCl2(aq)	1.4440E-13	-12.8404	0.0000	-12.8404
Fe(OH) 3(aq)	6.8486E-14	-13.1644	0.0000	-13.1644
HCl(aq)	5.0866E-14	-13.2936	0.0000	-13.2936
ZnCl2(aq)	2.1160E-15	-14.6745	0.0000	-14.6745
CuCl+	4.1239E-16	-15.3847	-0.1579	-15.5426
Zn(OH) 2(aq)	3.2903E-17	-16.4828	0.0000	-16.4828
Fe(OH) 2+	2.9552E-17	-16.5294	-0.1579	-16.6873
AlOH++	3.6334E-18	-17.4397	-0.6354	-18.0751
ZnCl3-	1.4692E-18	-17.8329	-0.1579	-17.9908
HO2-	1.4373E-18	-17.8424	-0.1579	-18.0003
Cu+	4.5784E-19	-18.3393	-0.1579	-18.4972
ClO-	3.7778E-19	-18.4228	-0.1579	-18.5806
CuCl2(aq)	2.6941E-19	-18.5696	0.0000	-18.5696
CuCl2-	9.6584E-20	-19.0151	-0.1579	-19.1730
ZnCl4--	4.9534E-20	-19.3051	-0.6692	-19.9743
CuCl3--	3.5927E-21	-20.4446	-0.6692	-21.1138
HClO(aq)	1.3551E-21	-20.8680	0.0000	-20.8680
FeOH++	3.7600E-23	-22.4248	-0.6354	-23.0602
Al+++	1.1770E-23	-22.9292	-0.9955	-23.9247
FeCO3+	1.0030E-23	-22.9987	-0.1579	-23.1566
ClO3-	8.3228E-25	-24.0797	-0.1579	-24.2376
FeCO3(aq)	7.2196E-25	-24.1415	0.0000	-24.1415
Mg4(OH) 4++++	3.7130E-25	-24.4303	-2.3454	-26.7757
ClO4-	1.7151E-25	-24.7657	-0.1777	-24.9435
FeHCO3+	3.0104E-26	-25.5214	-0.1579	-25.6793
Fe++	9.1449E-27	-26.0388	-0.5515	-26.5903
FeOH+	8.3269E-27	-26.0795	-0.1579	-26.2374
ClO2-	3.5100E-28	-27.4547	-0.1579	-27.6126
Fe(OH) 2(aq)	3.2772E-28	-27.4845	0.0000	-27.4845
Fe(OH) 3-	1.3375E-28	-27.8737	-0.1579	-28.0316
CuCl4--	7.5163E-29	-28.1240	-0.6692	-28.7932
FeCl+	6.0628E-30	-29.2173	-0.1579	-29.3752
Fe+++	1.8721E-30	-29.7277	-0.9955	-30.7231
Fe(OH) 4--	3.0940E-33	-32.5095	-0.6692	-33.1787
FeCl++	2.6229E-33	-32.5812	-0.6354	-33.2166
Al2(OH) 2++++	3.2481E-34	-33.4884	-2.3454	-35.8338
FeCl2+	1.1689E-34	-33.9322	-0.1579	-34.0901
HClO2(aq)	5.0193E-35	-34.2994	0.0000	-34.2994
FeCl2(aq)	4.9669E-35	-34.3039	0.0000	-34.3039
Formate	1.5949E-38	-37.7973	-0.1579	-37.9552
FeCl4--	3.0540E-39	-38.5151	-0.6692	-39.1843
H2(aq)	7.5398E-40	-39.1226	0.0291	-39.0935
Fe2(OH) 2++++	4.5182E-43	-42.3450	-2.3454	-44.6904
FeCl4-	4.4746E-43	-42.3492	-0.1579	-42.5071
Al3(OH) 4(5+)	1.8619E-43	-42.7300	-3.5127	-46.2427
Formic acid(aq)	9.7156E-45	-44.0125	0.0000	-44.0125
CO(aq)	5.6064E-47	-46.2513	0.0000	-46.2513
Fe3(OH) 4(5+)	2.8507E-56	-55.5450	-3.5127	-59.0577
Formaldehyde(aq)	2.6990E-85	-84.5688	0.0000	-84.5688
Al13O4(OH) 24(7+)	2.8424E-88	-87.5463	-6.8969	-94.4432

--- Summary of Solid Product Phases---

Product	Log moles	Moles	Mass, g	Volume, cc
Calcite	-3.6790	2.0943E-04	2.0961E-02	7.7351E-03
Dawsonite	-2.5249	2.9860E-03	4.2997E-01	1.4930E+00
Hematite	-5.5166	3.0435E-06	4.8602E-04	9.2139E-05
Magnesite	-4.7522	1.7695E-05	1.4919E-03	4.9578E-04
Tenorite	-4.2639	5.4467E-05	4.3326E-03	6.6559E-04
Zincite	-3.9756	1.0579E-04	8.6102E-03	5.2895E-02

	Mass, grams	Volume, cc
Created	4.658534E-01	1.554890E+00
Destroyed	0.000000E+00	0.000000E+00
Net	4.658534E-01	1.554890E+00

Warning-- these volume totals may be incomplete because of missing partial molar volume data in the data base

--- Summary of Pure Mineral Saturation States ---

Mineral	Log Q/K	Aff, kcal	State
Albite	-0.322	-0.491	
Albite high	-1.438	-2.193	
Albite low	-0.322	-0.491	
Amesite-14A	5.405	8.240	ssatd
Analcime	0.353	0.538	ssatd
Analcime-dehy	-5.247	-7.999	
Andalusite	-4.681	-7.136	
Andradite	-4.222	-6.436	
Anorthite	-5.450	-8.309	
Anthophyllite	-1.284	-1.957	
Antigorite	63.861	97.353	ssatd
Aragonite	-0.143	-0.218	
Artinite	-2.740	-4.178	
Beidellite-Ca	-3.354	-5.113	
Beidellite-H	-4.685	-7.142	
Beidellite-Mg	-3.244	-4.945	
Beidellite-Na	-2.716	-4.141	
Boehmite	0.168	0.257	ssatd
Borax	-2.371	-3.615	
Boric acid	-1.900	-2.896	
Brucite	-1.171	-1.785	
Calcite	0.000	0.000	satd
Chalcedony	-1.227	-1.870	
Chrysocolla	-4.201	-6.404	
Chrysotile	3.380	5.152	ssatd
Clinochlore-14A	7.620	11.616	ssatd
Clinochlore-7A	4.487	6.840	ssatd
Clinoptilolite-Na	-6.013	-9.166	
Clinoptilolite-hy-Na	-6.002	-9.150	
Clinozoisite	-5.020	-7.653	

Coesite	-1.715	-2.614	
Colemanite	-5.681	-8.660	
Corundum	-2.240	-3.415	
Cristobalite (alpha)	-1.465	-2.234	
Cristobalite (beta)	-1.831	-2.791	
Dawsonite	0.000	0.000	satd
Delafossite	-3.040	-4.634	
Diaspore	0.519	0.792	ssatd
Diopside	-1.174	-1.790	
Dioptase	-3.574	-5.449	
Dolomite	1.440	2.195	ssatd
Dolomite-dis	0.121	0.185	ssatd
Dolomite-ord	1.440	2.195	ssatd
Enstatite	-1.090	-1.661	
Epidote	-2.798	-4.265	
Epidote-ord	-2.800	-4.268	
Eucryptite	-4.039	-6.157	
Fe (OH) 3	-5.268	-8.031	
Ferrite-Ca	-5.926	-9.034	
Ferrite-Cu	-2.224	-3.390	
Ferrite-Mg	-5.069	-7.728	
Ferrite-Zn	-0.260	-0.396	
Forsterite	-2.271	-3.462	
Gaylussite	-3.554	-5.417	
Gibbsite	-0.231	-0.352	
Goethite	-0.561	-0.855	
Halite	-5.242	-7.991	
Hematite	0.000	0.000	satd
Huntite	-1.353	-2.062	
Hydroboracite	-4.427	-6.749	
Hydromagnesite	-6.389	-9.740	
Hydrozincite	-5.750	-8.766	
Ice	-0.289	-0.441	
Jadeite	-0.970	-1.479	
Kaolinite	-1.490	-2.272	
Kyanite	-4.490	-6.845	
Lansfordite	-3.421	-5.215	
Laumontite	-3.521	-5.367	
Lawsonite	-2.185	-3.332	
Magnesite	0.000	0.000	satd
Malachite	-3.230	-4.925	
Margarite	-4.611	-7.030	
Mesolite	2.330	3.552	ssatd
Monohydrocalcite	-0.979	-1.493	
Monticellite	-4.275	-6.518	
Montmor-Ca	-2.260	-3.446	
Montmor-Mg	-2.091	-3.188	
Montmor-Na	-1.563	-2.382	
Mordenite	-4.971	-7.578	
Na2CO3	-4.135	-6.304	
Na2CO3:7H2O	-4.364	-6.652	
Nahcolite	-2.863	-4.364	
Natrolite	1.004	1.531	ssatd
Natron	-4.354	-6.637	
Nepheline	-1.071	-1.632	
Nesquehonite	-3.391	-5.170	
Nontronite-Ca	-2.052	-3.129	
Nontronite-H	-3.382	-5.156	

Nontronite-Mg	-1.942	-2.961	
Nontronite-Na	-1.415	-2.157	
Okenite	-5.876	-8.957	
Paragonite	0.326	0.497	ssatd
Periclase	-5.480	-8.354	
Petalite	-2.110	-3.217	
Pirssonite	-3.702	-5.643	
Prehnite	-3.039	-4.633	
Pseudowollastonite	-3.920	-5.976	
Pyrophyllite	-4.770	-7.271	
Quartz	-0.984	-1.500	
Saponite-Ca	4.752	7.244	ssatd
Saponite-H	3.421	5.215	ssatd
Saponite-Mg	4.858	7.406	ssatd
Saponite-Na	5.389	8.216	ssatd
Scolecite	-0.967	-1.473	
Sepiolite	-1.542	-2.350	
SiO2 (am)	-2.051	-3.126	
Sillimanite	-4.986	-7.600	
Smithsonite	-1.945	-2.965	
Spinel	-5.899	-8.992	
Spodumene	-2.771	-4.224	
Talc	3.355	5.114	ssatd
Tenorite	0.000	0.000	satd
Thermonatrite	-4.158	-6.339	
Tremolite	2.655	4.047	ssatd
Tridymite	-1.140	-1.738	
Wollastonite	-3.736	-5.695	
Zincite	0.000	0.000	satd
Zn(OH) 2 (beta)	-0.867	-1.321	
Zn(OH) 2 (epsilon)	-0.621	-0.947	
Zn(OH) 2 (gamma)	-2.308	-3.519	
Zoisite	-5.058	-7.711	

--- Summary of Gases ---

Gas	Fugacity	Log fugacity
Al (g)	3.9622-169	-168.4021
B (g)	2.9950-178	-177.5236
C (g)	6.8268-170	-169.1658
C2H4 (g)	3.9227-213	-212.4064
CH4 (g)	6.8560-130	-129.1639
CO (g)	7.8214E-44	-43.1067
CO2 (g)	2.4595E-04	-3.6092
Ca (g)	1.7207-132	-131.7643
Chlorine	9.3880E-30	-29.0274
Cu (g)	7.2400E-66	-65.1403
H2 (g)	1.1114E-36	-35.9541
H2O (g)	1.6234E-01	-0.7896
HCl (g)	3.1712E-18	-17.4988
Li (g)	2.0882E-78	-77.6802
Mg (g)	1.5125-111	-110.8203
Na (g)	1.0553E-62	-61.9766
O2 (g)	1.9940E-01	-0.7003
Si (g)	5.0464-197	-196.2970
Zn (g)	2.7298E-64	-63.5639

-
--- No reaction path is defined (path) ---

Start time = 15:50:32 10/07/05
End time = 15:50:32 10/07/05

Run time = 0.330 seconds
User time = 0.330 seconds
Cpu time = 0.330 seconds

Normal exit

APPENDIX C

SIMULATION CALCULATION SUMMARY FOR INTEGRATED CHEMICAL EFFECTS TEST (ICET) #1 AT 60 °C [140 °F] AT 148 HOURS, USING STREAM ANALYZER, VERSION 2.0

Calculation Summary

Calculation Summary

ICET#1 148h Calculation for Work2

Unit Set: Default

Automatic Chemistry Model
 Aqueous (H+ ion) Databanks:
 Public
 Excluding 2 solid phases
 Redox selected

Isothermal Calculation

Pressure 1.00000 atm

1

Stream Inflows

H2O	55.5080	mol
B(OH)3	0.259000	mol
LiOH	1.01000e-4	mol
HCl	2.74000e-3	mol
Zn	1.06000e-4	mol
Al	4.09000e-3	mol
Fe	6.09000e-6	mol
Cu	5.46000e-5	mol
SiO2	4.49000e-4	mol
Al(OH)3	2.98000e-5	mol
Ca(OH)2	2.19000e-4	mol
Mg(OH)2	2.40000e-5	mol
NaOH	2.20000e-1	mol

Speciation Summary

Total number of species: 265

User Inflows	Related Inflows	Aqueous Species	Vapor Species	Solid Species	Second Liquid Species
H2O	Fe3Al2Si8O12	H2O	H2O	Al	
B(OH)3	AlCl3	Al(OH)2Cl	H2	Al(OH)2Cl	
LiOH	Al(OH)2Cl	AlOHCl+1	HCl	AlCl3.6H2O	
HCl	AlCl3.6H2O	Al(OH)2+1	O2	AlOHCl2	
Zn	AlOHCl2	Al(OH)3	SiCl4	AlO(OH)	
Al	AlO(OH)	Al+3		B(OH)3	
Fe	CaCl2	AlOH+2		CaCl2	
Cu	CaCl2.2H2O	Al(OH)4-1		CaCl2.2H2O	
SiO2	CaCl2.6H2O	B(OH)3		CaCl2.6H2O	
Al(OH)3	CaCl2.H2O	B(OH)4-1		CaCl2.H2O	
Ca(OH)2	CaCl2.CaO	CaCl2		CaCl2.4H2O	
Mg(OH)2	CaCl2.CaO.2H2O	CaH2BO3+1		CaCl2.CaO.2H2O	
NaOH	CaCl2.4H2O	CaHSiO3+1		Ca(OH)2	
	Ca(Al2Si6O16).5H2O	CaOH+1		Ca3(BO3)2	
	Ca(Al2Si5O14).5H2O	Ca+2		Cu	
	Ca(OH)Cl	CaCl+1		CuCl	
	Ca3(BO3)2	CaSiO2(OH)2		Cu2O	
	CaSiO2(OH)2	Cl-1		CuCl2	
	CuCl	Cu+1		CuCl2.2H2O	
	CuOH	CuCl2		Cu(OH)2	
	Cu2O	Cu(OH)2		Cu(OH)2	
	CuCl2	Cu+2		Al2(OH)5Cl	
	CuCl2.2H2O	Cu+1		Fe	
	Cu(OH)2	CuOH+1		FeCl3	
	Mg7Si8O22(OH)2	Cu(OH)4-2		FeCl2	
	CaAl2Si4O12.6H2O	CuCl3-1		FeCl2.2H2O	
	Al2(OH)5Cl	Cu(OH)3-1		FeCl2.6H2O	
	Fe2Al2SiO5(OH)4	B2O(OH)5-1		FeCl2.4H2O	
	FeAl2SiO5(OH)2	H2SiO4-2		Fe(OH)2	
	Al2SiO5(OH)4	Fe2(OH)2+4		FeCl3.2.5H2O	
	Ca2Fe5Si8O22(OH)2	H2		FeCl3.2H2O	
	Ca2Al4Si8O24.7H2O	HCl		FeCl3.6H2O	
	Fe2Al9Si4O23(OH)	H+1		Fe(OH)3	
	Mg2Al2SiO5(OH)4	OH-1		LiCl	
	Na2Al2Si3O10.2H2O	FeCl3		LiCl.2H2O	
	Al2Si2O5(OH)4	Fe+2		LiCl.1H2O	
	Fe7Si8O22(OH)2	Fe+3		LiOH	
	CaAl2Si7O18.6H2O	FeCl2		LiOH.1H2O	
	H2	Fe(OH)2		LiBO2	
	FeCl3	FeCl+1		LiBO2.2H2O	
	FeCl2	FeOH+1		LiBO2.8H2O	
				MgCl2	

FeCl₂.2H₂O
 FeCl₂.6H₂O
 FeCl₂.4H₂O
 Fe(OH)₂
 FeCl₃.2.5H₂O
 FeCl₃.2H₂O
 FeCl₃.6H₂O
 Fe(OH)₃
 FeNaSi₂O₆
 LiCl
 LiCl₂.2H₂O
 LiCl₂.1H₂O
 LiH₂BO₃
 Fe(OH)₄-2
 Fe(OH)₃-1
 FeCl₂+1
 Fe(OH)₂+1
 Fe(OH)₃
 FeCl₂+2
 FeOH+2
 FeCl₄-1
 Fe(OH)₄-1
 LiH₂BO₃
 LiOH
 Li+1
 MgSiO₂(OH)₂
 MgCl₂.2H₂O
 MgCl₂.6H₂O
 MgClOH
 MgCl₂.4H₂O
 Mg(OH)₂
 SiO₂
 NaAlO₂
 Na₂O.Ai₂O₃.2.5H₂O
 NaCl
 NaOH
 NaOH.1H₂O
 NaBO₂
 Na

BO₂.2H₂O
 C₃

LiOH.1H₂O
 LiBO₂
 LiBO₂.2H₂O
 LiBO₂.8H₂O
 MgCl₂
 MgCl₂.2H₂O
 MgCl₂.6H₂O
 MgClOH
 MgCl₂.4H₂O
 MgSiO₂(OH)₂
 O₂
 Fe₅Al₂Si₃O₁₀(OH)₈
 H₄SiO₄
 SiCl₄
 NaAlO₂
 Na₂O.Ai₂O₃
 Na₂O.Ai₂O₃.2.5H₂O
 Na₂Al₂Si₅O₁₄.5H₂O
 NaB(OH)₄
 NaCl
 NaH₂BO₃
 NaHSiO₃
 NaOH.1H₂O
 NaBO₂
 NaBO₂.2H₂O
 MgHSiO₃+1
 MgOH+1
 Mg+2
 O₂
 SiO₂
 SiCl₄
 NaB(OH)₄
 NaHSiO₃
 Na+1
 B₄O₅(OH)₄-2
 B₃O₃(OH)₄-1
 H₃SiO₄-1
 ZnCl₂
 ZnCl+1
 Zn(OH)₂
 Zn+2
 ZnOH+1
 Zn(OH)₄-2
 ZnCl₃-1
 Zn(OH)₃-1
 NaBO₂.0.5H₂O
 NaBO₂.4H₂O
 Na₂SiO₃
 Na₂SiO₃.6H₂O
 Na₂SiO₃.9H₂O
 Na₂SiO₃.5H₂O
 NaB₅O₈.5H₂O
 Na₂B₄O₇
 Na₂B₄O₇.10H₂O
 Na₂B₄O₇.5H₂O
 Na₂B₄O₇.4H₂O
 Zn
 ZnCl₂
 ZnCl₂.1H₂O
 ZnCl₂.3H₂O
 ZnCl₂.5ZnO.8H₂O
 Zn(OH)₂

NaBO2.0.5H2O
 NaBO2.4H2O
 Na2SiO3
 Na2SiO3.6H2O
 Na2SiO3.9H2O
 Na2SiO3.5H2O
 NaB5O8
 NaB5O8.5H2O
 Na2B4O7
 Na2B4O7.10H2O
 Na2B4O7.5H2O
 Na2B4O7.4H2O
 Al4Fe5Si6O22(OH)2
 Fe2Fe(FeSiO5)(OH)4
 Mg4Al4Si2O10(OH)8
 Fe3Si2O5(OH)4
 Fe3Si4O10(OH)2
 ZnCl2
 ZnCl2.1H2O
 ZnCl2.3H2O
 ZnCl2.5ZnO
 ZnCl2.5ZnO.8H2O
 Zn(OH)2

Stream Parameters

Mixture Properties

Stream Amt - Total Inflow
Temperature
Pressure

55.9948 mol
 60.0000 °C
 1.00000 atm

Aqueous Properties

pH
Ionic Strength
ORP
Osmotic Pressure
Electrical Cond, specific
Electrical Cond, molar
Viscosity, absolute
Viscosity, relative

9.75308 pH
 3.78719e-3 mol/mol
 -0.617624 V (SHE)
 9.99601 atm
 0.0326152 1/(ohm-cm)
 68.4065 cm2/ohm-mol
 0.478653 cP
 1.02603 cP/cP H2O

Density
Total
Aqueous
Vapor
Solid
2nd Liquid

--
 --
 1.00390 g/ml
 1.88507e-4 g/ml
 26.8197 g/ml
 0.0 g/ml

Enthalpy	Total cal	Aqueous cal	Vapor cal	Solid cal	2nd Liquid cal
	-3.85093e6	-3.85084e6	-78.2451	-11.8131	0.0
Heat Capacity	Total cal/g K	Aqueous cal/g K	Vapor cal/g K	Solid cal/g K	2nd Liquid cal/g K
	0.0	0.0	0.0	0.0	0.0

Total and Phase Flows (Amounts)

Mole (True)	Total mol	Aqueous mol	Vapor mol	Solid mol	2nd Liquid mol
	55.7573	55.9855	7.05772e-3	1.33210e-4	0.0
Mole (App)	Total mol	Aqueous mol	Vapor mol	Solid mol	2nd Liquid mol
	55.9948	56.2230	7.05772e-3	1.33210e-4	0.0
Mass	Total g	Aqueous g	Vapor g	Solid g	2nd Liquid g
	1025.08	1025.03	0.0363742	0.0112723	0.0
Volume	Total L	Aqueous L	Vapor L	Solid L	2nd Liquid L
	1.21401	1.02105	0.192959	4.20298e-7	0.0

Species Output (True Species)

H2O	Total mol	Aqueous mol	Vapor mol	Solid mol	2nd Liquid n/a
	55.5418	55.5404	1.38419e-3	0.0	0.0
B(OH)3	Total mol	Aqueous mol	Vapor mol	Solid mol	2nd Liquid mol
	0.0208344	0.0208344	0.0	0.0	0.0
LiOH	Total mol	Aqueous mol	Vapor mol	Solid mol	2nd Liquid mol
	1.01709e-7	1.01709e-7	0.0	0.0	0.0
HCl	Total mol	Aqueous mol	Vapor mol	Solid mol	2nd Liquid mol
	1.722e-18	1.68382e-18	3.81726e-20	0.0	0.0
Cu	Total mol	Aqueous mol	Vapor mol	Solid mol	2nd Liquid mol
	5.46e-5	0.0	0.0	5.46e-5	0.0
SiO2	Total mol	Aqueous mol	Vapor mol	Solid mol	2nd Liquid mol
	2.11168e-5	2.11168e-5	0.0	0.0	0.0
Al(OH)3	Total mol	Aqueous mol	Vapor mol	Solid mol	2nd Liquid mol
	6.75639e-7	6.75639e-7	0.0	0.0	0.0
Al(OH)2Cl	Total mol	Aqueous mol	Vapor mol	Solid mol	2nd Liquid mol
	2.02697e-30	2.02697e-30	0.0	0.0	0.0
CaCl2	Total mol	Aqueous mol	Vapor mol	Solid mol	2nd Liquid mol
	2.68945e-24	2.68945e-24	0.0	0.0	0.0
CaSiO2(OH)2	Total mol	Aqueous mol	Vapor mol	Solid mol	2nd Liquid mol
	3.90525e-8	3.90525e-8	0.0	0.0	0.0
CuCl2	Total mol	Aqueous mol	Vapor mol	Solid mol	2nd Liquid mol
	2.26892e-35	2.26892e-35	0.0	0.0	0.0
Cu(OH)2	Total mol	Aqueous mol	Vapor mol	Solid mol	2nd Liquid mol
	1.12052e-23	1.12052e-23	0.0	0.0	0.0

H2	6.24709e-3	5.73566e-4	5.67353e-3	0.0	0.0
FeCl3	6.73151e-39	6.73151e-39	0.0	0.0	0.0
FeCl2	1.00813e-17	1.00813e-17	0.0	0.0	0.0
Fe(OH)2	2.2606e-6	1.01802e-6	0.0	1.20805e-6	0.0
Fe(OH)3	2.69358e-10	2.69358e-10	0.0	0.0	0.0
LiH2BO3	1.4604e-5	1.4604e-5	0.0	0.0	0.0
MgSiO2(OH)2	1.15099e-7	1.15099e-7	0.0	0.0	0.0
O2	3.01194e-75	3.23566e-76	2.68837e-75	0.0	0.0
SiCl4	7.65924e-97	2.75177e-100	7.65648e-97	0.0	0.0
NaB(OH)4	0.0125225	0.0125225	0.0	0.0	0.0
NaHSiO3	2.97618e-4	2.97618e-4	0.0	0.0	0.0
ZnCl2	8.31405e-14	8.31405e-14	0.0	0.0	0.0
Zn(OH)2	9.21229e-5	1.4721e-5	0.0	7.74019e-5	0.0
AlOHCl+1	1.47938e-19	1.47938e-19	0.0	0.0	0.0
Al(OH)2+1	4.62119e-12	4.62119e-12	0.0	0.0	0.0
Al+3	1.0206e-21	1.0206e-21	0.0	0.0	0.0
AlOH+2	7.92781e-17	7.92781e-17	0.0	0.0	0.0
Al(OH)4-1	4.11912e-3	4.11912e-3	0.0	0.0	0.0
B(OH)4-1	0.179084	0.179084	0.0	0.0	0.0
CaH2BO3+1	1.6668e-4	1.6668e-4	0.0	0.0	0.0
CaHSiO3+1	2.13667e-8	2.13667e-8	0.0	0.0	0.0
CaOH+1	3.77276e-7	3.77276e-7	0.0	0.0	0.0
Ca+2	5.18825e-5	5.18825e-5	0.0	0.0	0.0
CaCl+1	1.23307e-11	1.23307e-11	0.0	0.0	0.0
Cl-1	2.74e-3	2.74e-3	0.0	0.0	0.0
Cu+1	1.09675e-17	1.09675e-17	0.0	0.0	0.0
Cu+2	9.85354e-30	9.85354e-30	0.0	0.0	0.0
Cu+1	5.57247e-32	5.57247e-32	0.0	0.0	0.0
CuOH+1	4.76589e-27	4.76589e-27	0.0	0.0	0.0
Cu(OH)4-2	5.33283e-27	5.33283e-27	0.0	0.0	0.0
CuCl3-1	1.29921e-40	1.29921e-40	0.0	0.0	0.0
Cu(OH)3-1	2.82225e-25	2.82225e-25	0.0	0.0	0.0
B2O(OH)5-1	7.20697e-3	7.20697e-3	0.0	0.0	0.0
H2SiO4-2	2.00389e-7	2.00389e-7	0.0	0.0	0.0
Fe2(OH)2+4	7.41469e-43	7.41469e-43	0.0	0.0	0.0
H+1	2.47718e-10	2.47718e-10	0.0	0.0	0.0
OH-1	7.30972e-4	7.30972e-4	0.0	0.0	0.0
Fe+2	4.19031e-7	4.19031e-7	0.0	0.0	0.0
Fe+3	3.30799e-28	3.30799e-28	0.0	0.0	0.0
FeCl+1	1.54912e-12	1.54912e-12	0.0	0.0	0.0
FeOH+1	2.36078e-6	2.36078e-6	0.0	0.0	0.0
Fe(OH)4-2	3.07353e-10	3.07353e-10	0.0	0.0	0.0

Fe(OH)3-1	1.07745e-6	1.07745e-6	0.0	0.0	0.0
FeCl2+1	1.13944e-34	1.13944e-34	0.0	0.0	0.0
Fe(OH)2+1	1.21803e-15	1.21803e-15	0.0	0.0	0.0
FeCl2+2	4.80099e-32	4.80099e-32	0.0	0.0	0.0
FeOH+2	8.82039e-21	8.82039e-21	0.0	0.0	0.0
FeCl4-1	7.58951e-44	7.58951e-44	0.0	0.0	0.0
Fe(OH)4-1	6.09956e-9	6.09956e-9	0.0	0.0	0.0
Li+1	8.62943e-5	8.62943e-5	0.0	0.0	0.0
MgHSiO3+1	1.00242e-8	1.00242e-8	0.0	0.0	0.0
MgOH+1	8.99695e-7	8.99695e-7	0.0	0.0	0.0
Mg+2	2.29752e-5	2.29752e-5	0.0	0.0	0.0
Na+1	0.20718	0.20718	0.0	0.0	0.0
B4O5(OH)4-2	4.36341e-3	4.36341e-3	0.0	0.0	0.0
B3O3(OH)4-1	4.83687e-3	4.83687e-3	0.0	0.0	0.0
H3SiO4-1	1.29879e-4	1.29879e-4	0.0	0.0	0.0
ZnCl+1	7.80144e-11	7.80144e-11	0.0	0.0	0.0
Zn+2	1.16143e-8	1.16143e-8	0.0	0.0	0.0
ZnOH+1	1.34029e-6	1.34029e-6	0.0	0.0	0.0
Zn(OH)4-2	1.50756e-7	1.50756e-7	0.0	0.0	0.0
ZnCl3-1	6.3027e-17	6.3027e-17	0.0	0.0	0.0
Zn(OH)3-1	1.23743e-5	1.23743e-5	0.0	0.0	0.0
Total (by phase)	55.9927	55.9855	7.05772e-3	1.3321e-4	0.0

C-7

Molecular Output (Apparent Species)

	Total	Aqueous	Vapor	Solid	2nd Liquid
	mol	mol	mol	mol	n/a
H2O	56.0005	55.9991	1.38419e-3	0.0	0.0
LiOH	1.01000e-4	1.01000e-4	0.0	0.0	0.0
HCl	2.68247e-3	2.68247e-3	3.81726e-20	0.0	0.0
Cu	5.46000e-5	0.0	0.0	5.46000e-5	0.0
SiO2	4.44128e-4	4.44128e-4	0.0	0.0	0.0
Fe3Al2Si3O12	1.62307e-6	1.62307e-6	0.0	0.0	0.0
Ca3(BO3)2	7.30000e-5	7.30000e-5	0.0	0.0	0.0
Cu2O	5.91400e-19	5.91400e-19	0.0	0.0	0.0
CuCl2	1.14975e-23	1.14975e-23	0.0	0.0	0.0
H2	6.24709e-3	5.73566e-4	5.67353e-3	0.0	0.0
Fe(OH)2	1.20805e-6	0.0	0.0	1.20805e-6	0.0
MgCl2	2.40000e-5	2.40000e-5	0.0	0.0	0.0
O2	3.01194e-75	3.23566e-76	2.68837e-75	0.0	0.0
SiCl4	7.65648e-97	0.0	7.65648e-97	0.0	0.0

NaAlO2	4.11655e-3	4.11655e-3	0.0	0.0	0.0
NaBO2	0.205141	0.205141	0.0	0.0	0.0
NaB5O8	0.0107426	0.0107426	0.0	0.0	0.0
Fe2Fe(FeSiO5)(OH)4	3.18446e-9	3.18446e-9	0.0	0.0	0.0
ZnCl2.5ZnO	4.76635e-6	4.76635e-6	0.0	0.0	0.0
Zn(OH)2	7.74019e-5	7.74019e-5	0.0	7.74019e-5	0.0
Total (by phase)	56.2302	56.2230	7.05772e-3	1.33210e-4	0.0

Element Balance

	Total	Aqueous	Vapor	Solid	2nd Liquid
	mol	mol	mol	mol	n/a
H(+1)	112.004	112.001	2.76839e-3	1.57220e-4	0.0
NA(+1)	0.220000	0.220000	0.0	0.0	0.0
CA(+2)	2.19000e-4	2.19000e-4	0.0	0.0	0.0
ZN(+2)	1.06000e-4	2.85981e-5	0.0	7.74019e-5	0.0
CU(+2)	1.14975e-23	1.14975e-23	0.0	0.0	0.0
FE(+2)	6.08363e-6	4.87558e-6	0.0	1.20805e-6	0.0
MG(+2)	2.40000e-5	2.40000e-5	0.0	0.0	0.0
AL(+3)	4.11980e-3	4.11980e-3	0.0	0.0	0.0
FE(+3)	6.36892e-9	6.36892e-9	0.0	0.0	0.0
O(-2)	56.5066	56.5050	1.38419e-3	1.57220e-4	0.0
CL(-1)	2.74000e-3	2.74000e-3	3.81726e-20	0.0	0.0
LI(+1)	1.01000e-4	1.01000e-4	0.0	0.0	0.0
SI(+4)	4.49000e-4	4.49000e-4	7.65648e-97	0.0	0.0
H	0.0124942	1.14713e-3	0.0113471	0.0	0.0
O	6.02387e-75	6.47132e-76	5.37674e-75	0.0	0.0
B(+3)	0.259000	0.259000	0.0	0.0	0.0
FE(0)	0.0	0.0	0.0	0.0	0.0
CU(+1)	1.09675e-17	1.09675e-17	0.0	0.0	0.0
CU(0)	5.46000e-5	0.0	0.0	5.46000e-5	0.0
AL(0)	0.0	0.0	0.0	0.0	0.0
Zn(0)	0.0	0.0	0.0	0.0	0.0

Species Activity Coefficients

H2O	1.00131	Act-Coef
Al(OH)2Cl - Aq	57.0965	Act-Coef
AlOHCl+1	37.6753	Act-Coef
Al(OH)2+1	37.7544	Act-Coef
Al(OH)3 - Aq	57.0965	Act-Coef
Al+3	1.64769	Act-Coef
AlOH+2	11.6536	Act-Coef
Al(OH)4-1	38.4785	Act-Coef
B(OH)3 - Aq	57.0965	Act-Coef
B(OH)4-1	39.9008	Act-Coef
CaCl2 - Aq	57.0965	Act-Coef
CaH2BO3+1	39.5940	Act-Coef
CaHSiO3+1	37.6843	Act-Coef
CaOH+1	39.6254	Act-Coef
Ca+2	16.8482	Act-Coef
CaCl+1	45.4679	Act-Coef
CaSiO2(OH)2 - Aq	57.0965	Act-Coef
Cl-1	39.9009	Act-Coef
Cu+1	37.7114	Act-Coef
CuCl2 - Aq	57.0965	Act-Coef
Cu(OH)2 - Aq	57.0965	Act-Coef
Cu+2	11.5361	Act-Coef
Cu+1	37.7114	Act-Coef
CuOH+1	37.7114	Act-Coef
Cu(OH)4-2	11.5013	Act-Coef
CuCl3-1	37.6753	Act-Coef
Cu(OH)3-1	37.6753	Act-Coef
B2O(OH)5-1	37.6753	Act-Coef
H2SiO4-2	12.7047	Act-Coef
Fe2(OH)2+4	0.102775	Act-Coef
H2 - Aq	57.0965	Act-Coef
HCl - Aq	57.0965	Act-Coef
H+1	39.9057	Act-Coef
OH-1	40.4274	Act-Coef
FeCl3 - Aq	57.0965	Act-Coef
Fe+2	11.5617	Act-Coef
Fe+3	1.60603	Act-Coef
FeCl2 - Aq	57.0965	Act-Coef
Fe(OH)2 - Aq	57.0965	Act-Coef
FeCl+1	37.7115	Act-Coef
FeOH+1	37.7115	Act-Coef
Fe(OH)4-2	11.5013	Act-Coef
Fe(OH)3-1	37.6803	Act-Coef

FeCl2+1	37.6920	Act-Coef
Fe(OH)2+1	37.7114	Act-Coef
Fe(OH)3 - Aq	57.0965	Act-Coef
FeCl2+2	11.5707	Act-Coef
FeOH+2	11.5707	Act-Coef
FeCl4-1	37.6753	Act-Coef
Fe(OH)4-1	37.6753	Act-Coef
LiH2BO3 - Aq	57.0965	Act-Coef
LiOH - Aq	57.0965	Act-Coef
Li+1	39.6439	Act-Coef
MgSiO2(OH)2 - Aq	57.0965	Act-Coef
MgHSiO3+1	37.6843	Act-Coef
MgOH+1	37.7128	Act-Coef
Mg+2	11.5693	Act-Coef
O2 - Aq	57.0965	Act-Coef
SiO2 - Aq	57.0881	Act-Coef
SiCl4 - Aq	57.0965	Act-Coef
NaB(OH)4 - Aq	57.0965	Act-Coef
NaHSiO3 - Aq	57.0965	Act-Coef
Na+1	39.6447	Act-Coef
B4O5(OH)4-2	11.5013	Act-Coef
B3O3(OH)4-1	37.6753	Act-Coef
H3SiO4-1	39.8997	Act-Coef
ZnCl2 - Aq	57.0965	Act-Coef
ZnCl+1	37.7038	Act-Coef
Zn(OH)2 - Aq	57.0965	Act-Coef
Zn+2	11.5323	Act-Coef
ZnOH+1	37.6830	Act-Coef
Zn(OH)4-2	12.7023	Act-Coef
ZnCl3-1	39.8945	Act-Coef
Zn(OH)3-1	39.8945	Act-Coef
H2O - Vap Fug.Coef.	0.995928	Fug-Coef
HCl - Vap Fug.Coef.	0.998169	Fug-Coef
H2 - Vap Fug.Coef.	1.00108	Fug-Coef
O2 - Vap Fug.Coef.	0.999801	Fug-Coef
SiCl4 - Vap Fug.Coef.	0.994679	Fug-Coef

Species K(eq)-Values

H2O	9.38243e-14
H2O - Vap	5.08561
Al - Sol	1.11336e14

Al(OH)2Cl - Aq	7.90562e-3
Al(OH)2Cl - Sol	7.12112e-17
AlCl3.6H2O	5.88942e5
AlOHCl+1	3.10997e-10
AlOHCl2 - Sol	1.91458e-10
Al(OH)2+1	2.79508e-9
Al(OH)3 - Aq	2.38725e-9
AlOH+2	9.60769e-10
AlO(OH) - Sol	0.134623
Al(OH)4-1	1.28470e-7
B(OH)3 - Sol	2.38396
B(OH)4-1	9.36567e8
CaCl2 - Aq	7.12980e9
CaCl2 - Sol	9.60517e9
CaCl2.2H2O	3.22427e6
CaCl2.6H2O	24394.8
CaCl2.H2O	5.14621e10
CaCl2.CaO.2H2O	1.43760e12
CaCl2.4H2O	2.00914e5
CaH2BO3+1	0.0170185
CaHSiO3+1	0.101160
Ca(OH)2 - Sol	1.43053e-6
CaOH+1	0.0308634
CaCl+1	3044.68
Ca3(BO3)2 - Sol	2782.89
CaSiO2(OH)2 - Aq	1.78271e-5
Cu - Sol	39464.5
Cu+1	2.65724e6
CuCl - Sol	1.17113e-6
Cu2O - Sol	1.73253e-28
CuCl2 - Aq	0.334609
CuCl2 - Sol	1069.63
CuCl2.2H2O	1.00797
Cu(OH)2 - Aq	1.48282e-7
Cu(OH)2 - Sol	4.83372e-19
Cu+1	0.105630
CuOH+1	3.33837e-7
Cu(OH)4-2	0.0915059
CuCl3-1	172.937
Cu(OH)3-1	0.0317599
Al2(OH)5Cl - Sol	1.29061e-44
B2O(OH)5-1	5.27204e8
Fe2(OH)2+4	1.84326e-20

H2 - Aq	1.56368e8
H2 - Vap	7.26875e-4
HCl - Aq	2.00791e5
HCl - Vap	0.318083
Fe - Sol	1.53693e11
FeCl3 - Aq	21.8210
FeCl3 - Sol	344.987
Fe+2	2.25624e-28
FeCl2 - Aq	198.195
FeCl2 - Sol	2.58538e7
FeCl2.2H2O	749.525
FeCl2.6H2O	188.760
FeCl2.4H2O	172.837
Fe(OH)2 - Aq	8.08472e-4
Fe(OH)2 - Sol	2.41100e-14
FeCl+1	161.946
FeOH+1	2.87238e-5
Fe(OH)4-2	6.06216
Fe(OH)3-1	7.55710e-4
FeCl3.2.5H2O	19.4986
FeCl3.2H2O	31.4444
FeCl3.6H2O	11.7092
FeCl2+1	0.252587
Fe(OH)2+1	1.17278e-9
Fe(OH)3 - Aq	1.57650e-9
Fe(OH)3 - Sol	1.49946e-36
FeCl2+2	1.86761
FeOH+2	2.74772e-12
FeCl4-1	262.489
Fe(OH)4-1	3.53253e-5
LiCl - Sol	3.39820e7
LiCl.2H2O	2.83423e6
LiCl.1H2O	2.66160e5
LiH2BO3 - Aq	0.527152
LiOH - Aq	0.310950
LiOH - Sol	28.3435
LiOH.1H2O	2.45171
LiBO2 - Sol	1.96745
LiBO2.2H2O	0.493293
LiBO2.8H2O	1.78619
MgCl2 - Sol	2.30346e18
MgCl2.2H2O	2.10264e8
MgCl2.6H2O	38695.4

MgClOH - Sol	4.49339
MgCl ₂ .4H ₂ O	1.44933e5
MgSiO ₂ (OH) ₂ - Aq	1.83929e-6
MgHSiO ₃ +1	0.0655676
Mg(OH) ₂ - Sol	3.23657e-12
MgOH+1	4.13509e-3
O ₂ - Vap	8.66481e-4
SiO ₂ - Aq	7.69210e-10
SiO ₂ - Sol	3.47020e-3
SiCl ₄ - Aq	6.76192e23
SiCl ₄ - Vap	2.60075e-6
NaAlO ₂ - Sol	3278.02
Na ₂ O.Al ₂ O ₃ .2.5H ₂ O	29720.9
NaB(OH) ₄ - Aq	1.46620
NaCl - Sol	36.0599
NaHSiO ₃ - Aq	0.0450396
NaOH - Sol	1.10933e6
NaOH.1H ₂ O	30123.8
NaBO ₂ - Sol	754.131
NABO ₂ .2H ₂ O	21.7654
NaBO ₂ .0.5H ₂ O	20447.5
NaBO ₂ .4H ₂ O	13.8871
Na ₂ SiO ₃ - Sol	2.31637e15
Na ₂ SiO ₃ .6H ₂ O	1.07508e13
Na ₂ SiO ₃ .9H ₂ O	5.84030e12
Na ₂ SiO ₃ .5H ₂ O	1.38270
Na ₅ O ₈ .5H ₂ O	5.01027e8
Na ₂ B ₄ O ₇ - Sol	5.18879e-15
Na ₂ B ₄ O ₇ .10H ₂ O	1.75239e14
Na ₂ B ₄ O ₇ .5H ₂ O	2.62878e-22
Na ₂ B ₄ O ₇ .4H ₂ O	2.01079e-22
B ₄ O ₅ (OH) ₄ -2	7.44075e15
B ₃ O ₃ (OH) ₄ -1	1.69151e7
H ₃ SiO ₄ -1	8.67455e-14
Zn - Sol	6.81985e19
ZnCl ₂ - Aq	1.21003
ZnCl ₂ - Sol	1.01251
ZnCl+1	0.0889214
ZnCl ₂ .1H ₂ O	1.53075
ZnCl ₂ .3H ₂ O	7.84931e-13
ZnCl ₂ .5ZnO.8H ₂ O	23.0878
Zn(OH) ₂ - Aq	3.17175e-5
Zn(OH) ₂ - Sol	6.66554e-16

ZnOH+1
Zn(OH)4-2
ZnCl3-1
Zn(OH)3-1

1.39979e-6
0.136075
3.68673
8.98700e-4

APPENDIX D

**SIMULATED OUTPUT FILE FOR INTEGRATED CHEMICAL EFFECTS TEST
(ICET) #1 AT 60 °C[140 °F] AT 148 HOURS, USING PHREEQC VERSION 2.8**

Input file: D:\My Modelling Files\2006_GSI-191\PHREEQC informed cases\app-ip-1a.pqi
Output file: D:\My Modelling Files\2006_GSI-191\PHREEQC informed cases\app-ip-1a.pqi
Database file: C:\Programs\USGS\Phreeqc_Interactive-2.8\gsi-191.dat

Reading data base.

LLNL_AQUEOUS_MODEL_PARAMETERS
NAMED_EXPRESSIONS
SOLUTION_MASTER_SPECIES
SOLUTION_SPECIES
PHASES
END

Reading input data for simulation 1.

DATABASE C:\Programs\USGS\Phreeqc_Interactive-2.8\gsi-191.dat
TITLE ICET #1 solution at 148h
SOLUTION 1
 units mol/kgw
 pH 7.0 charge
 temp 60
 pe 2.0
Al 4.12E-03
B 2.593E-01
Ca 2.193E-04
Cl 2.740E-03
Cu 5.459E-05
Fe 6.087E-06
Li 2.93E-05
Mg 2.404E-05
Na 2.202E-01
Si 4.492E-04
Zn 1.058E-04
EQUILIBRIUM_PHASES
 CO2(g) -3.48
SAVE solution 1
END

TITLE

ICET

Beginning of initial solution calculations.

Initial solution 1.

-----Solution composition-----

Elements	Molality	Moles
Al	4.120e-003	4.120e-003
B	2.593e-001	2.593e-001
Ca	2.193e-004	2.193e-004
Cl	2.740e-003	2.740e-003
Cu	5.459e-005	5.459e-005
Fe	6.087e-006	6.087e-006
Li	2.930e-005	2.930e-005

Mg	2.404e-005	2.404e-005
Na	2.202e-001	2.202e-001
Si	4.492e-004	4.492e-004
Zn	1.058e-004	1.058e-004

-----Description of solution-----

pH	=	9.470	Charge balance
pe	=	2.000	
Activity of water	=	0.992	
Ionic strength	=	1.998e-001	
Mass of water (kg)	=	1.000e+000	
Total alkalinity (eq/kg)	=	2.307e-001	
Total carbon (mol/kg)	=	0.000e+000	
Total CO2 (mol/kg)	=	0.000e+000	
Temperature (deg C)	=	60.000	
Electrical balance (eq)	=	1.388e-013	
Percent error, 100*(Cat- An)/(Cat+ An)	=	0.00	
Iterations	=	11	
Total H	=	1.112725e+002	
Total O	=	5.614144e+001	

-----Distribution of species-----

Species	Molality	Activity	Log Molality	Log Activity	Log Gamma
OH-	3.814e-004	2.690e-004	-3.419	-3.570	-0.152
H+	4.222e-010	3.390e-010	-9.374	-9.470	-0.095
H2O	5.553e+001	9.921e-001	1.744	-0.003	0.000
Al	4.120e-003				
AlO2-	3.994e-003	2.866e-003	-2.399	-2.543	-0.144
NaAlO2	1.253e-004	1.253e-004	-3.902	-3.902	0.000
HALO2	6.891e-007	6.891e-007	-6.162	-6.162	0.000
Al(OH)2+	3.118e-011	2.238e-011	-10.506	-10.650	-0.144
AlOH+2	1.585e-015	4.216e-016	-14.800	-15.375	-0.575
Al+3	1.227e-020	1.448e-021	-19.911	-20.839	-0.928
Al2(OH)2+4	5.006e-029	3.663e-031	-28.301	-30.436	-2.136
Al3(OH)4+5	4.753e-036	2.931e-039	-35.323	-38.533	-3.210
Al13O4(OH)24+7	0.000e+000	0.000e+000	-60.404	-66.704	-6.300
B(-5)	0.000e+000				
BH4-	0.000e+000	0.000e+000	-140.797	-140.942	-0.144
B(3)	2.593e-001				
BO2-	1.926e-001	1.382e-001	-0.715	-0.860	-0.144
B(OH)3	4.609e-002	4.609e-002	-1.336	-1.336	0.000
NaB(OH)4	2.048e-002	2.048e-002	-1.689	-1.689	0.000
CaB(OH)4+	1.511e-004	1.084e-004	-3.821	-3.965	-0.144
MgB(OH)4+	1.817e-005	1.304e-005	-4.741	-4.885	-0.144
B2O(OH)5-	1.803e-012	1.294e-012	-11.744	-11.888	-0.144
Ca	2.193e-004				
CaB(OH)4+	1.511e-004	1.084e-004	-3.821	-3.965	-0.144
Ca+2	6.817e-005	2.125e-005	-4.166	-4.673	-0.506
CaCl+	1.446e-008	1.038e-008	-7.840	-7.984	-0.144
CaOH+	1.224e-008	8.785e-009	-7.912	-8.056	-0.144
CaCl2	1.779e-011	1.779e-011	-10.750	-10.750	0.000
Cl(-1)	2.740e-003				
Cl-	2.677e-003	1.852e-003	-2.572	-2.732	-0.160
NaCl	6.075e-005	6.075e-005	-4.216	-4.216	0.000
CuCl2-	1.186e-006	8.512e-007	-5.926	-6.070	-0.144
Zn(OH)Cl	1.790e-007	1.790e-007	-6.747	-6.747	0.000
CuCl3-2	4.055e-008	1.013e-008	-7.392	-7.995	-0.603
ZnCl+	3.561e-008	2.555e-008	-7.448	-7.593	-0.144
CaCl+	1.446e-008	1.038e-008	-7.840	-7.984	-0.144
MgCl+	5.000e-009	3.588e-009	-8.301	-8.445	-0.144
LiCl	1.774e-009	1.774e-009	-8.751	-8.751	0.000

	CuCl+	1.591e-009	1.142e-009	-8.798	-8.943	-0.144
	ZnCl2	3.672e-011	3.672e-011	-10.435	-10.435	0.000
	CaCl2	1.779e-011	1.779e-011	-10.750	-10.750	0.000
	CuCl2	1.114e-012	1.114e-012	-11.953	-11.953	0.000
	HCl	1.378e-013	1.378e-013	-12.861	-12.861	0.000
	ZnCl3-	2.617e-014	1.878e-014	-13.582	-13.726	-0.144
	FeCl+	1.208e-014	8.667e-015	-13.918	-14.062	-0.144
	ZnCl4-2	8.029e-016	2.005e-016	-15.095	-15.698	-0.603
	FeCl2	1.089e-019	1.089e-019	-18.963	-18.963	0.000
	CuCl4-2	2.872e-022	7.170e-023	-21.542	-22.145	-0.603
	FeCl4-2	6.516e-024	1.627e-024	-23.186	-23.789	-0.603
	FeCl+2	7.565e-025	2.011e-025	-24.121	-24.697	-0.575
	FeCl2+	7.732e-026	5.548e-026	-25.112	-25.256	-0.144
	FeCl4-	3.189e-034	2.289e-034	-33.496	-33.640	-0.144
Cl (1)	6.938e-033					
	ClO-	6.876e-033	4.935e-033	-32.163	-32.307	-0.144
	HClO	6.203e-035	6.203e-035	-34.207	-34.207	0.000
Cl (3)	0.000e+000					
	ClO2-	0.000e+000	0.000e+000	-54.935	-55.079	-0.144
	HClO2	0.000e+000	0.000e+000	-61.379	-61.379	0.000
Cl (5)	0.000e+000					
	ClO3-	0.000e+000	0.000e+000	-65.293	-65.444	-0.152
Cl (7)	0.000e+000					
	ClO4-	0.000e+000	0.000e+000	-79.739	-79.890	-0.152
	ZnClO4+	0.000e+000	0.000e+000	-84.409	-84.553	-0.144
Cu (1)	6.445e-006					
	Cu+	5.218e-006	3.745e-006	-5.283	-5.427	-0.144
	CuCl2-	1.186e-006	8.512e-007	-5.926	-6.070	-0.144
	CuCl3-2	4.055e-008	1.013e-008	-7.392	-7.995	-0.603
Cu (2)	4.815e-005					
	CuOH+	4.740e-005	3.401e-005	-4.324	-4.468	-0.144
	Cu+2	7.228e-007	2.253e-007	-6.141	-6.647	-0.506
	CuO2-2	2.388e-008	5.963e-009	-7.622	-8.225	-0.603
	CuCl+	1.591e-009	1.142e-009	-8.798	-8.943	-0.144
	CuCl2	1.114e-012	1.114e-012	-11.953	-11.953	0.000
	CuCl4-2	2.872e-022	7.170e-023	-21.542	-22.145	-0.603
Fe (2)	2.254e-011					
	Fe+2	1.598e-011	4.982e-012	-10.796	-11.303	-0.506
	FeOH+	6.425e-012	4.611e-012	-11.192	-11.336	-0.144
	Fe(OH)2	1.072e-013	1.072e-013	-12.970	-12.970	0.000
	Fe(OH)3-	1.740e-014	1.249e-014	-13.759	-13.903	-0.144
	FeCl+	1.208e-014	8.667e-015	-13.918	-14.062	-0.144
	Fe(OH)4-2	1.464e-019	3.655e-020	-18.834	-19.437	-0.603
	FeCl2	1.089e-019	1.089e-019	-18.963	-18.963	0.000
	FeCl4-2	6.516e-024	1.627e-024	-23.186	-23.789	-0.603
Fe (3)	6.087e-006					
	Fe(OH)4-	3.079e-006	2.209e-006	-5.512	-5.656	-0.144
	Fe(OH)3	3.005e-006	3.005e-006	-5.522	-5.522	0.000
	Fe(OH)2+	3.059e-009	2.195e-009	-8.514	-8.658	-0.144
	FeOH+2	8.520e-015	2.265e-015	-14.070	-14.645	-0.575
	Fe+3	1.017e-021	1.199e-022	-20.993	-21.921	-0.928
	FeCl+2	7.565e-025	2.011e-025	-24.121	-24.697	-0.575
	FeCl2+	7.732e-026	5.548e-026	-25.112	-25.256	-0.144
	Fe2(OH)2+4	1.888e-026	1.381e-028	-25.724	-27.860	-2.136
	Fe3(OH)4+5	1.027e-031	6.336e-035	-30.988	-34.198	-3.210
	FeCl4-	3.189e-034	2.289e-034	-33.496	-33.640	-0.144
H (0)	8.530e-026					
	H2	4.265e-026	4.473e-026	-25.370	-25.349	0.021
Li	2.930e-005					
	Li+	2.930e-005	2.222e-005	-4.533	-4.653	-0.120
	LiCl	1.774e-009	1.774e-009	-8.751	-8.751	0.000
	LiOH	1.490e-009	1.490e-009	-8.827	-8.827	0.000
Mg	2.404e-005					
	MgB(OH)4+	1.817e-005	1.304e-005	-4.741	-4.885	-0.144
	Mg+2	5.863e-006	2.148e-006	-5.232	-5.668	-0.436

	MgCl+	5.000e-009	3.588e-009	-8.301	-8.445	-0.144
	Mg4 (OH) 4+4	3.795e-023	2.777e-025	-22.421	-24.556	-2.136
Na	2.202e-001					
	Na+	1.993e-001	1.430e-001	-0.701	-0.845	-0.144
	NaB (OH) 4	2.048e-002	2.048e-002	-1.689	-1.689	0.000
	NaHSiO3	2.745e-004	2.745e-004	-3.561	-3.561	0.000
	NaAlO2	1.253e-004	1.253e-004	-3.902	-3.902	0.000
	NaCl	6.075e-005	6.075e-005	-4.216	-4.216	0.000
	NaOH	6.743e-006	6.743e-006	-5.171	-5.171	0.000
O(0)	1.085e-031					
	O2	5.423e-032	5.688e-032	-31.266	-31.245	0.021
Si	4.492e-004					
	NaHSiO3	2.745e-004	2.745e-004	-3.561	-3.561	0.000
	HSiO3-	1.010e-004	7.247e-005	-3.996	-4.140	-0.144
	SiO2	7.367e-005	7.367e-005	-4.133	-4.133	0.000
	H2SiO4-2	2.771e-008	6.919e-009	-7.557	-8.160	-0.603
	H6 (H2SiO4) 4-2	2.207e-011	5.511e-012	-10.656	-11.259	-0.603
	H4 (H2SiO4) 4-4	6.570e-013	2.404e-015	-12.182	-14.619	-2.437
Zn	1.058e-004					
	ZnOH+	5.507e-005	3.952e-005	-4.259	-4.403	-0.144
	Zn(OH) 2	4.624e-005	4.624e-005	-4.335	-4.335	0.000
	Zn+2	3.687e-006	1.149e-006	-5.433	-5.940	-0.506
	Zn(OH) 3-	5.845e-007	4.195e-007	-6.233	-6.377	-0.144
	Zn(OH) Cl	1.790e-007	1.790e-007	-6.747	-6.747	0.000
	ZnCl+	3.561e-008	2.555e-008	-7.448	-7.593	-0.144
	Zn(OH) 4-2	8.382e-010	2.093e-010	-9.077	-9.679	-0.603
	ZnCl2	3.672e-011	3.672e-011	-10.435	-10.435	0.000
	ZnCl3-	2.617e-014	1.878e-014	-13.582	-13.726	-0.144
	ZnCl4-2	8.029e-016	2.005e-016	-15.095	-15.698	-0.603
	ZnClO4+	0.000e+000	0.000e+000	-84.409	-84.553	-0.144

-----Saturation indices-----

Phase	SI	log IAP	log KT	
B2O3	-7.82	-2.66	5.16	B2O3
Boehmite	2.10	7.56	5.46	AlO(OH)
Borax	-1.65	11.89	13.54	Na2 (B4O5 (OH) 4) : 8H2O
Boric_acid	-1.54	-1.34	0.21	B(OH) 3
Brucite	-0.99	13.26	14.26	Mg(OH) 2
Cuprite	9.43	1.64	-7.79	Cu2O
Diaspore	2.45	7.56	5.11	AlO(OH)
Fe(OH) 3	2.38	19.10	16.72	Fe(OH) 3
Gibbsite	1.74	7.56	5.82	Al(OH) 3
Hydroboracite	-0.84	19.52	20.36	MgCaB6O11:6H2O
SiO2(am)	-1.73	-4.13	-2.41	SiO2
Tenorite	5.81	12.29	6.48	CuO
Tobermorite-14A	-12.75	46.49	59.24	Ca5Si6H21O27.5
Xonotlite	-21.73	60.78	82.51	Ca6Si6O17(OH) 2
Zn(OH) 2 (gamma)	1.11	12.99	11.88	Zn(OH) 2

Beginning of batch-reaction calculations.

Reaction step 1.

Using solution 1.

Using pure phase assemblage 1.

-----Phase assemblage-----

Phase	SI	log IAP	log KT	Moles in assemblage		
				Initial	Final	Delta
CO2(g)	-3.48	-11.54	-8.06	1.000e+001	9.988e+000	-1.236e-002

-----Solution composition-----

Elements	Molality	Moles
Al	4.122e-003	4.120e-003
B	2.594e-001	2.593e-001
C	1.236e-002	1.236e-002
Ca	2.194e-004	2.193e-004
Cl	2.741e-003	2.740e-003
Cu	5.461e-005	5.459e-005
Fe	6.090e-006	6.087e-006
Li	2.931e-005	2.930e-005
Mg	2.405e-005	2.404e-005
Na	2.203e-001	2.202e-001
Si	4.494e-004	4.492e-004
Zn	1.058e-004	1.058e-004

-----Description of solution-----

equilibrium

pH = 9.308 Charge balance
 pe = -0.057 Adjusted to redox

Activity of water = 0.992
 Ionic strength = 2.037e-001
 Mass of water (kg) = 9.996e-001
 Total alkalinity (eq/kg) = 2.308e-001
 Total CO2 (mol/kg) = 1.236e-002
 Temperature (deg C) = 60.000
 Electrical balance (eq) = 1.387e-013
 Percent error, 100*(Cat-|An|)/(Cat+|An|) = 0.00
 Iterations = 14
 Total H = 1.112725e+002
 Total O = 5.616615e+001

-----Distribution of species-----

Species	Molality	Activity	Log Molality	Log Activity	Log Gamma
OH-	2.634e-004	1.854e-004	-3.579	-3.732	-0.152
H+	6.129e-010	4.918e-010	-9.213	-9.308	-0.096
H2O	5.553e+001	9.918e-001	1.744	-0.004	0.000
Al	4.122e-003				
AlO2-	3.995e-003	2.862e-003	-2.398	-2.543	-0.145
NaAlO2	1.254e-004	1.254e-004	-3.902	-3.902	0.000
HA1O2	9.983e-007	9.983e-007	-6.001	-6.001	0.000
Al(OH)2+	6.565e-011	4.703e-011	-10.183	-10.328	-0.145
AlOH+2	4.871e-015	1.286e-015	-14.312	-14.891	-0.579
Al+3	5.478e-020	6.406e-021	-19.261	-20.193	-0.932
Al2(OH)2+4	4.779e-028	3.407e-030	-27.321	-29.468	-2.147
Al3(OH)4+5	9.647e-035	5.731e-038	-34.016	-37.242	-3.226
Al13O4(OH)24+7	0.000e+000	0.000e+000	-57.148	-63.480	-6.332
B(-5)	0.000e+000				
BH4-	0.000e+000	0.000e+000	-123.081	-123.226	-0.145
B(3)	2.594e-001				
BO2-	1.785e-001	1.279e-001	-0.748	-0.893	-0.145
B(OH)3	6.185e-002	6.185e-002	-1.209	-1.209	0.000
NaB(OH)4	1.898e-002	1.898e-002	-1.722	-1.722	0.000

	CaB(OH) 4+	1.019e-004	7.300e-005	-3.992	-4.137	-0.145
	MgB(OH) 4+	1.553e-005	1.112e-005	-4.809	-4.954	-0.145
	B2O(OH) 5-	2.242e-012	1.606e-012	-11.649	-11.794	-0.145
C(-2)	0.000e+000					
	C2H4	0.000e+000	0.000e+000	-128.882	-128.882	0.000
C(-3)	0.000e+000					
	C2H6	0.000e+000	0.000e+000	-85.563	-85.563	0.000
C(-4)	0.000e+000					
	CH4	0.000e+000	0.000e+000	-59.334	-59.334	0.000
C(2)	1.144e-028					
	CO	1.144e-028	1.144e-028	-27.941	-27.941	0.000
C(4)	1.236e-002					
	HCO3-	8.117e-003	5.815e-003	-2.091	-2.235	-0.145
	CO3-2	3.239e-003	8.549e-004	-2.490	-3.068	-0.579
	NaHCO3	6.401e-004	6.401e-004	-3.194	-3.194	0.000
	NaCO3-	1.978e-004	1.417e-004	-3.704	-3.849	-0.145
	CaCO3	6.572e-005	6.572e-005	-4.182	-4.182	0.000
	Cu(CO3) 2-2	3.683e-005	9.121e-006	-4.434	-5.040	-0.606
	CuCO3	9.761e-006	9.761e-006	-5.011	-5.011	0.000
	ZnCO3	7.711e-006	7.711e-006	-5.113	-5.113	0.000
	CO2	5.185e-006	5.444e-006	-5.285	-5.264	0.021
	MgCO3	2.852e-006	2.852e-006	-5.545	-5.545	0.000
	CaHCO3+	1.856e-006	1.329e-006	-5.732	-5.876	-0.145
	CuCO3(OH) 2-2	1.363e-006	3.376e-007	-5.866	-6.472	-0.606
	ZnHCO3+	6.172e-007	4.422e-007	-6.210	-6.354	-0.145
	MgHCO3+	2.397e-007	1.718e-007	-6.620	-6.765	-0.145
	FeCO3	6.054e-008	6.054e-008	-7.218	-7.218	0.000
	FeHCO3+	8.658e-009	6.203e-009	-8.063	-8.207	-0.145
	FeCO3+	2.778e-016	1.990e-016	-15.556	-15.701	-0.145
Ca	2.194e-004					
	CaB(OH) 4+	1.019e-004	7.300e-005	-3.992	-4.137	-0.145
	CaCO3	6.572e-005	6.572e-005	-4.182	-4.182	0.000
	Ca+2	4.991e-005	1.547e-005	-4.302	-4.811	-0.509
	CaHCO3+	1.856e-006	1.329e-006	-5.732	-5.876	-0.145
	CaCl+	1.053e-008	7.540e-009	-7.978	-8.123	-0.145
	CaOH+	6.152e-009	4.407e-009	-8.211	-8.356	-0.145
	CaCl2	1.291e-011	1.291e-011	-10.889	-10.889	0.000
Cl(-1)	2.741e-003					
	Cl-	2.678e-003	1.849e-003	-2.572	-2.733	-0.161
	NaCl	6.077e-005	6.077e-005	-4.216	-4.216	0.000
	CuCl2-	1.169e-006	8.374e-007	-5.932	-6.077	-0.145
	Zn(OH) Cl	1.875e-007	1.875e-007	-6.727	-6.727	0.000
	ZnCl+	5.423e-008	3.885e-008	-7.266	-7.411	-0.145
	CuCl3-2	4.015e-008	9.944e-009	-7.396	-8.002	-0.606
	CaCl+	1.053e-008	7.540e-009	-7.978	-8.123	-0.145
	MgCl+	4.611e-009	3.303e-009	-8.336	-8.481	-0.145
	LiCl	1.770e-009	1.770e-009	-8.752	-8.752	0.000
	ZnCl2	5.573e-011	5.573e-011	-10.254	-10.254	0.000
	CuCl+	1.377e-011	9.866e-012	-10.861	-11.006	-0.145
	CaCl2	1.291e-011	1.291e-011	-10.889	-10.889	0.000
	FeCl+	4.927e-012	3.530e-012	-11.307	-11.452	-0.145
	HCl	1.996e-013	1.996e-013	-12.700	-12.700	0.000
	ZnCl3-	3.971e-014	2.845e-014	-13.401	-13.546	-0.145
	CuCl2	9.607e-015	9.607e-015	-14.017	-14.017	0.000
	ZnCl4-2	1.224e-015	3.032e-016	-14.912	-15.518	-0.606
	FeCl2	4.427e-017	4.427e-017	-16.354	-16.354	0.000
	FeCl4-2	2.661e-021	6.591e-022	-20.575	-21.181	-0.606
	FeCl+2	2.721e-024	7.183e-025	-23.565	-24.144	-0.579
	CuCl4-2	2.489e-024	6.164e-025	-23.604	-24.210	-0.606
	FeCl2+	2.761e-025	1.978e-025	-24.559	-24.704	-0.145
	FeCl4-	1.135e-033	8.130e-034	-32.945	-33.090	-0.145
Cl(1)	2.544e-037					
	ClO-	2.512e-037	1.799e-037	-36.600	-36.745	-0.145
	HClO	3.282e-039	3.282e-039	-38.484	-38.484	0.000

Cl (3)	0.000e+000					
ClO2-	0.000e+000	0.000e+000	-63.810	-63.955	-0.145	
HClO2	0.000e+000	0.000e+000	-70.093	-70.093	0.000	
Cl (5)	0.000e+000					
ClO3-	0.000e+000	0.000e+000	-78.605	-78.757	-0.152	
Cl (7)	0.000e+000					
ClO4-	0.000e+000	0.000e+000	-97.488	-97.641	-0.152	
ZnClO4+	0.000e+000	0.000e+000	-101.976	-102.121	-0.145	
Cu (1)	6.370e-006					
Cu+	5.161e-006	3.697e-006	-5.287	-5.432	-0.145	
CuCl2-	1.169e-006	8.374e-007	-5.932	-6.077	-0.145	
CuCl3-2	4.015e-008	9.944e-009	-7.396	-8.002	-0.606	
Cu (2)	4.824e-005					
Cu (CO3) 2-2	3.683e-005	9.121e-006	-4.434	-5.040	-0.606	
CuCO3	9.761e-006	9.761e-006	-5.011	-5.011	0.000	
CuCO3 (OH) 2-2	1.363e-006	3.376e-007	-5.866	-6.472	-0.606	
CuOH+	2.833e-007	2.029e-007	-6.548	-6.693	-0.145	
Cu+2	6.294e-009	1.951e-009	-8.201	-8.710	-0.509	
CuO2-2	4.704e-011	1.165e-011	-10.328	-10.934	-0.606	
CuCl+	1.377e-011	9.866e-012	-10.861	-11.006	-0.145	
CuCl2	9.607e-015	9.607e-015	-14.017	-14.017	0.000	
CuCl4-2	2.489e-024	6.164e-025	-23.604	-24.210	-0.606	
Fe (2)	7.759e-008					
FeCO3	6.054e-008	6.054e-008	-7.218	-7.218	0.000	
FeHCO3+	8.658e-009	6.203e-009	-8.063	-8.207	-0.145	
Fe+2	6.557e-009	2.033e-009	-8.183	-8.692	-0.509	
FeOH+	1.810e-009	1.296e-009	-8.742	-8.887	-0.145	
Fe (OH) 2	2.077e-011	2.077e-011	-10.683	-10.683	0.000	
FeCl+	4.927e-012	3.530e-012	-11.307	-11.452	-0.145	
Fe (OH) 3-	2.328e-012	1.668e-012	-11.633	-11.778	-0.145	
FeCl2	4.427e-017	4.427e-017	-16.354	-16.354	0.000	
Fe (OH) 4-2	1.358e-017	3.363e-018	-16.867	-17.473	-0.606	
FeCl4-2	2.661e-021	6.591e-022	-20.575	-21.181	-0.606	
Fe (3)	6.012e-006					
Fe (OH) 3	3.519e-006	3.519e-006	-5.454	-5.454	0.000	
Fe (OH) 4-	2.488e-006	1.783e-006	-5.604	-5.749	-0.145	
Fe (OH) 2+	5.206e-009	3.730e-009	-8.283	-8.428	-0.145	
FeOH+2	2.116e-014	5.585e-015	-13.674	-14.253	-0.579	
FeCO3+	2.778e-016	1.990e-016	-15.556	-15.701	-0.145	
Fe+3	3.668e-021	4.289e-022	-20.436	-21.368	-0.932	
FeCl+2	2.721e-024	7.183e-025	-23.565	-24.144	-0.579	
FeCl2+	2.761e-025	1.978e-025	-24.559	-24.704	-0.145	
Fe2 (OH) 2+4	1.178e-025	8.395e-028	-24.929	-27.076	-2.147	
Fe3 (OH) 4+5	1.101e-030	6.542e-034	-29.958	-33.184	-3.226	
FeCl4-	1.135e-033	8.130e-034	-32.945	-33.090	-0.145	
H (0)	2.333e-021					
H2	1.166e-021	1.224e-021	-20.933	-20.912	0.021	
Li	2.931e-005					
Li+	2.931e-005	2.221e-005	-4.533	-4.653	-0.120	
LiCl	1.770e-009	1.770e-009	-8.752	-8.752	0.000	
LiOH	1.026e-009	1.026e-009	-8.989	-8.989	0.000	
Mg	2.405e-005					
MgB (OH) 4+	1.553e-005	1.112e-005	-4.809	-4.954	-0.145	
Mg+2	5.429e-006	1.981e-006	-5.265	-5.703	-0.438	
MgCO3	2.852e-006	2.852e-006	-5.545	-5.545	0.000	
MgHCO3+	2.397e-007	1.718e-007	-6.620	-6.765	-0.145	
MgCl+	4.611e-009	3.303e-009	-8.336	-8.481	-0.145	
Mg4 (OH) 4+4	6.354e-024	4.530e-026	-23.197	-25.344	-2.147	
Na	2.203e-001					
Na+	2.000e-001	1.433e-001	-0.699	-0.844	-0.145	
NaB (OH) 4	1.898e-002	1.898e-002	-1.722	-1.722	0.000	
NaHCO3	6.401e-004	6.401e-004	-3.194	-3.194	0.000	
NaHSiO3	2.559e-004	2.559e-004	-3.592	-3.592	0.000	
NaCO3-	1.978e-004	1.417e-004	-3.704	-3.849	-0.145	
NaAlO2	1.254e-004	1.254e-004	-3.902	-3.902	0.000	

	NaCl	6.077e-005	6.077e-005	-4.216	-4.216	0.000
	NaOH	4.657e-006	4.657e-006	-5.332	-5.332	0.000
O(0)	0.000e+000					
	O2	0.000e+000	0.000e+000	-40.141	-40.120	0.021
Si	4.494e-004					
	NaHSiO3	2.559e-004	2.559e-004	-3.592	-3.592	0.000
	SiO2	9.943e-005	9.943e-005	-4.002	-4.002	0.000
	HSiO3-	9.409e-005	6.740e-005	-4.026	-4.171	-0.145
	H2SiO4-2	1.791e-008	4.435e-009	-7.747	-8.353	-0.606
	H6 (H2SiO4) 4-2	3.501e-011	8.670e-012	-10.456	-11.062	-0.606
	H4 (H2SiO4) 4-4	5.080e-013	1.797e-015	-12.294	-14.745	-2.451
Zn	1.058e-004					
	ZnOH+	5.790e-005	4.148e-005	-4.237	-4.382	-0.145
	Zn(OH)2	3.344e-005	3.344e-005	-4.476	-4.476	0.000
	ZnCO3	7.711e-006	7.711e-006	-5.113	-5.113	0.000
	Zn+2	5.647e-006	1.750e-006	-5.248	-5.757	-0.509
	ZnHCO3+	6.172e-007	4.422e-007	-6.210	-6.354	-0.145
	Zn(OH)3-	2.918e-007	2.091e-007	-6.535	-6.680	-0.145
	Zn(OH)Cl	1.875e-007	1.875e-007	-6.727	-6.727	0.000
	ZnCl+	5.423e-008	3.885e-008	-7.266	-7.411	-0.145
	Zn(OH)4-2	2.903e-010	7.188e-011	-9.537	-10.143	-0.606
	ZnCl2	5.573e-011	5.573e-011	-10.254	-10.254	0.000
	ZnCl3-	3.971e-014	2.845e-014	-13.401	-13.546	-0.145
	ZnCl4-2	1.224e-015	3.032e-016	-14.912	-15.518	-0.606
	ZnClO4+	0.000e+000	0.000e+000	-101.976	-102.121	-0.145

-----Saturation indices-----

Phase	SI	log IAP	log KT	
Artinite	-2.99	14.27	17.26	Mg2CO3(OH)2:3H2O
Azurite	-0.22	6.63	6.85	Cu3(CO3)2(OH)2
B2O3	-7.57	-2.41	5.16	B2O3
Boehmite	2.26	7.72	5.46	AlO(OH)
Borax	-1.46	12.08	13.54	Na2(B4O5(OH)4):8H2O
Boric_acid	-1.42	-1.21	0.21	B(OH)3
Brucite	-1.35	12.91	14.26	Mg(OH)2
Calcite	0.94	2.26	1.32	CaCO3
CO2(g)	-3.48	-11.54	-8.06	CO2
Cuprite	9.09	1.31	-7.79	Cu2O
Diaspore	2.61	7.72	5.11	AlO(OH)
Fe(OH)3	2.45	19.17	16.72	Fe(OH)3
Gibbsite	1.90	7.72	5.82	Al(OH)3
Huntite	-0.60	6.37	6.97	CaMg3(CO3)4
Hydroboracite	-0.89	19.47	20.36	MgCaB6O11:6H2O
Lansfordite	-3.49	1.35	4.84	MgCO3:5H2O
Magnesite	-0.06	1.37	1.43	MgCO3
Malachite	3.76	8.26	4.50	Cu2CO3(OH)2
Monohydrocalcit	-0.05	2.26	2.31	CaCO3:H2O
Nesquehonite	-3.36	1.36	4.72	MgCO3:3H2O
Siderite	-0.78	-1.62	-0.84	FeCO3
SiO2(am)	-1.60	-4.00	-2.41	SiO2
Smithsonite	1.46	1.32	-0.14	ZnCO3
Tenorite	3.43	9.90	6.48	CuO
Tobermorite-14A	-14.28	44.96	59.24	Ca5Si6H21O27.5
Xonotlite	-23.72	58.80	82.51	Ca6Si6O17(OH)2
Zn(OH)2(gamma)	0.97	12.85	11.88	Zn(OH)2
ZnCO3:H2O	1.17	1.31	0.14	ZnCO3:H2O

End of simulation.

 Reading input data for simulation 2.

```

USE solution 1
EQUILIBRIUM PHASES
      CO2(g)      -3.48
B2O3           0      0
Borax          0      0
Boric_acid     0      0
Brucite        0      0
Cuprite        0      0
Fe(OH)3        0      0
Hydroboracite  0      0
SiO2(am)       0      0
Tenorite       0      0
Tobermorite-14A 0      0
Xonotlite     0      0
Zn(OH)2(gamma) 0      0
Artinite       0      0
Azurite        0      0
Huntite        0      0
Lansfordite    0      0
Magnesite      0      0
Malachite      0      0
Monohydrocalcit 0      0
Nesquehonite  0      0
Siderite       0      0
Smithsonite    0      0
ZnCO3:H2O     0      0
END
  
```

 Beginning of batch-reaction calculations.

Reaction step 1.

Using solution 1. Solution after simulation 1.
 Using pure phase assemblage 1. PHASES

-----Phase assemblage-----

Phase	SI	log IAP	log KT	Moles in assemblage		
				Initial	Final	Delta
Artinite	-2.99	14.27	17.26	0.000e+000		0.000e+000
Azurite	-10.51	-3.66	6.85	0.000e+000		0.000e+000
B2O3	-7.57	-2.41	5.16	0.000e+000		0.000e+000
Borax	-1.46	12.08	13.54	0.000e+000		0.000e+000
Boric_acid	-1.42	-1.21	0.21	0.000e+000		0.000e+000
Brucite	-1.35	12.91	14.26	0.000e+000		0.000e+000
CO2(g)	-3.48	-11.54	-8.06	1.000e+001	1.000e+001	-1.019e-005
Cuprite	0.00	-7.79	-7.79	0.000e+000	3.222e-006	3.222e-006
Fe(OH)3	0.00	16.72	16.72	0.000e+000	6.066e-006	6.066e-006
Huntite	-0.60	6.37	6.97	0.000e+000		0.000e+000
Hydroboracite	-0.89	19.47	20.36	0.000e+000		0.000e+000
Lansfordite	-3.49	1.35	4.84	0.000e+000		0.000e+000
Magnesite	-0.06	1.37	1.43	0.000e+000		0.000e+000
Malachite	-3.09	1.41	4.50	0.000e+000		0.000e+000
Monohydrocalcit	-0.05	2.26	2.31	0.000e+000		0.000e+000
Nesquehonite	-3.36	1.36	4.72	0.000e+000		0.000e+000
Siderite	-4.34	-5.19	-0.84	0.000e+000		0.000e+000
SiO2(am)	-1.60	-4.00	-2.41	0.000e+000		0.000e+000
Smithsonite	0.00	-0.14	-0.14	0.000e+000	1.021e-004	1.021e-004
Tenorite	0.00	6.48	6.48	0.000e+000	4.813e-005	4.813e-005

Tobermorite-14A	-14.28	44.96	59.24	0.000e+000	0.000e+000
Xonotlite	-23.72	58.80	82.51	0.000e+000	0.000e+000
Zn(OH)2 (gamma)	-0.49	11.39	11.88	0.000e+000	0.000e+000
ZnCO3:H2O	-0.29	-0.15	0.14	0.000e+000	0.000e+000

-----Solution composition-----

Elements	Molality	Moles
Al	4.122e-003	4.120e-003
B	2.594e-001	2.593e-001
C	1.227e-002	1.227e-002
Ca	2.194e-004	2.193e-004
Cl	2.741e-003	2.740e-003
Cu	1.819e-008	1.818e-008
Fe	2.146e-008	2.145e-008
Li	2.931e-005	2.930e-005
Mg	2.405e-005	2.404e-005
Na	2.203e-001	2.202e-001
Si	4.494e-004	4.492e-004
Zn	3.665e-006	3.663e-006

-----Description of solution-----

	pH =	9.308	Charge balance
	pe =	1.061	Adjusted to redox
equilibrium	Activity of water =	0.992	
	Ionic strength =	2.036e-001	
	Mass of water (kg) =	9.996e-001	
	Total alkalinity (eq/kg) =	2.304e-001	
	Total CO2 (mol/kg) =	1.227e-002	
	Temperature (deg C) =	60.000	
	Electrical balance (eq) =	1.392e-013	
	Percent error, 100*(Cat- An)/(Cat+ An) =	0.00	
	Iterations =	5	
	Total H =	1.112725e+002	
	Total O =	5.616580e+001	

-----Distribution of species-----

Species	Molality	Activity	Log Molality	Log Activity	Log Gamma
OH-	2.634e-004	1.854e-004	-3.579	-3.732	-0.152
H+	6.128e-010	4.917e-010	-9.213	-9.308	-0.096
H2O	5.553e+001	9.919e-001	1.744	-0.004	0.000
Al	4.122e-003				
AlO2-	3.995e-003	2.862e-003	-2.398	-2.543	-0.145
NaAlO2	1.254e-004	1.254e-004	-3.902	-3.902	0.000
HALO2	9.982e-007	9.982e-007	-6.001	-6.001	0.000
Al(OH)2+	6.564e-011	4.703e-011	-10.183	-10.328	-0.145
AlOH+2	4.869e-015	1.285e-015	-14.313	-14.891	-0.578
Al+3	5.475e-020	6.403e-021	-19.262	-20.194	-0.932
Al2(OH)2+4	4.772e-028	3.405e-030	-27.321	-29.468	-2.147
Al3(OH)4+5	9.628e-035	5.726e-038	-34.016	-37.242	-3.226
Al13O4(OH)24+7	0.000e+000	0.000e+000	-57.150	-63.481	-6.331
B(-5)	0.000e+000				
BH4-	0.000e+000	0.000e+000	-132.027	-132.172	-0.145
B(3)	2.594e-001				
BO2-	1.785e-001	1.279e-001	-0.748	-0.893	-0.145
B(OH)3	6.185e-002	6.185e-002	-1.209	-1.209	0.000
NaB(OH)4	1.898e-002	1.898e-002	-1.722	-1.722	0.000
CaB(OH)4+	1.019e-004	7.300e-005	-3.992	-4.137	-0.145
MgB(OH)4+	1.553e-005	1.112e-005	-4.809	-4.954	-0.145

	B2O(OH) 5-	2.242e-012	1.606e-012	-11.649	-11.794	-0.145
C(-2)	0.000e+000					
	C2H4	0.000e+000	0.000e+000	-142.300	-142.300	0.000
C(-3)	0.000e+000					
	C2H6	0.000e+000	0.000e+000	-101.218	-101.218	0.000
C(-4)	0.000e+000					
	CH4	0.000e+000	0.000e+000	-68.280	-68.280	0.000
C(2)	6.639e-031					
	CO	6.639e-031	6.639e-031	-30.178	-30.178	0.000
C(4)	1.227e-002					
	HCO3-	8.117e-003	5.816e-003	-2.091	-2.235	-0.145
	CO3-2	3.239e-003	8.551e-004	-2.490	-3.068	-0.578
	NaHCO3	6.402e-004	6.402e-004	-3.194	-3.194	0.000
	NaCO3-	1.979e-004	1.418e-004	-3.704	-3.848	-0.145
	CaCO3	6.573e-005	6.573e-005	-4.182	-4.182	0.000
	CO2	5.185e-006	5.444e-006	-5.285	-5.264	0.021
	MgCO3	2.852e-006	2.852e-006	-5.545	-5.545	0.000
	CaHCO3+	1.856e-006	1.329e-006	-5.732	-5.876	-0.145
	ZnCO3	2.670e-007	2.670e-007	-6.574	-6.574	0.000
	MgHCO3+	2.398e-007	1.718e-007	-6.620	-6.765	-0.145
	ZnHCO3+	2.137e-008	1.531e-008	-7.670	-7.815	-0.145
	Cu(CO3)2-2	1.375e-008	3.405e-009	-7.862	-8.468	-0.606
	CuCO3	3.643e-009	3.643e-009	-8.439	-8.439	0.000
	CuCO3(OH)2-2	5.087e-010	1.260e-010	-9.294	-9.900	-0.606
	FeCO3	1.644e-011	1.644e-011	-10.784	-10.784	0.000
	FeHCO3+	2.351e-012	1.684e-012	-11.629	-11.774	-0.145
	FeCO3+	9.901e-019	7.094e-019	-18.004	-18.149	-0.145
Ca	2.194e-004					
	CaB(OH)4+	1.019e-004	7.300e-005	-3.992	-4.137	-0.145
	CaCO3	6.573e-005	6.573e-005	-4.182	-4.182	0.000
	Ca+2	4.990e-005	1.547e-005	-4.302	-4.811	-0.509
	CaHCO3+	1.856e-006	1.329e-006	-5.732	-5.876	-0.145
	CaCl+	1.054e-008	7.548e-009	-7.977	-8.122	-0.145
	CaOH+	6.152e-009	4.408e-009	-8.211	-8.356	-0.145
	CaCl2	1.293e-011	1.293e-011	-10.888	-10.888	0.000
Cl(-1)	2.741e-003					
	Cl-	2.680e-003	1.851e-003	-2.572	-2.733	-0.161
	NaCl	6.084e-005	6.084e-005	-4.216	-4.216	0.000
	CaCl+	1.054e-008	7.548e-009	-7.977	-8.122	-0.145
	Zn(OH)Cl	6.499e-009	6.499e-009	-8.187	-8.187	0.000
	MgCl+	4.616e-009	3.307e-009	-8.336	-8.481	-0.145
	ZnCl+	1.879e-009	1.346e-009	-8.726	-8.871	-0.145
	LiCl	1.772e-009	1.772e-009	-8.752	-8.752	0.000
	CuCl2-	3.329e-011	2.385e-011	-10.478	-10.622	-0.145
	CaCl2	1.293e-011	1.293e-011	-10.888	-10.888	0.000
	ZnCl2	1.933e-012	1.933e-012	-11.714	-11.714	0.000
	CuCl3-2	1.145e-012	2.836e-013	-11.941	-12.547	-0.606
	HCl	1.997e-013	1.997e-013	-12.700	-12.700	0.000
	CuCl+	5.143e-015	3.685e-015	-14.289	-14.434	-0.145
	ZnCl3-	1.379e-015	9.880e-016	-14.860	-15.005	-0.145
	FeCl+	1.339e-015	9.593e-016	-14.873	-15.018	-0.145
	ZnCl4-2	4.254e-017	1.054e-017	-16.371	-16.977	-0.606
	CuCl2	3.592e-018	3.592e-018	-17.445	-17.445	0.000
	FeCl2	1.204e-020	1.204e-020	-19.919	-19.919	0.000
	FeCl4-2	7.254e-025	1.797e-025	-24.139	-24.745	-0.606
	FeCl+2	9.707e-027	2.563e-027	-26.013	-26.591	-0.578
	FeCl2+	9.860e-028	7.064e-028	-27.006	-27.151	-0.145
	CuCl4-2	9.323e-028	2.309e-028	-27.030	-27.636	-0.606
	FeCl4-	4.061e-036	2.910e-036	-35.391	-35.536	-0.145
Cl(1)	4.389e-035					
	ClO-	4.333e-035	3.104e-035	-34.363	-34.508	-0.145
	HClO	5.661e-037	5.661e-037	-36.247	-36.247	0.000
Cl(3)	0.000e+000					
	ClO2-	0.000e+000	0.000e+000	-59.337	-59.481	-0.145
	HClO2	0.000e+000	0.000e+000	-65.620	-65.620	0.000

Cl (5)	0.000e+000					
ClO3-	0.000e+000	0.000e+000	0.000e+000	-71.895	-72.047	-0.152
Cl (7)	0.000e+000					
ClO4-	0.000e+000	0.000e+000	0.000e+000	-88.542	-88.695	-0.152
ZnClO4+	0.000e+000	0.000e+000	0.000e+000	-94.491	-94.636	-0.145
Cu (1)	1.811e-010					
Cu+	1.467e-010	1.051e-010		-9.834	-9.978	-0.145
CuCl2-	3.329e-011	2.385e-011		-10.478	-10.622	-0.145
CuCl3-2	1.145e-012	2.836e-013		-11.941	-12.547	-0.606
Cu (2)	1.800e-008					
Cu(CO3)2-2	1.375e-008	3.405e-009		-7.862	-8.468	-0.606
CuCO3	3.643e-009	3.643e-009		-8.439	-8.439	0.000
CuCO3(OH)2-2	5.087e-010	1.260e-010		-9.294	-9.900	-0.606
CuOH+	1.057e-010	7.573e-011		-9.976	-10.121	-0.145
Cu+2	2.348e-012	7.278e-013		-11.629	-12.138	-0.509
CuO2-2	1.756e-014	4.349e-015		-13.756	-14.362	-0.606
CuCl+	5.143e-015	3.685e-015		-14.289	-14.434	-0.145
CuCl2	3.592e-018	3.592e-018		-17.445	-17.445	0.000
CuCl4-2	9.323e-028	2.309e-028		-27.030	-27.636	-0.606
Fe (2)	2.107e-011					
FeCO3	1.644e-011	1.644e-011		-10.784	-10.784	0.000
FeHCO3+	2.351e-012	1.684e-012		-11.629	-11.774	-0.145
Fe+2	1.780e-012	5.518e-013		-11.750	-12.258	-0.509
FeOH+	4.913e-013	3.520e-013		-12.309	-12.453	-0.145
Fe(OH)2	5.640e-015	5.640e-015		-14.249	-14.249	0.000
FeCl+	1.339e-015	9.593e-016		-14.873	-15.018	-0.145
Fe(OH)3-	6.322e-016	4.529e-016		-15.199	-15.344	-0.145
FeCl2	1.204e-020	1.204e-020		-19.919	-19.919	0.000
Fe(OH)4-2	3.688e-021	9.136e-022		-20.433	-21.039	-0.606
FeCl4-2	7.254e-025	1.797e-025		-24.139	-24.745	-0.606
Fe (3)	2.143e-008					
Fe(OH)3	1.254e-008	1.254e-008		-7.902	-7.902	0.000
Fe(OH)4-	8.872e-009	6.356e-009		-8.052	-8.197	-0.145
Fe(OH)2+	1.856e-011	1.330e-011		-10.731	-10.876	-0.145
FeOH+2	7.540e-017	1.991e-017		-16.123	-16.701	-0.578
FeCO3+	9.901e-019	7.094e-019		-18.004	-18.149	-0.145
Fe+3	1.307e-023	1.528e-024		-22.884	-23.816	-0.932
FeCl+2	9.707e-027	2.563e-027		-26.013	-26.591	-0.578
FeCl2+	9.860e-028	7.064e-028		-27.006	-27.151	-0.145
Fe2(OH)2+4	1.495e-030	1.067e-032		-29.825	-31.972	-2.147
FeCl4-	4.061e-036	2.910e-036		-35.391	-35.536	-0.145
Fe3(OH)4+5	4.981e-038	0.000e+000		-37.303	-40.528	-3.226
H (0)	1.353e-023					
H2	6.767e-024	7.105e-024		-23.170	-23.148	0.021
Li	2.931e-005					
Li+	2.931e-005	2.221e-005		-4.533	-4.653	-0.120
LiCl	1.772e-009	1.772e-009		-8.752	-8.752	0.000
LiOH	1.026e-009	1.026e-009		-8.989	-8.989	0.000
Mg	2.405e-005					
MgB(OH)4+	1.553e-005	1.112e-005		-4.809	-4.954	-0.145
Mg+2	5.429e-006	1.981e-006		-5.265	-5.703	-0.438
MgCO3	2.852e-006	2.852e-006		-5.545	-5.545	0.000
MgHCO3+	2.398e-007	1.718e-007		-6.620	-6.765	-0.145
MgCl+	4.616e-009	3.307e-009		-8.336	-8.481	-0.145
Mg4(OH)4+4	6.352e-024	4.532e-026		-23.197	-25.344	-2.147
Na	2.203e-001					
Na+	2.000e-001	1.433e-001		-0.699	-0.844	-0.145
NaB(OH)4	1.898e-002	1.898e-002		-1.722	-1.722	0.000
NaHCO3	6.402e-004	6.402e-004		-3.194	-3.194	0.000
NaHSiO3	2.559e-004	2.559e-004		-3.592	-3.592	0.000
NaCO3-	1.979e-004	1.418e-004		-3.704	-3.848	-0.145
NaAlO2	1.254e-004	1.254e-004		-3.902	-3.902	0.000
NaCl	6.084e-005	6.084e-005		-4.216	-4.216	0.000
NaOH	4.658e-006	4.658e-006		-5.332	-5.332	0.000

O(0)		4.295e-036				
	O2	2.147e-036	2.254e-036	-35.668	-35.647	0.021
Si		4.494e-004				
	NaHSiO3	2.559e-004	2.559e-004	-3.592	-3.592	0.000
	SiO2	9.942e-005	9.942e-005	-4.003	-4.003	0.000
	HSiO3-	9.408e-005	6.740e-005	-4.026	-4.171	-0.145
	H2SiO4-2	1.790e-008	4.435e-009	-7.747	-8.353	-0.606
	H6 (H2SiO4) 4-2	3.500e-011	8.669e-012	-10.456	-11.062	-0.606
	H4 (H2SiO4) 4-4	5.076e-013	1.797e-015	-12.295	-14.745	-2.451
Zn		3.665e-006				
	ZnOH+	2.004e-006	1.436e-006	-5.698	-5.843	-0.145
	Zn(OH)2	1.158e-006	1.158e-006	-5.936	-5.936	0.000
	ZnCO3	2.670e-007	2.670e-007	-6.574	-6.574	0.000
	Zn+2	1.954e-007	6.059e-008	-6.709	-7.218	-0.509
	ZnHCO3+	2.137e-008	1.531e-008	-7.670	-7.815	-0.145
	Zn(OH)3-	1.011e-008	7.240e-009	-7.995	-8.140	-0.145
	Zn(OH)Cl	6.499e-009	6.499e-009	-8.187	-8.187	0.000
	ZnCl+	1.879e-009	1.346e-009	-8.726	-8.871	-0.145
	Zn(OH)4-2	1.005e-011	2.490e-012	-10.998	-11.604	-0.606
	ZnCl2	1.933e-012	1.933e-012	-11.714	-11.714	0.000
	ZnCl3-	1.379e-015	9.880e-016	-14.860	-15.005	-0.145
	ZnCl4-2	4.254e-017	1.054e-017	-16.371	-16.977	-0.606
	ZnClO4+	0.000e+000	0.000e+000	-94.491	-94.636	-0.145

-----Saturation indices-----

Phase	SI	log IAP	log KT	
Artinite	-2.99	14.27	17.26	Mg2CO3 (OH) 2 : 3H2O
Azurite	-10.51	-3.66	6.85	Cu3 (CO3) 2 (OH) 2
B2O3	-7.57	-2.41	5.16	B2O3
Boehmite	2.26	7.72	5.46	AlO (OH)
Borax	-1.46	12.08	13.54	Na2 (B4O5 (OH) 4) : 8H2O
Boric_acid	-1.42	-1.21	0.21	B (OH) 3
Brucite	-1.35	12.91	14.26	Mg (OH) 2
Calcite	0.94	2.26	1.32	CaCO3
CO2 (g)	-3.48	-11.54	-8.06	CO2
Cuprite	0.00	-7.79	-7.79	Cu2O
Diaspore	2.61	7.72	5.11	AlO (OH)
Fe(OH)3	0.00	16.72	16.72	Fe (OH) 3
Gibbsite	1.90	7.72	5.82	Al (OH) 3
Huntite	-0.60	6.37	6.97	CaMg3 (CO3) 4
Hydroboracite	-0.89	19.47	20.36	MgCaB6O11 : 6H2O
Lansfordite	-3.49	1.35	4.84	MgCO3 : 5H2O
Magnesite	-0.06	1.37	1.43	MgCO3
Malachite	-3.09	1.41	4.50	Cu2CO3 (OH) 2
Monohydrocalcit	-0.05	2.26	2.31	CaCO3 : H2O
Nesquehonite	-3.36	1.36	4.72	MgCO3 : 3H2O
Siderite	-4.34	-5.19	-0.84	FeCO3
SiO2 (am)	-1.60	-4.00	-2.41	SiO2
Smithsonite	0.00	-0.14	-0.14	ZnCO3
Tenorite	0.00	6.48	6.48	CuO
Tobermorite-14A	-14.28	44.96	59.24	Ca5Si6H21O27.5
Xonotlite	-23.72	58.80	82.51	Ca6Si6O17 (OH) 2
Zn(OH)2 (gamma)	-0.49	11.39	11.88	Zn (OH) 2
ZnCO3 : H2O	-0.29	-0.15	0.14	ZnCO3 : H2O

End of simulation.

Reading input data for simulation 3.

End of run.
